DETERMINATION OF THE SEISMIC PARAMETERS AND UPPER CRUSTAL STRUCTURE OF THE WESTERN MIDLAND VALLEY, SCOTLAND

by

FAWZI SHAREEF AHMED

B.Sc. University of Mosul

Thesis submitted for the degree of Doctor of Philosophy (by research) at the University of Glasgow, Department of Geology and Applied Geology, August 1991

ProQuest LLC.
789 East Eisenhower Parkway
P.O. Box 1346
Ann Arbor, MI 48106 – 1346

Dedicated to my mother

DECLARATION

The material presented in this thesis is the result of research undertaken by the author between February 1987 and August 1991 in the Department of Geology and Applied Geology, University of Glasgow, under the supervision of Dr. J. J. Doody.

This thesis is based on my own independent research and any published or unpublished material used by me has been given full acknowledgment in the text.

F. S. AHMED

J. J. DOODY
(Supervisor)

Department of Geology and Applied Geology,
University of Glasgow, Glasgow.

ACKNOWLEDGEMENTS

I would like to thank everybody in the Department who has helped and supported me to finish this thesis.

I express my deep gratitude to my supervisor Dr Doody not just for his guidance through this work, but for the great help, encouragement and devotion of much of his time to finish this work.

I would like to thank every member of staff in the Department for their moral and financial support to finish this thesis during the most difficult times of recent months. My special thanks and gratitude to Professor Russell and Professor Smythe for their support. I also thank my Arab colleagues for their support.

Thanks are due to Professor Leake for the use of the facilities of the Department and to Dr Farrow for his assistance with the computer facilities.

Many thanks are due to Bob Cumberland for his help and to Zayd, Eddie and Kenny for their help in the fieldwork over a long time.

I should thank the managers of the quarries used in this study and the landowners for the use of their land for the data acquisition.

Finally my thanks to the Iraqi Government for the scholarship which made this study possible.

LIST OF CONTENTS

LIST OF FIGURES

SUMMARY

This project was designed to investigate the western part of the Midland Valley of Scotland. A number of seismic profiles had been undertaken to investigate the centre, eastern and southern Midland Valley. The main feature of the western Midland Valley is the wide presence of the Carboniferous Clyde Plateau Lavas and the presence of major NE-SW trending faults. The main profile was chosen to cross such features: the Dusk Water Fault which played a big role in the deposition of Carboniferous rocks and the distribution of the Carboniferous igneous activity, Paisley Ruck, and Gartness Fault.

This project consists of 2 seismic refraction lines. Three component seismic data were recorded from quarry blast sources. A short line was intended to study near vertical reflections using three component recording. The line is about 15 km long and was recorded in Ayrshire eastward from Hillhouse quarry. The main line is about 70 km long and extends NNE-SSW in the west of the Midland Valley, crossing major faults which played key roles in the deposition and distribution of Carboniferous rocks. The line crosses mostly Carboniferous sediments and the Clyde Plateau Lavas, crossing the Upper and Lower Old Red Sandstone to the north of the Clyde. It passes through Hillhouse, Loanhead and Sheephill quarries. Frequency and polarization filters were used to improve the data quality.

Four layers are recognised in this study for the upper crust from their P-wave velocities. The first layer has a P-wave velocity of 3.5-5.0 km/s and occurs at depths of 0-2 km. This layer is considered as Carboniferous and Upper Old Red Sandstone sediments. The second layer has velocity of 5.0-5.6 km/s and occurs at 1-4 and 0-3 km depth and it shows considerable lateral velocity variation related to the Paisley Ruck. It is interpreted as Lower Old Red Sandstone. This layer is thinned in the area between the Dusk Water Fault and Paisley Ruck and to the east near Troon. The third layer has a P-wave velocity of 5.8 km/s and is restricted to between the Dusk Water Fault and Paisley Ruck. This layer lies at 2.5-3.5 km depth and may represent a Lower ORS volcanic ridge. The fourth layer has a velocity of 5.99-6.08 km/s

and its top is at depth 3-4 km. This layer is interpreted as upper crystalline basement.

Some faults seen at surface affected the basement: the Dusk Water Fault, Paisley Ruck and Gartness Fault which have a Caledonian NE-SW trend. This suggests that these faults, which controlled Carboniferous basins, may be older fractures in the basement reactivated at that time. The lateral velocity variation of the Lower ORS suggest that the Paisley Ruck represents a strike-slip fault. Previous studies considered that such faults in the Midland Valley sole out with depth above or at top crystalline basement.

Deep wide-angle reflections were observed from depths of 8, 12, 15 and 20 km, and are interpreted as being from the boundaries of, and within, a mid-crustal layer.

INTRODUCTION

The Midland Valley of Scotland has been the subject of many geological and geophysical studies to investigate the upper crust and the tectonic regime of this area. In particular, the role of the crystalline basement in the evolution of the Carboniferous sedimentary basins.

This project was undertaken to determine the upper crustal seismic velocity distribution and structure in the western part of Midland Valley of Scotland. A particular study was relation of the crystalline basement with the surface geology across the NE-SW trending major faults in this part of the Midland Valley. These faults controlled the deposition and distribution of the Carboniferous sedimentary and igneous rocks. Quarry blasts were used as seismic sources for a medium length refraction profile to obtain information about the upper and middle crustal layers. Three component recording was undertaken. The study of near vertical reflections from an additional short line length was undertaken to compare the interfaces determined with those obtained from the longer profile. There have been relatively few such short range reflection studies using quarry blasts.

Various processing methods were employed. Frequency filtering was applied to all of the data. Three component recording allowed us to apply more processing methods to apply and study the effect of different polarization filters parameters for the signal enhancement. Various interpretation methods were applied to the data and, finally, raytracing to model the study area.

This thesis describes the data acquisition, processing and interpretation of the above data. General geology and tectonics of the area are reviewed in chapter one and a review of the previous geophysical studies is presented in chapter two. Processing methods are described in chapter three and the interpretation methods discussed in chapter four. Chapter five summarises the results of this study.

CHAPTER ONE

GEOLOGY

1.1 INTRODUCTION

This study was undertaken to investigate the upper crust within the western Midland Valley of Scotland using the seismic method. The study involved a north-south seismic traverse across mostly Carboniferous outcrop. Fig. 1.1 shows the geology of the Midland Valley of Scotland. Also refer to Fig. 3.1b for the detailed geology in the vicinity of the profiles of this study. The Clyde Plateau Lavas (Lower Carboniferous) are a major feature at outcrop. The main geological structures in the area are the Dusk Water Fault, Inchgotrick Fault and Paisley Ruck. These major fractures trend NE-SW, which is the the same as the dominant Caledonian structural trend.

The Midland Valley of Scotland is a NE-SW trending block now exposing mainly Upper Palaeozoic rocks and is bounded on the north by the Highland Boundary Fault and on the south by the Southern Uplands Fault. It is an important unit within the Caledonide Orogeny. It is viewed as a terrane.

1.2 TECTONIC FRAMEWORK

There are many theories about the evolution of the Midland Valley of Scotland (MVS). Kennedy (1958) and George (1960) interpreted the Midland Valley as a graben receiving its detritus from the Grampian Highlands and the Southern Uplands during the Devonian times. Dewey (1971) and Leggett (1980) had broadly similar views, suggesting a destructive plate tectonic model and considering the Midland Valley to be a fore-arc basin dividing the accretionary prism to the south from a basement arc terrane to the north. The Southern Uplands trench received its deposits from the erosion of the metamorphosed and uplifting Dalradian terrane (Yardley *et al.* 1982). Bluck *et al.* (1980) considered the Midland Valley was an arc at least for part of its history and supplied detritus to the basins to the south. The fore-arc model of

the Midland Valley was rejected because of the interpretation of the Ordovician sequence at Girvan in the SW of the Midland Valley. These rocks were generated in a proximal fore-arc basin immediately to the south of a contemporaneous plutonic-volcanic arc. Further the Silurian sediments in the southern Midland Valley show an igneous and metamorphic source of sediments and not from the rising trench-slope. Thus the MVS is considered as an arc-inter-arc basin during the Ordovician-Devonian time (Bluck 1983). Much of the fore-arc basin is missing and the Southern Uplands accretionary prism is thought to have been thrust over this basin and the continental crust of the Midland Valley (Fig. 1.2).

Bluck (1984, 1985) interpreted the MVS as a suspect terrane which was juxtaposed with the Grampian Highlands by strike-slip movement during the Devonian (Fig. 1.3). Bluck (1984) considered the tectonic elements to have been juxtaposed by strike-slip and thrust faulting, both of which affected a 300% reduction in the width of the orogenic belt. While Hutton (1987) considered that there was no shortening and the British Caledonides were affected by major sinistral strike-slip faults in the end-Silurian and pre-Devonian time. Such research on the displaced terranes in the British Caledonides has challenged the traditional concept of the plate tectonic theory of the British Caledonides.

The terrane concept for the evolution of the Midland Valley has been supported by many studies, such as the palaeomagnetic study by Trench *et al.* (1989) which showed that the three terranes (Highland, Midland Valley and Southern Uplands) were adjacent by Devonian times. Another study by Haughton (1988) showed that the Lower Old Red Sandstone in north-east of the Midland Valley was derived from the Midland Valley itself and not from elsewhere, based on the petrographic examination and chemical analysis of clasts. An important mafic/ultramafic provenance was identified which shows that ophiolitic source rocks may have been part of the source. The chemical analysis showed that these rocks are isotopically unrelated to either Southern Uplands shales and greywackes or Dalradian metasedimentary rocks. Some authors went one step further. Trench & Haughton (1990) adopt the name North Midland Valley terrane for the Highland Border Complex and its hidden extension beneath the Devonian and Carboniferous cover, and considered the Midland Valley terrane itself may conceal important terrane boundaries. They suggest that the separation of the Northern Midland Valley and Grampian terranes inferred for the Ordovician period

was largely removed by late Silurian times, and the two terranes have a relative displacement of only tens kilometres after Lower Old Red Sandstone time.

Strike-slip tectonics superimposed on this framework were a critical control on Carboniferous sedimentary bsin development.

1.3 GEOLOGICAL SEQUENCE

1.3.1 Precambrian basement

There has been much speculation about the origin of the MVS, whether it is continental or oceanic. No pre-Palaeozoic basement is exposed, so there is a wide variety of models for the evolution and the type of the basement, such as Dalradian rocks (Yardley *et al.* 1982), oceanic crust (Mitchell & McKerrow 1975), or a Pre-Dalradian block (Kennedy 1958, George 1960). There is only indirect evidence of the type and evolution of the basement.

1-Provenance studies.

Provenance studies were based on the lithology of conglomerates in the Lower Palaeozoic which is exposed near Girvan and Lesmahagow. These conglomerates contain igneous clasts of acid to basic composition. Bluck (1983, 1984) suggests the source of these clasts was a volcanic plutonic arc in the Midland Valley, and which would be now concealed by the later deposits.

2- Geophysical studies

P-and S-wave measurement of Lewisian rocks (Hall & Al-haddad 1976) and the calculation of Poisson's ratio by Assumpcao & Bamford (1978) suggest that a layer with velocity of 6.4 km/s identified in the LISPB seismic experiment (see later) is of pre-Caledonian basement, which is composed of intermediate granulite gneiss similar to Lewisian Gneiss. Other studies by Hall *et al.* (1983) and Davidson *et al.* (1984) also suggest an acid to intermediate basement composition under the Midland Valley. The LISPB 7.0 km/s layer is considered as lower crust and so interpreted as basic rock of dominantly gabbro to diorite composition.

3- Xenoliths from volcanic vents

Xenoliths are found in vents in Ayrshire, Renfrewshire and along the Fife coast in the east of the Midland Valley. These are inferred to be samples of the basement (Upton *et al.* 1976). These rocks yield information on crustal and upper mantle composition layers. Upton *et al.* (1984) integrated these with the seismic velocities of LISPB to show that the xenoliths of foliated quartzo-feldspathic granulite gneisses and unfoliated plutonic rocks are correlated with the LISBP 6.4 km/s mid crustal layer while the basic granulite, is represented by foliated peridotites and other unfoliated ultramafics rocks are correlated to the 7.0 km/s lower crustal layer. There is no evidence of low grade metamorphic rocks as might be expected if Dalradian rocks underlie the Lower Palaeozoic rocks (Dewey 1971, Upton *et al.* 1983).

The Precambrian rocks (i.e crystalline crust) can be summarised according to the seismic velocity into:-

1- Upper crystalline rock layer with a velocity of 6.0 km/s of mainly feldspathic granulite composition.

2- Lower crystalline basement which represent the pre-Caledonian basement, which has the velocity of 6.4 km/s and is mainly acidic to intermediate granulite in composition.

3- Lower crustal layer with a velocity of 7.0 km/s which is dominantly gabbro to diorite in composition.

1.3.2 Lower Palaeozoic

The oldest rocks seen at the surface in the Midland Valley are at Ballantrae and at the Highland Border (Fig.1.4). The rocks at Ballantrae comprise a suite of intrusive and extrusive, predominantly basic igneous rocks and are associated with marine sediments (Church & Gayer 1973, Dewey 1974), and are of Arenig age (Stone & Rushton 1983). These rocks show the history of the subduction on the southern margin of the Laurentian continent and are variously considered as a remnant of a Pacific ocean island (Barret *et al.* 1982) or as an obducted part of a marginal basin including a small oceanic island (Bluck *et al.* 1980, Bluck & Halliday 1982, Bluck 1983). The complex is unconformably overlain by a conglomeratic and turbiditic sequence of

Llanvrn-Ashgillian age deposited in a series of fault bounded basins (Williams 1962). Bluck (1983) interpreted the later sequence as being formed in a proximal fore-arc basin and postulates the presence of a major arc massif to the north and a fore-arc basin to the south (Fig. 1.5).

The rocks of the Highland Border Complex (HBC) occur as a series of discontinous outcrops adjacent to the Highland Boundary Fault. The HBC consists of serpentinite and possibly other ophiolitic rocks of early pre-Arenig age, and a sequence of limestones and conglomerates, shale, cherts and quartz. There has been much speculation about the rocks of the complex, particularly whether they are a Dalradian subgroup or a discrete group. Fossils discovered by Curry *et al.* (1984) confirmed that the complex is of Ordovician age (Arenig to late Caradoc age) and thus the rocks were not involved in the early Grampian deformational event which affected the Dalradian group.

The complex is unconformably overlain by Downtonian strata at Stonehaven and by the Lower Old Red Sandstone at Loch Lomond. Bluck (1984) suggested that it was deposited in a marginal basin. He compared the complex with the Dalradian and demonstrated that the two crustal blocks were not adjacent at this time and the Highland Boundary Fault is the boundary between the two terranes. Trench & Haughton (1990) combined palaeomagnetic studies and a geochemical analysis to study terrane positions in late Silurian times. They suggested that the separation of the Northern Midland Valley and Grampian terranes inferred for the Ordovician period was largely removed by late Silurian, with relative displacements of tens of kilometres after Lower Old Red Sandstone deposition.

A number of Lower Palaeozoic inliers occur in the southern part of the Midland Valley and range in age from Llandovery to Ludlow. These rocks show the transition through the Silurian from marine turbidites, shales and conglomerates to terrestrial conglomerates and sandstones and show a high proportion of acidic rock fragments. The base of this sequence is seen near Girvan where this conglomerate oversteps Ashgillian rocks of the Girvan sequence (Ingham 1978). Bluck (1983) showed that this sequence was deposited in an inter-arc basin, and the source of the deposit came from the south. The Southern Uplands accretionary prism is not far from the outcrop and cannot be the source, thus the prism either covers the source which supplied the sediments, or there has been subsequent relative movement of the MVS and Southern Uplands.

1.3.3 Old Red Sandstone.

The lithologically based name Old Red Sandstone (ORS) is used particularly in Scotland to refer to the Devonian age. The ORS is divided into Upper, Middle and Lower parts. The Middle ORS is missing in the Midland Valley, and the Upper ORS rests unconformably on the Lower ORS.

1.3.3.1 Lower Old Red Sandstone

Fig. 1.6 shows the ORS outcrop in the Midland Valley. The Lower ORS is characterised by red, drab conglomerate and lithic arenites which are interstratified with lavas of basalt, andesite, trachyte, dacite and rhyolite composition (Bluck 1967). The thickness of this varies in the Midland Valley, but generally it decreases southwestwards along the northern margin of the Midland Valley (Friend & Macdonald 1968) and the estimated thickness of the Lower ORS in Kincardineshire is 6600 m (Armstrong & Paterson 1970), and it reaches about 1800 m at Loch Lomond (Qureshi 1970). Within the upper Firth of Clyde there is a general decrease of the ORS thickness under the Carboniferous rocks northwestwards towards the Highland Boundary Fault (McLean & Walker 1978). The thickest development of the Lower ORS in the southern part of the Midland Valley is probably in the Pentland Hills (Mykura 1960). The sediments consist of about 600 m of conglomerates and coarse pebbly sandstones.

The sediments thin towards the north-east where they interdigitate with and are replaced by a sequence of lavas and tuffs up to 1800 m thick. The lava is varying in composition from basalt to rhyolite. At Maybole the sequence consists of conglomerate and sandstone and it may include 1200 m of sediments overlain by up to 450 m of lava in south Ayrshire (Eyles *et al.* 1949). The Lower ORS rest unconformably on the Arenig to Caradoc Highland Border Complex in the north of the Midland Valley. While in the south the Lower ORS rests unconformably on the Lower Palaeozoic in the Pentland Hills (Mykura 1960) and at Girvan (Cock & Toghill 1973) and rests conformably on the Silurian rocks at Lesmahagow and in Hagshaw Hills (Rolfe 1961).

Using palaeoflow and clast provenance data, Bluck (1983,1984) suggested that the Lower ORS was deposited in two basins, the Lanark and Strathmore basins and the sediments were dispersed off a volcanic ridge which was the

southwesterly extension of the Ochil-Sidlaw chain and which is now partly exposed south of Ayr (Fig. 1.5). The sedimentation took place in a series of small sub-basins (Fig. 1.7). These basins were probably controlled by strike-slip motion on a pre-cursor of the Highland Boundary Fault which is now concealed by the post-ORS Highland Boundary Fault (Bluck 1984, Haughton 1986, Haughton & Bluck 1989 & Haughton 1989).

The Lower ORS age for this sequence is questioned by geochronological studies which have placed most of the vulcanicity of the Lower ORS as late Silurian (Thirlwall 1983), and also suggest that there is a minor intrusion at Tinto of late Silurian age (Bluck 1984).

1.3.3.2 Upper Old Red Sandstone

The Upper ORS rests unconformably on the Lower ORS in the Midland Valley. The Upper ORS is composed of terrestrial clastic sediments. It is more matture and characterised by finer grain sediments than the Lower ORS. There are no volcanic rocks within the succession. The thickest development of the formation is 1 km in the northwestern part of the Midland Valley and it thins to 0.5 km to the south and the east (Fig. 1.8).

In the north-west part of the area the outcrop occupies a strip on the north and west of the Clyde Plateau Lavas, below which the Lower ORS dips gently to the south-east and east. In Ayrshire outcrops are generally aligned NW-SE and emerge from below the cover of Carboniferous rocks on either side of the Mauchline syncline.

Palaeocurrent studies (Bluck 1978) suggest an East or Northeast drainage direction through the Upper ORS. Change of distribution grain size and provenance show the lowest of the Upper ORS was confined to a series of small fault-controlled basins in the NW Midland Valley which may be due to local stresses resulting from sinistral movements along the Highland Boundary Fault.

1.3.4 Carboniferous

1.3.4.1 Sedimentation

Most of the Midland Valley outcrop is Carboniferous sedimentary and extrusive igneous rocks. Most of the western part of outcrop is the Clyde Plateau Lavas which have a NW-SE trend. Permian NE-SW dykes cut the

sequence. Fig. 1.9 shows the Carboniferous outcrop.

The Carboniferous sedimentary sequence formed in either shallow marine or fluviatile environments with localised, often persistent, contemporaneous volcanic activity which often exerted control over sedimentation (Francis 1968, 1983). Red beds reappeared at the end of the Carboniferous showing the return of arid conditions in the Permian. Fig. 1.10 shows the subdivision and classification of the sequence in the Midland Valley. The thickness of the Carboniferous rocks has a considerable variation in the western part of the Midland Valley and has a maximum thickness in Ayrshire (Fig 1.11). The Calciferous Sandstone Measures (CSM) in the Midland Valley show extreme lateral facies changes. It includes a large volume of basic igneous rocks and records an increasing marine influence on sedimentation. Within the CSM, the Cementstone Group consists of argillaceous limestone interbedded with mudstone and sandstone of probably lagoonal origin. The thickest sediment (480 m) occurs near Dailly in south Ayrshire and thins northwards. In Renfrewshire the Cementstones are overlain by the Clyde Plateau Lavas which divides the CSM into lower and upper sedimentary groups, in which the upper group rests unconformably on the lava and its deposition is controlled by the lava topography (Whyte 1981). To the north of Ardrossan the Clyde Plateau Lava rest on ORS and to the north, around the upper Firth of Clyde, there is no clear contrast between the ORS and the Calciferous Sandstone.

The Limestone Coal Group consists of deltaic sandstones, siltstones and shales and it contains coal beds. This group shows a similar pattern of sedimentation to the Lower Limestone Group but with a thicker coals and thinner marine limestone. Its thickness varies from 90 m in south Ayrshire to 150 m at Dalry in north Ayrshire. Sedimentation has been controlled by contemporaneous movement on NE-SW faults such as the Dusk Water, Inchgotrick and Kerse Loch Faults.

The Passage Group consists mainly of sandstone with locally thick beds of clay rocks. In Ayrshire, basaltic lava separates two sedimentary groups, the upper group containing bauxite clay. The volcanics are up to 150 m thick, near Troon, decreasing to the east and are absent further east and south.

The Coal Measures consist of white or grey sandstone, grey or dark siltstones and mudstones with ironstones. The Lower and Middle Coal Measures reach their maximum thickness in south Ayrshire, near Dalmellington and decrease to the north-west. The Upper Coal Measures

consist mainly of shales and sandstones, and are found only in central Ayrshire under the New Red Sandstone in Mauchline. It varies in thickness from 380 m on the north-western side of the Mauchline Basin to 540 m in the south-east.

Sedimentation was greatly influenced by contemporaneous tectonics. Hall (1971,1974) recognised two zones of different structural style separated by the N-S trending line "Lanark line". To the east of this line N-S folds are cut by E-W normal faults and dykes are common. To the west, E-W faulting is less apparent with NW trending folds and faults being important. Both patterns are superimposed on an older NE-SW trend within the pre-Carboniferous basement. During the Carboniferous, the NE-SW and the E-W trend of active structures changed gradually to NW-SE trend which controlled the Permian deposition. However, the major control on sedimentation in the Carboniferous was the differential subsidence along NE-SW trending faults in the Midland Valley.

The nature of the Highland Boundary Fault at this time is not clear due to lack of outcrop, the Carboniferous sediments cross the fault near Loch Lomond suggesting little or no relief on the fault line.

In the western Midland Valley, parallel NE-SW structures are the Paisley Ruck, Dusk Water, Inchgotrick & Kerse Loch Faults. McLean (1961, 1978) considered that the abrupt change of the stratigraphic units across these faults indicate syn-depositional fault movements (Fig 1.12). The tectonic models of the Midland Valley in the Carboniferous can be divided into those advocating pure shear in an E-W stress field (Russell 1971, Haszeldine 1987), pure shear in a N-S stress field (Leeder 1976, Bott *et al.* 1984) and dextral, strike-slip models (Dewey 1982, Read 1987). Read (1989) considered that the Dewey (1982) model provides the best explanation of the evidence for right-lateral strike-slip during the late Carboniferous found along a lineament in the eastern part of the Campsie Fault and the eastern part of the Ochil Fault. He considered that the lineament extends WSW below the eastern part of the Milngavie-Kilsyth Fault to underlie the Paisley Ruck. This lineament may have been initiated as a Riedel Shear by dextral strike-slip faulting along the Highland Boundary Fault, or it may reflect a reactivated Late-Caledonian sinistral strike-slip fault system (Fig 1.13). Gibbs (1987) suggested a "mixed mode " combination of right-lateral strike-slip and dip-slip fault arrays and postulated a complex series of shallow detachments within the Upper Palaeozoic sediments.

Based on seismic information, Dentith (1987) postulated the presence of a low angle detachment horizon controlling the observed structures, which may be at less than 2 km in some places. He compared the high relief on the mid-ORS refractor, which follows surface structures, with the virtually planar crystalline basement top, and considered the detachment to be usually between 2 & 4 km depth. Thin skinned processes with multiple detachment levels have been postulated for the region by Gibbs (1984) who suggests a dextral strike-slip environment during the Carboniferous times. Dentith (1987) found this in agreement with his data, particularly with regard to the structure of the Ochil Fault, a major E-W listric fault in the central Midland Valley.

During the late Carboniferous the direction of the regional stress switched from a N-S tension to a NE-SW tension giving rise to a broad fault-bounded basin in which subsidence kept pace with sedimentation through to Permian times. In Ayrshire the Mauchline basin is separated from the East Arran basin by a block bounded by the Dusk Water and Inchgotrick faults in which there is no evidence of structural continuity. To the SE, the Kerse Loch and Southern Upland Faults similarly divide the Mauchline Basin from the Sanquhar basin. Associated with these feature is the anticlinal swell running from Renfrew to Lesmahagow which exposes the Clyde Plateau Lavas north of the Inchgotrick fault and the Silurian rocks of the Lesmahagow inlier to the south. Bluck (1978) invoked the presence of a series of approximately NW-SE trending faults generated in Upper ORS times as a result of transitional stress along the Highland Boundary Fault producing pull-apart basins in the region of Renfrew and the Firth of Clyde. The basins of Arran and Mauchline may be related to the reactivation of these fractures. In addition to the syn-depositional folding, and faulting the sediments were controlled by the topography of the lava bodies.

1.3.4.2 Igneous activity

The Carboniferous succession contains large volumes of intrusive and extrusive alkali igneous rocks. The greatest eruption of lava was the Clyde Plateau Lavas (CPL) during the Dinantian. The main mass of the lava consists of olivine-basalt with subordinate trachyte, and forms a horseshoe-shaped outcrop extending from Strathaven in the south through Ayrshire and shows irregular thickness. It is about 800m south of the Paisley Ruck,

decreasing to 600m to the north of it (Cotton 1968). Further north it reaches about 800 m to the south of Campsie Fault in the Kilpatrick Hills. It is only about 200 m at the Campsie Hills and dies out within a short distance to the east.

The lavas show well-developed boles indicating contemporaneous sub-aerial weathering (Macdonald, 1973). The CPL may have originated from the many associated vents, though fissure eruption has been suggested due to the lateral persistence of some flows (Francis *et al.* 1970). In some areas vents, plugs and local dykes are grouped together in linear zones with a predominant NE-SW trend, which may reflect deep-seated fractures along Caledonian structures in the underlying basement (Cameron & Stephenson 1985). These fractures exerted a major structural control on the lava and marked changes in thickness of the lava occur across the NE-SW faults such as the Dusk Water Fault. Other less well defined volcanic lineaments have been postulated on a NW-SE trend in the western Midland Valley where such trends become more important during later igneous activity. At the end of the Dinantian the activity concentrated around Bathgate and probably overlapped the CPL (Anderson 1963).

In Silesian times the igneous activity continued and flows are seen interbedded with the Passage Group in Ayrshire. Lava flows of this age are predominant only in Ayrshire, but large volumes of magma solidified at depth occur in most areas as sill-complexes.(Fig. 1.14). Fig. 1.15 is a cross section of the Midland Valley showing the distribution of the Carboniferous lavas. The late Carboniferous activity gave a large number of E-W tholeiitic dykes and these dykes acted as feeders to the Midland Valley Sill Complex. Most of these dykes are concentrated in central Ayrshire in the Kilmarnock basin and are found to be thick in the basinal area.

1.3.5 Permian

The Permian (New Red Sandstone) rocks consist mainly of red sandstone and mudstone with basalt lava at the base and are known as the New Red Sandstone. These rocks have a very restricted outcrop in the Midland Valley: the Mauchline basin, Stranraer Basin, on Arran and offshore in the Firth of Clyde (McLean & Deegan 1978). The thickness of the red aeolian sandstone in the Mauchline Basin is about 450 m and it is about 1300-1600 m in Stranraer Basin as measured by the gravity method. The New Red Sandstone present

in the Firth of Clyde rests on the Lower Palaeozoic, south-west from Girvan (McLean & Deegan 1978), and it has a regional dip south-west-ward to the North Channel to reach its maximum thickness in the extreme south-west of the plateau within the Southwest Arran Trough (McLean & Wren 1978). Due to the lack of outcrop it is difficult to know the tectonic environment. Hall (1974) suggested that the NW fractures originating in the Carboniferous became more important in the Permian, exerting controls on sediment deposition.

1.3.6 Tertiary

Tertiary dolerite dykes associated with the Arran and Mull central igneous complexes are abundant in the western Midland Valley and dolerite sills occur in Ayrshire. Most of the Tertiary dykes are alkali olivine - dolerite or tholeiitic and have NW-SE trend. Faults of NW-SE trend are common in the west of Midland Valley and were assumed to be of Tertiary age (Anderson 1951), though Mykura(1967) and Hall (1974) showed the NW structures to have been active in the late Carboniferous and Permian.

1.4 STRUCTURE

Fig. 1.16 shows the principal structures in the Midland Valley. The tectonic setting of these structures will be discussed here in general and more attention will be paid to the structures which affected the sediments of the Carboniferous age.

The Midland Valley is a NE-SW trending block, mainly covered by Upper Palaeozoic rocks (Fig. 1.1) and bounded by the Highland Boundary Fault (HBF) to the north which separates the younger sediment of the Midland Valley from the older sequence of the Dalradian rocks. To the south it is bounded by the Southern Upland Fault (SUF) which separates its younger outcrops from the older sediment of the Southern Uplands. No margins to the Midland Valley equivalent to the HBF and SUF were observed from the WINCH deep seismic reflection section (Hall *et al.* 1984).

1.4.1 Highland Boundary Fault

The Highland Boundary Fault (HBF) extends from Stonehaven in the north-east to near Helensburgh on the Firth of Clyde. The fault represents a wide zone of displacement which includes two or more major faults. It becomes

unclear to the west of Loch Lomond near to the present study area. To the east of Loch Lomond the fault is the southern of two major fractures about 1 km apart. To the west the northern branch fault splays at a low angle from the other important fracture, and this trends NE-SW and swings to the south in the western part of the Midland Valley and the Firth of Clyde (Qureshi 1970). Along the NW side of the fault Dalradian rocks are exposed and the Lower Old Red Sandstone is on its southern side near Loch Lomond and the Carboniferous rocks further southwest near Greenock (Qureshi 1970).

This fault separates the Highland Border Complex of Ordovician age from the Dalradian rocks which represent the Late Pre-Cambrian metasedimentary and metavolcanic rocks deformed by the Grampian Orogeny. The youngest rocks affected by major faulting along this line are the Lower Carboniferous, but there is much evidence of folding and dislocation prior to this time (Harte *et al.* 1984). The complexity of the movement is further indicated by the presence of the Highland Border Complex itself. The HBF is interpreted as a sinistral strike-slip fault in the end-Silurian and pre-Devonian period (Hutton 1987). The HBF is interpreted as a reverse fault dipping northwest at an angle of 60-80 degrees to the northeast of Loch Lomond. To the southwest of the Loch Lomond the fault is interpreted as a normal fault, with a downthrow to the northwest. It is considered as a reverse fault of Carboniferous age by Bluck (1984). Its tectonism ceased before Permo-Carboniferous quartz-dolerite dykes were intruded since these dykes cross the fault zone without being crushed (Anderson 1947). Some studies considered the fault as a strike-slip fault (Anderson 1951). Recently, most models of the Caledonide orogeny considered that the HBF is a terrane boundary and as a large scale sinistral strike-slip fault from the Ordovician till the end of the Old Red Sandstone times (Bluck 1984, 1985).

1.4.2 Southern Uplands Fault

The SUF runs from Glen App in the south-west to Leadburn in Midlothian where the fault apparently is buried by the cover of Carboniferous sediments. The displacement of the fault began at least as early as Mid-Devonian and was renewed during Carboniferous times. The main displacement was probably in the Lower and Middle Devonian with a downthrow to the northwest along the whole fault. Late Carboniferous movement took place

during the Carboniferous with local effects. Differential subsidence caused abrupt changes of thickness in the Carboniferous of Ayrshire and south Lanarkshire. Recently, the fault has been interpreted as a terrane boundary. Studies by Elders (1987) compared the Ordovician conglomerates to the rocks in Newfoundland and he suggested a large sinistral translation along the SUF. There is some uncertainty about the time of the movement, constrained by the comparison which showed that the movement must be post Ordovician and pre-ORS, the age of the oldest overstep sediments across the structure in the northeast Midland Valley.

The presence of distinct sequences within the Northern Belt led McKerrow & Elders (1989) to suggest that the SUF lies 5 km to the north of the 'conventional' line in Scotland and NE Ireland. They compared the lithology of the Northern Belt and the southern part of the Midland Valley to suggest that the Downan point lavas in the Belt are younger than the Early Ordovician Ballantrae Igneous Complex, and that the SUF probably coincides with the Stinchar Fault, which would then separate the Llandeilo sequence from the Arenig on the west coast. The comparison of clasts in mass flow conglomerates in the Southern Uplands with granites in western Newfoundland suggest large Ordovician and Silurian strike-slip movements, while southerly-derived clasts in Late Silurian Midland Valley conglomerates suggest post-Silurian movements. The evidence for post Silurian movements comes from the Silurian inliers of the Midland Valley. The evidence for large scale strike-slip movements on the SUF suggest that the rocks now present in the Southern Uplands may have still been situated well to the west of the Scottish Midland Valley during the Late Silurian.

1.4.3 Other faults

In the western part of the Midland Valley, there are three major tectonic features which affected the deposition of the Upper Palaeozoic rocks. These are the Dusk Water and Inchgotrick Faults and Paisley Ruck. These faults and ruck trend ENE and swing to NE as they approach the Firth of Clyde. This swing might reflect a reorientation of the regional stress near an inhomogeneity in the crust (McLean & Qureshi 1966). These faults played a big role in the deposition and distribution of Carboniferous sediments. Abrupt changes in the sediment thickness show that these faults were active at the time of deposition.

1.4.3.1 Paisley Ruck

The Paisley Ruck has a NE-SW trend, the same as the common trend of the faults in the west of Midland Valley. It is a wide shatter-belt and the downthrow reverses as it is traced WSW. This fault affected the Carboniferous sediments and the distribution of the Clyde Plateau Lavas. The lava thickness is about 600 m on the NW side and it is about 800 m to the SE (Cotton 1968). From the variation of the lava thickness across the fault, Cotton (1968) suggested that the fault was active either as a normal fault contemporaneously with the extrusion of the Clyde Plateau Lavas and controlling the development of the lava pile, or was a strike-slip fault at a later date which brought lava of different thickness into juxtaposition.

The east-west and ESE-WNW alignments of minor faults on either side of the Ruck resemble a pattern of Riedel shears and extensional fractures created by a dextral strike-slip fault. This feature of the fault led Gibbs (1984) to consider that the Paisley Ruck is a positive flower structure produced by right-lateral transpression. Read (1989) proposed that a basement lineament probably extends WSW below the eastern part of Milngavie-Kilsyth fault to underlie the Paisley Ruck and this lineament may have been initiated as a Riedel Shear by dextral strike-slip fault along the Highland Boundary Fault, or it may reflect a reactivated Late-Caledonian sinistral strike-slip fault system.

1.4.3.2 Dusk Water Fault

This fault is present in north Ayrshire, and strikes NE-SW. At outcrop the fault dies before it reaches the coast (IGS sheet 22) but the gravity and magnetic results (McLean & Wren 1978) indicate that the fault persists to the south-west across the Firth of Clyde as far as the North Channel. The fault controlled the deposition of the Carboniferous sediments and also affected the distribution of the Clyde Plateau Lavas. The fault showed a contemporaneous movement with the eruption of the Clyde Plateau Lavas which are 1.25 km thick to the south of the fault and about 0.75 km to the north (Alomari 1980). The lavas thin towards the fault from the north-west, as the overlying sediments do, but thicken to the south-east (Hall 1974). The continuation of a reflector from the north-west of one line across the fault

led Hall (1974) to suggest the fault is not very steep to the south-east and so appears as a reverse fault in its effect on the Carboniferous.

1.4.3.3 Inchgotrick fault

The Inchgotrick Fault extends from the coast in central Ayrshire to the east near Lesmahagow. Along much of its length, in central Ayrshire, Upper Carboniferous rocks on the northern side are thrown down against Lower ORS. The most striking stratigraphic change across the fault is the near-absence of the Clyde Plateau Lavas on the southern side of the fault compared to the thickness at the northern side. The precise decrease cannot be determined from the geology as the base of the lava is not exposed.

1.4.4 Structure summary

The Caledonide framework of the Midland Valley exerted a great influence on later sedimentation and tectonics. However, transverse structures trending NW exercise the most important control on the present outcrop distribution of Upper Palaeozoic rocks in the west. A broad anticlinal high extending south-eastward from Renfrewshire, is the near surface expression of a lava pile thickest close to the present fold axis (Hall 1974). A broad syncline in southern Ayrshire, the Mauchline basin, is of similar trend and probably developed during Carboniferous time (McLean 1966). Mykura (1967) concludes from detailed study of the Upper Carboniferous rocks of south Ayrshire that activity along a NE line was replaced by movement, and differential subsidence along northwest lines during that interval.

CHAPTER TWO

PREVIOUS GEOPHYSICAL WORK

2.1 INTRODUCTION

A great deal of geophysical work has been done in the Midland Valley of Scotland to study the crustal structure, and to outline its tectonic framework. Data from the Firth of Clyde are summarised by McLean & Deegan (1978) and Hall *et al.* (1984) in addition to the gravity, magnetic and seismic work which has been carried out in the west of Midland Valley. Generally the previous work has been interpreted in terms of the upper crust as a top layer representing the Carboniferous and Upper Old Red Sandstone, a second layer representing the Lower Old Red Sandstone and Lower Paleozoic and a third layer interpreted as a crystalline basement.

This study which has taken place in west Midland Valley is to study the upper crust and a particular concern has been paid to the wide angle reflections.

2.2 REGIONAL STUDIES

The first regional study in the Midland Valley was carried out by McLean & Qureshi (1966) who used the gravity method to study the crustal structure. They constructed a profile across the western part of the Midland Valley perpendicular to the Highland Boundary Fault and the Southern Upland Fault (Fig. 2.1). It showed that the Bouguer gravity anomaly increases to the west and there is a high anomaly over the central zone of the Midland Valley. The data were stripped to the base of the Old Red Sandstone such that the sedimentary cover was represented by an equivalent thickness of Lower Palaeozoic sediment with a density of 2.7 g/cm^3. They produced a model of two crustal layers which showed the crust has a thickness of 32 km in the Midland Valley and is bounded by thicker crust to the north and south, the thickening of 5 km occuring in the upper crust. This study showed some local gravity effects in the area as well, such as the high

residual anomaly of +15 mgal observed over the Campsie Fells, but no explanation for that was given. From the geological map the Clyde Plateau Lavas thin abruptly at the Inchgotrick fault, but the high regional gravity contour of +20 mgal crosses the fault. They considered the local anomalies to be due to the extensive Upper Palaeozoic vulcanicity. By using different thickness of stratigraphic unit across these faults they were able to estimate syndepositional movement. For example, 800 m of synsedimentary movement is suggested across the Inchgotrick fault during Carboniferous times.

Crampin *et al.* (1970) described the Lowlands Seismological Network (LOWNET) located in the central and eastern part of the Midland Valley (Fig. 2.2). They studied the P-wave arrivals from data recorded from quarry blasts to produce a preliminary model of three layers. Layers 1 and 2 have velocities of 3 and 5.65 km/s respectively and these two layers were interpreted as Palaeozoic sediments. A refractor of velocity 6.45 km/s was interpreted as crystalline basement and its top occurs at 7-8 km depth.

The Lithospheric Seismic Profile in Britain (LISPB) was carried out in 1974 to study the structure of the crust and upper mantle in Britain. It crossed Britain from north to south (Fig. 2.3). Bamford *et al.* (1976, 1977, 1978) interpreted the data and showed 4 crustal layers: the top 4-5 km/s velocity is interpreted as the Old Red Sandstone and Carboniferous whereas the second layer which is less than 6.2 km/s represents the Lower Palaeozoic, the third segment of velocity greater than 6.2 km/s is crystalline basement, and the lower crustal layer with a velocity of 7.0 km/s from a depth of 20 km to the Moho at 25-32 km. A velocity of about 8 km/s represents the Moho refractor (Fig. 2.4a). The velocity of the basement is 6.0-6.2 km/s in the Highlands and is interpreted as Caledonian metasediments and intrusions. It has a lower velocity of 5.93 km/s beneath the Midland Valley, interpreted as Lower Palaeozoic rocks and 5.84 km/s beneath the Southern Uplands. The second layer has the velocity of 6.48 km/s north of the Southern Uplands Fault and was interpreted as Caledonian foreland basement which extends into the Midland Valley. It appears to terminate at the Southern Uplands Fault. The depth of this layer is 6-14 km. Its velocity is 6.28 km/s south of the Southern Uplands Fault and it underlies the Lower Palaeozoic layer at a depth of 8-14 km.

Assumpcao & Bamford (1978) used the shear waves of the LISPB data to study the Poisson's ratio of the crust by measuring the arrival time of the

shear wave relative to that of the P-wave (ts/tp). The particle motion was used to pick the onset of the shear wave with the help of the lowpass Hanning window to avoid any high frequency and ringing effect which is often caused by narrow band filtering. Fig. 2.5 shows the ts/tp method for the interpretation data. The P, S wave time can be measured directly from the data, removing the need to calculate the velocity of both P & S, thus minimising the cumulative effect of the error in the calculation. The disadvantage of this method is in the assumption of the common raypath and raypath length of both P and S waves, especially in a medium with lateral velocity variation such as the Midland Valley. The Poisson's ratio was used to model the crust (Fig. 2.4b). From this study the Poisson's ratio values were close to 0.25 except for layer 1 in the Southern Upland (0.231) and layer 2 under Midland Valley (0.224). They postulated that these low values are a result of tectonic activity close to the Southern Upland Fault.

MacBeth & Burton (1985) describe surface wave data obtained in the Midland Valley from the Kintail earthquake, recorded during the LISPB experiment. Seven regions of relatively homogeneous velocity are recognised within a 17 km depth into the upper crust. Velocities in the top 2 km are consistently low, 3.0 and 3.4 km/s and increasing slowly to 3.8 km/s . Lower layers have a mean velocity of 3.6 km/s.

Hall *et al.* (1983) used the Southern Upland Seismic Profile (SUSP), local LISPB data and seismic arrays at Eskdalemuir and Broughton to interpret the crustal structure of the Southern Uplands (Fig. 2.6). SUSP shows a P-wave velocity of 6.0 km/s at a depth of about 1 km increasing to 6.3 km/s at 3-4 km depth. Examination of data from quarry blasts recorded at the Broughton array (BTN), which is centred in the middle of the SUSP line, shows similar high apparent velocities along strike (parallel to SUSP) and in the Midland Valley to the north and west, but a low velocity to the south and east. The observations at the Eskdalemuir array show a high velocity along the strike and low velocity across it. The data are interpreted as being due to high (6.0 km/s) and low velocity (5.60 km/s) blocks of 10-12 km width (Fig. 2.7). It was concluded that the high velocities are due to crystalline rocks of granodioritic and dioritic composition, while the lower velocities are of greywackes and suggested that the high velocity crust of the Midland Valley continues south of the Southern Upland Fault. Oliver *et al.* (1984) has considered this variation of velocity is due to a transition from poorly foliated prehnite-pumpellyte facies to well foliated greenschist facies

schist, but the experiment used by Oliver as a comparison was poorly constrained and this view is not considered appropriate for the Southern Uplands.

Hall *et al.* (1984) interpreted the data of the Western Isles - North Channel (WINCH) deep seismic reflection profile. WINCH is a marine seismic reflection profile across the British Caledonides from the foreland north and west of the Outer Hebrides, to the Irish Sea and Cardigan Bay (Fig. 2.3). Locally WINCH runs through the North Channel across the extension of the Midland Valley into the Firth of Clyde. Recording to 15 s two way time permitted investigation down to the upper mantle. This study showed that a variety of shallow Carboniferous and younger sedimentary basins dominate the upper crust, and that these basins are usually formed by reactivation of earlier structures, but Hall *et al.* (1984) found it difficult to identify the causal stress patterns. The lower crust reflection shows no margin to the Midland Valley equivalent to the bounding faults seen at surface on land. Thrusts below the Highlands and the Southern Uplands have a variety of dip directions indicating a zig-zag crustal shortening of 100 km in the Highlands and 60 km in the Southern Uplands (Fig. 2.8).

The Firth of Clyde basin represents the deepest basin in this study and it contains up to 1.5 km of Permo-Triassic rocks and 2 km of Carboniferous. The Carboniferous has a rapid increase of thickness to the SE of the Highland Boundary Fault. Major Caledonide faults were reactivated and played a role in the control of sedimentation. The direction of the basin axes changed with time from the Carboniferous basin in the Firth of Clyde which is a pericline of NE-SW trend to the Permo-Triassic Portpatrick basin which is a NW-SE half graben. Generally the velocities which were obtained from this study are 3 km/s for Mesozoic and younger rocks, 4 km/s for Upper Palaeozoic, 6 km/s for crystalline upper crust, 7 km/s for lower crust and 8 km/s for the mantle. The Moho varies between 25 and 32 km between the Great Glen Fault Zone and Isle of Man. It is shallow below Dalradian areas and is deep below the Firth of Clyde. Variation of the Moho depth can be linked to the overlying thin, dense lower crust layer at Islay where a thick pile of Dalradian sediments preserved. This is interpreted as a crustal stretching.

Conway *et al.* (1987) interpreted the Midland Valley Investigation by Seismology (MAVIS, see Fig. 3.1) data as four upper crustal layers. The first layer shows a curved time-distance graph with apparent velocity increasing

from 2.7 km/s to 4.0 km/s and represents the Carboniferous and Upper Old Red Sandstone (ORS) and is of 1.5-3.0 km thickness under the southern line and 3.0-3.5 km beneath the northern line, reaching its maximum thickness to the west (Fig. 2.9). This layer has a high velocity at the western end of the north and southern lines associated with the presence of the Clyde Plateau Lavas. The second layer has a velocity of 5.2-5.7 km/s and represents the Lower Old Red Sandstone and Lower Palaeozoic. The thickness ranges from 0.1-5.0 km. This layer shows a higher velocity under the northern line relative to the southern one and they considered that to be a result of the presence of Devonian igneous rocks which are exposed to the north of the Ochil fault only 10 km from the northern line. Layer 3 has a velocity of 5.9-6.1 km/s and represents crystalline igneous and metamorphic rocks which occur at shallow depth at about 4 km and drop to 7 km at the western end of the northern line. The fourth layer has velocities of 6.4-6.6 km/s and was recognised as a velocity change within crystalline basement, possibly due to a more basic composition at depth. The depth to this layer is not less than 7 km (Fig. 2.9).

There are some differences between this interpretation of MAVIS and that by Dentith (1987). Dentith reduced the velocity of layer 1 to be in agreement with Davidson *et al.* (1984, see section 2.3), causing some changes in the depths of the layers to take place (Fig. 2.10). Layer 1 with velocity 3-5 km/s extends to 2.0 km depth which is shallower than predicted from the surface geology at Trearne near to the current study area. Layer 1 represents the Carboniferous and Upper ORS. The Lower ORS and Lower Palaeozoic rocks are represented by layer 2 with a velocity of 5.4 km/s and little change in depth but it becomes deeper to the east. Layer 3 has a velocity of 6.04 km/s and thickness of 3 km and no longer deepens to over 7 km, this is the crystalline basement. Layer 4 has a velocity of 6.43 km/s and was considered as higher velocity crystalline basement (Fig. 2.10). So the MAVIS upper crustal model by Dentith (1987) can be summarised as:

Layer	Velocity (km/s)	Depth (km)	Interpretation
1	3.0-3.5	0.5-3.0	Carboniferous & Upper ORS
2	5.4	0.5 -4.0, 3.0-6.0	L ORS & or L Palaeozoic
3	6.04	4.0-6.0	Crystalline Basement
4	6.43	7.0-8.5	Crystalline Basement

Thin-skinned tectonic processes with multiple detachment were postulated by Gibbs (1984) who suggested a dextral strike-slip environment during Carboniferous times. Dentith (1987) adopted the same idea to interpret the tectonic features he determined in the upper crust.

Hall & Dagley (1970) constructed a regional aeromagnetic map of the Midland Valley which shows anomalies which correlate with exposures of igneous rocks, and linear features associated with the Southern Upland Fault and the Highland Boundary Fault. Hossain (1976) interpreted the gravity and magnetic data around Bathgate. Two models were produced, representing the shallow and deep extremes of possible sources. The shallow model consists of a cone of lava , identical to those exposed at the surface in the Midland Valley and extending to a depth of 5 km. The second model consist of a deep ultra-basic intrusion at 10-14 km depth (Fig. 2.11).

Hutton *et al.* (1980) extended the electric resistivity data which had been described by Jones & Hutton (1979) from the Southern Uplands with thirty new stations forming a traverse approximately coincident with the LISPB profile. Ingham & Hutton (1982a, 1982b) extended the data into the Midland Valley and they correlated the depth of the lower crust on LISPB with the decrease of the resistivity in their data. They considered the increase in depth of the conducting zone towards the north gives support to the hypothesis that the Highland Boundary Fault is the location of an ancient subduction zone. This study showed that there is an electrical conductivity anomaly across the Southern Uplands Fault at 20 km depth, and they considered that this difference is due to the fundamental differences in the lower crustal structure to the north and south of the Southern Uplands Fault. They were not able to include the subduction zone along the Solway Firth in their model, but they considered the high conductivity under the Southern Uplands and the sharp boundary near the Southern Uplands Fault to be of special tectonic significance.

2.3 LOCAL STUDIES

There are many studies in the Midland Valley directly related to the present project area. McLean & Wren (1978) carried out a gravity and magnetic study in the Firth of Clyde and they showed that there is a high gravity anomaly

lying symmetrically about the central axis of the Midland Valley with a gradient of about 1.0 mgal/km away from it toward the Highlands to the north and Southern Uplands to the south. They proposed that the gravity high is generated at a deep crustal level, but is partly obscured by the effect of thick, low density Upper Palaeozoic sediments. The same study showed that the Dusk Water and Inchgotrick Faults continue to the west (though these two faults are dying before reaching the coast). This view is strengthened by the pattern of magnetic anomalies.

Cotton (1968) studied the thickness of the Clyde Plateau Lavas by the gravity method in the Campsie Hills and Kilpatrick Hills and found the thickness of the lava is very variable in the area, varying from 200 m in the Campsie Hills to 800 m in the Kilpatrick Hills and reaching its maximum thickness of 1000 m beneath Giffnock. The faults and Ruck in Renfrewshire and Ayrshire affected the Carboniferous sequence, the lava thickness increasing from about 600 m on the NW side of the Paisley Ruck to about 800 m on the SE side. Cotton suggested this variation was due to either the Paisley Ruck being active as a normal fault contemporaneously with the extrusion of the Clyde Plateau Lava thus controlling the development of the lava, or it was a strike-slip fault at a later date thus bringing lavas of different thickness into juxtaposition.

Hall (1970, 1974) studied the Clyde Plateau Lavas in the western part of Scotland to determine the thickness variation of the lava pile and to discriminate whether this is due to post extrusion folding or the maximal development of the lava along their NW-SE trending outcrop. The study pointed to the second model. The lava thins to NE and SW and the major structure trends NW-SE in the west of Midland Valley. In addition the study shows the presence of local changes in the lava thickness across NE-SW faults, indicating that these faults were active in the early Carboniferous extrusional period, as well as in the later Carboniferous. In this study the results of the seismic survey were combined with the geology of the area and the gravity study to construct a contour map and isopach map of the lava (Fig. 2.12).

Alomari (1980) undertook a gravity and magnetic study in the western Midland Valley and estimated the maximum thickness of the Clyde Plateau Lavas to be 1.25 km, thinning to 0.5 km under Hamilton and to the north of the Clyde. The Dusk Water Fault played an important role at the time of the eruption since the lavas are thicker to the south (1.25 km) than to the north

(0.75 km). The author interpreted the Hamilton low anomaly either as a granitic batholith intruded into the crystalline basement, which might be controlled by the extension of the Inchgotrick Fault, or as a local NE-SW striking Old Red Sandstone basin.

Davidson *et al.*(1984) used the gravity, magnetic and seismic data described above and additional short range refraction data to interpret the upper crustal structure of the Midland Valley (Fig. 2.13). For comparison, the LISPB model of the Midland Valley upper crustal structure is shown in Fig. 2.14. Davidson *et al.* identified two relatively low velocity layers: 3.0-3.7 km/s due to the Carboniferous and Upper ORS rocks and a higher velocity layer of 4.0-5.5 km/s due to the Lower ORS and Lower Palaeozoic rocks. This suggests the unconformity between the Upper and Lower ORS is a refractor. Both layers occur within LISPB layer 1. They concluded that the thickest sequence of Lower Palaeozoic occurs under the Silurian inliers and is not more than 3 km in thickness. The second layer of 5.7-5.9 km/s of the LISPB study is not recognised by Davidson *et al.* (1984). Rather their third layer has a velocity 6.0-6.1 km/s which they correlate to LISPB layer 2. It seemed to continue beneath the Southern Upland Fault at about 2.5 km and they proposed that the nature of this layer is crystalline rock of acidic to intermediate composition. Fig. 2.15 shows the velocity of this refractor to plot within the field for acid-intermediate gneisses, confirming the presence of crystalline rock at depth of 3 km. The LISPB 6.4 km/s layer was not defined by this study but they suggest it might reflect the change from amphibolite to granulite facies.

Davidson (1986) interpreted seismic data in the southern and central Midland Valley and he divided the Palaeozoic sequence into a top layer which has a velocity of 3.0-4.0 km/s for the Carboniferous and Upper ORS, 4.0-5.2 km/s for the Lower ORS layer and 3.5-5.5 km/s for the Silurian and, possibly, Ordovician. He concluded that the basement is probably of quartz-feldspar rich crystalline rocks. There is no evidence of any affect on the basement related to the pre-late Carboniferous faults. He suggested that either these faults sole out into a shallow (<4 km) decollement zone, and/or root into a major basement strike-slip lineament.

The far SW part of the Midland Valley and the western edge of the Southern Uplands have been studied by Al-Mansouri (1986). Three layers are considered for the upper crust. A layer of velocity 3.7-4.0 km/s to represent the Carboniferous and Upper ORS, a velocity of 5.0-5.5 km/s for

Lower ORS and Lower Palaeozoic, and 6.0-6.4 km/s for the crystalline basement. He interpreted the Ballantrae Complex with a low velocity layer as serpentinite (*c.* 4.0 km/s) and gabbro with velocity as high as 6.3 km/s. The basement is shallow (2 km) under the Ballantrae Complex with a velocity of 6.0 km/s which increases rapidly to 6.4 km/s at depth of 6 km and extends under the Southern Upland at about 2 km depth.

CHAPTER THREE

DATA ACQUISITION AND PROCESSING

3.1 INTRODUCTION

Three component seismic data were recorded from quarry blasts in the western part of the Midland Valley along a traverse trending nearly NNE-SSW. All the quarries are located on Carboniferous igneous rocks. The quarries are: Sheephill near Dumbarton, Loanhead near Beith and Hillhouse near Troon. Fig. 3.1a shows the seismic lines in the context of the whole Midland Valley and previous seismic lines. Fig. 3.1b shows the lines in relation to the local geology. The line was extended to the north and south of Sheephill and Hillhouse respectively to improve coverage of the basement. Total line length is 70 km. An unreversed line was also recorded to the east from Hillhouse. The profiles are termed "main" and "Hillhouse-Kilmarnock". This chapter will deal with the data acquisition, processing and presentation.

3.2 DATA ACQUISITION

An optimum line length to study the upper crust in this region is similar to that described by Davidson *et al.* (1984). The time-distance graph predicted by their model is shown in Fig. 3.2. Crossover distances of 7, 33 and 82 km are obtained for first arrivals from three refractors. The length of the main profile in this study is more than 70 km and it is recorded from the three sources with reversed coverage. The line crosses at least three major structures: Dusk Water Fault, Paisley Ruck and the Gartness Fault. It traverses various lithologies: Carboniferous sediments, the Clyde Plateau Lavas and the Old Red Sandstone (ORS). Stations were spaced at regular intervals (about 2 km). A second line of about 10 km length was recorded east from Hillhouse quarry with a receiver interval of 1 km to assess the study of deep crustal near-vertical reflections using three component recording and quarry blast sources. This line was recorded on Carboniferous

rocks parallel to the regional strike and was designed to avoid major faults and exposed igneous rocks.

Most of the receivers are less than 1 km off the ideal line. To find a rock site or easier access were factors in going off the line. Receivers and shots were located to within 10 m using Ordnance Survey maps. Because the maps are not up to date, especially due to the quarry expanding with time, a fixed location in the quarry or outside the quarry was used to record the shot instant, so a slight shift in the shot point location does not affect the travel time. Appendix 1 shows the location of the receiver sites used in this study. The receiver offset is calculated by a simple computer program using the equation

$$D = ((E_R - E_N)^2 + (N_R - N_S)^2)^{1/2} \quad \text{.....(3-1)}$$

where

N_S, E_S are the northing and easting grid coordinates of the shot point,

N_R, E_R are the northing and easting grid coordinates of the receiver.

The previous studies by Al-Mansouri (1986), Davidson (1986) and Dentith (1987) showed that the good coupling of a geophone waxed to rock gave a higher signal to noise ratio than an array spiked and buried in drift. For this reason rock sites were used wherever possible, but drift sites were used especially in the south, because few rock sites were available. The vertical and horizontal geophones were mounted on a circular base that was waxed to rock or spiked in drift. The radial component was oriented toward 020^{o} for all stations. Hence some radial components were positive away from the shot and the others toward the shot. Account of this was taken in all processing.

The P and SV waves propagate in the vertical-radial plane. To study the particle motion of different types of the wave we need to plot the particle motion of that event. P-waves propagate in the same direction as the wave propagation (i.e. away from the source), but the SV is perpendicular to the P-wave in the same plane.

The main sources of the background noise are the wind and local urban and industrial sources. Most of the sites were selected in a quiet area. To reduce the effect of wind, the geophones were sheltered by an inverted

plastic bucket, with varying degrees of success. Some records were repeated many times because of high noise levels or due to the bad reception of the time signal (MSF) in the area.

The use of a quarry blast as a seismic source has been discussed by Davidson (1986) and Sola (1985). They concluded that it is a reasonable source of P-wave first breaks, but the second arrivals are obscured by the length of the first break wavetrain, typically 500 ms in duration. In spite of this problem, Davidson (1986) was able to discriminate S-waves successfully by frequency filtering. The duration of any arrival is due to the quarry blast consisting of a series of time delayed charges in closely spaced holes, so creating a long source waveform. A further problem with the quarry source is that it is designed to send the energy upwards. Usually a quarry blast used in this study consisted of 10-15 holes of 30 m depth drilled about 10 m from the quarry face. The shot is fired as a series of paired holes with a delay of 25 ms between each pair. The charge is about 150-250 kg/pair. This type of blast is used because it fragments the maximum volume of rock whilst reducing vibration outside the quarry. The effective size of the seismic source is that of first hole (or pair) detonated.

The gain was set using the range of the receiver and the charge size, according to empirical rules established by the MAVIS study (Dentith 1987). The rules are for instantaneous charges, so the charge assumed was 150-200 kg. In addition to this relation for the gain setting, the site location and weather were taken into consideration. Sometimes the selected gain was too low, because of an unexpectedly low charge size or a non-ideal quarry face direction.

3.3 THE RECORDING SYSTEM

FM seismographs were used to record the data which were designed and built at the Department of Geology, University of Glasgow in 1984. The "Mark 2" instruments were developed from prototypes built in 1981 and are designed to be cheap, portable and easy to use. Wear and tear have reduced an original 50 recorders to a total of 25. Fig. 3.3 shows the recording process of the Glasgow "Mark2". Appendix 2 contains information about the recording sets and geophones used in this study.

The recorder uses a standard stereo cassette tape in conjunction with a four track recording head and contains a clock for remote starting up to 24

hours ahead. This is very useful for quarry blast recording. The use of C120 audio cassettes allows an hour long window to be recorded. Each set was used to record one component. Two tracks of seismic data from a single component geophone were recorded on a 3 kHz carrier. A high gain channel was selectable in 6 db steps over a range of 88-118 db and a low gain channel set automatically 18 db down from the selected high gain. Channel 3 was not used. Channel 4 was used to record the 60 kHz MSF time signal broadcast from Rugby. The use of three independent systems to obtain a three-component recording is not ideal, especially if any system fails to receive a good MSF signal. To overcome this problem Mr G. Gordon devised the "MSF SYN" device (see Fig. 3.4). This samples the three MSF records and distributes the best one to all of the systems. The three components were gathered in one file to give a three component record.

3.4 INITIAL PROCESSING AND DIGITISATION

The playback and digitising system used is shown in Fig. 3.5.

3.4.1 Playback.

The Glasgow playback system consists of a tape-head similar to that of the recorders. The recording is passed through a demodulator and then analogue filters usually set to pass frequencies between 3-40 Hz. These filters were to assist in the detection of arrivals on noisy traces. The output is then amplified and passed to a UV oscillograph. This instrument has the facility to run at a variety of paper speeds, whilst adjustment of the amplifier gain allows the amplitude of the trace to be varied. The MSF signal is also demodulated, but is passed directly to the amplifier and then oscillograph after cleaning via a Schmidt triger, if required. This signal is also passed to a decoder which displays the time of recording to assist in the location of arrivals.

3.4.2 Digitisation

The analogue data were converted to digital form using a Programmable Data Processor (PDP) 11/23 PLUS micro computer and software configured by R.T. Cumberland. The same playback system is used with the output passing through 40 Hz anti-aliasing analogue filters. An ADV 11-C analogue input board accepts sixteen single-ended bipolar inputs sampling the data at

200 samples/second to produce a binary form output. The internal programmable gain is set to 8 for the data, corresponding to a variation of +/- 1.25 volts. The program was configured to receive three input channels. A total of 20 sec of data was extracted to obtain all the useful arrivals. The data were converted to integer form and then transferred to the SUN computer network in the department for further processing. The binary data were stored on floppy disk.

3.4.3 Initial Processing

Now all the data are loaded on the computer for presentation and the digital processing. Variation in the field recording tape speed may cause a difference from the required sampling rate (i.e. more or less than 200 samples per second). To tackle this problem, Doody (1985) used a computer routine to correct these differences. The RESAMPLE program was written using the same routine to resample the data to 200 samples/s by assuming the tape has the same speed throughout the digitised record. The program calculates the number of samples between the MSF pulses and the number of pulses along the entire data length, then extrapolates the data to the required sampling rate. For noisy or inverted MSF, a short computer program ZMSF was used to clean up the MSF channel by manual picking of the MSF pulse after displaying the trace using the 'S' package. For a few traces without MSF an initial sampling rate of 204 sample/s was assumed. This figure was got by averaging more than 20 data files. The MSF pulse itself is not always sharp, which may cause an uncertainty of 1 or 2 samples for the onset of the pulse.

Program MSFPLOT was written to determine the start time of the digital processing of the data. The program plots the two seismic channels and the MSF channel. The recognition of known MSF pulses allows the time and therefore a number of samples between shot and file start times to be calculated. In the case of bad MSF on one component, the first arrival was compared with that of other components and the number of samples calculated to the beginning of the file according to that. This was used for just a few traces which have a short range from the shot point and a clear first arrival to be more confident about this calculation. This was done before the MSF SYNC devices were developed. The three components were recorded by individual seismographs and then each component was stored as a separate digital file. Each data file contains a header which specifies the station name, range and time difference to the shot in samples. To save

storage and ease of processing, the computer program CON was written to combine the three files depending on the start of each file relative to the shot instant, so the new file contains the three component recording starting at the same time relative to the shot instant.

Appendix 6 contains listings of programs RESAMPLE, ZMSF, MSFPLOT and CON.

3.5 DATA QUALITY AND PRESENTATION

The PLOT program is a general purpose refraction processing package developed and used at Glasgow University. It employs FORTRAN and "S". It was modified by the author to add three-component processing routines. The main program and adapted subroutines are listed in Appendix 6. This program can plot unfiltered and filtered data processed by frequency or polarization filters, in addition to spectral analysis determination. All seismic data plots of the main line of this project were plotted with SSW on the left.

Fig. 3.6 shows the unfiltered vertical component data recorded from Hillhouse quarry. These data are digitised for 20 s and recorded out to about 70 km range from the source. The vertical component shows a good S/N ratio up to 40 km, except trace 12 at 22 km. Up to 20 km stations were in drift. Most of the traces were fixed to a rock site beyond 20 km, and this gave a good signal, especially at the far traces. The traces recorded north of the Clyde (at > 40 km) show a lower signal to noise ratio. Traces at 41-47 km range were recorded at rock sites, but they are noisy. At this range we are at the limit of usefulness of the usual shot size. An unusually big shot (about 5 tonnes) gave the opportunity to extend the line further north by another 5 stations with good S/N ratio. Traces at 50-55 km offset were recorded at drift sites. The radial and transverse components (Figs 3.7 and 3.8 respectively) show a weaker first arrival and higher noise level on some traces. The transverse component shows a good shear wave segment up to 20 km. Filtering improved the S-wave data (see later).

Fig. 3.9 shows the S/N ratio relation of the three components and its relation to offset. The S/N ratio is measured at the first arrival within a window of 0.5 s. Generally the vertical component shows a higher S/N ratio than the radial and transverse components. All components show a decrease of the S/N ratio after a certain range, note the decrease at about 20

km. It is difficult to recognise the first arrival of horizontal components beyond 20 km offset. A similar relation was seen from the other shots.

The vertical component data recorded from Loanhead quarry is shown in Fig. 3.10. The data were recorded up to 40 km on both sides of the source. The data show a good S/N ratio to the north but it becomes poor to the south at a distance of 20 km. All the sites to the south were in drift due to the difficulty of finding outcrop in the area. Most of these sites contain a lot of pebbles causing poor geophone coupling with the ground. Figs 3.11 & 3.12 show the radial and transverse components respectively.

Data were recorded from Sheephill quarry up to 40 km offset and show a good S/N ratio on the vertical component (Fig. 3.13). The data show good shear waves. Figs 3.14 & 3.15 show the radial and transverse components respectively. Higher noise occurs on both the radial and transverse components, but good shear waves are observed.

Data were recorded from Hillhouse to the east (the HK line). Fig. 3.16 shows the vertical component data which have good S/N. The horizontal components have high noise levels on most the traces and some traces are overloaded. Figs 3.17 & 18 show the radial and transverse components.

3.6 PRINCIPLES AND APPLICATION OF DIGITAL PROCESSING

Seismic data contain useful energy (signal) and unuseful energy (noise). The filtering process discriminates signal from the noise. Filter design may be dependent or independent of data. Independent filters, such as frequency filters, are not derived from the data to be filtered, but are designed according to some parameter. In the case of dependent filters, such as the polarization filter, the characteristic of the filter is derived from the data to be filtered (Hatton *et al.* 1986).

The digital filtering process is described by a number of authors (e.g. Robinson & Treitel 1980). A brief description of the basic idea of the filter is given here. The filter is the output of a spike function input (Fig. 3.19). That is, the effect of the filter is defined by its impulse response. The effect of the filter is obtained by the convolution of the input data with the impulse response of the filter. The actual impulse response is infinitely long and therefore of no practical use. Truncation is necessary to get a useable filter. The truncation of the operator is an important control on the character of the filter.

Seismic data form a non-periodic wave but may be considered as periodic with an infinitely long period. To deal with the seismic wave, the amplitude and phase spectra are subdivided into a number of slices. The concept is illustrated in Fig. 3.20. The continuous amplitude and phase spectra (A) have been divided into sixteen components represented by sinusoidal waves of different frequency and phase (B). The waveform shown in C is the sum of these waves. Thus the time function (C) and the frequency function (A) are seen to be equivalent. Fourier transformation is used to convert time functions into the frequency domain and *vice versa.*

The digital processing carried out on the data included band-pass and low-pass frequency filtering. With the availability of three component data, processing involved use of the polarization filters. The result of each kind of filter was compared with the others to pick out the second arrival events.

3.7 FREQUENCY FILTER

The design of a frequency filter can be done by defining a desired amplitude spectrum for the filter operator with a desired cut-off frequency. This is known as the boxcar amplitude spectrum, such an operator is infinitely long for an ideal frequency filter and must be truncated for practical use as a convolution operator. Another approach is the gradual truncation of the operator by multiplying it with some other window function. The window function employed here consists of one cycle of cosine wave with its trough raised slightly greater than zero, known as the Hamming window.

Frequency filters are described in terms of their form of frequency response. The low pass filter will pass only frequencies less than the defined frequency. The band pass filter will pass all the frequencies within the band and cut the others. Filters are either zero-phase or minimum phase. Minimum phase filters have all filter coefficients for value of $t<0$ set to zero, where t is the time at which the filter is applied. So the filter has only a memory component and can only operate on the present and past components of a time series. The output has no time shift.

Zero-phase filters have anticipation and memory components, centred symmetrically about $t=0$. This allows the operation of the filter on the part of the trace in front of $t=0$ and this gives a greater control over the desired frequency response, but causes a time shift of the output. The time shift is half the filter length.

The frequency filter is not very efficient if the signal and noise spectra are similar. In this case another kind of filter should be used.

Figs 3.21-3.22 show the frequency filters which were used in this study

3.7.1 Spectral Analysis

The aim of any frequency filter is to discriminate against unwanted signal (noise) in the record to improve the signal. The PLOT program was used to determine the frequencies of both the signal and the noise to enable design of a suitable filter. The program has the facility for spectral analysis. Spectral analysis was undertaken for the following windows: pre-first arrival data to study the noise; 0.5 s window beginning at the first arrival for the P-wave; and a window of 1 s was used at the expected S-wave arrival time.

The first window, which represents the noise, showed a wide range of frequencies from 0-30 Hz (Fig. 3.23). The data from Hillhouse showed that the dominant range of the P-wave is 10-16 Hz (Fig. 3.24). This frequency range shows a decrease with offset, becoming 5-10 Hz beyond 40 km. The S-wave has a range of 4-10 Hz and becomes weak and unrecognisable after 30 km range (Fig. 3.25). The data from Sheephill showed lower frequencies of the P-wave at 5-15 Hz with a consistent peak of less than 10 Hz (Fig. 3.26). The shear wave has a frequency 4-8 Hz and it shows a very clear relation of frequency with range (Fig. 3.27).

Fig. 3.28 is the spectral analysis of the P-wave data recorded from Loanhead which show a wide frequency range of 5-15 Hz. The traces which are near the shotpoint show a lower frequency that might be due to the presence of the lava which affected the direct wave more than the headwave.The S-wave has a frequency range of less than 10 Hz, the frequency peak of spectra from data to the north of this shotpoint is a little higher than that to the south (Fig. 3.29)

Fig. 3.30 is the spectral analysis of the P-wave data of the Hillhouse-Kilmarnock line. These data show a P-wave frequency of 10-15 Hz. Spectral analysis of the S-waves shows a range from 5-10 Hz (Fig. 3.31).

All the quarries are located in igneous rocks. The frequency variation of the data show that the quarry has a big control on the frequency. This may be due to the different shot patterns and the kind of explosive of the different quarries.

3.7.2 Filter Application

Frequency filters can be applied using the PLOT program. The filter response is first obtained by runing the program FWFIR which is capable of designing bandpass, highpass, lowpass and bandstop filters with different windows, such as Hamming. The filter was designed based upon the spectral analysis of the data within certain windows which contain the signal or noise,. Dentith (1987) tried to use a good combination of the window length and filter type. He noticed that the filter length does not affect data quality but there is a slight smearing of the data with increasing length. The dominant frequency of the P-wave is 5-16 Hz which is very close to the S-wave frequency. Significant noise occurs within this range but also at other frequencies. So the frequency filter has to be chosen very carefully and even then will not give a complete cut out of the unwanted noise.

In most of the traces the first arrival was clear enough to pick without filtering, but the band-pass filter was used to enhance the second arrivals, especially the reflections. A 8-16 Hz band-pass filter was chosen because it covers the range of the P-wave frequencies. Minimum phase was chosen because this gives no phase shift of the data and so it is easier to compare with the unfiltered data or with data filtered using other filters, such as the polarization filter. Figs 3.32-3.35 show the filtered data (vertical component) from different sources plotted using a reduction velocity of 6 km/s. A 8 Hz low-pass filter with a Hamming window was used to separate the shear wave from P-wave second arrivals. Figs 3.36-3.39 show the filtered data plotted using a reduction velocity 3.5 km/s. The low pass filter showed a good influence on the data and highlighted some of the shear wave events.

3.8 POLARIZATION FILTER

3.8.1 Introduction

Seismic recordings are always contaminated by noise which makes the detection and interpretation of a seismic event difficult. Polarization analysis has been used to devise filters which will separate elastic body waves into compressional (P) and shear wave (S) and also enhance or attenuate surface waves (Archambeau & Flinn 1965, Montalbetti & Kanasewich 1970).

In geophysics the main problem is to pick the event from the recorded data which contain a lot of noise or unwanted signal. When the signal and noise have similar spectral character, the frequency filters are not effective.

The availability of three component seismograms allows one to determine a filter function which takes advantage of the polarization properties of both body and surface waves. The theory of polarization is discussed by Kanasewich (1981), but a brief discussion about the polarization properties and the filters will be given here.

Generally body waves have a high degree of linear polarization. Rayleigh surface waves are generally elliptically polarized in the vertical-radial plane, the waves displaying retrograde particle motion. Surface Love waves are found to be rectilinearly polarized in a horizontal plane and orthogonal to the direction of wave propagation. According to these properties of the signal and noise, the polarization filter is designed to preserve the desired signal and attenuate others. Fig. 3.40 shows the particle motion of a P-wave signal with a rectilinear motion and noise showing random motion.

Shimshoni & Smith (1964) suggested that the time averaged cross product of vertical and radial components of ground motion may be used as a measure of rectilinearity. The computed cross product is multiplied by the original signal so that a function of ground motion which enhances rectilinearly polarized signal is obtained. Another process described by the same workers computes the parameters of an equivalent ellipse at each instant in time from the Fourier components of the vertical and radial motion eccentricity. The major axis and angle of inclination of the ellipse from the vertical are displayed for the frequency at which maximum power is arriving and used to provide a criterion for the identification of P and SV type motion.

The measure of the variance-covariance matrix and the eigenvalue of the data within a certain window can give an indication of the rectilinearity of the event in certain plane. The rectilinearity is the measure of the maximum to minimum axis of the particle motion. The eigenvalue can give the degree of the rectilinearity within the window. Sliding this window down the trace and measuring the eigenvalue within the successive windows, one can then see the maximum value giving the higher rectilinearity. This gives the rectilinearity of the event in one polarization direction. Since the polarization direction varies, depending on the incident angle and the surface irregularity (i.e. the raypath), it is better to rotate the data with different rotation angles and then measure the rectilinearity. By rotating the data within the window for a series of rotation angles 0-180

degrees, that will give the maximum rectilinearity and the polarization direction.

Another method is used to measure this ratio by Boulfoul (pers. comm.), who finds the energy of the two components within a certain window gives the ratio of the rectilinearity similar to that of the variance-covariance method. In this method the energy is measured within a certain window for two components and then maximum and minimum of the energy found which will give the degree of the rectilinearity of the wave motion at that window. Generally the waves deviate from the wave propagation direction and are polarized in a different direction due to the presence of the anisotropy or irregularity of the refracting surface. Since the polarization direction is variable in this case, so the data are rotated with a range of rotation angles (for example, $0\text{-}90^{o}$ with 5^{o} increment) and the energy for the rotated data measured within the window in each case. This exercise will give the maximum and minimum energy and its rotation angle. To search for any event, use the same steps and slide the window by a certain increment along the desired length of the trace.

The variance-covariance and the energy method were used to study the polarization direction and the S-wave behaviour to find any indication about the anisotropy (see chapter 4).

Various workers have applied polarization filtering techniques to enhance the signal to noise ratio. Lewis & Meyer (1968) applied a phase filter of the REMODE type as described by Archambeau & Flinn (1965) and originally by Mim & Sax (1965). Montalbetti & Kanasewich (1970) designed a polarization filter which varied from that described by Flinn (1965) by taking both rectilinearity and direction of particle motion in consideration.

Two types of filter were used in this study and are now described.

3.8.2 Shimshoni and Smith filter

The filter depends on the rectilinearity of the signal polarization as compared with the elliptical polarization of noise. In this filter we consider the cross-product (Mj) of the vertical (V_j) and the radial (H_j) components within a certain window length. If the sampling interval is δt, then the average cross-product Mj at time $j\,\delta t$ for a window ranging from $(j\text{-}n)\,\delta t$ to $(j+n)\,\delta t$ is given by

$$M_j = \sum_{i=-n}^{+n} H_{i+j} V_{i+j} \qquad \text{.....(3-2)}$$

The cross-product gives a measure of the rectilinearity and the total signal power. Then the cross-product is multiplied by an original component, producing a function of ground motion in which rectilinearly polarized motion is enhanced.

$$VM_j = M_j * V_j \qquad \text{.....(3-3)}$$

$$HM_j = M_j * H_j \qquad \text{.....(3-4)}$$

where VMj, HMj are the output after the application of the polarization filter to the vertical and horizontal components respectively.

The window length (2n+1 samples) is critical to the filter efficiency, and was obtained by trial and error. Doody (1985) used the same filter and found that the best window length is about 0.5 s.

Originally the filter was designed to process the vertical and radial components. Some data show that some events are stronger on one component than the others. Figs 3.6-3.8 for data recorded from Hillhouse, for example, show that the shear wave is stronger on the transverse component than on the other two. Hence the filter was adapted to use the vertical, radial and transverse components or any two of the three.

$$M_j = \sum_{i=-n}^{+n} V_{i+j} R_{i+j} T_{i+j} \qquad \text{.....(3-5)}$$

This adaptation was tested on synthetic data. In the case of a negative value the cross-product, multiplication of the cross-product by the original trace, distorts the signal. For that reason the absolute value of the cross-product was taken.

$$VM_j = |M_j| * V_j \qquad \text{.....(3-6)}$$

$$HM_j = |M_j| * H_j \qquad \text{.....(3-7)}$$

The filter efficiency depends on the filter window length and it was found that the best window length is about 30 samples (0.15 s). Fig. 3.41 shows the application of the filter on one trace to show the effect of the filter window length. A large window causes smearing of the signal; the shorter window causes a distortion of the signal but it seems better for event picking. If we examine the effect of different window length on the first arrival of this trace, the small window shows a sharper first arrival than the bigger window length. The second arrival, at about 3 s, is clear on the unfiltered vertical data; the small window length produces a better enhancement of this event than the big window.

To check if this event is real, this output can be compared with the same trace after applying a frequency filter. Fig. 3.33 is the relevant frequency filtered plot. This trace is at 17 km in that Figure, and a clear event can be seen over a number of traces.

A random sample of many traces of the data was chosen and the ratio of the S/N ratios of the filtered and unfiltered data was plotted as a function of window length (Fig. 3.42). The same test was applied on the data by using the three components, and it shows that the small window is good. Fig. 3.43 is a comparison of using two or three components in the filter, using the same window length.

The polarization filter was included in the PLOT program. Figs. 3.44-3.47 show the data of this study, using the vertical and radial components to create the filter which was multiplied with the original vertical component. Note the effect of the filter on the first and second arrivals. The second arrivals show an alignment between some traces. The filter shows a good effect on the S-waves. The filter helps the S-wave picking, because it gives a sharp onset of the event. The small window was used here to pick the onset after comparing the same event by using other filters. Then the events were compared with the unfiltered section to pick the right onset time. This technique was used because it is known the filters cause some distortion of the data and so to minimise error in the picking of the event.

As mentioned earlier, the spectral analysis of the data showed that the noise has a wide range of frequencies which overlaps or is close to the signal frequency, so the frequency filtering is not very effective. Another trial to enhance the data is to use the polarization filter after applying the frequency filter to clean the data to a certain level. It is known that the frequency filter distorts the signal and that will affect the following polarization filter. To see

the effect on the S-wave the polarization filter was used after applying an 8 Hz lowpass filter. Comparing Fig. 3.48 with Fig. 3.44 for data recorded from Hillhouse shows that the combined effect is good on the second arrival. Note the S-wave on traces at 0-15 km, they have a higher signal, and the effect of this combination on noisy traces, such as the trace at about 50 km range. This shows a good improvement of the events. Figs. 3.49-3.50 show the result of applying the polarization filter after a low-pass of 8 Hz to Loanhead and Sheephill.

3.8.3 REMODE filter

The REctilinear MOtion DEtector (REMODE) filter considers the rectilinearity in the radial and vertical directions instead of the three dimensions it was originally designed for by Mims & Sax (1965). The vertical (Z) and radial (R) components are rotated so that the expected direction of the incident body wave bisects the angle between the two orthogonal components (Fig. 3.51)

$$Z' = Z\cos(\pi / 4\phi) + N\cos\alpha.\sin(\pi / 4\phi) + E\sin\propto.\sin(\pi / 4\phi) \quad \text{.....(3-8)}$$

$$R' = Z\sin(\pi / 4\phi) - N\cos\alpha.\cos(\pi / 4\phi) - E\sin\propto.\cos(\pi / 4\phi) \quad \text{.....(3-9)}$$

where ϕ is the angle of incidence, α is the azimuth of a great circle path, and Z, N, E are the vertical, radial and transverse components. The filter operator is obtained from a cross correlation function, C(T), of Z(t) and R(t) over a window, W, centred at some time, t, on the record

$$C(+T) = \sum_{t-w/2}^{t+w/2} Z(t)R(t+T) \quad \text{.....(3-10)}$$

To ensure that the operator is an even function and introduces no phase distortion, the negative lags are generated from the positive lags.

$$C(-T) = C(+T) \quad \text{.....(311)}$$

C(T) is large if the polarization is rectilinear, and small if the motion is elliptical. The output from the filter is given by

$$Y_R(t) = P_P K \sum_{T=-L}^{L} R(t-T)C(T) \qquad \text{.....(3-12)}$$

$$Y_z(t) = P_P K \sum_{T=-L}^{L} Z(t-T)C(T) \qquad \text{.....(3-13)}$$

where P is the polarization operator and K is a normalizing factor

$$K(t) = \left[\sum_{t-w/2}^{t+w/2} R^2(t) \sum_{t-w/2}^{t+w/2} Z^2(t) \right]^{-1/2} \qquad \text{.....(3-14)}$$

The REMODE program was written, using the REMODE subroutine from Leicester University. The program can process data in "GLAMK2" format. The outputs are saved in files for input to the PLOT program or for plotting the filtered and unfiltered data using the "S" package. The program can process the data with different rotation angles and calculate the S/N ratio for the filtered/unfiltered vertical component data within the requested window.

The REMODE filter was used on the data and produced a good improvement in the signal to noise ratio. The filter parameters are slightly different from those applied by Henry (1987). He found that the best window length for the cross correlation is about 0.5 s but a good enhancement of the signal was obtained with a window of 30 samples (0.15 s) in this study after trials. The rotation angle required depends on the incident angle. Hence the window length and the rotation affected the filter parameters. A fixed incident angle (50^{o}) was used to find the best window. Fig. 3.52 shows the effect of the window length. See, for example, the effect of different window lengths on the first arrival. A big window smears some noise just before the first arrival, while the small window attenuates the noise. The same comparison with the second arrivals show some differences with the window length. For example, the clear event at about 3 s on the unfiltered trace. The application of the filter with a small window (0.15 s) highlights the event, whereas the bigger window does not. Another kind of comparison was tried by comparing the REMODE filter with other frequency filtering. Compare the same event with the trace at 17 km in Fig. 3.33 after applying frequency filter, it shows that this event is consistent with the other traces. Similarly with the S-wave at about 4 s on the same trace.

To obtain the appropriate rotation angle, the filter was employed with a fixed window of 0.15 s and with different rotation angles. Then the S/N ratio of the filtered to unfiltered data was measured. Henry (1987) considered the maximum enhancement of signal to noise ratio was obtained for a rotation of 35^{o} which corresponds to 10^{o} incidence angle. In this work the best enhancement was got by different rotation angles which depend on the incident angle at the station. Fig. 3.53 shows the effect of different rotation angles on one recording.

Fig. 3.54 shows the effect of different polarization filters on a sample recording. Each filter is set to the optimum parameters for the recording.

3.9 VELOCITY ANALYSIS

Seismic velocity can be measured to give an indication of the lithology and for use in determining the thicknesses of the layers in the area. Seismic energy travels from the shotpoint to the receivers along different raypaths: direct, refracted and reflected. The travel time of the energy to a receiver depends on the offset of the receiver and the length of the path. To measure the velocity we need to correct the data by removing the effect of the offset.

In refraction work the direct wave travels with the velocity of the top layer, the head wave travels mostly by the appropriate layer velocity. The velocity of each layer can be given by the slope of the curve. In reflection the wave travels by the velocity of the overburden above the reflector. Said (1990) worked on velocity analysis and used the hyperbolic (reflection) and straight line trajectories (direct and refraction) as a function of the time intercept and velocity to correct data for analysis.

In velocity analysis the coherency is measured to see how well the data fit an assumed time-distance trajectory (Fig. 3.55). The parameters of the best fit time correction can be used as attributes of an observed arrival across a receiver array.

Different methods of velocity coherency have been described such as unnormalised crosscorrelation (Schneider & Backus 1968), energy normalised crosscorrelation, statistical normalised crosscorrelation sum (Neidell & Taner 1971), and semblance (Taner & Koehler 1969). The coherency measurement is taken in a certain window length. These methods were written into a computer program by Said (1990). He concluded that the window length for the semblance method was very close to the

period of the event (typically 35 ms in this study). Other parameters which affect the computation are the velocity and time increments between measures. Bigger increments degrade the result, and smaller ones require a very long computational time.

In this work the semblance method was chosen. Semblance is defined to be a normalised output/input energy. Semblance has a value in the range $0<s<1$. It exhibits a unity value if the signal of all traces have the same phase and amplitude and zero if they are out of phase.

This method was employed here, using similar parameters to those suggested by Said (1990), to check identified velocity segments and to determine parameters of any reflections in the data. Appendix 7 shows the application of the method on data recorded from Sheephill.

3.10 P-WAVE PICKING

The accuracy of the first arrival picking depends on the S/N ratio of the recorded data. At the near traces, there is no problem with picking due to high S/N ratios. The uncertainty of the picking increases with the offset, partly due to poor S/N ratio and partly due to misidentification of the first arrival from the stronger reflection events which are close to the first arrival at certain ranges.

The analogue record was used at the beginning for the first arrival picking. The variation of the tape speed (as mentioned earlier), the noise on the time signal channel and the different speed of the playback paper cause some uncertainty of the picking. To achieve better picking the digital data were used for that purpose. Since all the data were resampled, the uncertainty of the picking will be less. Furthermore the correlation of the events on different traces is easy and the confused picking of any reflection events is less. The uncertainty of the picking was taken as 0.03 s and this is the accumulated error of the location of the shotpoint and the receivers, and the clarity of the time signal of the data. If there was any doubt about some events, they were compared with the analogue. Appendix 7 shows the details in picking of all unfiltered and filtered plots produced, using Sheephill data as an example. Figs. 3.56-3.59 show the first arrival time-distance plot with the error bars plotted with a reduction velocity of 6 km/s.

3.11 S-WAVE PICKING

Hall & Ali (1985) described the difficulties of S-wave picking as being due to the long train of the signal waveform, similarity in the waveforms of the signal and noise, and shingling effects particularly in noisy traces. S-wave picking is difficult because it is a second arrival and the onset is not sharp. To have more confidence in the picking of the shear wave, the signal properties can be used. The signal shows a linear polarization in a certain plane. The P and the SV waves are polarized in the vertical-radial plane and the SH wave polarized in the horizontal plane. Plotting the particle motion can give a good indication of the propagation of the signal in a certain window. So the signal has a high rectilinearity. The rectilinearity is a measure of the long axis to the short axis of the elliptical movement of the wave in a certain plane. Fig. 3.60 shows the particle motion within a certain window for both the P- and S-waves in vertical-radial plane. Note the direction of the particle motion for both. The particle motions of the P- and the S-waves show good linear polarization.

The S-waves were picked in the same way as the P-wave from the digital data. The S-waves were picked from the filtered data and, in most cases, these picks were compared with the same events after applying different filter processing. Filters cause some distortion on the data, so the filtered sections were superimposed on the unfiltered to pick the more reliable event. The uncertainty of the S-wave picking was taken as 0.05 s and this is related to the same kind of uncertainty as for the P-wave picking, in addition to the uncertainty of picking the right onset. Appendix 7 shows the details in picking of all unfiltered and filtered plots produced, using Sheephill data as an example. Figs 3.61-64 show the S-wave picking of the data.

CHAPTER FOUR

INTERPRETATION OF SEISMIC DATA

4.1 INTRODUCTION

The data were subject to a variety of methods of interpretation. Direct arrivals show a curved nature in the Midland Valley and were subjected to the WHB and Tau-P methods to calculate the velocity distribution of the first layer. Head waves were subject to the horizontal and dipping layer calculations. The wide-angle reflection events which have been recognised in the data were subjected to the T^2-X^2 method to calculate the depth and the overburden average velocity. Finally ray tracing was applied to model the data. In this chapter a brief description of these methods and their results will be discussed.

Fig. 4.1 shows the time-distance graph of the first arrivals recorded along the main profile, using a reduction velocity of 6 km/s. Figs 4.2-4.4 show the interpreted vertical component data of the main line. Fig. 4.5 shows the time-distance graph of the data recorded along the Hillhouse-Kilmarnock (HK) line with a reduction velocity of 6.0 km/s. Fig. 4.6 shows the interpreted vertical component data of the HK profile. Appendix 3 is a list of picked first arrival travel times. Symbols for different arrivals are explained in Table 4.2. The first segment (direct arrival) is curved for all shots due to vertical and horizontal velocity variation. The second layer headwave is received from about 10-12 km. Headwaves from crystalline basement are detected from about 30 km. The crossover distances agree well with previous studies (Davidson 1986, Dentith 1987).

4.2 METHODS: OVERVIEW

Good knowledge of the first layer is critical to the interpretation of the deeper structure. The data interpretation will begins with direct arrivals through the top layer. The time-distance graph of the recorded data shows

that the direct arrivals have a curved nature in the Midland Valley. This shows that the top layer has vertical and/or lateral velocity variation. Al-Mansouri (1986), Davidson (1986) and Dentith (1987) considered this kind of curvature is due to lateral and vertical velocity variation within the first layer. To measure the velocity of the first layer, the Wiechert-Herglotz-Bateman (WHB) and the Tau-P methods were used. WHB and Tau-P methods provide a means of direct inversion from the time-distance data to a velocity-depth relation, but assume no lateral velocity variation.

The velocity of the top layer was obtained from the WHB and Tau-P inversion methods. The velocities of deeper layers were obtained by regression using the "S" package. Standard methods of refraction interpretation were applied to the data to find the thicknesses of layers.

4.3 TOP LAYER VELOCITY ESTIMATION

4.3.1 Wiechert-Herglotz-Bateman Method

The Wiechert-Herglotz-Bateman (WHB) method allows the direct inversion of time-distance data to a velocity-depth function by means of the solution of this equation.

$$z(v) = \frac{1}{\pi} \int_{x=0}^{x=x} \cosh^{-1}(v dt / dx)\, dx \qquad \text{.....(4-1)}$$

where

$$v = (dx / dt)_{x=x} \qquad \text{.....(4-2)}$$

where the velocity is derived at depth Z, Z being the turning point of a ray arriving at the surface at a range X from the source. The method is used where there is no velocity inversion and assumes no lateral velocity variation.

4.3.2 Tau-P Method

Diebold & Stoffa (1981) showed that the travel time can be expressed in terms of the horizontal (p) and vertical (q) components of wave slowness

$$\Delta T = p\Delta X = q\Delta z \qquad \text{.....(4-3)}$$

where

$$p = \frac{\sin i}{v} \qquad \text{.....(4-4)}$$

$$q = \frac{\cos i}{v} \qquad \text{.....(4-5)}$$

where
v= velocity of the medium
i=direction of the raypath

Wave slowness, U , is given by

$$U = \frac{1}{v} = (p^2 + q^2)^{1/2} \qquad \text{.....(4-6)}$$

and for a series of horizontal layers a refracted ray has travel time

$$T = p_x + 2\sum_{i=1}^{n} q_i z_i \qquad \text{.....(4-7)}$$

At each point (t,x) on a time-distance curve the tangent is defined by the eq. 4.7 with a gradient P and time-intercept tau (τ). This method represents the time-distance curve as a series of straight lines. The depth calculation is based on planar method equations (see section 4.5).

$$Z_1 = \frac{Tau(P_2) / 2}{(U_1 2 - p_2 2)^{1/2}} \qquad \text{.....(4-8)}$$

to derive Z_1 and then

$$Z_i = \frac{tau(P_{i+1}) / 2 \sum_{j=1}^{j=i+1} Z_j (U_j - P_{i+1})^{1/2}}{(U_i^2 - P_{i+1}^2)^{1/2}} \qquad \text{.....(4-9)}$$

for the i-th planar layer.

4.3.3 Application of the WHB and Tau-P methods

These two methods were applied to the direct wave arrivals to estimate the top layer velocity. The program WHB10 was originally written by J. Hall to calculate the velocity-depth function from the time-distance graph. The program was designed to use data with an even spacing. The difficulties of getting an even spacing for the receivers due to some equipment failure or the access to the sites led Dentith (1987) to modify the program to accept uneven spacing. The program uses five curves to invert the time-distance to velocity-depth, these curves are the best fit, maximum, minimum, most curved and most straight curves through the data. The program uses the resulting velocity-depth curves to determine maximum and minimum value for a given data point and plot an error bar centred on the point of the best-fit curve. The error bars are not true error but define an envelope of possible velocity-depth curves.

Dentith (1987) did a lot of testing on the effect of receiver spacing and he found that increasing the spacing causes a slight decrease in the velocity at a given depth for both methods. The Tau-P method depends on this estimation of the surface velocity (v_0) and Dentith found that increasing the velocity causes a given velocity to be predicted at a greater depth. The underestimating of v_0 causes over-estimation of velocity at a given depth, while the over-estimation distorts the shape of the velocity depth curve near the surface. The difficulties of estimating the optimum surface velocity led Dentith (1987) to consider that the WHB is more useful for the data because it does not depend on another variable. Dentith (1987) modelled a lateral velocity variation to see the effect of that on the data after applying WHB inversion. He found that data recorded in the direction of lateral increase show considerably higher apparent velocities than those from the same part of the model recorded against the increase.

The application of the WHB method to the data of this study showed that the top layer velocity varies from shot to shot. A comparison of the top layer velocity will be given to 1 km depth for all the shots and some more information below this depth if it is available. The velocity was taken from the velocity-depth curve every 0.2 km.

Fig. 4.7 shows the time-distance and velocity-depth graphs by applying WHB to the Hillhouse (main line) data. The data show that the P-wave

velocity is 3.4-4.1 km/s to about 0.8 km depth with a gradient of 0.9 s^{-1}, reaching about 4.3 km/s at 1 km depth. This is in good agreement with the previous studies of Hall (1974), Davidson *et al.* (1984) and Dentith (1987) for the Carboniferous layer which occurs at outcrop in the Hillhouse area.

Data recorded from Loanhead show a higher velocity near the surface (4.0 km/s) due to the presence of significant igneous rocks within the top layer. The velocity-depth curves of the Loanhead shotpoint show that the velocity has a slight difference when the data are recorded in opposite directions. Figs 4.8 & 4.9 show the WHB inversion of the data recorded from Loanhead to the north and south respectively. The velocity is 4.0 km/s at the surface. It increases to about 4.5 km/s at 1 km depth when the line is recorded to the south from Loanhead; it is 4.8 km/s at 1 km depth when it is recorded to the north. Given the work of Dentith (1987), see above, these results suggest a lateral increase of the velocity to the north.

Fig 4.10 shows the data recorded from Sheephill. A high velocity (4 km/s) occurs at the surface going to 4.6 km/s at 1 km depth with a gradient of 0.6 s^{-1}.

Results were quoted at 1 km depth for comparison. But some curves sampled deeper. Top layer velocity reaches 5.0 km/s at 2 km depth based upon Hillhouse (main line) and 5.0 km/s at about 1.7 km beneath Sheephill.

WHB inversion was applied to the S-wave arrivals. The data recorded from Hillhouse (main line) showed the S-wave velocity ranges from 1.0 km/s at surface to 2.2 km/s at 1 km depth with a gradient of 1.2 s^{-1} (Fig. 4.11). The low S-wave velocity is due to the presence of pores and cracks which affect the S-wave more than the P-wave.

The data recorded from Loanhead to the north showed that the S-wave velocity is 1.5 km/s at the surface reaching 2.2 km/s at a depth of 0.5 km and then increases slowly with depth to be about 2.8 km/s at 1 km depth with a gradient of 0.75 s^{-1} (Fig. 4.12). The data recorded from Loanhead to the south showed a similar velocity within the top 0.5 km, but it has a higher velocity below that rising to 2.4 km/s at 1 km depth with gradient of 0.60 s^{-1} (Fig. 4.13). The S-waves from both directions show a similar relation to that of the P-wave, i.e. the gradient to the north is higher. However, the Vp/Vs ratio is different to the north (Fig. 4.18b) and south (Fig. 4.18c) of Loanhead.

Data recorded from Sheephill showed that the S-wave velocity is higher than that from the other shots (Fig. 4.14). It has a velocity of 1.8 km/s

at the surface and increases gradually to 2.4 km/s at 1 km depth with a gradient of 0.60 s^{-1}.

4.3.4 Vp/Vs and Poisson's ratio

Theory

The velocities of P- and S-waves in the earth depend on the elastic constants of rocks, which in turn are dependent on mineral constitution and rock texture. Christensen & Fountain (1975), O'Connell & Budiansky (1974, 1977) and others confirm that petrography, geochemical and physical properties of rocks influence P- and S-waves differently. The Vp/Vs ratio in this case can give more information about the lithology than each velocity separately and, alternatively, the Poisson's ratio can differentiate the rocks according to their properties. Tatham (1982) considered that not just the physical properties of the rocks affected the velocity but even the shape and distribution of the pores and cracks (Fig. 4.15).

The Poisson's ratio (σ) is defined as the ratio of the strain normal to strain parallel to uniaxial stress applied to a unit cube of rocks. σ varies from 0-0.5 and it can be obtained from Vp/Vs using the relation

$$\sigma = \frac{0.5(V_p / V_s)^2 - 1}{(V_p / V_s)^2 - 1} \qquad \text{.....(4-10)}$$

Vp/Vs varies among minerals and so some lithological discrimination is possible on the basis of this parameter. Domenico (1984) showed that the Poisson's ratio can be used to discriminate sandstone from limestone, for example:

Rock type	Poisson's ratio
Sandstone	0.17-0.26
Dolomite	0.27-0.29
Limestone	0.29-0.33

Sandstone has a wide variation and the separation of sandstone from limestone depends on the difference in Poisson's ratio of quartz (σ=0.056) and calcite (σ=0.316) (Fig. 4.16). The substantially higher S-wave reciprocal velocity of quartz results in a Poisson's ratio of less than one-fifth that of

calcite. Poisson's ratio is affected also by the porosity. Domenico established an empirical function for this: $1/v=A+B\phi$, where ϕ is the porosity at each differential pressure, A and B are reciprocals of the matrix velocity and rate of change of reciprocal velocity with porosity respectively. These factors show that the porosity is affected by depth and pressure. The higher pressure with depth causes the closure of pores which affects the velocity of P- and S-waves propagating through that medium. Figs 4.17a and 4.17b show the P- and S-wave affected by the porosity at different pressure. The porosity density which varies from one rock to another causes variation in P- and S-wave velocities. O'Connell & Budiansky (1974, 1977) and others modelled the effect of the porosity on the Vp/Vs relation and demonstrated that the effects of pore density, pore shape and whether the pores and cracks are dry or saturated.

The Poisson's ratio can provide a good discrimination of the lithology and the internal structure of rocks. Ali (1983) and Hall & Ali (1985) studied P- and S-waves from Lewisian rocks in the North of Scotland to see the variation of the Vp/Vs and Poisson's ratio from different lithological units. They found that σ has a vertical and lateral variation. They interpreted the vertical variation as a result of closing cracks due to overburden pressure and the lateral variation to be due to the effect of lateral changes in lithology.

Application

Fig. 4.18 shows the Vp/Vs and σ of the data. Vp/Vs and σ decrease with depth. Note that the Vp/Vs varies from one shot to another. Poisson's ratio has a high value (0.40) near the surface but it decreases to 0.30 at about 0.6 km and this may be due to the closure of the cracks with depth. The Vp/Vs relation and the Poisson's ratio of this study showed that the average value of σ in the first layer ranges from 0.30-0.24. This value is within the same range as previous studies. Assumpcao (1978) found the Poisson's ratio of the first layer to be within the range of 0.33-0.27 from the LISPB study. Dentith (1987) found that σ is 0.29 for the first layer and he considered that to be in good agreement with the LISPB study for the top layer.

4.4 DEEPER LAYERS : VELOCITIES AND INTERPRETATION OVERVIEW

The velocities determined for refractors are presented and discussed here. The velocity of each refractor velocity segment was calculated by regression using the "S" package. These velocities are listed in the tables below. Direct velocities are included for completeness. After obtaining the velocities of the top layer and refractors, various interpretation methods were used to build a model for the upper crustal structure in the studied area, as described in following sections.

Table 4.1 P- and S-wave velocities. A minus range value implies recording to the SSW of the shotpoint; positive implies to the NNE. Ranges in km; P- and S-wave velocities are in km/s. PR= Poisson's ratio. Arrival names are explained in table 4.2.

Hillhouse shot (main line)

Arrival	Receiver ranges	P-wave	S-wave	PR
a1	0.00 to 8.33	3.40 - 4.30	1.00 - 2.20	0.40 - 0.32
a2	8.33 to 14.01	5.50 ± 0.02	2.86 ± 0.11	0.31
a3	16.21 to 26.12	5.83 ± 0.04	3.37 ± 0.07	0.24
a4	28.20 to 38.52	6.08 ± 0.06	-	-
a4	41.96 to 59.83	6.03 ± 0.03	-	-
a4	62.68 to 65.90	6.08 ± 0.06	-	-

Loanhead shot

Arrival	Receiver ranges	P-wave	S-wave	PR
a4	-33.43 to -25.96	6.06 ± 0.07	3.40 ± 0.02	0.27
a3	-23.29 to -12.87	5.88 ± 0.06	3.34 ± 0.04	0.26
a2	-11.02 to -7.04	5.19 ± 0.13	2.96 ± 0.01	0.25
a1	-7.04 to 0.00	4.00 - 4.50	1.50 - 2.40	0.36 - 0.30
a1	0.00 to 7.23	4.00 - 4.80	1.50 - 2.20	0.24 - 0.40
a2	7.23 to 11.20	5.24 ± 0.02	2.97 ± 0.01	0.26
a3	11.20 to 17.83	5.78 ± 0.03	3.24 ± 0.03	0.27
a4	21.26 to 39.17	5.99 ± 0.02	3.34 ± 0.03	0.27

Sheephill shot

Arrival	Receiver ranges	P-wave	S-wave	PR
a1	0.00 to -9.45	4.00 - 4.60	1.80 -2.40	0.33 - 0.29
a2	-9.45 to -13.39	5.58 ± 0.01	2.93 ± 0.13	0.30
a3	-25.20 to -15.54	5.86 ± 0.01	3.21 ± 0.04	0.28
a4	-29.71 to -39.52	5.94 ± 0.04	3.52 ± 0.01	0.22

Hillhouse-Kilmarnock line

Arrival	Receiver ranges	P-wave	S-wave	PR
a1	1.64 to 6.47	3.84 ± 0.04	1.86 ± 0.09	0.34
a2	9.53 to 13.06	5.05 ± 0.05	2.53 ± 0.05	0.33

These velocities can be interpreted as 4 groups, corresponding to 4 upper crustal layers:

1 - The first segment with a velocity of 3.8-4.2 km/s for the top layer which is taken to represent the Carboniferous and Upper Old Red Sandstone (ORS). This segment is curved due to both lateral and vertical velocity variation. This layer was studied by applying the WHB and Tau-P methods (see above). This layer has a higher value from the data recorded from Loanhead and Sheephill than recorded from Hillhouse. The higher velocity is due to the presence of the Carboniferous igneous rocks (Clyde Plateau Lavas) which cover most of the northern part of the profile.

2 - A segment with a velocity of 5.5 km/s is clear on the time-distance graphs from both Hillhouse (main line) and Sheephill quarries, but it has a velocity of 5.2 km/s on the graph from Loanhead on both sides. The data recorded along the HK line show a lower velocity of 5.0 km/s for this layer. Davidson (1986) and Dentith (1987) considered that this layer represents the Lower ORS and/or Lower Palaeozoic. Dentith(1987) found that this layer has a higher velocity on MAVIS I north than that on MAVIS I south, but the data recorded from Sheephill (our northern shotpoint) do not show a higher velocity on the time-distance graph. However, raytracing (see later) does require higher velocities for layer 2 north of the Paisley Ruck.

3 - A velocity of 5.8 km/s is clear on the data, especially from Sheephill in the area between the DWF and PR. This layer may represent a Lower ORS volcanic ridge (see chapters 1 and 5).

4 - A segment with a velocity of 5.99-6.08 km/s is observed from all three quarries, which represents the crystalline basement in the Midland Valley based on previous studies.

Note that the HK line is too short to obtain first arrivals of group 3 and 4.

Some shots show good S-waves; some to a considerable offset, such as from Sheephill. S-waves on data recorded from Hillhouse (main line) were observed up to about 30 km. S-waves from the first layer for all the shots were subjected to the WHB inversion method as mentioned above. S-wave segments from deep layers were calculated by regression using the "S" package. The velocities of the S-wave are listed in the table above.

As mentioned above, S-waves do not cover all of the main profile. Accordingly the Poisson's ratios of these segments were calculated where possible. The Poisson's ratio of the second layer is 0.26, obtained from Hillhouse (main line) and Sheephill. The Poisson's ratio of the third layer is 0.28 from Sheephill. The Poisson's ratio of the basement is 0.31 and this value was obtained from Hillhouse (main line) and Loanhead.

These velocities and their time intercepts were used to determine the thickness and depths of the upper crustal layers by applying horizontal, dipping layer and plus-minus methods, as described below.

4.5 HORIZONTAL LAYER INTERPRETATION

When a seismic wave is incident on an interface between two layers of different velocity it is reflected and/or transmitted (Fig. 4.19). Refraction is according to Snell's Law:

$$\frac{\sin i}{\sin r} = \frac{V1}{V2} \qquad \text{.....(4-11)}$$

where

i = incidence angle

r = transmission angle

v1 = velocity in the first layer
v2 = velocity in the second layer

Fig. 4.20 shows the main raypaths in a ground of three layers. All the layers have a constant velocity and are separated by planar horizontal interfaces. The direct wave travels horizontally though layer 1 at a velocity of V_1. The travel-time curve is a straight line with a slope of $1/V_1$. When a ray hits the first interface at the critical angle (θ) it is transmitted at 90^o to the normal and runs along the interface between the two layers. In this case sin r=1. Plotting the time-distance graph of this arrival gives a straight line with a gradient of $1/V_2$. The line cuts the time axis at a positive time called the time intercept. The derivation of the equation for depth to the interface will not be mentioned as it is available in many textbooks (e.g. Dobrin 1976, Kearey & Brooks 1984). The final equation is presented here. The depth to the first refractor, which is the thickness of the first layer, is given by

$$Z1 = \frac{Ti1\,V1\,V2}{2(V2^2 - V1^2)^{1/2}} \qquad \text{.....(4-12)}$$

where
V1 = velocity of the first layer
V2 = velocity of the second layer
Ti = time intercept

In the case of the second refractor, critical refraction is from the top of the third layer. The time-distance graph has a slope of 1/V3, where V3 is the velocity of the third layer. From the intercept on the time axis (T_{i2}) we can obtain the thickness of the second layer:

$$Z2 = 0.5\left[Ti2 - 2Z1\frac{(V3^2 - V1^2)^{1/2}}{V3\,V1}\right]\frac{V3\,V2}{(V3^2 - V2^2)^{1/2}} \qquad \text{.....(4-13)}$$

where
V1, V2, V3, Ti2 and Z1 are defined as above
Depth to the third layer = Z1+Z2

This method was applied to the data by using the velocities which were obtained from the WHB for the first layer and regression for the refractors.

Fig. 4.1 shows the direct and head wave segments of the upper crust for the data gathered from the main profile, and Fig. 4.5 for the shorter HK line. Fig. 4.21 shows the horizontal layer interpretation of the main profile.

The application of the horizontal layer interpretation to the data recorded on the HK line showed that the thickness of the first layer is 0.8 km, in good agreement with Davidson (1986). Horizontal layer interpretation on the main line showed that the thickness of the first layer is about 2 km beneath Hillhouse, 1 km near Loanhead and increases to about 2 km to the north of the Paisley Ruck (PR, Fig. 4.21). The difference in thickness of the first layer under Hillhouse from that under Loanhead, and the presence of the DWF between these two quarries, leads us to assume that this variation is most likely due to the fault. Similarly the Paisley Ruck is assumed to cause the thickness change of this layer between Loanhead and Sheephill. Thus big throws of about 0.8-1.0 km on the Dusk Water Fault and Paisley Ruck are suggested.

A thickness of 0.8 km for this layer was detected below MAVIS I south near Trearne which is at the far west of the MAVIS I south, see Fig. 3.1. The closest point on the main profile is Loanhead quarry.

Layer 1 disappears a few kilometres to the north of Sheephill where deeper layers come to surface, according to the geological map (Clyde sheet) which shows the outcrop of the Upper ORS for a short distance followed by the Lower ORS. The data recorded from Hillhouse (main line) showed that there is a step forward of the basement refracted arrival at about 64 km offset. This indicates that there is a fault in the basement refractor at this position which may be the cause of the cropping out of the Lower ORS.

The second layer has a velocity of 5.0-5.6 km/s. This velocity was determined from the time-distance graph, it is 5.2 km/s on the data from Loanhead and about 5.5 km/s from Hillhouse (main line) and Sheephill. This velocity is 5.0 km/s on the HK line where it lies at 1 km depth. The thickness here of this layer was not calculated because there is no refraction coverage of the underlying layer on the HK line. Note that the thickness was taken to be the same as below the main line for the raytrace modelling. The depth to the second layer, of course, varies along the main profile with the thickness of layer 1. It is about 2 km beneath Hillhouse, it occurs at 1 km under Loanhead in the area between the DWF and PR, and its depth increases again under Sheephill. This layer crops out to the north of the Clyde, beyond the Gartness Fault.

A velocity of 5.8 km/s was observed on the data fron Hillhouse and Sheephill. The data from Loanhead did not not show the same velocity. The horizontal layer calculation show that this layer lies at 2.5 km and it was considered that this layer is restricted to the middle of the line.

A velocity of 5.99-6.08 km/s is observed at ranges of over 30 km. The refractor is crystalline basement and lies at 3-4 km depth beneath the main line, which agrees with Davidson (1986) and Dentith (1987). The data show that this segment is affected by faulting. At some faults different velocities are observed on both sides of the fault; at a fault to the north of the Clyde the same refractor is observed on both sides. These faults were compared with the faults which are known at the surface. Note that the HK profile is too short for headwave coverage of the basement, but reflections were observed from a depth of about 4 km, in accord with depth for basement obtained from the main line and Davidson (1986).

Previous studies had showed no indication of any substantial faults affecting the basement in the Midland Valley, but the data gathered here show that the basement is affected by some faulting. Two of these faults are the Dusk Water Fault and Paisley Ruck. Another fault to the north of the Clyde shows a big throw of about 0.8 km to the south. This fault is located at 60 km from Hillhouse in Fig. 4.21. However, raytrace modelling shows a more realistic location for the step to be beneath the Gartness Fault, which separates the Upper ORS from the Lower ORS at surface.

In the cases where velocity segments from different layers were observed on either side of a fault position the calculation of depths and fault throw were limited. To calculate the thickness of these layers and the throw of the faults a different approach was used. An estimate of depth of each layer is calculated by shifting the whole segment up or down as if it is not affected by faulting and assuming the crossover point is at the fault location. The shift is assumed to represent the time difference caused by this displacement of the layer (Δt). The velocity of the layers above the shifted interface were averaged to find the velocity of the overburden layer to calculate the displacement of the refractor. From the time-intercept difference (Δt), the step of the fault (Δz) was calculated.

$$\Delta z = \Delta t V_1 V_2 / (V_2^2 - V_1^2)^{1/2} \qquad \text{.....(4-14)}$$

Δz was added or subtracted from the calculated depth to find the depth after the fault according to its relation with the whole segment, i.e stepping forward or backward on the time-distance graph.

4.6 DIPPING LAYERS INTERPRETATION

4.6.1 Reversal coverage

When the interfaces are not horizontal, the velocity which is obtained from the time-distance plot is not the true velocity and is called the apparent velocity. This velocity is affected by the true refractor velocity and its dip along the profile. The apparent velocity shooting down dip is less than the true velocity, because the rays returning to the surface pass through an increasing thickness of layer 1 with offset. The reverse happens when shooting up dip. In both cases the apparent velocities depend on the dip angle. Thus the previous equations are invalid. Reverse shooting coverage gives information about the dip direction from the time intercepts on the reversed time-distance graph. Fig. 4.22 shows a boundary between two layers with velocities V_1 and V_2 and dipping at an angle ϕ. See Telford *et al.* (1987) for the derivation of the equations, but only the final derived equation of the method will be presented here. The critical angle of refraction is given by:

$$\theta = \frac{1}{2}\left\{\sin^{-1}\left(\frac{V_1}{V_d}\right) + \sin^{-1}\left(\frac{V_1}{V_u}\right)\right\} \qquad \text{.....(4-15)}$$

and the dip of the refractor is:

$$\phi = \frac{1}{2}\left\{\sin^{-1}\left(\frac{V_1}{V_d}\right) - \sin^{-1}\left(\frac{V_1}{V_u}\right)\right\} \qquad \text{.....(4-16)}$$

where
V_1= top layer velocity
V_u= updip direction refractor velocity
V_d= downdip direction refractor velocity.

Knowing V_1 and θ, the true refractor velocity V_2 may be derived using Snell's Law

$$V_2 = V_1 / \sin \theta \qquad \text{.....(4-17)}$$

The depth at the updip shot can be obtained by

$$Z_u = \frac{V_u t_u}{2 \cos \theta} \qquad \text{.....(4-18)}$$

and at the downdip shot by

$$Z_d = \frac{V_d t_d}{2 \cos \theta} \qquad \text{.....(4-19)}$$

where

t_u= time intercept of updip shooting

t_d= time intercept of downdip shooting

This method was employed on the data where there is reversed coverage and an indication of dip of the first refractor. It was applied separately to the data recorded between Hillhouse-Loanhead and Loanhead-Sheephill. Application to the data between Hillhouse and Loanhead shows the first refractor dipping to the south at 1.7^o and the depths below the shotpoints (1.7 and 1.0 km) to be similar to those of the horizontal layer interpretation. The true refractor velocity is 5.33 km/s, which is slightly different from the velocities obtained from the horizontal layer interpretation. Whereas the same refractor between Loanhead and Sheephill dips to the north at 2.0^o, and occurs at 0.8 km beneath Loanhead and 1.5 km beneath Sheephill, the true refractor velocity was found to be 5.39 km/s. This method was not employed on the data between Hillhouse and Sheephill because of the opposite dips determined above.

The application of the horizontal layer method to this refractor showed that this layer is affected by the DWF and PR. These two faults occur between Hillhouse-Loanhead and Sheephill-Loanhead respectively. Applying this method on these shots does not give the true dip, but it shows an average dip of the layer between the two shots by ignoring the effect on the refractor of the throw of these faults. The dipping layer method gave a similar depth of the refractor under each source to that which has been obtained by the horizontal layer method.

4.6.2 Split spread shooting (Loanhead)

The availability of data in the split spread shooting pattern gave a chance to use another adaptation of the dipping layer interpretation to Loanhead shot. In the case of a dipping layer and split spread recording, Johnson (1976) interpreted the split spread profile using the general formula of the planar layer:

$$t(k) = \frac{x \sin \beta_1}{v_1} + \sum_{i=1}^{k-1} \frac{H_i}{v_i} .(\cos \alpha_i + \cos \beta_i) \qquad \text{.....(4-20)}$$

where

k designates the interface along which the wave is refracted,

Hi = the vertical thickness of the i-th layer beneath the source,

Vi = the velocity of the i-th layer,

α_i = the angle with respect to the vertical made by the downgoing ray in the i-th layer,

β_i = the angle with respect to the vertical made by the upgoing ray in the i-th layer

X = distance

In this method Johnson used the apparent velocity to find the incident and dip angles for each layer. By starting the calculation for the first refractor and finding its dip, then the second and so on to build up the model.

The split spread method was applied to the data from Loanhead quarry. To obtain the first refractor, a velocity of 4.0 km/s was assumed for the first layer, estimated from the WHB method. It was found that this refractor has a velocity of 5.19 km/s, occurs beneath Loanhead at about 1.0 km depth and dips at less than one degree to the south. This depth is in agreement with those derived from the horizontal and reversed dipping layer calculations. By applying this depth and dip angle, the depth and dip angle of the second refractor were obtained. A first interpretation used times picked and used in the horizontal layer interpretation. However, the split spread results suggested that the third layer (second refractor) was basement at 2.5 km, which is a shallower depth than suggested by the other methods of interpretation and our knowledge about the crystalline basement depth in the area. The relevant traces from Loanhead have poor signal to noise ratios. Repicking suggested velocities closer to those of layer 3. Re-

interpretation by split spread on this basis shows the second layer has a thickness of 1.9 km and dips to the north with an angle of about 1.5 degrees (Fig. 4.23). Layer 3 has a velocity of about 5.89 km/s and lies at about 2.9 km depth below Loanhead. This shows a slight difference of depth to this layer from the horizontal layer interpretation.

4.6.3 Summary

The application of dipping layer interpretations to the data showed that it is difficult to measure the dip of the first refractor, in this case, because it is affected by the DWF between Hillhouse and Loanhead and by the PR between Loanhead and Sheephill, but it shows a similar depth under the shots to what was obtained from the horizontal layer. Using the split spread method on the data from Loanhead showed that the thicknesses of the first and second layer are similar to that of the horizontal layer, the first refractor dips at less than 1 degree to the south, the second refractor dips at little more than 1 degree to the north. These dips are small, so there is no big modification to the model obtained by the horizontal layer interpretation.

4.7 PLUS-MINUS INTERPRETATION

The plus-minus method (Hagedoorn 1959) is used to investigate non-planar refractors. It requires the calculation at each receiver of a plus time for conversion to the refractor depth and a minus time for the estimation of the refractor velocity. In this method reverse shooting is required and local dips of the refractor should not be more than about 5^{o}. The plus time is the sum of the arrival times of the two refracted arrivals minus the total time of the refracted arrival between the two shot points. When the data has no reverse coverage (at the ends of the reversed coverage) the plus time can be calculated by extrapolating the data using the refractor velocity derived from the minus times (see below). Such a plus time is calculated from the deviation of the observed arrival from the travel-time given by extrapolating the gradient of the refractor velocity from the travel-time at the last station which has reversed coverage. The differences were doubled and added to the plus time at the last station at which a plus time was obtained.

The minus time is the difference between arrival times of the two refracted arrivals at a station. The minus time is used to calculate the

refractor velocity by plotting distance versus minus-time. Refractor velocity V2 is given by

$$\text{Gradient} = \frac{V2}{2} \qquad \text{.....(4-21)}$$

The depth of the refractor below a station (K) is given by

$$Z(K) = \frac{\text{Tplus}(K)V2V1}{2(V2^2 - V1^2)^{1/2}} \qquad \text{.....(4-22)}$$

where
V1 = top layer velocity
V2 = refractor velocity
Tplus = plus-time of the refractor

The plus-minus method was applied to the reversed coverage of the basement refractor between Hillhouse and Sheephill. The minus, plus times and the depth of the refractor are shown in Appendix 4. The velocity from the minus time was 5.99 ± 0.03 km/s . V1 was taken by averaging the layers above the basement refractor, weighted according to the thickness of the overburden layers. Fig. 4.24 shows the plus-minus interpretation of the basement refractor. The method shows that the basement lies at 4 km in the south and shallows to the north. The interpretation shows that there is a step at about 30 km which can be correlated with the southern margin of layer 3 on the raytrace model (Fig. 4.28) and which might be correlated with the DWF. Similarly, a step at about 54 km can be correlated with the northern margin of layer 3 and also which may reflect the PR at the basement. The shallower depth to basement determined beneath layer 3 (between the DWF and PR) may be due to an underestimate of overburden velocity in this zone.

The effect of the Gartness Fault on the basement refractor is clear after applying this method. The refractor north of the Gartness Fault is much shallower than that obtained from the horizontal layer interpretation. The overburden velocity was taken as 5.1 km/s and this may be the reason for the underestimation of the depth of this refractor. Note that the raytracing model is in better agreement with the horizontal layer interpretation.

4.8 INTERPRETATION OF WIDE-ANGLE REFLECTIONS

Fig 4.25 illustrates a horizontal interface separating two media. The incident ray is reflected with an angle which is equal to the incident angle. The rays travel with the velocity of the upper layer. The travel-time to a receiver at distance x can be written as

$$V^2t^2 = x^2 + 4h^2 \qquad \text{.....(4-23)}$$

where
V = overburden velocity of the reflector
t = time
x = offset of receiver
h = depth to the reflector

This equation can be re-arranged as:

$$\frac{V^2t^2}{4h^2} - \frac{x^2}{4h^2} = 1 \qquad \text{.....(4-24)}$$

Thus the travel time is a hyperbola as shown in Fig. 4.25. The depth of the reflector is determined by measuring t_o, the travel time for a geophone at the shotpoint. Setting x=0

$$h = \frac{1}{2}Vt_0 \qquad \text{.....(4-25)}$$

The plot of t^2 against x^2 gives a straight line of slope $(1/V^2)$and intercept t_o^2. The difference in travel time for a given reflection for two geophone locations is known as moveout and is represented here by Δt. In the case that the reference offset is zero, the moveout is called the normal moveout, Δt_o.

$$\Delta t_n \approx \frac{x^2}{2V^2t_0} \qquad \text{.....(4-26)}$$

From the above equation it is seen that the normal moveout increases as the square of the offset x, inversely as the square of the velocity and

inversely with the traveltime. Thus the curvature increases rapidly with the far geophones and becomes less with the increasing recording time. The concept of the normal moveout is important to decide whether the event is a reflection or not. If the normal moveout is different from the value which is given by equation by more than the experimental error, then the event is not from a horizontal reflector.

Reflection events which were picked (see sections 3.7-3.9) were subjected to the T^2-X^2 plotting by using the "S" package and checking that the data lie on a straight line. Some of the data were omitted from the dataset because they are well scattered. This happened at the far traces, sometimes due to the mis-identification of the event. The overburden velocity and time intercept were measured by regressing the dataset using the "S" package. The depth to each reflector was calculated by using this velocity and the time intercept in eq. 4-25. The picked events were compared with the refraction model obtained from the horizontal layer interpretation to see if they represent the same interfaces as the refractors, or not.

An event was observed on the data recorded from Hillhouse quarry (main line) within the range of 22-38 km. The T^2-X^2 application on this event shows that it has an overburden velocity of 5.87 km/s and it represents a reflector at 9.5 km depth (a6). The same reflector was observed in the data at a range of about 60 km from the same shot. Another event was observed at the same data and this shows a reflector at 11.5 km (a7) with overburden velocity of 5.97 km/s and also an event of a reflector at 14.7 km (a8) with an overburden velocity of 6.08 km/s. The data from Sheephill show the same event at 13 to 28 km range with an average velocity of 5.87 km/s and depth to this reflector is 8.6 km (a6). Another two events were observed on the data at the same range and they have overburden velocities of 5.70 km/s and 6.08 km/s and occur at 11.1 and 15.5 km depth (a7 and a8). Loanhead data show the presence of some events and these gave a reflectors at 8.7 km (a6) with overburden velocity of 5.87 km/s and 12.8 km (a7) with a velocity of 6.02 km/s and 18.8 km (a8) with an overburden velocity of 6.08 km/s.

These results were compared to establish any common reflectors. Some of the events show a low interval velocity of the reflector and that was considered to be either due to the mispicking of the event or complexity of the area.

The data recorded from the HK line show some events which were picked and treated with the T^2-X^2 method. This showed the presence of a reflector at 4.5 km with average velocity of 5.27 km/s. Other reflectors were seen in the data but the T^2-X^2 calculation showed that these reflectors have low overburden velocities.

4.9 ANISOTROPY

4.9.1 Background

The anisotropic nature of rocks has been recognised since at least the 1930's (McCollum & Snell 1932). In anisotropic media seismic velocity varies with propagation direction. In stratified rocks the velocity parallel to the bedding is different from that perpendicular. In crystalline rocks any fabric produces a similar effect on the velocity. Fractures also produce a different velocity along the fracture alignment from the perpendicular direction.

A number of studies have been carried out on the anisotropic character of media. Carlson & Christensen (1979) and Bachman (1979) studied velocity variation in calcareous sediments and they found the reason for the anisotropy in their study was due to the fabric orientation. A medium consisting of a series of planar parallel isotropic layers with different physical properties behaves as an anisotropic media when the seismic wavelength is greater than the thickness of the individual layers. This is called a transversly isotropic media and may be analogous to sedimentary layers. Refraction occurs at interfaces between layers thick relative to the seismic wavelength when there is a contrast in the seismic velocity of the layers to cause a deviation of the raypath depending on the incidence angle. All these factors affect the velocity measurement in any studied area. Dentith (1987) tried to study the anisotropy in the Midland Valley by combining the data which he had from his refraction profiles, commercial reflection lines and well logs. He concluded that the anisotropic variation in velocity did not affect the final model of the area, because its effects were within the uncertainty of his study.

Observation of seismic anisotropy can provide a lot of information about the mineralogy and internal structure of the anisotropic rocks, and the orientation of the stress field that aligned the anisotropy when it was last fixed (Crampin *et al.* 1984). Both P- and S-waves are affected when propagating in an anisotropic medium by some kind of deviation of the

waves from the propagation direction. The effect of the polarization is very small on the P-wave. The S-wave gives more information about the anisotropy. Crampin (1985) considered that the S-wave has about three times more information than the P-wave. A lot of studies within the last ten years concentrated on the S-wave behaviour in isotropic and anisotropic media.

Shear waves entering an anisotropic media split into two phases with different velocities and approximately orthogonal polarization directions which are fixed relative to the anisotropic symmetry (Crampin *et al.* 1986). This splitting is not lost after the wave leaves the anisotropic medium and so information is preserved along its path. The study of the SV and SH waves can give an idea about the anisotropy of the rock. Seismic anisotropy is most likely diagnosed through the shear wave splitting (Crampin 1981).

Nuttli (1961) showed that the particle motion of a linearly-polarized plane shear wave incident at a free surface would be either linear or non-linear, depending on whether the angle of incidence was less than or greater than the critical angle $i_c=\sin^{-1}(Vp/Vs)$, where Vp and Vs are the P and S-wave velocities. The curved shear wavefront incident on the free surface at the critical angle generates a P-headwave along the surface of the half space. At large angles of incidence the SP phase appears as a precursor to the direct S arrival and its amplitude is largest on the radial component. The particle motion of the SP and S in the sagittal and horizontal planes could be attributed to anisotropy induced shear wave splitting. The transverse plane which is orthogonal to the sagittal and horizontal planes may be used to discriminate between S and SP arrivals and for the shear wave splitting (Booth & Crampin 1985).

The azimuthal anisotropy which causes shear-wave splitting in most crustal rocks is caused by oriented fluid-filled inclusions. These inclusions are usually caused by preferentially oriented pore space in sedimentary rocks and fluid microcracks in igneous and metamorphic rocks (Booth *et al.* 1987). Such fabrics relate to stress regimes of the region. The shape of the fractures and the pore space and whether these pores are saturated or dry has a great role in the polarization and the anisotropic velocity.

4.9.2 Polarization of seismic waves

Both compressional and shear waves exhibit a high degree of linear polarization. The P-wave polarization is the deviation of the polarized

wave from the propagation vector and it is almost the direction of the group velocity. The energy propagation follows the raypath, so the apparent deviation is the difference of the polarized and group velocity deviation. The S-wave is more sensitive to the anisotropic medium than the P-wave because when it passes through anisotropic media it splits into two quasi shear waves (qs1, qs2) which travel with different velocities (Crampin 1977).

The particle motions of some traces were plotted for certain windows covering the first (P) arrivals. By this kind of plotting we tried to find any consistent relation of the first arrivals that could give an indication of the wave behaviour along the raypath and the incident angle. Particle motion plotting was applied also to the S-wave within a window of 1 sec beginning at its onset to see the S-wave behaviour, since the S-waves on some traces show some pulses within the wavetrain. The particle motion for the S-wave was plotted in the three planes to see the wave propagation and if it is possible to recognise any time difference between any SV and SH phases which would arise due to any anisotropy.

The variance-covariance and the measure of the eigenvalue and the energy technique, which were mentioned in Chapter 3, were applied to the data. The data were rotated every 5 degrees and the energy measured, and the maximum polarization and its rotation angle taken. The maximum rotation angle was plotted as a function of offset to see if there is any consistent orientation of the data and from that the polarization direction can be obtained. The polarization direction can give a good indication of the anisotropy. The data show no consistency of angle.

Another thing tried was to measure the ratio of the maximum to minimum polarization in the horizontal plane, to see if there is any time difference of the SV and SH which gives an indication of the degree of anisotropy. Again, no consistent results were obtained.

4.10 RAYTRACE MODELLING

4.10.1 Introduction to the method

The model developed by the previous methods of interpretation (Figs 4.21, 4.23 and 4.24) were tested using the SEIS83 raytracing package. This package consists of the main raytracing program (also called SEIS83) and a ray plotting program (RAYPLOT), and programs SYNTPL and SEISPL to calculate and plot synthetic seismograms based upon the output of SEIS83.

The program can handle a model involving curved interfaces, block structures and isolated bodies. All layers may be inhomogeneous.

The raypath is defined from the model and the travel times computed from the source to any surface receivers by rays leaving the source at a range of specified angles. When successive rays terminate at the surface at locations on either side of a receiver an iterative process is initiated to select an intermediate initial angle and raypath through the model. This process is repeated a specified number of times, or until the ray terminates within a specified distance of the receiver.

The program depends on the raytracing method (Cerveny *et al.* 1974). The raypath is calculated as

$$\frac{dx}{dt} = V \sin D \qquad \text{.....(4-27)}$$

$$\frac{dz}{dt} = V \cos D \qquad \text{.....(4-28)}$$

$$\frac{dD}{dt} = \frac{-\partial v}{\partial x} \cos D + \frac{\partial v}{\partial z} \sin D \qquad \text{.....(4-29)}$$

where

x = horizontal direction
z = vertical direction
D = declination from the horizontal of the raypath
t = arrival time at a point in the model
$\partial v / \partial x$ = partial derivative of velocity with respect to x
$\partial v / \partial z$ = partial derivative of velocity with respect to z

Velocities within each layer are given as a grid. The velocity at a point is calculated either by fitting bicubic splines to the data or by linear interpolation between the grid points, or by specifying velocities at the top and bottom of a layer.

4.10.2 Application of Raytracing

In raytracing both profiles, rays were used that came to surface within 100 m of a receiver.

Main line

The raytracing model was designed according to the velocities of the first layer derived from the WHB method and the velocities and depths of deeper layers obtained by the horizontal, dipping layer and plus-minus calculations. The poor S/N of some traces in the Loanhead data had needed us to reconsider their picking. In the raytracing these traces were treated as with the split spread interpretation. The surface geology was taken into account to determine the velocity distribution of the first layer. Specifically, account was taken of the outcrop of different geological units and the effect of the faults on these units, especially in the areas away from the seismic sources where there are no direct arrivals to control the velocity distribution of the top layer.

In the initial model a lot of care was given to the distribution of velocity in the first layer, especially as this layer shows a lateral velocity variation along the profile due to the Carboniferous basins and the presence of the Clyde Plateau Lavas. The velocity at the surface of layer 1 was set to about 3.5 km/s in the south. It increases to the north partly due to the outcrop of the Lower Carboniferous Clyde Plateau Lavas which increases the surface velocity to 4 km/s. The ability of the modelling program to accept the lateral velocity variation made it easy to model this layer. Layer 1 thickness was set in agreement with the horizontal layer interpretation. This layer disappears where layer 2 comes to the surface a few kilometres to the north of Sheephill.

Layer 2 was given a velocity of 5.2-5.7 km/s with a thickness of 1.5 km. The velocity gradient of this layer was assumed as 0.05 s^{-1}, similar to the MAVIS study. Layer 3 was modelled with velocity of 5.8 km/s at a depth of about 2.5 km depth and the basement at 4 km with 6.08 km/s velocity in the initial model. A velocity gradient of 0.03 s^{-1} was used for both layers 3 and 4.

The model was extended deeper by including the 6.4 km/s layer which was identified by Dentith (1987) at 8 km depth and which was seen on the LISPB data (Bamford *et al.* 1978). The depth to this layer was compared with a reflection seen on the data recorded from Hillhouse quarry at about 20-40 km offset (Fig. 4.2) and the data recorded from Sheephill (Fig. 4.4). The detection of deeper wide angle reflections in the data permit extending the model further down. For this, the same velocity distribution of the deeper crustal layers was used as in the MAVIS study, because these velocities were

considered to be more reliable than those calculated from the reflections observed in this study.

This model was then adjusted to match the data. Travel times of direct and head waves were modelled to within 0.03 s of observed travel-times. 0.03 s is the uncertainty believed to exist on the picked travel times. For deep reflections a larger discrepancy of 0.10 s was allowed. Discrepancies are listed in Appendix 5.

The final raytracing model of the upper crust beneath the main line is shown in Fig. 4.26. Fig. 4.27 shows the velocity distribution of this model. Fig. 4.28 shows the raypaths of the arrivals used to construct the model. The codes for the ray paths of the entire model are shown in Table 4.2. Note that the lithological interpretation of layer 3 given here is particularly uncertain (see chapter 5).

Table 4.2 Raypath codes.

Symbol	Interpretation
a1	direct arrival through Carb. and Upper ORS
a2	headwaves from Lower ORS
a3	headwaves from ? Lower ORS volcanic ridge (layer 3)
a4	headwaves from the crystalline basement.
a5	reflection from top crystalline basement.
a6	reflection from top middle crust
a7	reflection from within middle crust.
a8	deeper reflection from within mid-crust.
a9	reflection from the top of the lower crust.

The final model derived by raytracing shows no big changes for layer 1 and layer 2 from Hillhouse and Loanhead. In the raytracing model, the same velocity of layer 2 was applied initially for the whole line. This gave a good agreement of the arrival times of headwaves from the second and third layers from all the shots, except that arrivals from layer 3 show a consistent delay of 0.1 s in the data recorded from Sheephill. To remove this delay a higher velocity was applied in the northern part of layer 2. Minor adjustments had to be made to the top of layer 2 in the north to refit layer 2 head waves from Sheephill.

The change of velocity was best modelled as occuring across the PR. A number of observations suggest strike slip movement at the Paisley Ruck. Cotton (1969) found that the thickness of the Clyde Plateau Lavas changes across the fault and he suggested the PR brought different lava thicknesses into juxtaposition. Read (1989) suggested that the PR is a strike slip fault, its movement being pre-late Carboniferous. Dentith (1987) suggested that the Lower ORS is not uniform, with the seismic velocity being higher in the north due, he proposed, to the presence of Lower ORS lavas. Strictly, Dentith's increased velocity was applied to his entire undifferentiated Lower ORS/Lower Palaeozoic layer, although the Lower ORS is probably dominant in this layer. So the raytrace modelling of layer 2 in this study shows some support for strike slip movement along the PR, from the modelling of a lateral velocity change at the fault. Dentith's explanation of the change is considered to be reasonable.

An alternative explanation of velocity change, however, is that there was a highland to the south of the PR which separated two Lower ORS depositional basins. Haughton (1989), through his map of the Lower ORS deposition, shows that major channels flowed parallel and near to the PR (see Fig. 1.7). This may support the model that the area immediately to the south of the PR was highland (specifically a volcanic ridge which may be our layer 3) during that time.

Layer 3 occurs at 2 km depth in between the DWF and PR and extends down to rest on the crystalline basement at 3.6-4.0 km, a thickness of 2 km. It has a velocity of about 5.8 km/s. A velocity gradient of 0.03 s^{-1} was used for this layer.

Previous studies showed that crystalline basement has a velocity of 5.99-6.05 km/s. This layer was found to have the same range of velocity in this study. A velocity gradient of 0.03 s^{-1} was used for this layer, as in the MAVIS project. Previous studies of Davidson (1986) and Dentith (1987) showed that this layer is not affected by any faulting and there is no correlation between the near surface structure and the basement. This study shows that the basement is affected by some faults, specifically the DWF, PR, Gartness Fault, which are also important features at surface.

The model shows that the basement lies at 4 km in the south and it has a small step up to the north at the DWF. Another step of about 0.2 km up to the north again is clear under the PR and at this range the basement occurs

at about 3.5 km depth. The raytrace modelling shows a step of about 0.6 km up to the north beneath Gartness Fault (see Fig. 4.28).

Reflectors were modelled at 8, 12, 15 and 20 km depth. The reflector at 8 km is considered to be the top of the mid-crust and is the top of the 6.4 km/s layer seen in other studies. The two reflectors at 12 and 15 km depth are considered as intra mid-crust reflectors. The reflector at 20 km, also seen by the MAVIS experiment, may represent the top of the lower crust. Fig. 4.29 shows the velocity distribution of the entire main line model down to 20 km depth. Fig. 4.30 shows the reflection raypaths used to construct deeper parts of the model along the model. Synthetic data were created from the model (Fig. 4.31). Some reflections are clear, but others are not clear on the synthetic data due to their small amplitudes.

The synthetic data show that the model can be improved, by giving greater attention to details of layers (e.g. velocity gradients). However, the main features of the model are considered to be very robust.

HK line

The data obtained from the HK profile show only 2 layers as first arrivals due to the small length of the line. Layer 1 has a velocity of 3.5-4.6 km/s, the same as the main line. The thickness of this layer is less than 1 km and that is in agreement with Davidson (1986). The second layer has a velocity of 5.0 km/s obtained from the time-distance graph. The raytrace model shows that the velocity of this layer is about 4.7 km/s at 1 km depth. A velocity gradient of 0.05 s^{-1} was used for this layer, similar to the main line.

The HK line is a short line and does not show first arrival refractions from the deeper layers, but observation of a good reflection permitted modelling of the crystalline basement at 4 km depth, which is the same depth as beneath the southern part of the main line. A similar velocity to the basement on the main line was applied to this line. The data showed the presence of another reflector (a5) at 5.5 km representing an interface of 6.3 km/s. Figs 4.32 & 4.33 show the raytracing section of the HK line and velocity distribution respectively. Fig. 4.34 shows the rays used to construct the model.

Other reflectors were observed on the data similar to those on the main line and these reflectors were included within the model using the same velocity distribution. Synthetic data were plotted for the line to compare with the observed data (Fig. 4.35).. Again, the synthetic data show

that the model can be improved, but the main features are considered to be robust.

4.11 SUMMARY

The data interpretation showed the presence of four upper crustal layers in the area. The first layer represents the Carboniferous and Upper ORS; the second layer represents the Lower ORS; a third layer, which occurs only between the DWF and PR, is most likely due to the presence of a Lower ORS volcanic ridge (see chapter 5) between these two major faults and the fourth layer is crystalline basement. The crystalline basement was affected by faults trending NE-SW and which are seen at the surface.

Wide angle reflections show the presence of a reflector at 8 km depth and that is similar to the third refractor of the LISPB study with a velocity of 6.4 km/s. This interface was also recognised by the MAVIS study and it may represent the top of the middle crust. A reflector at 20 km, considered as the top of the lower crust from previous studies, was also observed in this study. Two intra-mid crust reflectors were observed at 12 and 15 km.

CHAPTER FIVE

DISCUSSION AND CONCLUSIONS

5.1 INTRODUCTION

This study was a seismic investigation of the upper and mid-crustal layers of the western Midland Valley of Scotland. Specific targets were the relationships of crystalline basement, overlying Carboniferous basins and major NE-SW trending faults seen at the surface. The use of three-component recording and appropriate processing techniques improved the data and some wide-angle reflections were detected. Data were acquired along a reversed, medium length refraction line and a short, unreversed profile. The near vertical reflections from the short line gave more information about the deep layers in the upper and mid-crust. This chapter will concentrate on some arguments about the layers determined and the conclusions of this study.

5.2 DATA ACQUISITION AND PROCESSING

A few general comments can be made. A quarry blast source may distort much useful information, due to the long wavetrain which is generated by the blasting routine may cause events to overlap. However, very good first arrivals were usually obtained and some good S-waves.

The availability of three component data is very useful for the refraction method to study S-wave arrivals and wide angle reflections. More processing can be done by applying the polarization filters on the data and studying particle motions. The data processing showed that the use of the polarization filters is effective for enhancing the data particularly the S-waves. It was demonstrated that, for polarization filtering, a small window length is more effective than a longer one for the picking of the the onset of an arrival.

5.3 SUMMARY OF THE SEISMIC MODEL

The upper crustal layers of the Midland Valley have been studied by many authors. Generally the top layer (1) has been considered to represent the Carboniferous and Upper ORS, layer 2 interpreted as the Lower ORS and/or Lower Palaeozoic, the third layer as the crystalline basement. A deeper higher velocity more basic crystalline layer has also been observed.

The present study shows a good agreement with these velocities. See the solid line of Fig. 5.1. The P-wave velocity of the first layer from the WHB method showed that the P-wave velocity near surface varies from 3.5 km/s in the south to 4.0 km/s in the north due to the presence of igneous rocks. It increases with the depth at different gradients. This layer has a Poisson's ratio of 0.30-0.24. This layer is interpreted as the Carboniferous and Upper ORS. The present thickness of this layer varies from 0-2 km.

Layer 2 has a velocity of 5.0-5.6 km/s. This layer has a higher velocity in the north than in the south. Dentith (1987) reported that the velocity of layer 2 is higher under MAVIS I north than that under MAVIS I south. See Fig. 3.1 for the locations of these lines. Dentith deduced that the Lower ORS in the north is different from that in the south. He suggested that the high velocity of the Lower ORS to the north is due to the presence of more volcanic rock. In this study, this layer is considered as the Lower ORS. The main lateral velocity change is seen to occur across the PR. An alternative explanation of the velocity change is that the Lower ORS was formed in two basins which may have had separate sources.

The data show the presence of a high velocity layer in the middle of the main line between the DWF and PR. Layer 2 occurs elsewhere at these depths. This layer (3) has a velocity of 5.8 km/s and lies at about 2 km depth. This layer was interpreted as Lower Palaeozoic or an ORS volcanic ridge, see below.

Layer 4 which represents the crystalline basement has a velocity of 6.0-6.1 km/s and its top lies at about 4 km depth in the south and shallows to the north. It is affected by major faults which may be correlated with faults at the surface.

A reflector was detected at 5.5 km depth from data of the Hillhouse-Kilmarnock line. It was interpreted as the top of the high velocity crystalline basement with a velocity of 6.3 km/s. The data show the presence of other reflectors at and within the mid-crust. Using the velocity distribution for

below the crystalline basement refractor from the previous studies showed the presence of a reflector at 8 km depth. This reflector occurs at the same depth as the 6.4 km/s refractor on LISPB and MAVIS. Wide angle reflections show two reflectors within the mid crust at 12 and 15 km depth. The top of the lower crust occurs at 20 km. It is clear that near vertical reflections from quarry blasts can provide reasonably good quality data from deeper crustal layers using a short line length with a relatively small receiver interval.

5.4 GEOLOGICAL DISCUSSION OF UPPER LAYERS

By upper layers we mean layers 1-3, which are interpreted to be rocks above crystalline basement. The thickness of the first layer is seen to vary significantly in the final raytracing model. The Gartness Fault, Paisley Ruck and Dusk Water Fault cross the main profile and are the main controls on the thickness. The variable thickness of this layer is not just seen along the main line, where it is interpreted as due to the presence of the faults, but the data on the HK line show a different thickness of layer 1 (less than 1 km) to that of the main profile near by. The cross section on the geological map (Ayrshire sheet) shows variable thicknesses of the Carboniferous strata. Most of the layers show thinning southward toward the Inchgotrick Fault, which is just south of the HK line. It is considered the main reason why the overall thickness of layer 1 to the north along the main line is different to that on the HK line.

The second layer (Lower ORS) is also affected by the DWF and PR. The thickness of this layer is about 1 km between these two faults, but 2-3 km beneath the rest of the main line. This suggests either this area was a high during most of the Lower ORS, or that this zone suffered vertical movement before Upper ORS times. The Lower ORS crops out to the north of the Clyde. The Lower ORS outcrop is bounded by the Inchmurrin Fault to the north, an element of the Highland Boundary Fault system, and to the south by the Gartness Fault. During the Lower Devonian the Greenock area was part of a major north-east-trending subsiding basin centered on the Midland Valley and it has been suggested that these basins were involved in strike slip movement along the Highland Boundary Fault system (Paterson *et al.* 1990). A minimum thickness of 2 km can be estimated for the Lower ORS (Paterson *et al.* 1990). The thickness of 3.0 km derived in this study revises the minimum estimate of Paterson *et al.*

The Lower ORS shows an increase in velocity to the north. The implications of this regarding increased volcanics in the northern Lower ORS and/or separate sedimentary basins are explained in section 5.3.

The data recorded along the HK line show that the Lower ORS lies at less than 1 km depth. The rocks at the surface in this area are Upper Carboniferous as along the main profile north of Hillhouse. As mentioned earlier, this suggests stratigraphic thinning of layer 1 south toward the Inchgotrick Fault.

This study indicated the presence of a local high velocity in the area between the DWF and PR. This is the layer 3 of this study with a velocity of 5.8 km/s and its top lies between 2.0 and 2.5 km depth. The Lower ORS (layer 2) occurs at either side of the high velocity block, separated from it by the DWF and PR, and is thinned over layer 3. Two hypotheses can be offered regarding the block. It is either Lower Palaeozoic sediments, or a Lower ORS volcanic ridge. The latter is preferred.

1- Lower Palaeozoic: previous workers interpreted layer 2 as Lower ORS and/or Lower Palaeozoic rocks giving no seismic indication about the thickness of the Lower ORS itself. Some geological studies estimate that the thickness of the Lower ORS is more than 2 km in the north west of the Midland Valley. Qureshi (1970) estimated the thickness of the Lower ORS to be 1.5-1.8 km near Loch Lomond based on gravity work. Most of the seismic studies estimated that the velocity of this layer is between 5.0-5.6 km/s and they used these velocities for raytrace modelling. The higher velocity of our layer 3 means we are probably dealing with a different layer. Our knowledge about the crystalline basement is that it is Precambrian, but the oldest rocks seen at the surface in the area are Silurian and Ordovician. Kamaliddin (pers. comm.) found no significant difference in the velocity of the Lower ORS and Silurian-Ordovician in this region and their velocities are much less than 5.8 km/s, so they are not layer 3. The presence of layer 3 above crystalline basement and below a (thinned) layer 2 would suggest a lowermost Palaeozoic age. There is no evidence of its nature. The presence of this layer only between the DWF and PR (and blocks of thicker layer 2) needs explaining. The PR may represent a strike slip fault (Cotton 1968 Read 1989). The DWF is considered to have been an active fault in the Carboniferous (and Devonian?), and it had a big role in control of the Carboniferous sedimentary deposition and distribution of the Carboniferous

igneous rocks. The limited presence of layer 3 in this location suggests that these three blocks were not adjacent to each other at pre-Devonian times.

2- Igneous ridge: the alternative interpretation for this layer is that it represents the Ayr-Ochil-Sidlaw volcanic ridge proposed by Bluck (1985). He considered that in late Silurian-early Devonian (Lower ORS) times there were two basins on either side of this ridge. Both basins, the Strathmore Basin in the north and the Lanark in the south, were flanked by the volcanic ridge which supplied sediments to the north and the south. Haughton (1989) also pointed to the existence of this volcanic ridge (see Fig. 1.7). In the seismic data, the 5.8 km/s is the highland built up of volcanics.The Lower ORS sedimentary layer (our layer 2) is thinned over this body, perhaps showing sedimentation on the ridge after volcanic activity had stopped and the adjacent basins were filled. Haughton (1989) considered that this ridge is possibly ephemeral, but our geophysical experiment shows the ridge to be of a significant size. It is worth emphasising that the ridge is Lower ORS in age which means that the volcanic activity of this ridge increased the velocity of the Lower ORS in this area. That is, the part of the Lower ORS affected by the igneous activity is recognised in this study as layer 3.

5.5 RELATION BETWEEN THE BASEMENT AND UPPER LAYERS

The velocity and depth of crystalline basement is in good agreement with previous studies. Davidson (1986) and Dentith (1987) suggested that this layer is approximately horizontal, that it is not significantly affected by any faults, and there is no simple comparison of the top basement structure with structures seen in the overlying layers. They suggested that the major faults in the Midland Valley sole out at the top of the basement or within their layer 2 (Lower ORS/Lower Palaeozoic). This study shows the presence of big faults in the basement and all these faults have some manifestation at the surface: the Dusk Water Fault, Paisley Ruck and Gartness Fault.

5.6 ROLE OF MAJOR FAULTS

An important feature of the western Midland Valley is the presence of large NE-SW faults. These faults played important roles in the deposition and distribution of the Carboniferous rocks in the area. Many geological studies

have been undertaken to investigate these faults regarding their active times and their relation with the other faults in the Midland Valley. Many hypotheses were given about the fault system of the Midland Valley. These hypotheses range between vertical movement, strike-slip movement, and the combination of the strike-slip and the vertical movements. Cotton (1968), Read (1989) considered the PR as a strike slip fault. Gibbs (1984) interpreted ESE-WNW alignments of minor faults on either side of the Paisley Ruck to resemble a pattern of Riedel Shear and extensional fractures created by right-lateral strike slip, and he considered the Paisley Ruck as a positive flower structure produced by right-lateral transpression. Read (1989) considered the lineament which extends WSW below the eastern part of the Milngavie-Kilsyth Fault to underlie the Paisley Ruck, and it may have been initiated as a Riedel Shear by right-lateral strike slip along the Highland Boundary Fault, or it may reflect a reactivated Late-Caledonian left-lateral strike slip fault system.

Dentith (1987) considered that many Midland Valley faults are soling out within the Lower ORS or Lower Palaeozoic or at the basement top. Paterson *et al.* (1990) described some faults having a vertical movement, such as the Inchmurrin Fault.

This study shows that the DWF and PR affect layers 1 and 2, bound layer 3 and have some vertical displacement on the basement. The lateral Lower ORS velocity changes across the PR supports that this fault a strike slip fault as suggested by Dentith (1987) and Read(1989). Whether these faults initiated in the basement and later reactivated to affect the above layers or if they initiated later and affected both the basement and the above layers, is not certain.

The strike of these faults suggest that they are Caledonide. If so, then the interpretation of layer 3 as lowermost Palaeozoic implies significant pre-Upper ORS strike slip on these faults (see section 5.4) with some possible pre-Upper ORS vertical faulting to thin the Lower ORS above layer 3. If, however, layer 3 is a Lower ORS volcanic ridge then its location may be due to the presence of these Caledonide faults. They could have acted as magma supply routes. Later reactivation controlled the Upper ORS/Carboniferous deposition.

If they are not Caledonian faults, then other possibilities arise depending on the nature of layer 3. If layer 3 is lowermost Palaeozoic, they originated during the Lower ORS to control layer 3 as a highland between

two basins, later reactivating in the Upper ORS and Carboniferous. If layer 3 is an ORS volcanic ridge, the faults may have developed in the Upper ORS/Carboniferous along planes of weakness at the sides of the ridge.

The model that would be prefered by most geologists is that the faults are Caledonian, that the volcanic ridge may be located due to them and that they reactivated to control Upper ORS and Carboniferous sedimentation. The deeper extent of the effects of the NE-SW faults crossed in this study supports the view from geological studies that the faults were the main controls on Carboniferous sedimentation in the western Midland Valley.

There is another fault on the basement showing a downthrow of about 0.8 km to the south, located north of the Clyde. The raytracing shows that this step correlates with a major fault at surface (the Gartness Fault). This fault separates the Upper and Lower ORS. The thickness of the Lower ORS estimated by gravity method is about 1.5-1.8 km near Loch Lomond (Qureshi 1970), this layer is exposed at the surface. The BGS report of the Greenock District (Paterson *et al.* 1990) shows that the thickness of the Lower ORS is thicker than that, being a minimum of 2.0 km.

The presence of a fault at the surface which shows no effect on a refractor may be interpreted that the fault soles out at a shallower depth than the refractor. For example, a fault to the north of the PR and south of the Clyde shows an effect on the top refractor only. Note that this fault cannot be correlated with any particular fault of the many that cross the main line in this area. The behaviour of this fault agrees with previous ideas of the depth of effect of faults in the Midland Valley (Dentith 1987). The major faults crossed by the main line have a NE-SW trend and show a vertical movement effect at the basement.

In the MAVIS study Dentith did not recognise the vertical movement of the basement. He used this to say that the tectonics controlling Carboniferous basins were thin-skinned, the faults soling out at or above the top of crystalline basement. The results of the main profile are against this. However, most of the MAVIS profiles did not cross NE-SW faults.

The geology of the Midland Valley shows the direction of the faults relates to their ages. The Caledonide faults show a NE-SW trend whereas the Carboniferous faults show an E-W trend which changed to NW-SE during Permian times. The direction change of these faults was due to the change of the stress direction at that time.

A look at the NE-SW faults shows that these faults have a vertical movement. This is very clear on the Gartness Fault. During the Middle Devonian compressive movement caused folding of the Lower Devonian rocks in a NE-SW trend and major thrust movement of elements of the Highland Boundary system. An especially large displacement on the South Inchmurrin Fault caused the erosion of any Lower Devonian rocks that may have been deposited to the north (Paterson *et al.* 1990). In our data we have a similar vertical movement to the north beneath the Gartness Fault.

The Paisley Ruck was considered as a strike slip fault (Cotton 1968, Read 1989) and this study shows that it has some vertical movement. In this case, it may be that some of the faults have a combination of strike slip and vertical movement. Paterson *et al.* (1990) reported that a series of NNE-SSW faults displaced the rocks in the axial zone of the Aberfoyle Anticline, and appear to combine sinistral strike-slip movement with vertical displacement.

It is argued that Dentith did not obtain a complete view of the upper crustal tectonics from the MAVIS experiment. From our study I suggest that the older Caledonide faults were reactivated to give vertical movement on the basement as a result of oblique stresses on them during the Upper ORS/Carboniferous strike-slip regime. Other faults that sole out in the sedimentary cover were either created at this time, or are old faults which were in the wrong orientation to be reactivated with any vertical movement. It is clear that the Midland Valley has a very complicated fault system.

5.7 SUMMARY OF CONCLUSIONS

This study has shown that the upper crust of the western Midland Valley consists of 4 layers as follows:

1- Layer 1 : this layer is the Carboniferous and Upper ORS. This layer has a velocity of 3.5-4.6 km/s and it has a lateral velocity variation due to the its complex basins and the presence of the Clyde Plateau Lavas. Thickness of this layer ranges from 0-2 km.

2- Layer 2 : this layer has a velocity of 5.2-5.6 km/s in the southern part, but it shows higher velocity to the north of the PR. The thickness of this layer

ranges from 1-3 km. The lateral velocity change is due to an increase of volcanic rocks in the northern part of the sequence, or a difference in the source composition of the sediments in the north and south.

3- Layer 3 : this layer shows the presence of higher velocity of 5.8 km/s above the crystalline basement. It is a Lower ORS volcanic ridge or lowermost Palaeozoic sediments. The ridge idea is preferred because it agrees with recent geological hypotheses.

4- Layer 4 : this layer represents the crystalline basement, it has a velocity of 6.0-6.1 km/s and its top occurs at a depth of 3-4 km.

High velocity crystalline basement of 6.4 km/s which was detected in the LISPB and MAVIS study is observed in this study from wide-angle reflections in the data. It is the top of the middle crust at 8 km depth. Reflections from the mid-crust are observed at 12 and 15 km depth and from the top of the lower crust at 20 km.

The data show the effects of some large faults. The faults which are observed on the data are very obvious at the surface, such as the DWF and PR. These two faults show some effect on layers 1 and 2 and they bound layer 3 and they have affected the crystalline basement. The two faults show a big throw on layer 1 of about 0.8 km. Their effect at the basement ranges from 0.2-0.4 km. The data show a big step of the basement in the north and this step is correlated with the Gartness Fault at the surface.

So the crystalline basement is affected by some faults in contrast to what is suggested by previous work. This may be due to this study being in a different area. It is suggested, however, that the reason may be that this is the first study to have sampled in detail across NE-SW trending Caledonian faults in the Midland Valley.

It is clear that the fault pattern in the upper crust of the Midland Valley is nore complex than was previously thought.

5.8 RECOMMENDATIONS FOR FURTHER WORK

There are some points that arise from this study regarding data acquisition and processing, as well as possible targets for further work. These points are:

1- The use of more sophisticated equipment, or to modify the present equipment, to record the three components on the same recorder. This would reduce the uncertainty of combining the three components, arising from variations of recording speed in the field and uncertainty in the time signal.

2- Using more three component records could help to obtain more information about the nature of the Midland Valley layers, by applying the polarization technique and studying the S-waves behaviour.

3- Further work could be undertaken on the S-wave actually obtained in this study, leading to a possible S-wave velocity model.

4- More concentrated lines should be recorded across the Paisley Ruck to study the velocity changes on both sides.

5- More lines are needed to cross the probable Lower ORS igneous ridge to study its behaviour along the Midland Valley and see if it is the Ayr-Ochil-Sidlaw structure.

6- The extension of the main profile to the north to study the relation of the HBF and some of the major faults to the south of it.

7- It is time for a thorough review to be made of the significant number of seismic experiments undertaken in the Midland Valley. Particularly since this study, and that of Kamaliddin (1991), show significant faulting of the crystalline basement that was previously not fully recognised.

REFERENCES

AL-MANSOURI, D. 1986. Seismological studies of upper crustal structure in the vicinity of the Girvan-Ballantrea Area, SW Scotland. *Ph.D. thesis (unpubl.), University of Glasgow.*

ALI, M. 1983. Study of shear wave velocities in the Lewisian metamorphic complex of NW Scotland. *Ph.D thesis (unpubl.), University of Glasgow.*

ALOMARI, M. I. 1980. Geological interpretations of the gravity field of the western Midland Valley of Scotland. *Ph.D.thesis (unpubl.), University of Glasgow.*

ANDERSON, F. M. 1951. The dynamics of faulting. 2nd ed. Oliver & Boyd.

ANDERSON, F. W. 1963. The geological survey bore at Rashiehill, Stirlingshire. *Bull. Geol. Surv. G.B.*, **20**, 43-106.

ARCHAMBEAU, C. B. & FLINN, E. A. 1965. Automated analysis of seismic radiation for source characteristics. *IEEE*, **53**, 1876-1844.

ARMSTRONG, M. & PATERSON, I. B. 1970. The Lower Old Red Sandstone of the Strathmore region. *Rep. Inst. Geol. Sci.* **70/12.**

ASSUMPCAO, M. & BAMFORD, D. 1978. LISPB-V studies of crustal shear waves. *Geophys. J. R. astr. Soc.*, **54**, 61-73.

ASSUMPCAO, M. S. 1978. Studies of crustal shear waves and Poisson's Ratio. *Ph.D thesis (unpubl.), University of Edinburgh.*

BACHMAN, R. T. 1979. Acoustic anisotropy in marine sediments and sedimentary rocks. *J. Geophys. Res.*, **84**, 7661-7663.

BAMFORD, D., FABER, S., JACOB, B., KAMINSKI, W., NUNN, K., PRODEHL, C., FUCHS, K., KING, R. & WILLMORE, P. 1976. A lithospheric seismic profile in Britain - I. Preliminary results. *Geophys. J. R. astr. Soc.*, **44**, 145-160.

BAMFORD, D., NUNN, K., PRODEHL, C. & JACOB, B. 1977. LISPB-III. upper crustal structure of Northern Britain. *J. Geol. Soc. Lond.*, **133**, 481-488.

BAMFORD, D., NUNN, K., PRODEHL, C. & JACOB, B. 1978. LISPB-IV. crustal structure of Northern Britain. *Geophys. J. R. astr. Soc.*, **54**, 43-60.

BARRETT, T. J., JENKYNS, H. C., LEGGETT, J. K. & ROBERTSON, A. H. F. 1982. Comment and reply on 'Age and origion of Ballantrae ophiolite and its significance to the Caledonian orogeny and the Ordovician time scale'. *Geology*, **9**, 331-333.

BLUCK, B. J. & HALLIDAY, A. N. 1982. Comment and reply on 'Age and origin of Ballantrae ophiolite and its significance to the Caledonian orogeny and Ordovician time scale'. *Geology*, **9**, 331-333.

BLUCK, B. J. 1967. Deposition of some Upper Old Red Sandstone conglomerates in the Clyde area: A study in the significance of bedding. *Scot. J. Geology*, **3**, 139-167.

BLUCK, B. J. 1978. Sedimentation in a late orogenic basin: the Old Red Sandstone of the Midland Valley of Scotland. In: BOWES, D. R. & LEAKE, B. E. (Eds) Crustal evolution in northwestern Britain and adjacent regions. *Geol. J. Spec. Issue*, **10**, 249-278.

BLUCK, B. J. 1983. Role of the Midland Valley of Scotland in the Caledonian orogeny. *Trans. R. Soc. Edin.*, **74**, 119-136.

BLUCK, B. J. 1984. Pre-Carboniferous history of the Midland Valley of Scotland. *Trans. R. Soc. Edin.*, **75**, 275-295.

BLUCK, B. J. 1985. The Scottish Paratectonic Caledonides. *Scott. J. Geol*, **21**, 437-464.

BLUCK, B. J., HALLIDAY, A. N., AFTALION, M. & MacINTYRE, R. M. 1980. Age of Ballantrae ophiolite and its significance to the Caledonian orogeny and the Ordovician time scale. *Geology*, **8**, 492-495.

BOOTH, D. C. & CRAMPIN, S. 1985. Shear-wave polarizations on a curved wavefront at an isotropic free surface. *Geophys. J. R. astr. Soc.*, **83**, 31-45.

BOOTH, D. C., CRAMPIN, S. & CHESNOKOV, E. M. 1987. Preface: proceedings of the second international workshop on seismic anisotropy. *Geophys. J. R. astr. Soc.*, **91**, 261-263.

BOTT, M. H. P., SWINBURNE, P. M. & LONG, R. E. 1984. Deep structure and origin of the Northumberland and Stainmore Troughs. *Proc. York. Geol. Soc.*, **44**, 479-495.

CAMERON, I. B. & STEPHENSON, D. 1985. The Midland Valley of Scotland. *British Geological Survey, Third edition.*

CARLSEN, R. L. & CHRISTENSEN, N. I. 1979. Velocity anisotropy in semi-indurated calcareous deep sea sediments. *J. Geophys. Res.*, **84**, 205-211.

CERVENY, V., LANGER, J. & PSENCIK, I. 1974. Computation of geometric spreading of seismic body waves in laterally inhomogeneous media with curved interfaces. *Geophys. J. R. astr. Soc.*, **38**, 9-20.

CHRISTENSEN, N. I. & FOUNTAIN, D. M. 1975. Constitution of the lower continental crust based on experimental studies of seismic velocities in granulite. *Geol. Soc. Am. Bull.*, **86**, 227-236.

CHURCH, W. R. & GAYER, R. A. 1973. The Ballantrae ophiolite. *Geol. Mag.*, **110**, 497-510.

COCKS, L. R. M. & TOGHILL, P. 1973. Biostratigraphy of the Silurian of Girvan. *Quart. J. Geol. Soc. Lond.*, **129**, 209-243.

CONWAY, A., DENTITH, M. C., DOODY, J. J. & HALL, J. 1987. Preliminary interpretation of upper crustal structure across the Midland Valley of Scotland from two East-West seismic refraction profiles. *J. Geol. Soc. Lond.*, **144**, 865-870.

COTTON, W. R. 1968. A geological survey of the Campsie and Kilpatrick Hills. *Ph.D. thesis (unpubl.), University of Glasgow.*

CRAMPIN, S. 1977. A review of the effects of anisotropic layering on the propagation of seismic waves. *Geophys. J. R. astr. Soc.*, **49**, 9-27.

CRAMPIN, S. 1981. A review of wave motion in anisotropic and cracked elastic-media: *Wave Motion*, **3**, 343-391.

CRAMPIN, S. 1985. Evaluation of anisotropy by shear-wave splitting. *Geophysics*, **50**, 142-152.

CRAMPIN, S., BOOTH, D. C., KRASNOVA, M. A., CHESNOKOV, E. M., MAXIMOV, A., B. & TARASOV, N. T. 1986. Shear-wave polarizations in the Peter the First range indicating crack-induced anisotropy in a thrust -fault regime. *Geophys. J. R. astr. Soc.*, **84**, 401-412.

CRAMPIN, S., CHESNOKOV, E. M. & HIPKIN, R. G. 1984. Seismic anisotropy - the state of the art: II. *Geophys. J. R. astr. Soc.*, **76**, 1-6.

CRAMPIN, S., JACOB, A. W. B., MILLER, A. & NEILLSON, A. 1970. The LOWNET radio-linked seismometer network in Scotland. *Geophys. J. R. astr. Soc.*, **21**, 207-216.

CURRY, G. B., BLUCK, B. J., BURTON, C. J., INGHAM, J. K., SIVETER, D. J. & WILLIAMS, A. 1984. Age, evolution and tectonic history of the Highland Border Complex, Scotland. *Trans. R. Soc. Edin.*, **75**, 113-133.

DAVIDSON, K. A. S. 1986. Seismological studies of upper crustal structure of the Southern Midland Valley of Scotland. *Ph.D. thesis (unpubl.), University of Glasgow.*

DAVIDSON, K. A. S., SOLA, M., POWELL, D. W. & HALL, J. 1984. Geophysical model for the Midland Valley of Scotland. *Trans. R. Soc. Edin.*, **75**, 175-181.

DENTITH, M. C. 1987. Geophysical constraints on upper crustal structure in the Midland Valley of Scotland. *Ph.D. thesis (unpubl.), University of Glasgow.*

DEWYEY, J. F. 1971. A model for the Lower Palaeozoic evolution of the Southern margin of the Southern Caledonides of Scotland and Ireland. *Scott. J. Geol.*, **7**, 219-240.

DEWEY, J. F. 1974. Continental margins and ophiolite obduction: Appalachian Caledonian Systems. In Burk, C.A. & DRAKE, C. L. (eds). *Geology of Continental Margins*, 933-950, Springer-Verlag, New York.

DEWEY, J. F. 1982. Plate Tectonics and the evolution of the British Isles. *J. Geol. Soc. Lond.*, **139**, 371-414.

DIEBOLD, J. B. & STOFFA, P. L. 1981. The traveltime equation, tau-P mapping, and inversion of common midpoint data. *Geophysics*, **46**, 238-254.

DOBRIN, M. B. 1976. *Introduction to geophysical prospecting.* McGRAW HIL, NEW YORK.

DOMENICO, S. N. 1984. Rock lithology and porosity determination from shear and compressional wave velocity. *Geophysics*, **49**, 1188-1195.

DOODY, J. J. 1985. Deep crustal seismic studies of Southwest Britain. *Ph.D. thesis (unpubl.), University of Wales.*

ELDERS, C. F. 1987. The provenance of granite boulders in conglomerates of the Northern and Central Belts of the Southern Uplands of Scotland. *J. Geol. Soc. Lond.*, **144**, 853-864.

EYLES, V. A., SIMPSON, J. B. & MacGEGOR, A. G. 1949. The geology of central Ayrshire. *Mem. Geol. Surv. U.K.*

FLINN, E. A. 1965. Signal analysis using rectiliniarity and direction of particle motion . *Proceedings of the IEEE*, **53**, 1874-1876.

FRANCIS, E. H. 1968. Review of Carboniferous-Permian volcanicity in Scotland. *Geologische Rundschau*, **57**, 219-247.

FRANCIS, E. H., FORSYTH, F. H., READ, W. A. & ARMSTRONG, M. 1970. The Geology of the Stirling district. *Mem. Geol. Surv. G. B.*

FRANCIS. E. H. 1983. Carboniferous. In: CRAIG, G. Y. (Ed), *Geology of Scotland*, 253-296. Scottish Academic Press.

FRIEND, P. F. & MacDONALD, R. 1968. Volcanic sediments, stratigraphy and tectonic background of the Old Red Sandstone of Kintyre, W. Scotland. *Scott. J. Geol.*, **4**, 265-282.

GEORGE, T. N. 1960. The Stratigraphical evolution of the Midland Valley. *Trans. Geol. Soc. Glasg.*, **24**, 33-107.

GIBBS, A. D. 1984. Structural interpretation with emphasis on extensional tectonics, *Part 2, J. A. P. E. C. Course Notes*, **28.**

GIBBS, A. D. 1987. Developments of extension and mixed-mode sedimentary basins. In COWARD, M. P., DEWEY, J. F. & HANCOCK, P. L. (eds.) continental extensional tectonics. *Spec. Publ. Geol. Soc. Lond.* **28**, 19-33.

HAGEDOORN, J. G. 1959. The Plus-Minus method of interpreting seismic refraction sections. *Geophys. prosp.*, **7**, 158-183.

HALL, D. H. & DAGLEY, P. 1970. Regional magnetic anomalies: an analysis of the smoothed aeromagnetic map of Great Britain and Northern Ireland. *Rep. Inst. Geol. Sci.*, **70/10**.

HALL, J. & AL-HADDAD, F. M. 1979. Variation of effective seismic velocities of minerals with pressure and its use in velocity prediction. *Geophys. J. R. astr. Soc.*, **57**, 107-118.

HALL, J. & ALI, M. 1985. Shear waves in a seismic survey of Lewisian basement: an extra control on lithological variation and porosity. *J. Geol. Soc., Lond.*, **142**, 677-688.

HALL, J. 1970. The correlation of the seismic velocities with formations in the South-West of Scotland. *Geophys. Prosp.*, **18**, 134-148.

HALL, J. 1974. A seismic reflection survey of the Clyde Plateau Lavas in North Ayrshire and Renfrewshire. *Scott. J. Geol.*, **9**, 253-279.

HALL, J. 1978. 'LUST' - a seismic refraction survey of the Lewisian basement complex in NW Scotland. *J. Geol. Soc., Lond.*, **35**, 555-563.

HALL, J., BREWER, J. A., MATTHEWS, D. H. & WARNER, M. R. 1984. Crustal structure across the Caledonides from the 'WINCH' seismic reflection profile; influences on the evolution of the Midland Valley of Scotland. *Trans. R. Soc. Edin.*, **75**, 97-109.

HALL, J., POWEL, D. W., WARNER, M. R., EL-ISA, Z. H. M., ADESANYA, O. & BLUCK, B. J. 1983. Seismological evidence for shallow crystalline basement in the Southern Uplands of Scotland. *Nature*, **305**, 418-420.

HARTE, B., BOOTH, J. E., DEMPSTER, T. J., FETTES, D. J., MENDUM, J. R. & WATTS, D. 1984. Aspects of the post-deposition and evolution of

Dalradian and Highland Border Complex rocks in the Southern Highlands of Scotland. *Trans. R. Soc. Edin.*, **75**, 151-163.

HASZELDINE, R. S. 1987. British Isles Carboniferous sediments viewed in an Atlantic rift setting. In: KELLING, G. & BESLEY, B. M. (Eds), *Sedimentation in a synorogenic Basin Complex: the Upper Carboniferous of North-West Europe.* Blackie.

HATTON, L., WORTHINGTON, M. H. & MAKIN, J. 1986. *Seismic data processing: Theory and Practise.* Blackwell Scientific Publications.

HAUGHTON, P. D. W. & BLUCK, B. J. 1989. Contrasting alluvial sequences in the Lower Old Red Sandstone of the Strathmore Region, Scotland. Implications for the relation between late Caledonian tectonics and sedimentation. *Preceedings of the Second International Symposium on the Devonian System, Calgary, Alberta.*

HAUGHTON, P. D. W. 1986. The sedimentology and provenance of the Dunnotar and Crawton Group, Lower Old Red Sandstone, Kincardineshire, Scotland. *Ph.D. thesis (unpubl.), University of Glasgow.*

HAUGHTON, P. D. W. 1988. A cryptic Caledonian flysh terrane in Scotland. *J. Geol. Soc. Lond.*, **145**, 685-704.

HAUGHTON, P. D. W. 1989. Structure of some Lower Old Red Sandstone conglomerates, Kincardineshire, Scotland: deposition from late-orogenic antecedent streams? *J. Geol. Soc. Lond.*, **146**, 509 -525.

HENRY, W. J. 1987. A seismic investigation of the Kenya Rift Valley. *Ph.D. thesis (unpubl.), University of Leicester.*

HOSSAIN, M. M. A. 1976. Analysis of the major gravity and magnetic anomalies centred about Bathgate, central Scotland. *M.Sc. thesis (unpubl.), University of Glasgow.*

HUTTON, D. H. W. 1987. Strike-slip terranes and a model for the evolution of the British and Irish Caledonides. *Geol. Mag.*, **124**, 405-425.

HUTTON, V. R. S., INGHAM, M. R. & MBIPOM, E. W. 1980. An electrical model of the crust and upper mantle in Scotland. *Nature*, **287**, 30-33.

INGHAM, J. K. 1978. Geology of a continental margin 2: middle and late Ordovician transgression, Girvan. In BOWES, D. R. & LEAKE, B. E. (eds), Crustal evolution in northwestern Britain and adjacent regions, *Geol. J. Spec. Issue*, **10**, 163-176.

INGHAM, M. R. & HUTTON, V. R. S. 1982a. Crustal and upper mantle electrical conductivity structure in Southern Scotland. *Geophys. J. R. astr. Soc.*, **69**, 579-594.

INGHAM, M. R. & HUTTON, V. R. S. 1982b. The interpretation and tectonic implications of the geoelectric structure of Southern Scotland. *Geophys. J. R. astr. Soc.*, **69**, 595-606.

JOHNSON, S. H. 1976. Interpretation of split-spread refraction data in terms of plane dipping layers. *Geophysics*, **41**, 418-424.

JONES, A. G. & HUTTON, V. R. S. 1979a. A multi-station magnetotelluric study of Southern Scotland- I. Fieldwork, data analysis and results. *Geophys. J. R. Astr. Soc.*, **56**, 329-349.

JONES, A. G. & HUTTON, V. R. S. 1979b. A multi-station magnetotelluric study of Southern Scotland - II. Monte-Carlo inversion of the data and its geophysical and tectonic implications. *Geophys. J. R. Astr. Soc.*, **56**, ,351-368.

KAMALIDDIN, Z. A. R., 1991. Seismic interpretation of the Southern Uplands Terrane. *Ph.D. thesis (unpubl.), University of Glasgow.*

KANASWICH, E. R. 1981. *Time sequence analysis in Geophysics.* University of Alberta Press.

KEAREY, P. & BROOKS, M. 1984. *An Introduction to Geophysical Exploration.* Blackwell Scientific Publications.

KENNEDY, W. Q. 1958. The tectonic evolution of the Midland Valley of Scotland. *Trans. Geol. Soc.*, **23**, 106-133.

LEEDER, M. R. 1976. Sedimentary facies and the origin of basin subsidence along the Northern margins of the supposed Hercynian Ocean. *Tectonophysics*, **36**, 167-179.

LEGGETT, J. K. 1980. The sedimentological evolution of a Lower Palaeozoic accretionary fore-arc in the Southern Uplands of Scotland. *Sedimentology*, **27**, 401-417.

LEWIS, T. R. & MEYER, R. P. 1968. A seismic investigation of the upper mantle to the west of Lake Superior. *Bull. Seism. Soc.*, **58**, 565-596.

MACBETH, C. D. & BURTON, P. W. 1985. Upper crustal shear velocity models from higher mode Rayleigh wave dispersion in Scotland. *Geophys. J. R. astr. Soc.*, **83**, 519-539.

MACDONALD, J. G. 1973. The Campsie and Lennoxtown district. In: BLUCK, B. J. (Ed), Excursion guide to the geology of the Glasgow District. 60-65. *Geol. Soc. of Glasgow.*

McCOLLUM, B. & SNELL, F. A. 1932. A symmetry of sound velocity in stratified formations. In: *Early Geophysical papers, S. E. G., Tulsa.*

McKERROW, W. S. & ELDERS, C. F. 1989. Movements on the Southern Upland Fault. *J. Geol. Soc. Lond.*, **146**, 393-395.

McLEAN, A. C. & DEEGAN, C. E. 1978. The solid geology of the Clyde sheet. *Rep. Inst. Geol. Sci.*, **78/9**.

McLEAN, A. C. & QURESHI, I. R. 1966. Regional gravity anomalies in the Western Midland Valley of Scotland. *Trans. R. Soc. Edin.*, **66**, 267-283.

McLEAN, A. C. & WALKER, A. E. 1978. The solid geology of the Clyde sheet. *Rep. Inst. Geol. Sci.*, **78/9**.

McLEAN, A. C. & WREN, J. 1978. The solid geology of the Clyde sheet. *Rep. Inst. Geol. Sci.*, **78/9**.

McLEAN, A. C. 1961. Density measurement of rocks in Southwest Scotland. *Trans. R. Soc. Edin.*, **68**, 103-111.

McLEAN, A. C. 1966. A gravity survey in Ayrshire and its geological interpretation. *Trans. R. Soc. Edin.*, **66**, 239-265.

McLEAN, A. C. 1978. Evolution of fault controlled Ensialic Basins in North-Western Britain. In: BOWES, D. R. and LEAKE, B. E. (Eds), Crustal evolution of North-Western Britain and adjacent regions. *Geol. J. Soc. Lond. Spec. Issue*, **10.**

MIMS, C. H. & SAX, R. L. 1965. "Recilinear motion detection(REMODE)", *Teledyne, Inc., Alexandria, Va., Seismic Data Lab. Rept. 118.*

MITCHELL, A. H. G. & McKERROW, W. S. 1975. Analogous evolution of Burma Orogen and the Scottish Caledonides. *Bull. Geol. Soc. Amer.* **86,** 305-315.

MONTALBETTI, J. F. & KANASEWICH, E. R., 1970. Enhancement of teleseismic body phases with a Polarization filter. *Geophys. J. R. astr. Soc.*, **72**, 119-129.

MYKURA, W. 1960. The Lower Old Red Sandstone rocks of the Pentland Hills. *Bull. Geol. Surv. G. B.*, **16**, 131-155.

MYKURA, W. 1967. The Upper Carboniferous rocks of South-West Ayrshire. *Bull. Geol. Surv. G. B.* **26**, 23-98.

NEIDELL, N. S. & TANER, M. T. 1971. Semblance and other coherency measures for multichannel data. *Geophysics*, **36**, 482-97.

NUTTLI, O., 1961. The effect of the Earth's surface on the S-wave particle motion. *Bull. seism. Soc. Am.*, **51**, 237-246.

O'CONNELL, R. J. & BUDIANSKY, B. 1974. Seismic velocities in dry and saturated cracked solids. *J. Geophys. Res.*, **79**, 5412-26.

O'CONNELL, R. J. & BUDIANSKY, B. 1977. Viscoelastic properties of fluid saturated cracked solids. *J. Geophys. Res.*, **82**, 5719-5735.

OLIVER, G. J. H., SMELLIE, J. L., THOMAS, L. J., CASEY, D. M., KEMP, A. E., EVANS, L. J., BALDWIN, J. R. & HEPWORTH, B. C. 1984. Early Palaeozoic metamorphic history of the Midland Valley, Southern Uplands-Longford-Down massif and the Lake District, British Isles. *Trans. R. Soc. Edin.*, **75**, 245-258.

PATERSON, I. B., HALL, I. H. S. & STEPHENSON, D. 1990. *Geology of the Greenock district.* British Geological Survey.

QURESHI, I. R. 1970. A gravity survey of a region of the Highland Boundary Fault, Scotland. *J. Geol. Soc. Lond.*, **125**, 481-502.

READ, W. A. 1987a. Controls on the Silesian sedimentation in the Midland Valley of Scotland. In: KELLING, G. & BESLEY, B. M. (Eds), *Sedimentation in a synorogenic Basin Complex; The Upper Carboniferous of North-West Europe.* Blackie.

READ, W. A. 1989. Sedimentological evidence for a major subsurface fracture system linking the eastern Campsie and the eastern Ochil faults. *Scott. J. Geol.*, **25**, 187-200.

ROBINSON, E. A. & TREITEL, S. 1980. *Geophysical Signal Analysis.* Prentice-Hall.

ROLFE, W. D. I. 1961. The geology of the Hagshaw Hill Silurian Inlier, Lanarkshire. *Trans. Edin. Geol. Soc.*, **18**, 240-269.

RUSSELL, M. J. 1971. North-South geofractures in Scotland and Ireland. *Scott. J. Geol.*, **8**, 75-84.

SAID, E. K. 1990. Development of seismic velocity analysis software. *M.Sc. thesis (unpubl.), University of Glasgow.*

SCHNEIDER, W. A. & BACKUS, M. M. 1968. Dynamic correction analysis. *Geophysics*, **33**, 105-26.

SHIMSHONI, M. & SMITH, S. 1964. Seismic signal enhancement with three-component detectors. *Geophysics*, **29**, 664-671.

SOLA, M. A. 1985. The seismic structure under the central Midland Valley from refraction measurements. *Ph.D. thesis (unpubl.), University of Glasgow.*

STONE, P. & RUSHTON, A. W. A. 1983. Graptolite faunas from the Ballantrae ophiolite complex and their structural implications. *Scott. J. Geol.*, **19**, 297-310.

TANER, M. T. & KOEHLER, F. 1969. Velocity spectra-digital computer derivation and applications of velocity functions. *Geophysics*, **34**, 859-881.

TATHAM, R. H. 1982. Vp/Vs and lithology. *Geophysics*, **47**, 336-344.

TELFORD, W. M., GELDART, L. P., Sherriff, R. E. & Keys, D. A. 1987. *Applied geophysics*. Cambridge University press

THIRLWALL, M. F. 1983. Discussion on implications for Caledonian plate tectonic models of chemical data from volcanic rocks of the British Old Red Sandstone. *J. Geol. Soc. Lond.*, **140**, 315-318.

TRENCH, A. & HAUGHTON, P. D. W. 1990. Palaeomagnetic and geochemical evaluation of a terrane-linking ignimbrite: evidence for the relative position of the Grampian and Midland Valley terranes in late Silurian time. *Geol. Mag.*, **127**, 241-257.

TRENCH, A., DENTITH, M. C., BLUCK, B. J., WATTS, D. R. & FLOYD, J. D. 1989. Short paper : palaeomagnetic constraints on the geological terrane models of the Scottish Caledonides. *J. Geol. Soc. Lond.*, **146**, 405-408.

UPTON, B. G. J., ASPEN, P. & GRAHAM, A. M. 1983. The upper mantle and crust beneath the British Isles: Evidence from inclusion suites in volcanic rocks. *J. Geol. Soc. Lond.*, **140**, 105-122.

UPTON, B. G. J., ASPEN, P. & HUNTER, R. H. 1984. Xenoliths and their implications for the deep geology of the Midland Valley and adjacent regions. *Trans. R. Soc. Edin.*, **75**, 65-70.

UPTON, B. G. J., ASPEN, P., GRAHAM, A. M. & CHAPMAN, N. A. 1976. Pre-Palaeozoic basement of the Scottish Midland Valley. *Nature*, **269**, 517-518.

WHYTE, M. A. 1981. The Upper Brigantian (Lower Carboniferous) of Central Strathclyde. *Scott. J. Geol.*, **17**, 227-246.

WILLIAMS, A. 1962. The barr and Lower Ardmillian series (Caradoc) of the Girvan District, South-West Ayrshire. *Mem. Geol. Soc. Lond.*, **3**.

YARDLEY, B. W. D., VINE, F. J. & BALDWIN, C. T. 1982. The plate tectonic setting of NW Britain and Ireland in Late Cambrian and Early Ordovician Time. *J. Geol. Soc. Lond.*, **139**, 455-463.

APPENDICES

APPENDIX 1

Receiver coordinates and geophone coupling

Main line

Site	Name	National Grid Easting	Northing	Geophone Coupling
1	Shwalton	34.53	34.60	drift
2	Drybridge	35.05	36.15	drift
3	Dreghorn	34.82	38.28	drift
4	Percton	35.25	40.52	drift
5	West Balgray	35.42	42.56	drift
6	Old mains	35.40	44.42	drift
7	Hill of Fergushill	35.61	46.10	drift
8	Sunnyside	35.82	48.38	drift
9	Nettlehirst House	36.57	50.52	rock
10	Border	36.10	52.26	drift
11	Mid Bogside	36.70	54.28	drift
12	Knowes Farm	36.85	56.46	drift
13	Newtown of Beitrees	37.40	58.10	rock
14	Castle Semple	37.70	60.30	rock
15	High Overton	38.50	62.30	rock
16	Monkland	39.45	63.46	rock
17	Houstonhead Dam	39.50	66.15	rock
18	Chapel Farm	40.86	67.83	rock
19	Boghill Cottage	41.15	69.80	rock
20	Crosshill	42.80	72.02	rock
21	Rigangower Quarry	43.75	75.33	rock
22	Black Linn Reservoir	44.48	76.95	rock
23	Dumbarton Muir	45.33	80.82	rock
24	Wester Cameron	46.22	83.17	drift
25	Low Gartachorrans	47.26	85.72	drift
26	Drumbeg	47.95	88.28	drift
27	Shandon	47.83	89.52	rock
28	Bat a Charchel	49.22	92.40	rock
29	Corrie	49.38	95.30	rock
30	Borland Farm	51.32	96.59	drift
31	Gartloaning	51.45	98.10	rock

Hillhouse-Kilmarnock line

Site	Name	National Grid Easting	Northing	Geophone Coupling
1	Dundonald Castle	34.60	36.32	drift
2	Newfield Mains	34.61	37.60	drift
3	Rowanhill	34.32	38.61	drift
4	Templeton	34.65	39.42	drift
5	Townend	34.75	40.65	drift
6	West Mosside	35.80	44.12	drift
7	Barleith	35.55	45.37	drift
8	Purroch	35.56	46.68	drift
9	West Ashyard	35.62	47.70	drift

APPENDIX 2

GLASGOW FM Mark 2 seismic recorder specifications

Detector:	Mark Products L15B 4.5 Hz geophones with 600 coil, or alternative.
Amplifier Gain:	adjustable 88-118 dB in 6 dB steps; second output at 18 dB lower than first; clipped 10 V p-p (less for better linearity). Input resistance of 4.7 k for 0.65 of critical damping of L15B geophones.
Modulator:	central frequency is 2 kHz; frequency deviation for 10 V p-p input is +/- 100%: current output is 250 A.
Recording:	saturation.
Demodulator:	produces 2 V output for maximum modulator input (10V); 14 dB loss reduces overall system gain to the range 56-104 dB (including both gain output).
Playback filters:	Kemo VBF/3.
Oscillograph:	Bryans 40000 6-channel.
System frequency response:	direct connection of modulator to modulator; 3 dB down points give approximate pass-band of 2-60 Hz.
Noise and distortion:	system noise limits dynamic range to 46 dB at maximum gain. Distortion is less than 1% at 70% of clipping level. Wow and flutter: less than 0.25%.
Power Requirements:	Amplifier-modulator 20 MA; 18V. Recorder (during recording) 115 mA; 18V.
Cassette recorder:	Tape speed 4.74 cm/s.

APPENDIX 3

Travel times of the recorded data

Main Line : Hillhouse

Station	Range (km)	Travel time (sec)	Reduced time (sec)
Hh01	0.42	0.12	0.05
Hh02	2.09	0.62	0.27
Hh03	4.02	1.10	0.43
Hh04	6.29	1.69	0.64
Hh05	8.33	2.14	0.75
Hh06	10.18	2.48	0.78
Hh07	12.13	2.83	0.80
Hh08	14.01	3.17	0.83
Hh09	16.21	3.50	0.80
Hh10	17.96	3.80	0.81
Hh11	20.33	4.19	0.80
Hh12	22.57	4.59	0.83
Hh13	24.26	4.89	0.85
Hh14	26.12	5.20	0.84
Hh15	28.20	5.50	0.80
Hh16	29.49	5.72	0.80
Hh17	32.15	6.18	0.82
Hh18	34.03	6.49	0.82
Hh19	36.02	6.79	0.79
Hh20	38.52	7.20	0.78
Hh21	41.96	7.73	0.74
Hh22	43.70	8.04	0.75
Hh23	47.66	8.67	0.72
Hh24	50.15	9.06	0.70
Hh25	52.87	9.53	0.72
Hh26	55.52	9.98	0.73
Hh27	56.70	10.17	0.72
Hh28	59.83	10.70	0.73
Hh29	62.68	11.06	0.61
Hh30	64.41	11.34	0.61
Hh31	65.90	11.58	0.60

Main Line : Loanhead

station	Range (km)	Travel time (sec)	Reduced time (sec)
Lh-7	33.43	6.25	0.67
Lh-4	27.74	5.31	0.69
Lh-3	25.96	5.00	0.67
Lh-2	23.29	4.59	0.70
Lh01	20.88	4.22	0.74
Lh02	19.29	3.95	0.74
Lh03	17.19	3.77	0.70
Lh04	14.92	3.18	0.69
Lh05	12.87	2.84	0.69
Lh06	11.02	2.51	0.67
Lh07	9.33	2.16	0.61
Lh08	7.04	1.74	0.57
Lh09	4.89	1.22	0.40
Lh10	3.15	0.78	0.25
Lh11	1.17	0.21	0.06
Lh12	1.17	0.32	0.12
Lh13	2.90	0.69	0.20
Lh14	5.080	1.23	0.38
Lh15	7.230	1.69	0.48
Lh16	8.640	1.95	0.51
Lh17	11.20	2.44	0.58
Lh18	13.22	2.78	0.58
Lh19	15.18	3.14	0.61
Lh20	17.83	3.59	0.62
Lh21	21.26	4.13	0.59
Lh22	23.03	4.40	0.56
Lh23	26.96	5.07	0.58
Lh24	29.47	-	-
Lh25	32.22	-	-
Lh26	34.87	-	-
Lh27	36.00	6.59	0.59
Lh28	39.17	7.10	0.58
Lh29	-	-	-
Lh30	-	-	-
Lh31	-	-	-

Main Line : Sheephill

station	Range (km)	Travel time (sec)	Reduced time (sec)
Sh01	41.15	-	-
Sh02	39.52	7.32	0.74
Sh03	37.49	6.97	0.72
Sh04	35.21	6.59	0.72
Sh05	33.19	6.25	0.72
Sh06	31.39	5.97	0.74
Sh07	29.71	5.66	0.70
Sh08	27.46	-	-
Sh09	25.20	4.84	0.64
Sh10	23.66	4.57	0.62
Sh11	21.56	4.22	0.62
Sh12	19.44	3.86	0.62
Sh13	17.71	3.56	0.61
Sh14	15.54	3.19	0.60
Sh15	13.39	2.94	0.70
Sh16	11.98	2.90	0.69
Sh17	9.45	2.18	0.60
Sh18	7.39	1.73	0.50
Sh19	5.44	1.31	0.40
Sh20	2.83	0.68	0.20
Sh21	-	-	-
Sh22	-	-	-
Sh23	6.35	1.38	0.32
Sh24	-	-	-
Sh26	-	-	-
Sh27	15.40	3.03	0.46
Sh28	18.57	3.61	0.51
Sh29	-	-	-
Sh30	-	-	-
Sh31	-	-	-

Hillhouse-Kilmarnock line

station	Range (km)	Travel time (sec)	Reduced time (sec)
Hk01	1.64	0.30	0.03
Hk02	2.91	0.62	0.13
Hk03	3.91	0.91	0.25
Hk04	4.73	1.12	0.33
Hk05	6.72	1.62	0.50
Hk06	9.53	2.18	0.59
Hk07	10.74	2.43	0.65
Hk08	12.04	2.67	0.66
Hk09	13.06	2.88	0.70

APPENDIX 4

Plus-minus interpretation

This appendix lists the plus and minus times and depth determined for the crystalline basement refractor between Hillhouse and Sheephill on the main line. Distances are from Hillhouse.

Distance(km)	t(-)	t(+)	Depth(km)
2.09		0.92	4.01
4.02		0.88	3.87
6.29		0.89	3.88
8.33		0.89	3.89
10.18		0.74	3.24
12.13		0.74	3.22
16.21	-1.33	0.73	3.21
17.96	-0.76	0.76	3.32
20.33	-0.02	0.80	3.48
22.57	0.73	0.83	3.64
24.26	1.33	0.84	3.68
26.12	2.00	0.77	3.38
28.20		0.69	3.57
29.49		0.69	3.56
32.15		0.72	3.72
34.03		0.72	3.72
36.02		0.65	3.38
38.52		0.64	3.29
41.96		0.55	2.86
43.70		0.59	3.03
47.66		0.52	2.68
50.15		0.48	2.51
52.87		0.52	2.67
55.52		0.53	2.74
56.70		0.51	2.66
59.83		0.53	2.74
62.68		0.28	1.48
64.41		0.28	1.48
65.90		0.25	1.30

APPENDIX 5

Raytracing results

This appendix shows the discrepancy between arrival times determined by raytracing and observed arrival times. A negative discrepancy shows the computed time is faster than observed. Data are grouped by shotpoint. In each group the data are listed by arrival type. The distances shown are the positions of the receivers along the raytracing model with zero being at the SSW end. Offsets of receivers can be seen by comparison of their position and that of the shotpoint. The arrival codes are explained in Table 4.2

Hillhouse shot

Arrival	Position (km)	Arrival time(sec)	Discrepancy (sec)
a1	20.42	0.11	-0.01
	22.09	0.59	-0.03
	24.02	1.11	+0.01
	26.28	1.68	-0.01
a2	28.33	2.12	-0.01
	30.18	2.47	0.00
	32.18	2.85	+0.03
	34.00	3.19	+0.02
a3	36.21	3.54	+0.04
	37.96	3.82	+0.02
	40.33	4.21	0.02
	42.57	4.59	-0.00
	44.25	4.87	-0.02
	46.12	5.19	0.00
a4	48.20	5.50	0.00
	49.49	5.71	-0.01
	52.15	6.18	0.00
	54.03	6.48	-0.01
	56.02	6.81	+0.02
	58.52	7.22	-0.02
	61.96	7.79	-0.06
	63.70	8.07	+0.03
	67.66	8.69	+0.03
	70.15	9.08	+0.02
	72.87	9.49	-0.04
	75.52	9.92	-0.06

	76.70	10.11	-0.06
	79.83	10.62	+0.03
	82.67	11.07	+0.02
	84.41	11.35	+0.01
	85.89	11.59	+0.01
a6	44.25	5.26	0.00
	46.12	5.52	+0.03
	48.20	5.83	+0.04
	49.49	6.01	+0.01
	52.15	6.44	+0.03
	54.03	6.72	+0.02
	56.02	7.02	+0.02
	58.52	7.41	+0.04
	61.96	7.96	+0.08
	79.83	10.67	-0.02
	82.67	11.12	-0.02
	84.41	11.40	+0.01
	85.89	11.64	+0.02
a7	40.33	5.46	+0.03
	42.57	5.71	-0.02
	44.25	5.90	+0.09
	46.12	6.12	+0.12
	48.20	6.39	+0.06
	49.49	6.54	+0.05
	52.15	6.93	+0.07
	54.03	7.17	-0.06
	56.02	7.44	+0.03
	58.52	7.78	+0.02
a8	48.20	6.96	-0.02
	49.49	7.10	-0.03
	52.15	7.44	-0.10
	54.03	7.66	-0.12
	56.02	7.90	-0.10
	58.52	8.22	-0.20
	61.96	8.69	-0.20
	63.70	8.90	-0.15
	67.66	9.42	-0.10
	70.15	9.74	-0.06
	72.87	10.09	-0.02
	75.52	10.46	-0.02
	76.70	10.63	-0.02
	79.83	11.08	+0.02
	82.67	11.48	+0.04
	84.41	11.73	+0.05

	85.89	11.95	+0.04
a9	48.20	7.88	+0.03
	49.49	8.07	+0.01
	52.15	8.19	+0.06
	54.03	8.38	-0.03
	56.02	8.66	+0.04
	58.52	8.87	+0.06
	61.96	9.14	+0.02
	63.70	9.56	+0.03
	67.66	9.74	+0.05

Loanhead shot south

Arrival	Position (km)	Arrival time(sec)	Discrepancy (sec)
a1	40.33	0.29	-0.04
	37.96	0.78	0.00
	36.21	1.21	0.00
a2	34.00	1.74	0.00
	32.18	2.16	0.00
	30.18	2.49	-0.02
	28.33	2.86	+0.03
a3	26.28	3.16	-0.02
	24.02	3.59	+0.02
	22.09	3.99	+0.04
	20.42	4.29	+0.07
a4	18.11	4.73	+0.14
	14.44	5.33	+0.33
	13.66	5.46	+0.17
	7.97	6.40	+0.16
a5	30.18	3.56	+0.12
	28.33	3.75	+0.09
	26.28	3.99	+0.08
	24.02	4.27	+0.10
a6	36.21	4.21	+0.05
	34.00	4.31	+0.07
	32.18	4.44	+0.08
	30.18	4.56	+0.08
	28.33	4.71	+0.06
	26.28	4.88	+0.05
	24.02	5.10	+0.10

Loanhead shot north

Arrival	Position (km)	Arrival time(sec)	Discrepancy (sec)
a1	42.57	0.29	+0.04
	44.25	0.72	+0.03
	46.12	1.25	+0.02
a2	48.20	1.70	+0.02
	49.49	1.95	0.00
	52.15	2.48	+0.04
a3	54.03	2.80	+0.02
	56.02	No arrival	
	58.52	3.61	+0.02
	61.96	4.23	+0.10
	63.70	4.51	-0.11
a4	67.66	5.13	+0.06
	76.70	6.57	+0.02
	79.83	7.08	-0.02
a5	52.15	3.55	-0.10
	54.03	3.74	-0.20
	56.02	3.96	-0.16
	58.52	4.28	-0.05
a6	48.20	4.29	+0.12
	49.49	4.38	+0.06
	52.15	4.55	+0.04
	54.03	4.69	+0.12
	56.02	4.85	+0.09
	58.52	5.11	+0.08

Sheephill shot south

Arrival	Position (km)	Arrival time(sec)	Discrepancy (sec)
a1	58.52	0.69	-0.01
	56.02	1.30	-0.01
	54.03	1.74	+0.01
a2	52.15	2.17	0.00
	49.49	2.67	-0.02
	48.20	2.93	-0.01
a3	46.12	3.24	+0.05
	44.25	3.62	+0.06
	42.57	3.92	+0.06
	40.33	4.28	+0.06
	37.96	4.65	+0.09
	36.21	4.92	+0.08

a4	32.18	5.66	0.00
	30.18	5.95	-0.02
	28.33	6.27	+0.02
	26.28	6.62	+0.03
	24.02	7.02	+0.05
	22.09	7.39	+0.07
a6	46.12	4.90	-0.08
	44.25	5.11	-0.07
	42.57	5.29	+0.10
	40.33	5.52	+0.12
	37.96	5.77	+0.09
a7	46.12	5.67	+0.05
	44.25	5.85	+0.03
	42.57	6.00	+0.07
	40.33	6.20	+0.10
	37.96	6.41	+0.12
	36.21	6.58	+0.11
a8	49.49	6.87	+0.07
	48.20	6.92	+0.06
	46.12	7.03	+0.04
	44.25	7.17	+0.06
	42.57	7.29	+0.03
	40.33	7.45	-0.03
	37.96	7.62	-0.05
	36.21	7.76	-0.08

Sheephill shot north

Arrival	Position (km)	Arrival time(sec)	Discrepancy (sec)
a1	67.66	1.41	+0.04
a2	76.70	3.07	+0.04
	79.83	3.65	+0.04

Hillhouse-Kilmarnock line

Arrival	Position (km)	Arrival time(sec)	Discrepancy (sec)
a1	1.64	0.40	+0.05
	2.91	0.72	+0.04
	3.91	0.96	+0.03
	4.73	1.16	+0.03
a2	6.72	1.59	+0.02

	9.53	2.17	+0.01
	10.74	2.42	+0.01
	12.04	2.69	+0.02
	13.06	2.90	+0.02
a5	9.53	2.54	+0.10
	10.74	2.73	+0.05
	12.04	2.94	+0.06
	13.06	3.12	+0.05
a6	9.53	3.50	+0.07
	10.74	3.61	+0.01
	12.04	3.74	+0.02
	13.06	3.86	+0.01
a7	9.53	4.49	+0.04
	10.74	4.57	+0.03
	12.04	4.66	+0.02
	13.06	4.74	+0.02

APPENDIX 6

Computer Programs

Some FORTRAN routines were written for this study, or considerably altered. These are listed in this Appendix. All are available on the SUN network of the Department of Geology and Applied Geology, University of Glasgow

The programs are listed in the following order:

1. REMODE
2. APLOT - the main program and adapted routines
3. RESAMPLE
4. ZMSF
5. CON

REMODE

```
C-------------------------------------------------
C REMODE FILTER
C-------------------------------------------------
C THIS PROGRAM IS DESIGNED TO PROCESS SYNTHETIC AND REAL
C DATA IN "GLAMK2" FORMAT. A FIXED INPUT FILE NAME WAS
C USED "testrem".

THE INPUT FILE IS AS FOLLOWS:

line 1      The actual number of data files to be processed
line 2      The title on the plot, such as the line name
line 3      The filter parameters:
            IMO,ITR,IK,IP,POLR,NR,SCALE,IWW,IFR,ILG,IHLG,IROT
line 4      The first input and output file names & some parameters
            e.g   FNAME1,FNAME2,SA,TA,IONS,IWL
line 5      The second input and output file names & some parameters
  ..          .....
  ..          ......
line n      The n-th input and output file names.


C DESCRIPTION OF THE PARAMETERS
C   IMO   = 1 FOR THE FIELD DATA
C   IMO   = 0 FOR SYNTHETIC DATA.
C   ITR   = 0 WHEN THE OUTPUT IS WANTED TO BE FREE FORMAT.
C   IT    = 1 FOR INTEGER FORMAT FOR USE IN THE "PLOT"
C           PROGRAM
C   IWW   = THE CROSS CORRELATION WINDOW (IN SAMPLES).
C   IFR   = THE START OF THE PROCESSED DATA FILE.
C   ILG   = THE END OF THE PROCESSED DATA FILE.
C   IHLG  = LENGTH OF THE FILTER OPERATOR.
C   NR    = NUMBER OF TIMES TO PASS TRACES THROUGH A
C           REMODE FILTER.
C   IROT  = DATA ROTATION
C   IROT  = 0 IS AN OPTION TO RUN THE FILTER WITH A CERTAIN
C           ROTATION ANGLE
C   IROT  =1 TO RUN THE FILTER WITH DIFFERENT ROTATION
C           ANGLES 0-90 DEGREES AND CALCULATE THE
C           SIGNAL/NOISE RATIO OF THE FILTERED TO UNFILTERED
C           DATA FOR EACH ROTATION ANGLE ( THE OUTPUT FILE
C           IS "STNOUT")
C   FNAME1 =THE INPUT FILE NAME.
C   FNAME2 =THE OUTPUT FILE NAME.
```

```
C    SA      = THE INCIDENT ANGLE TO ROTATE THE TWO
C              COMPONENT.
C    TA      = THE AZIMUTH.
C    IONS    = THE WINDOW CENTER FOR THE S/N CALCULATION.
C    IWL     = THE WINDOW LENGTH OF THE S/N.
 C
      PARAMETER(NTP=4, NTR=2000 )
      DIMENSION ITRACE(NTP, NTR),TRACE(NTP, NTR), X(NTR),
     *Y(NTR), Z(NTR)
      CHARACTER  FNAME1*10, FNAME2*6, DAT*8,RSN*6, SSN*6,
     *AUT*3, INSTR*6 , TITLE*20
      COMMON/MR/XH(NTR), YH(NTR), ZH(NTR), AMP(NTR),
     *YDIST(NTR), RH(NTR)
      COMMON/B/CT(600,100)
C
C TO READ FROM INPUT FILE CALLED "testrem".
C
      OPEN(3,FILE='testrem')
      READ(3,*)NFILE
      READ(3,*)TITLE
      READ(3,*)IMO,ITR,IK,IP,POLR,NR,SCALE,IWW,IFR,ILG,IHLG,IROT
      DO 11 KK=1,NFILE
      WRITE(6,*)'PROCESSING FILE NUMBER',KK
      READ(3,*)FNAME1,FNAME2,SA,TA,IONS,IWL
C
      OPEN (1,FILE=FNAME1)
      OPEN (2,FILE=FNAME2)
C
C READING THE INPUT PARAMETERS AND WRITING THE OUTPUT
C    FILES
C
      IF(IMO.EQ.1)THEN
      READ(1,110) RSN, SSN, AUT, DAT, NCHAN, INSTR
      WRITE(2,110) RSN, SSN, AUT, DAT, NCHAN, INSTR
      DO 10 M=1,NCHAN
      READ (1,111) POSIT,IGAIN,IPOL,ISAMP,AMPL
      WRITE(2,111) POSIT,IGAIN,IPOL,ISAMP,AMPL
10    CONTINUE
      END IF
C
      JI=2000
      III=0
      DO 20 J=1,JI
      IF(IMO.EQ.1) READ(1,130,END=2) (ITRACE(M,J),M=1,3)
      IF(IMO.EQ.0) READ(1,*,END=2) (TRACE(M,J),M=1,3)
      III=III+1
```

```
20    CONTINUE
2     IN = III
C
      DO 21 J=IFR,ILG
      IF (IMO.EQ.1) THEN
      X(J) = REAL(ITRACE(1,J))
      Y(J) = REAL(ITRACE(2,J))
      Z(J) = REAL(ITRACE(3,J))
      ELSE IF(IMO.EQ.0) THEN
      X(J) = TRACE(1,J)
      Y(J) = TRACE(2,J)
      Z(J) = TRACE(3,J)
      END IF
21     CONTINUE
      CLOSE (1)
C
C
C DATA PROCESSING.
C
      OPEN(10,FILE='stnout')
C
      IF(IROT.EQ.0) THEN
      CALL ROTATE(IN, X, Y, Z, XH, YH, SA, TA)
      CALL REMODE(IN, IWW, SCALE, CDA, ICW, ILG, IFR, IK, IP, POLR,
     *          NR, IHLG)
C
      ELSE IF (IROT.EQ.1) THEN
      DO 109 J=0,90,5
      SA=J
      CALL ROTATE(IN,X,Y,Z,XH,YH,SA,TA)
      CALL REMODE(IN, IWW, SCALE, CDA, ICW, ILG, IFR, IK, IP, POLR,
     *NR, IHLG)
      CALL STNRAT (IFR,ILG,X,Y,ZH,IONS,IWL,SNFU)
C
C to write the s/n ratio of the filtered to unfilter data
C
      WRITE(10,*) FNAME1,'ANGLE',SA,'S/N OF FIL./UNFIL.  ',SNFU
109   CONTINUE
      ENDIF
C
C To write the title and output for plotting using "S" package.
C
      OPEN(4,FILE='ttt')
      OPEN(7,FILE='partm')
      SSA=SA-45.0
      WW=IWW*0.005
```

```
      WRITE(4,132)  FNAME2,WW,SSA
C
C THE OUTPUT FILE.
C
      DO 12 J=1,ILG-1
C     DO 12 J=IFR,ILG-1
C
C to write the filtered V&R only.
C
C     WRITE(7,*) ZH(J),RH(J),0.0
C
C To write the unfiltered V, R and the filtered V
C
      WRITE(7,*)X(J, Y(J), ZH(J)
      IF(ITR.EQ.0) WRITE(2,*) ZH(J),RH(J),0.0
      IF (ITR.EQ.1)THEN
C
C to write the filtered data in the output file
      ITRACE(1,J)=NINT(ZH(J))
      ITRACE(2,J)=NINT(RH(J))
      WRITE (2,130) ITRACE(1, J), ITRACE(2,J), 0
      END IF
12    CONTINUE
      CLOSE (2)
      WRITE(6,*)'THE OUTPUT FILE IS ', FNAME2
C
      CLOSE(4)
      CLOSE(7)
11    CONTINUE
C
110   FORMAT (2(A,2X),A,2X,A,I3,2X,A)
111   FORMAT (F7.3,I3,I2,I6,F7.3)
130   FORMAT (3I5)
132   FORMAT('"',A,'REMODE filter (w.l= ',F4.2,' sec, rot.ang.=',F5.1,')"')
C
      STOP
      END
C
C
      SUBROUTINE REMODE (N, IW, BB, CDA, ICW, ILG, IFR, IK, IP,
     * POLR, NR, IHLG)
C
C PRODUCE A TIME-VARYING REMODE FILTER WHICH IS
APOLARIZATION FILTER CONSIDERS ONLY THE RECTILINEARITY
C IN THE RADIAL AND VERTICAL DIRECTIONS INSTEAD OF IN THREE
C DIMENSIONAL SPACE. THE FILTER OPERATOR IS OBTAINED FROM
```

```
C A CROSS-CORRELATION FUNCTION BETWEEN  VERTICAL AND
C RADIAL COMPONENTS OVER A WINDOW ,IW,CENTERED AT SOME
C TIME THEN CONVOLVING THE FILTER OPERATOR WITH THE
C ORIGINAL TIME SERIES(V OR R)
C
      PARAMETER ( NTR=2000 )
      DIMENSION FK(NTR), VC(1000), RC(1000), VR(1000)
      COMMON/MR/XH(NTR),YH(NTR), ZH(NTR), AMP(NTR),
     *  YDIST(NTR), RH(NTR)
      COMMON/B/CT(600,100)
      ICW=IHLG*2-1
      INC=ILG+IFR
      DO 10 I=1,N
10    AMP(I)=XH(I)

C  NORMALIZES VERTICAL COMPONENT
      CALL NRMLIZ(N, BB, CDA, AMP)
      DO 12 I=1,N
12    XH(I)=AMP(I)
C
C REVERSE POLARITY IF NECESSARY
      IF (POLR.NE.0.0)GO TO 17
      DO 13 I=1,N
13    AMP(I)=YH(I)
      GO TO 18
17    DO 19 I=1,N
19    AMP(I)=-1*YH(I)
C
C NORMALIZES RADIAL COMPONENT
18    CALL NRMLIZ(N, BB, CDA, AMP)
      DO 14 I=1,N
14    YH(I)=AMP(I)
C
C CALCULATE THE POLARIZATION OPERATOR IF NECESSARY
      IF (IP.EQ.0)GO TO 31
      DO 30 I=1,N
      IL=IFR+I-1
      PP=XH(IL)*YH(IL)
      IF(PP.GT.0.0)AMP(IL)=1.0
      IF(PP.LT.0.0)AMP(IL)=0.0
30    CONTINUE
31    CONTINUE
C
C RECURSIVE MODE IF NECESSARY
      DO 50 M=1,NR
      DO 15 I=1,ILG
```

```
      J=IFR+I-1
      II=J+IW
      IF(II.GT.N)GO TO 23
      DO 16 K=1,IW
      KK=J+K-1
      VC(K)=XH(KK)
16    RC(K)=YH(KK)

C CALCULATE CROSS-CORRELATION AND FOLD TO GET C(-T)=C(+T)
      CALL CROSS(N,VC,RC,VR,IHLG,IW)
      YDIST(I)=VR(1)
      CALL FOLD(N,AMP,VR,IHLG)
      DO 20 L=1,ICW
20    CT(I,L)=AMP(L)

C CALCULATE K THE NORMALIZING FACTOR IF NECESSARY
      IF(IK.EQ.0)GO TO 23
      CALL AUTZ(VC,AUZ,IW,IHLG)
      CALL AUTZ(RC,AUR,IW,IHLG)
      FK(J)=(AUZ*AUR)**(-0.5)
15    CONTINUE
23    CONTINUE
      CALL CONV(N,YH,ZH,ICW,INC,IFR)
      DO 35 I=1,INC
35    YH(I)=ZH(I)
      CALL CONV(N,XH,ZH,ICW,INC,IFR)
      DO 22 I=1,INC
22    XH(I)=ZH(I)
C
C APPLY THE FILTER
C
50    CONTINUE
      IF(IK.EQ.0)GO TO 37
      DO 36 I=1,ILG
      L=IFR+I-1
      ZH(L)=XH(L)*FK(L)
      RH(L)=YH(L)*FK(L)
36    CONTINUE
37    CONTINUE
      IF(IP.EQ.0)GO TO 46
      IF(IK.NE.0)GO TO 38
      DO 40 I=1,ILG
      L=IFR+I-1
      ZH(L)=XH(L)*AMP(L)
      RH(L)=YH(L)*AMP(L)
40    CONTINUE
```

```
      GO TO 46
38    DO 43 I=1,ILG
      L=IFR+I-1
      ZH(L)=ZH(L)*AMP(L)
      RH(L)=RH(L)*AMP(L)
43    CONTINUE
46    CONTINUE
      CALL NRMLIZ(N,BB,CDA,ZH)
      CALL NRMLIZ(N,BB,CDA,RH)
      DO 52 I=1,N
      XH(I)=0.0
      YH(I)=0.0
52    CONTINUE
      DO 53 I=1,ILG
      KL=IFR+IHLG+I-1
      XH(KL)=YDIST(I)
      YH(KL)=YDIST(I)
53    CONTINUE
      CALL NRMLIZ(N,BB,CDA,XH)
      CALL NRMLIZ(N,BB,CDA,YH)
      RETURN
      END
C
C CALCULATE CROSS-CORRELATION
C
C
      SUBROUTINE CROSS(L, X, Y, Z, ILG, IW)
C
      DIMENSION X(1000),Y(1000),Z(1000)
      DO 10 I=1,ILG
      SUM=0.0
      DO 15 K=1,IW
      J=K+I-1
      IF(J.GT.IW)GO TO 10
15    SUM=SUM+X(J)*Y(K)
      Z(I)=SUM/IW
10    CONTINUE
      RETURN
      END
C
C
C  CALCULATE AUTO-CORRELATION
C
      SUBROUTINE AUTZ(X, AUT, IW, ILG)
C
      DIMENSION X(200)
```

```
      AUT=0.0
      DO 10 K=1,IW
10    AUT=AUT+X(K)*X(K)
      RETURN
      END
C
C CALCULATE CONVOLUTION
C
C
      SUBROUTINE CONV(N, X, Z, ICW, INC, IFR)
C
      PARAMETER ( NTR=2000 )
      DIMENSION X(NTR), Z(NTR)
      COMMON/B/CT(600,100)
      LY=INC+ICW-1
      ILG=INC-IFR
      DO 10 I=1,LY
10    Z(I)=0.0
      DO 20 I=1,ILG
      K=IFR+I-1
      DO 20 J=1,ICW
20    Z(K+J-1)=Z(K+J-1)+X(K)*CT(I,J)
      IF(LY-N)30,40,40
30    DO 32 I=LY,N
32    Z(I)=0.0
40    CONTINUE
      RETURN
      END
C
C GENERATE THE NEGATIVE LAGS FROM THE POSITIVE LAGS TO
C ENSURE THE OPERATOR IS AN EVEN FUNCTION.
C
      SUBROUTINE FOLD(N,X,VR,ILG)
C
      DIMENSION X(400), VR(1000)
      DO 10 I=1,N
10    X(I)=0.0
      DO 15 I=1,ILG
      IC=ILG+I-1
15    X(IC)=VR(I)
      IG=ILG-1
      DO 20 I=1,IG
      IZ=ILG+1-I
20    X(I)=VR(IZ)
      RETURN
      END
```

```
C
C NORMALIZES AMPLITUDE OF TRACES
C
      SUBROUTINE NRMLIZ(L, SCALE, CDA, X)
C
      PARAMETER ( NTR=2000 )
      DIMENSION X(NTR)
      CALL MAXAMP(L,CDA,X)
      IF(CDA.EQ.0.0)CDA=1.0
      DO 10 I=1,L
10    X(I)=X(I)*SCALE/CDA
      RETURN
      END
C
C
      SUBROUTINE MAXAMP(L, CDA, X)
C
C CALCULATES MAXIMUM AMPLITUDE OF TRACE.
C
      PARAMETER ( NTR=2000 )
      DIMENSION X(NTR)
      AMAX=X(I)
      DO 10 I=1,L
      AX=ABS(X(I))
      IF (AX.GT.AMAX)AMAX=AX
10    CONTINUE
      CDA=AMAX
      RETURN
      END
C
C
      SUBROUTINE ROTATE(IN, X, Y, Z, XH, YH, SA, TA)
C
      PARAMETER(NTP=4, NTR=2000 )
      DIMENSION XH(NTR), YH(NTR), X(NTR), Y(NTR), Z(NTR)
C
C     T=0
C
      S=SA*(3.1416/180)
      T=TA*(3.1416/180)
      A=SIN((3.1416/4)-S)
      B=COS((3.1416/4)-S)
      C=SIN(T)
      D=COS(T)
C
      DO 70 J=1,IN
```

```
      XH(J)=X(J)*B+Y(J)*D*A+Z(J)*C*A
      YH(J)=X(J)*A-Y(J)*D*B-Z(J)*C*B
70    CONTINUE
      RETURN
      END
C
      SUBROUTINE STNRAT (IFR, ILG, X, Y, ZH, IONS, IWL, SNFU)
C
C This ROUTINE is to calculate the S/N ratio of the three component
C within a certain window length(in samples ) on both sideof the required
C point.
C
      PARAMETER(NTP=4, NTR=2000 )
      DIMENSION TRACE(NTP,NTR), SUM(NTP), SM(NTP),
      TR(NTP,NTR),
       * SP(NTP),  SPN(NTP),STN(NTP),X(NTR),Y(NTR),ZH(NTR)
C
C
      DO 1111 K=IFR,ILG
      TRACE(1,K)=X(K)
      TRACE(2,K)=Y(K)
      TRACE(3,K)=ZH(K)
1111          CONTINUE
C
      DO 15 I=1,3
C
C to standardise the signal and calculate the signal amp.
C
      ISTR=IONS
      IEND=ISTR+IWl
      SUM(I)=0.0
      DO 16 K=ISTR,IEND
      SUM(I)=SUM(I)+TRACE(I,K)
16    CONTINUE
      NNN=IWL+1
      SM(I)=SUM(I)/NNN
      DO 17 K=1,IEND
      TR(I,K)=TRACE(I,K)-SM(I)
17    CONTINUE
      SUM(I)=0.0
      DO 18 K=1,IEND
      SUM(I)=SUM(I)+TR(I,K)**2
18    CONTINUE
      SP(I)=SQRT(SUM(I)/NNN)
C
C to standardise the noise and calculate its amp.
```

```
C
      ISTR=IONS-IWL
      IEND=IONS
      SUM(I)=0.0
      DO 21 K=ISTR,IEND
      SUM(I)=SUM(I)+TRACE(I,K)
21    CONTINUE
      NNN=IWL+1
      SM(I)=SUM(I)/NNN
      DO 22 K=1,IEND
      TR(I,K)=TRACE(I,K)-SM(I)
22    CONTINUE
      SUM(I)=0.0
      DO 23 K=1,IEND
      SUM(I)=SUM(I)+TR(I,K)**2
23    CONTINUE
      SPN(I)=SQRT(SUM(I)/NNN)
C
C the signal to noise ratio
C
      STN(I)=SP(I)/SPN(I)
C
15    CONTINUE
C
C the s/n of the filter to unfiltered vertical trace
      SNFU=STN(3)/STN(1)
C
110   FORMAT (2(A,2X),A,2X,A,I3,2X,A)
      CLOSE (1)
      RETURN
      END
C
C
```

APLOT

This is a version of the Glasgow "plot" program adapted to interpret the three component processing of this study. The main program is listed, followed by adapted subroutines.

```
      PROGRAM APLOT
C
C
C For details of operation and instructions for the program use, see the plot-
C manual which is available in the Department.
C
C This package was compiled and developed by K Davidson,
C                                                  Dept. of Geology,
C                                                  University of Glasgow.
C                                                  Oct/Nov 1986.
C
C                                                  Adapted by F.S.AHMED,
C                                                  OCT 1988
C
C All imported subroutines are acknowledged individually.
C
C The parameter command is used to allow easy extension, (or
C contraction) of the array sizes. Similar statements can be
C found in the following subroutines:
C
C    DATIN1, DATIN2, DATWRT, BTISUB, TRNORM , FASTFILT, PWR2,
C    RFILT, INTSUB
C
C    NTP   = the maximum number of input channels in a digital file
C    NCH   = the maximum number of traces likely to be processed
C    NTR   = the maximum number of data samples to be processed
C    NTF   = the next power of 2, greater than NTR, then + 2
C    NTI   = the maximum number of data samples likely to be input
C    NT2   = ((NFT-2) * 2) + 2
C
     PARAMETER(NTP=4, NCH=80, NTR=4000, NTF=4098, NTI=4000,
    * NT2=8194)
C
     COMMON/C1/ XX(NTP,NTR), WR1, WR2, WR3,WR4,WR5,WR6
     COMMON/C2/ F(NT2), R(NT2), S(NTF)
     COMMON/C3/ TWIND1(NCH),TWIND2(NCH)
     COMMON/C4/ IX(NTP,NTI), POSIT(NTP), IGAIN(NTP), IPOL(NTP),
    *           ISAMP(NTP), AMPL(NTP)
     DIMENSION  LI(NCH), ITLAG(NCH), AUTFAC(NCH), XWK(NTF),
    *           X(NTF), XY(NTR,NCH), WRR1(NCH), WRR2(NCH),
C   *           WRR3(NCH), WRR4(NCH), WRR5(NCH), WRR6(NCH)
     CHARACTER TITLE(40)*1, ICHART*6, ISTORD*6, ICOMP*9,
    *          PCHAN*8, OPT1*6, OPT2*6, OPT3*20, OPT4*6,
    *          DATOUT*8, STSHFT*6, FFP(8)*40
DATA IERROR, RFACT, NEXTRA, SCLFCT, STAT, LIMAX/0, 1., 100, 0., 0.,
1/
```

```
C
      PI = 4.0 * ATAN(1.0)
C
C 1. CONTROL DATA INPUT SECTION
C
      READ (5,*) NFILE, VEL, TIMM, NSAMP, TWINDO, ICHART, ISTORD
      READ (5,*) ICOMP, PCHAN, DATOUT, STSHFT
C
      IF (ICHART.EQ.'INTGER') ICHAR = 0
      IF (ICHART.EQ.'BINARY') ICHAR = 1
      IF (ICHART.EQ.'INTRNL') ICHAR = 2
      IF (ICHAR.LT.0.OR.ICHAR.GT.2)          IERROR = 1
C
      IF (ISTORD.EQ.'PASS  ') ISTRD = 0
      IF (ISTORD.EQ.'STORE ') ISTRD = 1
      IF (ISTORD.EQ.'READIN') ISTRD = 2
      IF (ISTRD.LT.0.OR.ISTRD.GT.2)          IERROR = 2
C
      IF (ICOMP.EQ.'VERTICAL') ICMP = 0
      IF (ICOMP.EQ.'TRIAXIAL') ICMP = 1
c     IF (ICOMP.EQ.'TRICOMFL') ICMP = 2
      IF (ICMP.LT.0.OR.ICMP.GT.2)            IERROR = 3
C
      IF (ICMP.GT.0) THEN
      IF (PCHAN.EQ.'VERTICAL') IPLOT = 1
      IF (PCHAN.EQ.'HORIZNT1') IPLOT = 2
      IF (PCHAN.EQ.'HORIZNT2') IPLOT = 3
      IF (PCHAN.EQ.'MSF    ') IPLOT = 4
      ELSE
      IPLOT = 0
      ENDIF
      IF (DATOUT.EQ.'DATAPASS')  IDOUT = 0
      IF (DATOUT.EQ.'DATAOUT ')  IDOUT = 1
      IF (DATOUT.EQ.'DATAIN  ')  IDOUT = 2
C
      IF (STSHFT.EQ.'NOSTAT')    ISTAT = 0
      IF (STSHFT.EQ.'STATIC')    ISTAT = 1
C
      IF (ISTAT.EQ.1) READ (5,*) STAT
C
      READ(5,9999) TITLE
9999        FORMAT(40A)
C
C Write TITLE to a separate file for later input to 'S'
C
      OPEN (9,FILE='pwk3')
```

```
      WRITE (9,998) TITLE
998   FORMAT  ('"',40A,'"')
      CLOSE (9)
C
      READ(5,*) XMIN,XMAX,YYMIN,YYMAX
      IF (YYMIN.GT.YYMAX) THEN
      YMIN = YYMAX
      YMAX = YYMIN
      ELSE
      YMIN = YYMIN
      YMAX = YYMAX
      ENDIF
C
C Define processing and display options
C
      READ(5,*) OPT1, OPT2
C
      IF (OPT1.EQ.'NOFILT') IFIL = 0
      IF (OPT1.EQ.'FILTER') THEN
      IFIL  = 1
      ICORR = 0
      ENDIF
      IF (OPT1.EQ.'AUTOCR') THEN
      IFIL  = 1
      ICORR = 1
      ENDIF
      IF (OPT1.EQ.'FASTFT') IFIL = 2
      IF (OPT1.EQ.'BUBBLE') IFIL = 3
      IF(OPT1.EQ.'POLARI')THEN
      IPFIL=1
      ELSE IF (OPT1.EQ.'FILPOL')THEN
      IPFIL=2
      ELSE
      IPFIL=0
      END IF
      IF (IPFIL.EQ.2)THEN
      IFIL=1
      ICOOR=1
      END IF
C
      IF (IFIL.LT.0.OR.IFIL.GT.3.OR.IPFIL.GT.2)       IERROR = 4
C
      IF (OPT2.EQ.'POWER ') ISPT = 1
      IF (OPT2.EQ.'AMPLTD') ISPT = 2
      IF (OPT2.EQ.'PHASE ') ISPT = 3
      IF (ISPT.LT.1.OR.ISPT.GT.3)                     IERROR = 5
```

```
C
      IF (IFIL.EQ.3) THEN
      DO 10 I=1,NCH
      TWIND1(I) = 0.
      TWIND2(I) = 0.
10    CONTINUE
      READ (5,*) NBUB
      DO 20 I=1,NBUB
      READ (5,*) L, TWIND1(L), TWIND2(L)
      TWIND1(L) = TWIND1(L) * NSAMP
20    CONTINUE
      CALL INTSUB (NBUB,NCH)
      DO 25 I=1,NCH
      ITLAG(I)  = TWIND1(I)
      AUTFAC(I) = TWIND2(I)
25     CONTINUE
      ENDIF
C
C The components of the polarization filter and the half window length
C
      IF (ICMP.GT.0)THEN
C     READ(5,*)IHWL,OPT3,IPAR,SW,EW
      READ(5,*)IHWL,OPT3
      IF (OPT3.EQ.'VERTIC-RADIAL')                IPOLAR=1
      IF (OPT3.EQ.'VERTIC-TRANSV')                IPOLAR=2
      IF (OPT3.EQ.'RADIAL-TRANSV')                IPOLAR=3
      IF (OPT3.EQ.'VERTIC-RADIAL-TRANSV')         IPOLAR=4
      IF(IPOLAR.LT.0.OR.IPOLAR.GT.4)              IERROR=6
      END IF
C
      READ(5,*) OPT4, OPT5
C
      IF (OPT4.EQ.'NOSCAL') ITR  = 0
      IF (OPT4.EQ.'TRANRM') ITR  = 1
      IF (OPT4.EQ.'SECNRM') ITR  = 2
      IF (OPT4.EQ.'X1NORM') ITR  = 3
      IF (OPT4.EQ.'X2NORM') ITR  = 4
      IF (OPT4.EQ.'XXNORM') ITR  = 5
      IF (OPT4.EQ.'VLNORM') ITR  = 6
      IF (ITR.EQ.3)      SCLFCT = 1.
      IF (ITR.EQ.4)      SCLFCT = 2.
      IF (ITR.LT.0.OR.ITR.GT.6)                   IERROR = 7
C
      IF (OPT5.EQ.0.)            RFACT = 1.
      IF (OPT5.NE.0..OR.OPT5.NE.100.) RFACT = OPT5 / 100.
C
```

```
      IF (ITR.EQ.5) READ(5,*) SCLFCT
      IF (ITR.EQ.5.AND.SCLFCT.EQ.0.)                IERROR = 8
C
C If time-variant data windowing is required then read in the
C window start and end times.
C
      IF (TWINDO.GE.1) THEN
      DO 30 I=1,80
      TWIND1(I) = 0.
      TWIND2(I) = 0.
30     CONTINUE
      DO 40 I=1,TWINDO
      READ (5,*) L, TWIND1(L), TWIND2(L)
40    CONTINUE
      ENDIF
C
C Write subtitle on filter information to file 'pwk4'
C 'CALL SYSTEM' is a UNIX system command
C
      OPEN (8,FILE='pwk4')
      IF (IPFIL.EQ.0.OR.IPFIL.EQ.2)THEN
      IF (IFIL.EQ.0) WRITE(8,*)'"Unfiltered time section"'
      OPEN(9,FILE="fwk3")
      JJ=8
      III=0
      do 111 I=1,JJ
      READ(9,1055,END=11)FFP(I)
      III=III+1
111   CONTINUE
11    IND=III
      IF (IFIL.EQ.1.AND.ICORR.EQ.0) WRITE(8,1055)(FFP(I),I=1,IND)
      IF (IFIL.EQ.1.AND.ICORR.EQ.1) THEN
      WRITE (8,*) '"Autocorrelation plot"'
      ENDIF
      IF (IFIL.EQ.2) WRITE (8,*) '"Spectral analysis plot"'
      ELSE
      SAMP=REAL(NSAMP)
      WL=(2*IHWL+1)/SAMP
      IF(IPFIL.EQ.1)WRITE(8,997)WL
      END IF
997   FORMAT('"Polarization filter',F5.2,' s','"')
      IF(IPFIL.EQ.2)THEN
      WRITE(8,1055)(FFP(I),I=1,IND)
      SAMP=REAL(NSAMP)
      WL=(2*IHWL+1)/SAMP
      WRITE(8,999)WL
```

```
999  FORMAT('"pol. filter',F5.2,' s',"")
1055         FORMAT(A)
     END IF
     CLOSE (8)
C
C Calculate nos. of samples to be read in
C
     IF (VEL.EQ.0.) THEN
     JI  = INT(TIMM * NSAMP) + NEXTRA
     ELSEIF (VEL.GT.0.) THEN
     DXD = MAX(XMAX,ABS(XMIN))
     JI  = INT((TIMM + DXD / VEL) * NSAMP) + NEXTRA
     ENDIF
     IF (JI.GT.4000) JI = 4000
C
C Check for any incorrect option commands, if so then stop program
C
     IF (IERROR.NE.0) THEN
     WRITE (6,*) '** Error in the specification of control data **'
     IF (IERROR.EQ.1) WRITE (6,*) 'ICHART is incorrectly specified'
     IF (IERROR.EQ.2) WRITE (6,*) 'ISTORD is incorrectly specified'
     IF (IERROR.EQ.3) WRITE (6,*) 'ICOMP is incorrectly specified'
     IF (IERROR.EQ.4) WRITE (6,*) 'OPT1 is incorrectly specified'
     IF (IERROR.EQ.5) WRITE (6,*) 'OPT2 is incorrectly specified'
     IF (IERROR.EQ.6) WRITE (6,*) 'OPT3 is incorrectly specified'
     IF (IERROR.EQ.7) WRITE (6,*) 'OPT4 is incorrectly specified'
     IF (IERROR.EQ.8) WRITE (6,*) 'SCLFCT is equal to zero'
     STOP
     ENDIF
C
C 2. DIGITAL DATA INPUT SECTION
C
C Subroutine DATIN1 reads the data files specified in the control file.
C Alternatively, a complete dataset previously written by a call to
C subroutine DATWRT, may be read in using DATIN2.
C
     OPEN (16,FILE='workdata',FORM='UNFORMATTED')
     KF=NFILE
     IF (TWINDO.GE.1.AND.TWINDO.LT.KF) CALL INTSUB
(TWINDO,KF)
     DO 200 I=1,KF
C
     IF (ICHAR.EQ.0.OR.ICHAR.EQ.1) THEN
     CALL ADATIN1 (ICHAR, ICMP, IPLOT, I, LA, IPFIL, ISTRD, JI, XMIN,
    *  XMAX)
     IF (ISTRD.EQ.1) CALL ADATWRT (I)
```

```
      ELSEIF (ICHAR.EQ.2.AND.ISTRD.EQ.2) THEN
      CALL ADATIN2 (I,ICMP,IPFIL,IPLOT,LA)
      ELSEIF (IDOUT.EQ.2) THEN
      CALL ADATIN2 (I,ICMP,IPFIL,IPLOT,LA)
      LI(I) = WR4
      ELSE
      WRITE (6,*) 'Input data source incorrectly specified'
      STOP
      ENDIF
C
C 3. DATA REDUCTION (WINDOWING) SECTION
C
C
C     IF (TWINDO.GE.1.AND.TWINDO.LT.KF) CALL INTSUB
(TWINDO,KF)
      IF (IFIL.EQ.2) THEN
      YYMIN = 0.
      YYMAX = NSAMP / 2
      ENDIF
C
C If seismic data is input from a previous run of program 'plot',
C then skip this section.
C
      IF (IDOUT.EQ.2) GO TO 1
C
C Calculates position and index of first sample in data window
C
      WR5 = 0
      IN  = WR4
      IF (VEL.GT.0.) THEN
      RITA = ABS(WR1) / VEL
      REDT=RITA*NSAMP
      KK=INT(REDT+0.005+YMIN*NSAMP)+WR2
      ELSEIF (VEL.EQ.0..AND.WR2.LT.0) THEN
      KK = INT(WR2)+1+INT(YMIN*NSAMP)
      ELSEIF (VEL.EQ.0..AND.WR2.GE.0) THEN
      KK = INT(WR2)+INT(YMIN*NSAMP)
      ENDIF
      WR5 = MAX(KK,1)
      IF (WR5.GT.1) THEN
      WR6 = YMIN
      ELSEIF (VEL.EQ.0..AND.WR5.EQ.1) THEN
      WR6 = -1.0 * WR2/REAL(NSAMP)
      ELSEIF (VEL.GT.0..AND.KK.LE.1) THEN
      WR6=ABS(REAL(KK)/REAL(NSAMP))+YMIN
      ENDIF
```

```
C
      IF (TWINDO.GE.1) THEN
      IF (TWIND1(I).LT.WR6) TWIND1(I) = WR6
      TFACT1 = (TWIND1(I) - WR6) * NSAMP
      WR5 = WR5 + TFACT1
      WR6 = TWIND1(I)
      ENDIF
C
C II is the window upper limit
C
      KITT = IN-WR5+1
      NP = INT(TIMM*NSAMP)+1
      IF (NP.GE.KITT) NP = KITT
      II  = NP+WR5-1
      LI(I) = II - WR5
      LII = II - WR5
C
      IF (TWINDO.GE.1) THEN
      IF (TWIND2(I).GT.YMAX) TWIND2(I) = YMAX
      TFACT2 = (TWIND2(I) - TWIND1(I)) * NSAMP
      IF (TFACT2.GT.LII) TFACT2 = LII
      LI(I) = TFACT2
      LII  = TFACT2
      ENDIF
C
C 4. PROCESSING SECTION
C
C Copy each trace in turn into a single vector 'XWK',
C then baselevel each trace.
C
1     LII = LI(I)
      KI  = 0
      IF (VEL .EQ. 0. ) THEN
      IF ( (-1.0*WR2/NSAMP).LT.YMIN ) KI = WR2 + INT(YMIN*NSAMP)
      ELSE
      CKWR2 = -1.0*WR2/NSAMP - ABS(WR1/VEL)
      IF (CKWR2 .LT. YMIN ) KI = INT( (YMIN-CKWR2) * NSAMP )
      ENDIF
      IF(TWINDO.GT.0)  KI=WR5
C
C M is the number of components
C
C
      DO 76 M=1,LA
      WRITE(6,*) 'PROCESSING STATION NUMBER',I,' TRACE
     * NUMBER', M
```

```
      DO 80 J=1,LII
      XWK(J) = XX(M,J+KI)
80    CONTINUE
      CALL REMAV (LII,XWK)
C
C If 'FILTER' has been called, then filter each trace with the
C filter generated by 'fwfir' and stored in 'fwk1'.
C
      IF (IFIL.EQ.1) THEN
      IF (ICORR.EQ.1) THEN
      DO 120 J=1,LII
      XWK(J) = XWK(J) * SIN((PI * (J-1)) / LII - 1)
120   CONTINUE
      ENDIF
      CALL PWR2 (LII,XWK,JIL)
      CALL FASTFILT (XWK,JIL,I,ICORR)
C
C If 'FASTFT' has been called, then calculate the power spectra
C by the spectrogram method, and display as normalised traces
C on a (frequency,range) plot.
C
      ELSEIF (IFIL.EQ.2) THEN
      CALL PWR2 (LII,XWK,JIL)
      CALL FFA (XWK,JIL)
      NFFTB2 = JIL / 2 + 1
      DO 130 L=1,NFFTB2
      J = L - 1
      XREAL = XWK(2*J+1)
      XIMAG = XWK(2*J+2)
      CALL XPOLAR (XREAL,XIMAG,SPECTM,ISPT)
      XWK(L) = SPECTM
      IF (L.GE.2.AND.ISPT.EQ.3) THEN
      PHZ1 = XWK(L-1)
      PHZ2 = XWK(L)
      CALL XDRUM (PHZ1,PHZ2)
      XWK(L) = PHZ2
      ENDIF
130   CONTINUE
      LII = NFFTB2
C
C Needs to be applied from the first arrival time
C
      ELSEIF (IFIL.EQ.3) THEN
      LIA = LII - ITLAG(I)
      DO 135 J=1,LIA
      L = J + ITLAG(I)
```

```
      XWK(L) = XWK(L) + (XWK(J) * AUTFAC(I))
135   CONTINUE
      ENDIF
C
      DO 85 J=1,LII
      XX(M,J) = XWK(J)
85    CONTINUE
      IF (IFIL.EQ.2) LI(I) = NFFTB2
76    CONTINUE
C
C The polarization filter
C
      IF(IPFIL.EQ.1.OR.IPFIL.EQ.2)THEN
      CALL POLARIZ(XX,IHWL,I,IPLOT,IPOLAR,LII)
      END IF
C
C     IF (IFIL.EQ.0.OR.IFIL.EQ.1.AND.IDOUT.EQ.1) THEN
C     DO 90 I=1,KF
C     WR4(I) = LI(I)
C 90  CONTINUE
C     CALL DATWRT (KF)
C     ENDIF
C
      DO 202 J=1,LII
      XY(J,I)=XX(1,J)
202   CONTINUE
C
      WRR1(I)=WR1
      WRR2(I)=WR2
      WRR3(I)=WR3
      WRR4(I)=WR4
      WRR5(I)=WR5
      WRR6(I)=WR6
200   CONTINUE
      CLOSE(16)
C
C 5. SCALING SECTION
C
C Normalise trace amplitudes according to ITR
C
      WRITE (6,*) 'entering TRNORM'
      CALL ATRNORM (KF,ITR,SCLFCT,WRR1,WRR4,XY)
C
C
C 6. PLOT PREPARATION SECTION
C
```

```
C This section converts each trace to plotting coordinates,
C scales each trace according to the trace density and an
C externally applied gain facter.
C Shorter traces are padded out with zeros to create an array
C with dimensions (LIMAX,KF) which will be written to
C output file 'pwk2' for plotting using 'S'
C
      WRITE (6,*) 'entering plot prep. section'
      RMIN =  100000.
      RMAX = -100000.
C
C Write out plot control information to a file for later use in 'S'
      OPEN (14,FILE='pwk1')
      OPEN (12,FILE='pwk2')
      WRITE (14,*) XMIN, XMAX, YYMIN, YYMAX, NSAMP, KF, VEL
C
      DO 110 I=1,KF
      LII = LI(I)
      IF (LII.GT.LIMAX) LIMAX = LII
      IF (RMAX.LT.WRR1(I)) RMAX = WRR1(I)
      IF (RMIN.GT.WRR1(I)) RMIN = WRR1(I)
110   CONTINUE
C
      WRITE (6,*) 'final write-out section'
      WRITE (14,*) LIMAX
      RSCALE = ABS((RMAX - RMIN) / ((KF - 1) * 2)) * RFACT
      IF (IFIL.EQ.2) RSCALE = RSCALE * 2
C
C Add on static and write out to the 'S' files
C
      DO 100 I=1,KF
      DO 65 J=1,LIMAX
      IF (J.LE.LI(I)) X(J) = WRR1(I) + (XY(J,I) * WRR3(I) * RSCALE)
      IF (J.GT.LI(I)) X(J) = 0.000001e+00
65    CONTINUE
      WRR6(I) = WRR6(I) + STAT
      WRITE (14,970) WRR6(I), LI(I), WRR1(I)
      WRITE (12,980) (X(J),J=1,LIMAX)
100   CONTINUE
C
      WRITE (6,960)
960   FORMAT (/////,'To view the graphical output from this program',
     *//5X,'type "S", then RETURN',//,'followed by ',
     *//5x,'?seis',//,'then',
     *//5x,'"device"',//,'followed by either',
     *//5X,'?datplot or ?pwrplot',//,
```

```
     *'for seismograms or spectral output',//,
     *'"device" refers to the graphical device, eg tek14, tek4107, gould,
     * or unixplot',/
     *'When plotting to "gould" or "unixplot" use the following forms'/
     *'eg   ?datplot;?gould   or   ?pwrplot;?anplot')
970  FORMAT (F8.3,I5,F8.3)
980  FORMAT (5E14.6)
101  format(I3,2X,A,2x,I,2x,2F5.2)
     CLOSE (12)
     CLOSE (14)
C
     STOP
     END
```

Some subroutines which were modified are listed here.

```
C
     SUBROUTINE ADATIN1 (ICHAR, ICMP, IPLOT, I, LA, IPFIL, ISTRD,
C    *                              JI, XMIN, XMAX)
C
     PARAMETER(NTP=4, NCH=80, NTR=4000, NTF=4098, NTI=4000)
C
     COMMON/C1/ XX(NTP,NTR), WR1, WR2, WR3, WR4, WR5, WR6
     COMMON/C4/ ITRACE(NTP,NTI), POSIT(NTP), IGAIN(NTP),
     IPOL(NTP),
    *        ISAMP(NTP), AMPL(NTP)
     CHARACTER   FNAME*36,DAT*8,RSN*6,SSN*6,AUT*3,INSTR*6
C
C DIGITAL DATA INPUT SECTION
C
C This section reads the data files specified in the control file
C
     READ (5,100) FNAME
C
     IF (ICHAR.EQ.1) THEN
     CALL BTISUB (FNAME)
     OPEN (10,FILE='tempdata',FORM='FORMATTED')
     ELSEIF (ICHAR.EQ.0) THEN
     OPEN (10,FILE=FNAME,FORM='FORMATTED')
     ENDIF
C
     READ(10,110) RSN, SSN, AUT, DAT, NCHAN, INSTR
     DO 10 M=1,NCHAN
     READ(10,*) POSIT(M),IGAIN(M),IPOL(M),ISAMP(M),AMPL(M)
     IF (AMPL(M).EQ.0.) AMPL(M)  = 1.
```

```
      IF (IGAIN(M).EQ.0) IGAIN(M) = 1
10    CONTINUE
      III=1
      DO 20 J=1,JI
      IF(INSTR.EQ.'GEOSTR')THEN
      READ(10,150,END=2) (ITRACE(M,J),M=1,NCHAN)
      ELSEIF (INSTR.EQ.'GLAMK1') THEN
      READ(10,*,END=2) (ITRACE(M,J),M=1,NCHAN)
      ELSE
      READ(10,*,END=2) (ITRACE(M,J),M=1,NCHAN)
      ENDIF
      III=III+1
20    CONTINUE
C
2     INDATA = III - 1
      CLOSE (10)
C
C WR arrays used to store trace specific data
C WR1 = Range
C WR2 = Number of samples to relate start of file to shot instant
C WR3 = Scaling factor externally applied to each trace
C WR4 = Number of samples actually read in
C WR5 = Working trace length (assigned in main program)
C WR6 = Time of first plotting sample (again assigned later)
C
      LL=0
      DO 30 M=1,NCHAN
c
      IF (POSIT(M).EQ.0)GO TO 30
      IF (ICMP.GT.0.AND.IPFIL.EQ.0)THEN
      IF (ISTRD.EQ.1.AND.M.GT.3) GO TO 30
      IF(ISTRD.EQ.0.AND.IPLOT.NE.M) GO TO 30
      ELSE IF(ICMP.GT.0.AND.IPFIL.GT.0.)THEN
      IF(M.GT.3)GO TO 30
      END IF
      WR1 = POSIT(M)
      WR2 = REAL(ISAMP(M))
      WR3 = AMPL(M)
      WR4 = REAL(INDATA)
      IN = INDATA
      WR5 = 0.0
      WR6 = 0.0
C
C Alters trace polarity if necessary
C
      IF (IPOL(M).EQ.0) THEN
```

```
      POL=1.0
      ELSEIF (IPOL(M).EQ.1) THEN
      POL=-1.0
      ENDIF
C
C Test whether each trace is outside the plot limits, and
C extend the limits if necessary
C
C
      IF (WR1.GT.XMAX) XMAX = WR1 + WR1/20
      IF (WR1.LT.XMIN) XMIN = WR1 - WR1/20
C
C Construct the 2D digital data matrix
C
      IF (ICMP.GT.0.AND.IPFIL.GT.0.OR.ISTRD.EQ.1) THEN
      DO 40 J=1,IN
      XX(M,J) = REAL(ITRACE(M,J)) * POL
40    CONTINUE
      ELSE
      DO 60 J=1,IN
      XX(1,J) = REAL(ITRACE(M,J)) * POL
60    CONTINUE
      END IF
C
      LL=LL+1
30    CONTINUE
      LA=LL
C
100   FORMAT (A)
110   FORMAT (2(A,2X),A,2X,A,I3,2X,A)
130   FORMAT (3I5)
140   FORMAT (4I5)
150   FORMAT (11I6)
C
      RETURN
      END
C
C
      SUBROUTINE ADATIN2 (I,ICMP,IPFIL,IPLOT,LA)
C
C Subroutine ADATIN2 reads in digital data from a binary file
C previously created by a call to subroutine DATWRT
C
      PARAMETER (NTP=4, NCH=80, NTR=4000)
C
      COMMON/C1/ XX(NTP,NTR), WR1, WR2, WR3, WR4, WR5, WR6
```

```
C
C
      READ (16) I ,WR1,WR2,WR3,WR4,WR5,WR6
C
      IN = WR4
      LL=0
      DO 20 N=1,3
      READ (16) (XX(N,J),J=1,IN)
      LL=LL+1
20    CONTINUE
      LA=LL
      IF(ICMP.EQ.0.OR.ICMP.GT.0.AND.IPFIL.EQ.0)THEN
      LL=0
      DO 50 N=1,3
      IF(ICMP.EQ.0.AND.N.GT.1) GO TO 50
      IF(ICMP.GT.0.AND.IPLOT.NE.N) GO TO 50
      DO 60 J=1,IN
      XX(1,J)=XX(N,J)
60    CONTINUE
      LL=LL+1
50    CONTINUE
      LA=LL
      END IF
C
      RETURN
      END
C
C
      SUBROUTINE ABTISUB (FNAME, FN1, FN2, FN3, ICMP)
C
C Subroutine to read binary files and rewrite them as integers
C
      PARAMETER(NTP=4, NTR=4000, NTI=4000)
C
      COMMON/c4/ IX(NTP,NTI), POSIT(NTP), IGAIN(NTP), IPOL(NTP),
     *          ISAMP(NTP), AMPL(NTP)
      CHARACTER  FNAME*36,RSN*6,SSN*6,AUT*3,DAT*8,INSTR*6,
     *       FN1*10,FN2*10,FN3*10
C
      IF(ICMP.LT.2) THEN
      OPEN(8,FILE=FNAME,FORM='UNFORMATTED')
      OPEN(9,FILE='tempdata',FORM='FORMATTED')
      ELSE IF(ICMP.EQ.2)THEN
      OPEN(10,FILE=FN1,FORM='UNFORMATTED')
      OPEN(11,file=FN2,FORM='UNFORMATTED')
      OPEN(12,FILE=FN3,FORM='UNFORMATTED')
```

```
      OPEN(13,FILE='tempdata1',form='formatted')
      OPEN(14,FILE='tempdata2',FORM='formatted')
      OPEN(15,FILE='tempdata3',FORM='formatted')
      END IF
C
      READ(8) RSN, SSN, AUT, DAT, NCHAN, INSTR
      WRITE(9,1) RSN, SSN, AUT, DAT, NCHAN, INSTR
      READ(10) RSN, SSN, AUT, DAT, NCHAN, INSTR
      WRITE(13,1) RSN, SSN, AUT, DAT, NCHAN, INSTR
      READ(11) RSN, SSN, AUT, DAT, NCHAN, INSTR
      WRITE(14,1) RSN, SSN, AUT, DAT, NCHAN, INSTR
      READ(12) RSN, SSN, AUT, DAT, NCHAN, INSTR
      WRITE(15,1) RSN, SSN, AUT, DAT, NCHAN, INSTR
C
      READ(8) POSIT(I), IGAIN(I), IPOL(I), ISAMP(I),AMPL(I)
      WRITE(9,*) POSIT(I), IGAIN(I), IPOL(I), ISAMP(I),AMPL(I)
      READ(10) POSIT(I), IGAIN(I), IPOL(I), ISAMP(I),AMPL(I)
      WRITE(13,*) POSIT(I), IGAIN(I), IPOL(I), ISAMP(I),AMPL(I)
      READ(11) POSIT(I), IGAIN(I), IPOL(I), ISAMP(I),AMPL(I)
      WRITE(14,*) POSIT(I), IGAIN(I), IPOL(I), ISAMP(I),AMPL(I)
      READ(12) POSIT(I), IGAIN(I), IPOL(I), ISAMP(I),AMPL(I)
      WRITE(15,*) POSIT(I), IGAIN(I), IPOL(I), ISAMP(I),AMPL(I)
99    CONTINUE
C
      IF (INSTR.EQ.'GLAMK1') THEN
      JTIME = 2816
      ELSE
      IF (POSIT(1).LT.20.)              JTIME = 2048
      IF (POSIT(1).GE.20..AND.POSIT(1).LT.60.) JTIME = 2816
      IF (POSIT(1).GE.60.)              JTIME = 3840
      ENDIF
C
      READ(8) ((IX(I,J),I=1,NCHAN),J=1,JTIME)
      READ(10) ((IX(I,J),I=1,NCHAN),J=1,JTIME)
      READ(11) ((IX(I,J),I=1,NCHAN),J=1,JTIME)
      READ(12) ((IX(I,J),I=1,NCHAN),J=1,JTIME)
      IF (INSTR.EQ.'GEOSTR') THEN
      WRITE(9,5) ((IX(I,J),I=1,NCHAN),J=1,JTIME)
      ELSEIF (INSTR.EQ.'GLAMK1') THEN
      WRITE(9,4) ((IX(I,J),I=1,NCHAN),J=1,JTIME)
      ELSE
      WRITE(9,3) ((IX(I,J),I=1,NCHAN),J=1,JTIME)
      WRITE(13,3)((IX(I,J),I=1,NCHAN),J=1,JTIME)
      WRITE(14,3) ((IX(I,J),I=1,NCHAN),J=1,JTIME)
      WRITE(15,3) ((IX(I,J),I=1,NCHAN),J=1,JTIME)
      END IF
```

```
      WRITE(0,*) FNAME',   **CONVERSION COMPLETE **'
      WRITE(0,*) FNAME1',  **CONVERSION COMPLETE **'
      WRITE(0,*) FNAME2',  **CONVERSION COMPLETE **'
      WRITE(0,*) FNAME3',  **CONVERSION COMPLETE **'
      REWIND(9)
      REWIND(13)
      REWIND(14)
      REWIND(15)
      CLOSE(8)
      CLOSE(9)
      CLOSE(10)
      CLOSE(11)
      CLOSE(12)
      CLOSE(13)
      CLOSE(14)
      CLOSE(15)
C
1     FORMAT(2(A,2X),A,2X,a,I3,2X,A)
3     FORMAT(3I5)
4     FORMAT(4I5)
5     FORMAT(11I6)
C
      RETURN
      END
C
C
      SUBROUTINE POLARIZ(XX,IHWL,I,IPLOT,IPOLAR,LII)
C
      PARAMETER (NTP=4,NTR=4000,NCH=80)
      DIMENSION SUM(NTR),XX(NTP,NTR),XT(NTP,NTR)
C
      J=IHWl+1
      IEF=LII-IHWL
      DO 20 k=J,IEF
      SUM(k)=0.00
      DO 30 l=K-IHWL,K+IHWL
      IF (IPOLAR.EQ.1)THEN
      SUM(k)=SUM(K)+(XX(1,L)*XX(2,L))
      ELSE IF (IPOLAR.EQ.2)THEN
      SUM(k)=SUM(K)+(XX(1,L)*XX(3,L))
      ELSE IF (IPOLAR.EQ.3)THEN
      SUM(k)=SUM(K)+(XX(2,L)*XX(3,L))
      ELSE IF (IPOLAR.EQ.4)THEN
      SUM(K)=SUM(K)+(XX(1,L)*XX(2,L)*XX(3,L))
      END IF
30    CONTINUE
```

```
C     IF (IPAR.GT.0.AND.IPAR.EQ.I) THEN
C     XT(1,K)=ABS(SUM(K))*XX(1,K)
C     XT(2,K)=ABS(SUM(K))*XX(2,K)
C     XT(3,K)=ABS(SUM(K))*XX(3,K)
C     ELSE
      IF (IPLOT.EQ.1)   XT(1,K)=ABS(SUM(K))*XX(1,K)
      IF (IPLOT.EQ.2)   XT(1,K)=ABS(SUM(K))*XX(2,K)
      IF (IPLOT.EQ.3)   XT(1,K)=ABS(SUM(K))*XX(3,K)
C     END IF
20    CONTINUE
C
C     IF (IPAR.GT.0.AND.IPAR.EQ.I)  CALL PARTMO(XT,LII,SW,EW)
      DO 50 K=1,IEF
      XX(1,K)=XT(1,K)
50    CONTINUE
      RETURN
      END
C
C
      SUBROUTINE ATRNORM (KX,ITR,SF,WRR1,WRR4,XY)
C
      PARAMETER(NCH=80, NTR=4000,NTP=4)
C
      DIMENSION  BMAX (NCH), XY(NTR, NCH), WRR1(NCH),
     *WRR4(NCH)
C
C Find the nearest trace to the shot-point for relative scaling and
C find the maximum values for both each trace and the whole section
C
      INDEX = 1
      AMAX  = 0.
      WRITE (6,*) 'the scaling factor is X ** ',SF
      DO 1 I=1,KX
      LX = WRR4(I)
      BMX = 0.
      IF (ABS(WRR1(INDEX)).GT.ABS(WRR1(I))) INDEX = I
      DO 2 J=1,LX
      IF (AMAX.LT.ABS(XY(J,I))) AMAX = ABS(XY(J,I))
      IF (BMX.LT.ABS(XY(J,I)))   BMX = ABS(XY(J,I))
2     CONTINUE
      IF (BMX.EQ.0.000000) BMX = BMX + 0.000001
      BMAX(I) = BMX
1     CONTINUE
C
C Calculate trace normalisation according to the index ITR
C
```

```
      DO 3 I=1,KX
      LX = WRR4(I)
      DO 4 J=1,LX
      IF (ITR.EQ.0) XY(J,I) = XY(J,I) / BMAX(INDEX)
      IF (ITR.EQ.1) XY(J,I) = XY(J,I) / BMAX(I)
      IF (ITR.EQ.2) XY(J,I) = XY(J,I) / AMAX
      IF (ITR.GE.3.AND.ITR.LE.5) THEN
      XY(J,I)=XY(J,I) / BMAX(INDEX)
      XY(J,I)=XY(J,I)*(ABS(WRR1(I))**SF/ABS(WRR1(INDEX))**SF)
      ENDIF
4     CONTINUE
3     CONTINUE
      IF (ITR.LT.0.OR.ITR.GT.5) THEN
      WRITE (6,*) 'This scaling option is not operational'
      ENDIF
C
      RETURN
      END
C
C
      SUBROUTINE ADATWRT (I)
C
C Subroutine ADATWRT writes out digital data to a binary workfile
C for quicker access during subsequent processing runs.
C Use subroutine DATIN2 to read the digital data back into the
C program.
C
      PARAMETER(NTP=4, NCH=80, NTR=4000)
C
      COMMON/C1/ XX(NTP,NTR), WR1, WR2, WR3, WR4, WR5, WR6
C
      WRITE (16) I,WR1,WR2,WR3,WR4,WR5,WR6
C
      IN = WR4
      DO 20 N=1,3
      WRITE (16) (XX(N,J),J=1,IN)
20    CONTINUE
C
999   FORMAT(3(5E14.6))
C
      RETURN
      END
```

RESAMPLE

```
      PROGRAM RESAMP
C
C
C THIS PROGRAM IS TO RESAMPLE THE DATA IF THE SAMPLING
C RATE IS MORE THAN 200 SAMPLES/SEC. IT USES THE MSF SIGNAL
CHANNEL TO RESANPLE THE DATA.
C
C
C                                                    WRITTEN BY
                                                     F.S.AHMED
                                                     OCT. 1988
C
C
C If the msf signal is clear (put imsf=0) the program counts the sampes no.to
C find the actual digitisation time. If there is doubt of the msf signal
C (put imsf=1) the program will use the average time which was taken by
C trying about 30 traces, (204 sample/s).
C
C The control file is "input"  "output"   imsf
C
C
      PARAMETER(NTP=4, NTR=4000 )
      DIMENSION ITRACE(NTP,NTR), X(NTP, NTR), AMP(NTP, NTR),
     *                 SS(NTR), ITR(NTR)
      CHARACTER  FNAME1*10, FNAME2*10, DAT*8, RSN*6, SSN*6,
     *                  AUT*3, INSTR*6
C
C  reading from control file
C
      OPEN (3,FILE='resout')
      READ(5,*) NFILE
      DO 50 KKK=1,NFILE
      WRITE(6,*)'PROCESSING FILE',KKK
      READ(5,*) FNAME1,FNAME2,IMSF
      OPEN (1,FILE=FNAME1)
      OPEN (2,FILE=FNAME2)
C
C
C  reading the data
C
      READ(1,110) RSN, SSN, AUT, DAT, NCHAN, INSTR
      WRITE(2,110) RSN, SSN, AUT, DAT, NCHAN, INSTR
      DO 10 M=1,NCHAN
      READ(1,120) POSIT, IGAIN, IPOL, ISAMP, AMPL
      WRITE(2,120) POSIT, IGAIN, IPOL, ISAMP, AMPL
10    CONTINUE
```

```
C
      JI=4000
      III=0
      DO 25 J=1,JI
      READ(1,130,END=26) (ITRACE(M,J),M=1, NCHAN)
      III=III+1
25    CONTINUE
26    IN=III
C
      CLOSE(1)
C
C to fix the time according to msf signal
C
      IF(IMSF.EQ.1) THEN
      ISEC=NINT(IN/200.0)
      SEC=real(ISEC-1)
      SR=204.0
      GO TO 45
      END IF
C
      LL=0
      NN=0
      ISEC=0
      DO 20 J=1,IN
       ITR(J)=ITRACE(3,J)
      IF(NN.GT.0.AND.NN.LT.100) GO TO 40
      IF(NN.GT.100) GO TO 2
      GO TO 1
2     NN=0
1     IF(ITR(J).EQ.0)  GO TO 3
40    NN=NN+1
      IF(NN.EQ.2)   ISEC=ISEC+1
C
C     TO COUNT SAMP.NO AFTER LAST S
C
      ITT=IN-J
      MMM=0
      IF(ITT.LT.208)  THEN
      MMM=MMM+1
      IF(NN.EQ.1.AND.MMM.EQ.1)  IEND=J
      END IF
      GO TO 20
3     LL=LL+1
C
C     TO COUNT THE SAMP.NO.TO 1st S
C
```

```
      IF(ISEC.EQ.0)  IEVENT=LL
20    CONTINUE
C
C     ISEC=ISEC-1
      IEVENT=IEVENT
      IEND=IEND-1
      ISTOP=IN-IEND
      IMID=IEND-IEVENT
      SEC=REAL(ISEC-1)
C
C to find the average sampling rate.
C
      SR=(IEND-IEVENT)/SEC
C
45    SR=SR
C
      DO 6 M=1,NCHAN
      DO 7 J=1,IN
      X(M,J)=REAL(ITRACE(M,J))
7     CONTINUE
6     CONTINUE
C
C the actual digitised time.
      IF(IMSF.EQ.0 )     TNS=(IEVENT+IMID+ISTOP-1)/SR
      IF(IMSF.EQ.1.AND.SEC.EQ.9)  TNS=(1/204.0)*2047
      IF(IMSF.EQ.1.AND.SEC.EQ.13)  TNS=(1/204.0)*2815
      IF(IMSF.EQ.1.AND.SEC.EQ.18)  TNS=(1/204.0)*3839
C
C the interpolation.
C
      TR=0.0
      TDL=TNS/FLOAT(IN-1)
      TRL=0.005
      DO 8 I=1,IN
      IF(I.GE.2)GO TO 9
      SS(I)=0.0
      GO TO 8
9     SS(I)=SS(I-1)+TDL
8     CONTINUE
      DO 11 N=1,NCHAN
      AMP(N,1)=X(N,1)
11    CONTINUE
C
      DO 12 MM=2,IN
      TR=TR+TRL
      IK=INT(TR/TDL+1.0)
```

```
      II=IK+1
      DO 13 N=1,NCHAN
      AMP(N,MM)=X(N,IK)+(TR-SS(IK))*(X(N,II)-X(N,IK))/TDL
13    CONTINUE
12    CONTINUE
C
C to write the output
C
      DO 14 N=1,NCHAN
      DO 15 J=1,IN
      ITRACE(N,J)=NINT(AMP(N,J))
15    CONTINUE
14    CONTINUE
C
      DO 16 J=1,IN
      WRITE(2,130)(ITRACE(N,J),N=1,NCHAN)
16    CONTINUE
      CLOSE (2)
C
      WRITE(6,*)'THE OUTPUT IS ',FNAME2
      WRITE(3,*)FNAME1, 'SAM.RATE', SR, 'S.PULS', SEC+1
C
50    CONTINUE
      CLOSE (3)
C
110   FORMAT (2(A,2X),A,2X,A,I3,2X,A)
120   FORMAT (F7.3,I3,I2,I6,F7.3)
130   FORMAT (3I5)
      STOP
      END
```

ZMSF

```
      PROGRAM ZMSF
C
C This program is to rewrite the msf channel whether it is noisy or reverse.
C
C
      PARAMETER(NTP=4, NTR=4000 ,KLK=20)
      DIMENSION ITRACE (NTP, NTR), ITR(NTR), IPOL(NTP), IS(KLK),
     *IE(KLK)
      CHARACTER  FNAME1*10, FNAME2*10, DAT*8, RSN*6, SSN*6,
      *AUT*3, INSTR*6
C
      write(6,*)'The input and output files name'
      READ(5,*) FNAME1,FNAME2
C     write(6,*)'The lowest( or the higest value in case of reverse)
C     *  to be zero'
C     READ*,IMS
      OPEN (1,FILE=FNAME1)
      OPEN (2,FILE=FNAME2)
C
C
C reading the data
C
      READ(1,110) RSN, SSN, AUT, DAT, NCHAN, INSTR
      WRITE(2,110) RSN, SSN, AUT, DAT, NCHAN, INSTR
      DO 10 M=1,NCHAN
      READ(1,120) POSIT,IGAIN,IPOL(M),ISAMP,AMPL
      WRITE(2,120) POSIT,IGAIN,IPOL(M),ISAMP,AMPL
10    CONTINUE
C
      JI=4000
      III=0
      DO 25 J=1,JI
      READ(1,130,END=26) (ITRACE(M,J),M=1,NCHAN)
      III=III+1
25    CONTINUE
26    IN=III
C
      WRITE(6,*)'Is the MSF noisy or reverse?'
      WRITE(6,*)'Write "1"for the noisy trace and "0"for the reverse'
      READ(5,*) KKPP
C
C this part for the noisy channal.
C
      IF(KKPP.EQ.1)THEN
      WRITE(6,*)'Write the number of sec. pulses'
      READ (5,*)IP
```

```
      DO 11 KK=1,IP
      WRITE(6,*)'Write the start and end of',kk,'sec.pulse'
      READ(5,*) IS(KK),IE(KK)
11    CONTINUE
      I=1
      DO 12 J=1,IN
      ITR(J)=ITRACE(3,J)
      IF(J.LT.IS(I))  ITR(J)=0
      IF(J.GE.IS(I).AND.J.LE.IE(I)) ITR(J)=ITR(J)
      IF(J.GT.IE(I).AND.I.GT.IP) ITR(J=0
      IF (J.GT.IE(I)) I=I+1
      ITRACE(3,J)=ITR(J)
      WRITE(2,130)(ITRACE(N,J),N=1,NCHAN)
12    CONTINUE
C
C This part for the reverse MSF
C
      ELSE IF (KKPP.EQ.0)  THEN
      DO 20 J=1,IN
      ITR(J)=ITRACE(3,J)
      IF(ITR(J).EQ.0)         ITR(J)=3000
      IF(ITR(J).LT.3000)      ITR(J)=0
C     IF(IPOL(3).EQ.1.AND.ITR(J).GT.IMS)      ITR(J)=0
C     IF(IPOL(3).EQ.0.AND.ITR(J).LT.IMS)      ITR(J)=0
      ITRACE(3,J)=ITR(J)
      WRITE(2,130) (ITRACE(N, J), N=1, NCHAN)
20    CONTINUE
      ENDIF
C
C
      WRITE(6,*)'THE OUTPUT IS',FNAME2
C
110   FORMAT (2(A,2X),A,2X,A,I3,2X,A)
120   FORMAT (F7.3,I3,I2,I6,F7.3)
130   FORMAT (3I5)
      STOP
      END
```

CON

```
      PROGRAM CON
C
C This program is used for reading 3-components data and to start
C them at the same time according to the number of samples from
C the shotpoint .
C
C
      PARAMETER (NTR=4000,NTP=4)
      DIMENSION ITRACE(NTP, NTP, NTR), ITR(NTP, NTP, NTR),
     *                IXX(NTP, NTR), SL1(NTP), ISL2(NTP), ISL3(NTP),
     *                SL5(NTP), POSIT(NTP,NTP), AMPT(NTP,NTP),
     *                ISAMP(NTP), IGAIN(NTP,NTP), IPOL(NTP,NTP)
      CHARACTER FN1*10, FN2*10, FN3*10, FN4*10, DAT*8, RSN*6,
     *                  SSN*6, INSTR*6, AUT*3
C
      READ(5,*)NFILE
      DO 21 K=1,NFILE
      PRINT*,'PROCESSING STATION NUMBER',K
      READ(5,*) FN1,FN2,FN3,FN4
C
      OPEN(UNIT=1,FILE=FN1)
      OPEN(UNIT=2,FILE=FN2)
      OPEN(UNIT=3,FILE=FN3)
      OPEN(UNIT=4,FILE=FN4)
C
C reading the data
C
      READ (1,1)RSN,SSN,AUT,DAT,NCHAN,INSTR
      READ (2,1)RSN,SSN,AUT,DAT,NCHAN,INSTR
      READ (3,1)RSN,SSN,AUT,DAT,NCHAN,INSTR
C
      DO 8 I=1,NCHAN
      READ (1,2)POSIT(1,I),IGAIN(1,I),IPOL(1,I),ISAMP(1),AMPT(1,I)
      READ (2,2)POSIT(2,I),IGAIN(2,I),IPOL(2,I),ISAMP(2),AMPT(2,I)
      READ (3,2)POSIT(3,I),IGAIN(3,I),IPOL(3,I),ISAMP(3),AMPT(3,I)
8     CONTINUE
C
      JI=4000
      III=0
      DO 30 J=1,JI
      READ(1,3,END=29) (ITRACE(1,M,J),M=1,3)
      READ(2,3,END=29) (ITRACE(2,M,J),M=1,3)
      READ(3,3,END=29) (ITRACE(3,M,J),M=1,3)
      III=III+1
30    CONTINUE
29    IN=III
```

```
C
C
C To start the three files according to the number of samples from the
C shotpoint to the digitization time of each file.
C
      IF (ISAMP(1).LT.ISAMP(2).AND.ISAMP(1).LT.ISAMP(3).OR.ISAMP(2)
     *         .EQ.ISAMP(3).AND.ISAMP(3).LT.ISAMP(1))THEN
      J1=0
      J2=ISAMP(2)-ISAMP(1)
      J3=ISAMP(3)-ISAMP(1)
      IFL=ISAMP(1)
C
      ELSE IF(ISAMP(2).LT.ISAMP(1).AND.ISAMP(2).LT.ISAMP(3).OR.
     *  ISAMP(1).EQ.ISAMP(3).AND.ISAMP(2).LT.ISAMP(1))THEN
      J1=ISAMP(1)-ISAMP(2)
      J2=0
      J3=ISAMP(3)-ISAMP(2)
      IFL=ISAMP(2)
C
      ELSE IF(ISAMP(3).LT.ISAMP(1).AND.ISAMP(3).LT.ISAMP(2).OR.
     * ISAMP(1).EQ.ISAMP(2).AND.ISAMP(3).LT.ISAMP(1))THEN
      J1=ISAMP(1)-ISAMP(3)
      J2=ISAMP(2)-ISAMP(3)
      J3=0
      IFL=ISAMP(3)
C
      ELSE IF (ISAMP(1).EQ.ISAMP(2).AND.ISAMP(2).LT.ISAMP(3))THEN
      J1=0
      J2=0
      J3=ISAMP(3)-ISAMP(1)
      IFL=ISAMP(1)
C
      ELSE IF (ISAMP(1).EQ.ISAMP(3).AND.ISAMP(3).LT.ISAMP(2))THEN
      J1=0
      J2=ISAMP(2)-ISAMP(1)
      J3=0
      IFL=ISAMP(1)
C
      ELSE IF (ISAMP(2).EQ.ISAMP(3).AND.ISAMP(3).LT.ISAMP(1))THEN
      J1=ISAMP(1)-ISAMP(2)
      J2=0
      J3=0
      IFL=ISAMP(2)
      END IF
C
      IFL=IFL
```

```
C
C To truncate the files at the same time
C
      IF (j1.GT.j2) THEN
      LARGE=J1
      ELSE
      LARGE=J2
      END IF
      IF (LARGE.GT.J3) THEN
      LARGEST=LARGE
      ELSE
      LARGEST=J3
      END IF
      LF=LARGEST
C
      IDFL=IN-1
      IEF=IDFL-LF
C
C To read the data at the same time with the same length
C
C
      DO 11 I=1,NCHAN
      DO 12 N=J1,iEF
      ITR(1,I,(N-J1+1))=ITRACE(1,I,N)
12    CONTINUE
C
      DO 13 N=J2,iEF
      ITR(2,I,(N-J2+1))=ITRACE(2,I,N)
13    CONTINUE
C
      DO 14 N=J3,iEF
      ITR(3,I,(N-J3+1))=ITRACE(3,I,N)
14    CONTINUE
11    CONTINUE
C
C  To select one channel
C
      DO 15 M=1,3
      DO 16 I=1,NCHAN
      IF(POSIT(M,I).EQ.0)GO TO 16
      SL1(M)=POSIT(M,I)
      ISL2(M)=IGAIN(M,I)
      ISL3(M)=IPOL(M,I)
      ISL3(m)=1
      SL5(M)=AMPT(M,I)
C
```

```
      DO 17 N=1,iEF
C     IF(IPOL(M,I).NE.0) ITR(M,I,N)=-1*ITR(M,I,N)
      IXX(M,N)=ITR(M,I,N)
17    CONTINUE
16    CONTINUE
C
C write the output file
C
      WRITE(4,5)RSN,SSN,AUT,DAT,NCHAN,INSTR
      WRITE(4,2)SL1(1),ISL2(1),ISL3(1),IFL,SL5(1)
      WRITE(4,2)SL1(2),ISL2(2),ISL3(2),IFL,SL5(2)
      WRITE(4,2)SL1(3),ISL2(3),ISL3(3),IFL,SL5(3)
C
      DO 18 N=1,IEF
      IFI (FN3.EQ.FN2)     IXX(3,N)=0
      WRITE(4,3) IXX(1,N),IXX(2,N),IXX(3,N)
18    CONTINUE
C
      WRITE(6,*)'THE OUTPUT FILE IS ', fn4
21    CONTINUE
C
1     FORMAT (2(A6,2X),A3,2X,A8,I3,2X,A6)
2     FORMAT (F7.3,I3,I2,I6,F7.3)
3     FORMAT(3I5)
5     FORMAT (A4,4X,A6,2X,A3,2X,A8,I3,2X,A6)
C
      CLOSE(1)
      CLOSE(2)
      CLOSE(3)
      CLOSE(4)
C
      STOP
      END
```

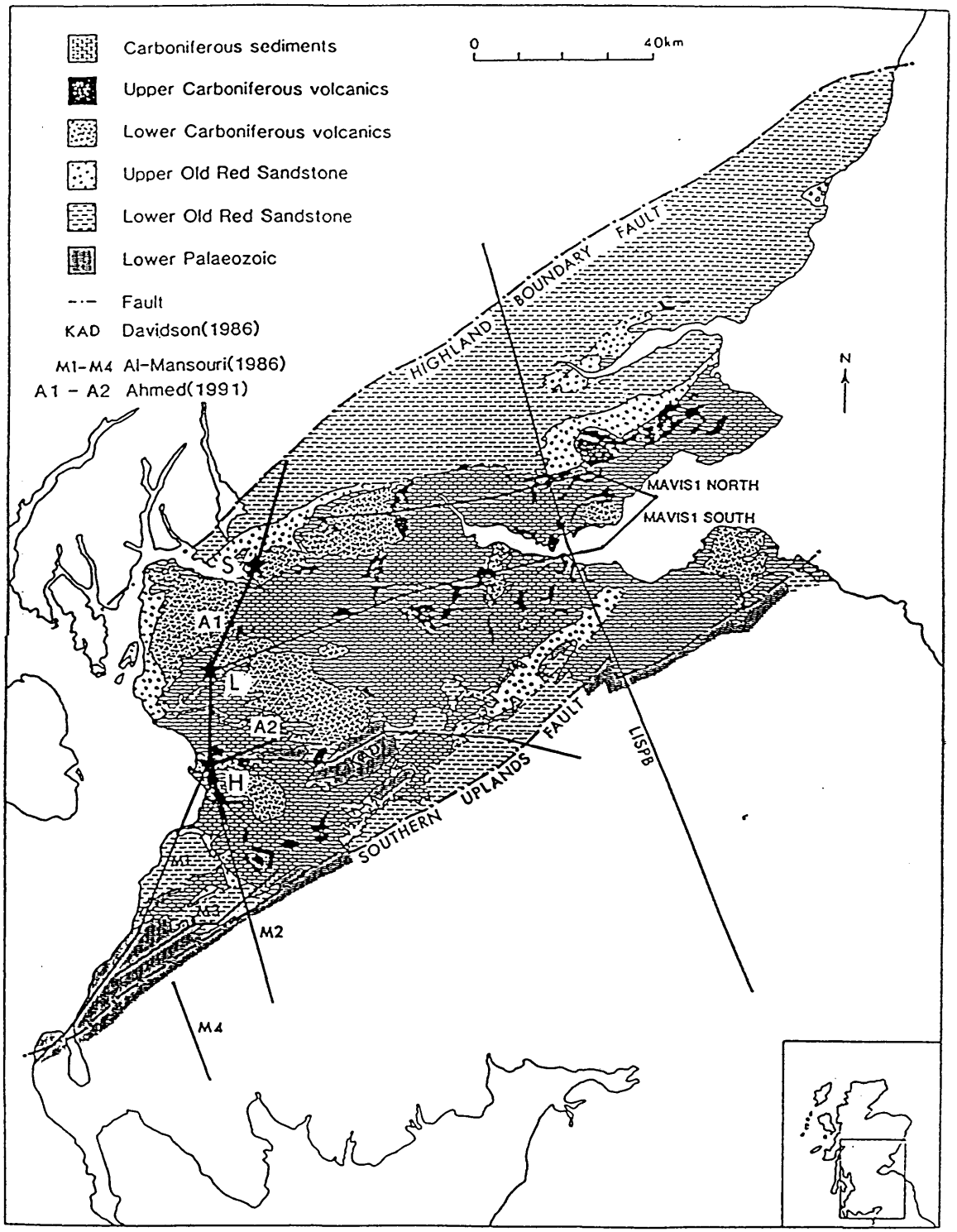

Fig. 1.1 Location and geological map of the Midland Valley of Scotland. Seismic profiles are shown, thick lines (A1, A2) are those of this study, thin lines are those of previous studies. A star indicates a shotpoint used in this study. From north to south these are: S = Sheephill, L = Loanhead, H = Hillhouse.

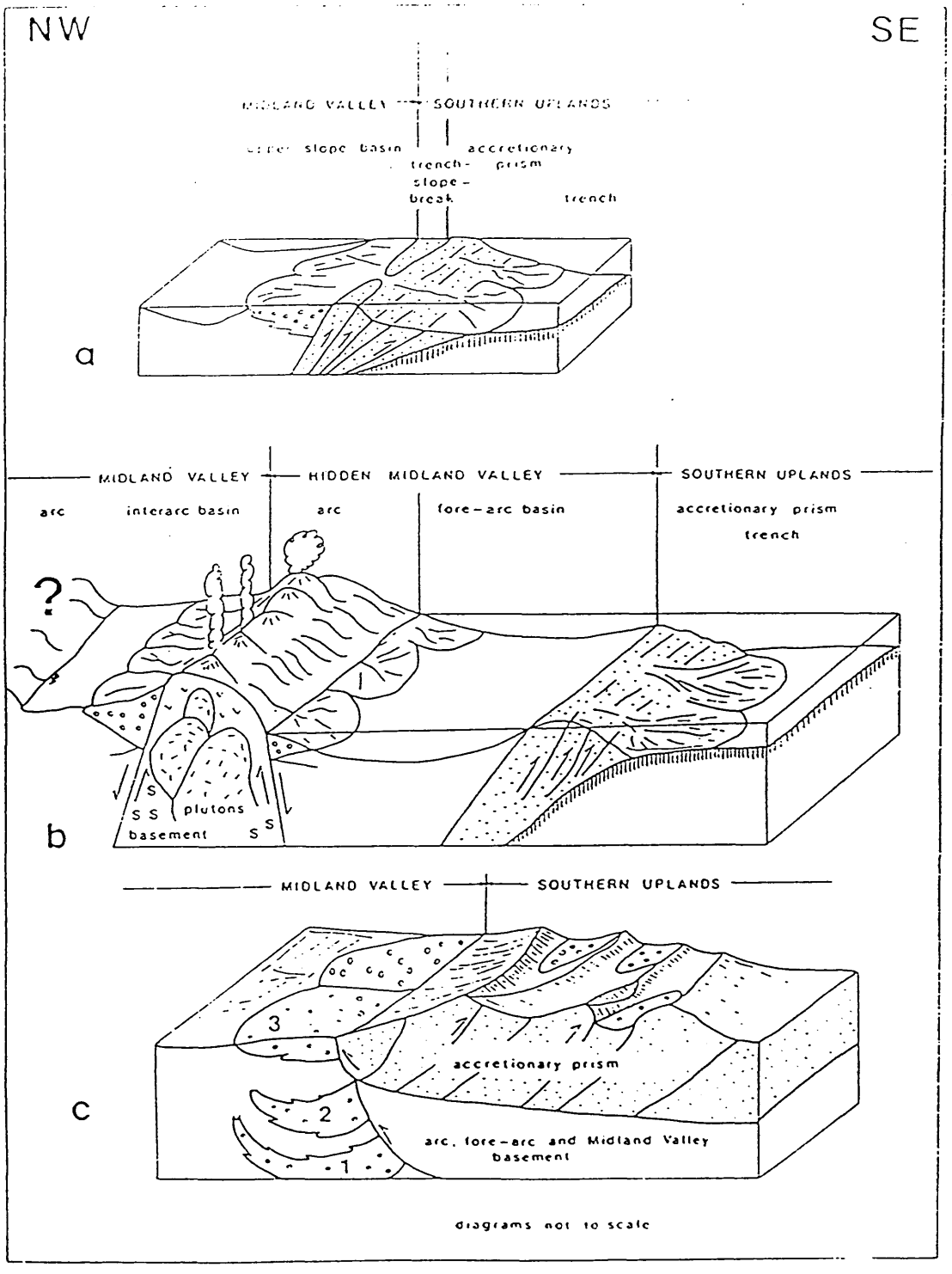

Fig. 1.2 Tectonic model of the Midland Valley during Ordovician-Devonian a)Midland Valley as fore-arc basin with trench-slope-break and upper-slope basin b) missing fore-arc basin beneath Southern Uplands and c) overthrusting of accretionary prism (after Bluck 1983).

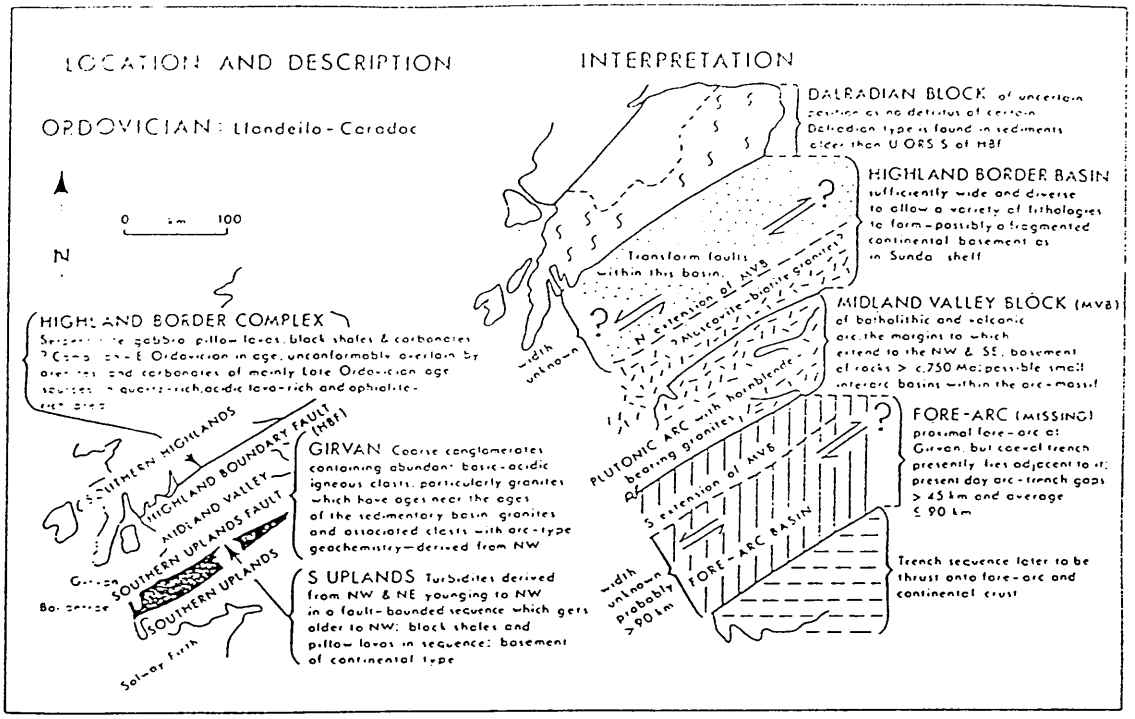

Fig. 1.3a Tectonic setting of the Midland Valley of Scotland during the Ordovician (after Bluck 1984).

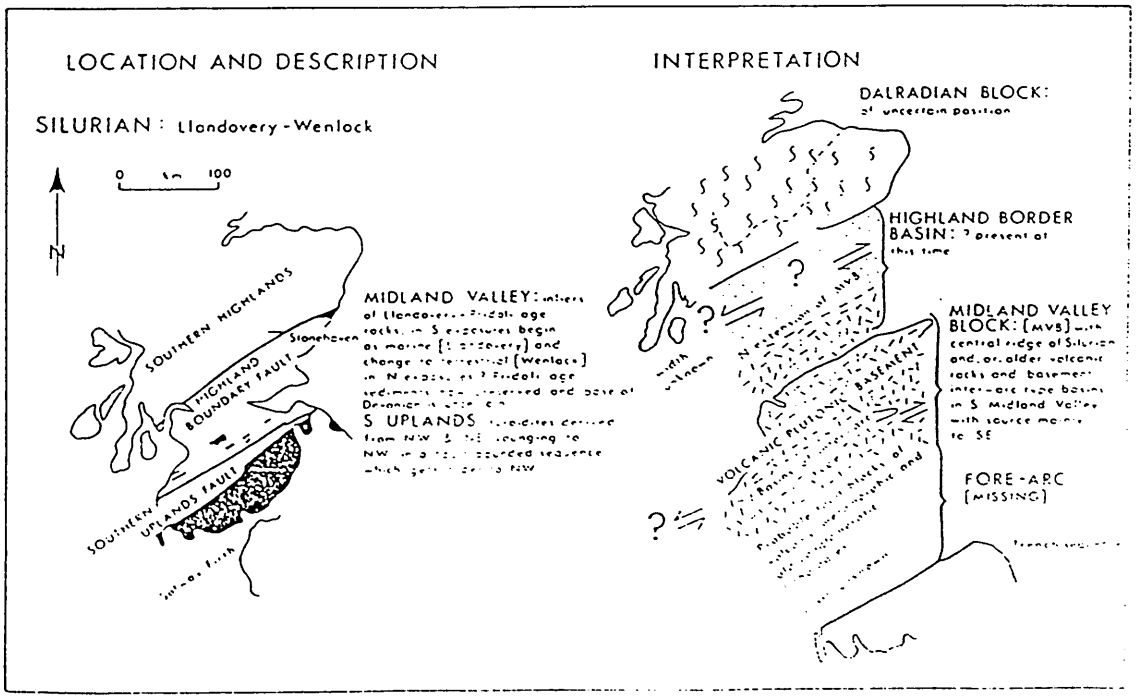

Fig. 1.3b Tectonic setting of the Midland Valley of Scotland during the Silurian (after Bluck 1984).

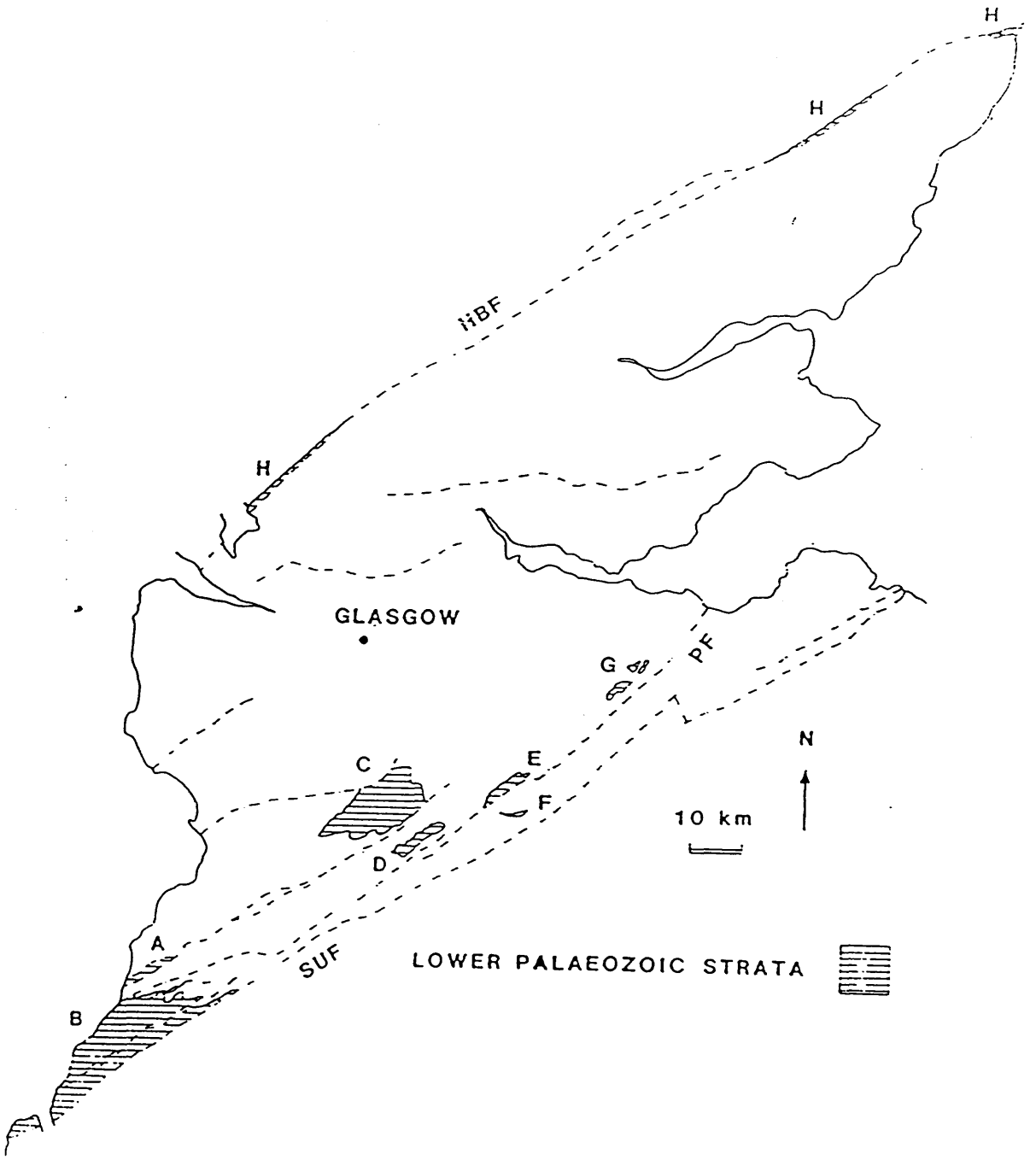

Fig. 1.4 Outcrop of Lower Palaeozoic rocks in the Midland Valley of Scotland. A - Craighead, B - Girvan, C - Lesmahagow, D - Hagshaw Hills, E - Carmichael, F - Eastfield, G - Pentland Hills, H - Highland Border, HBF - Highland Boundary Fault, SUF - Southern Uplands Fault (after Dentith 1987).

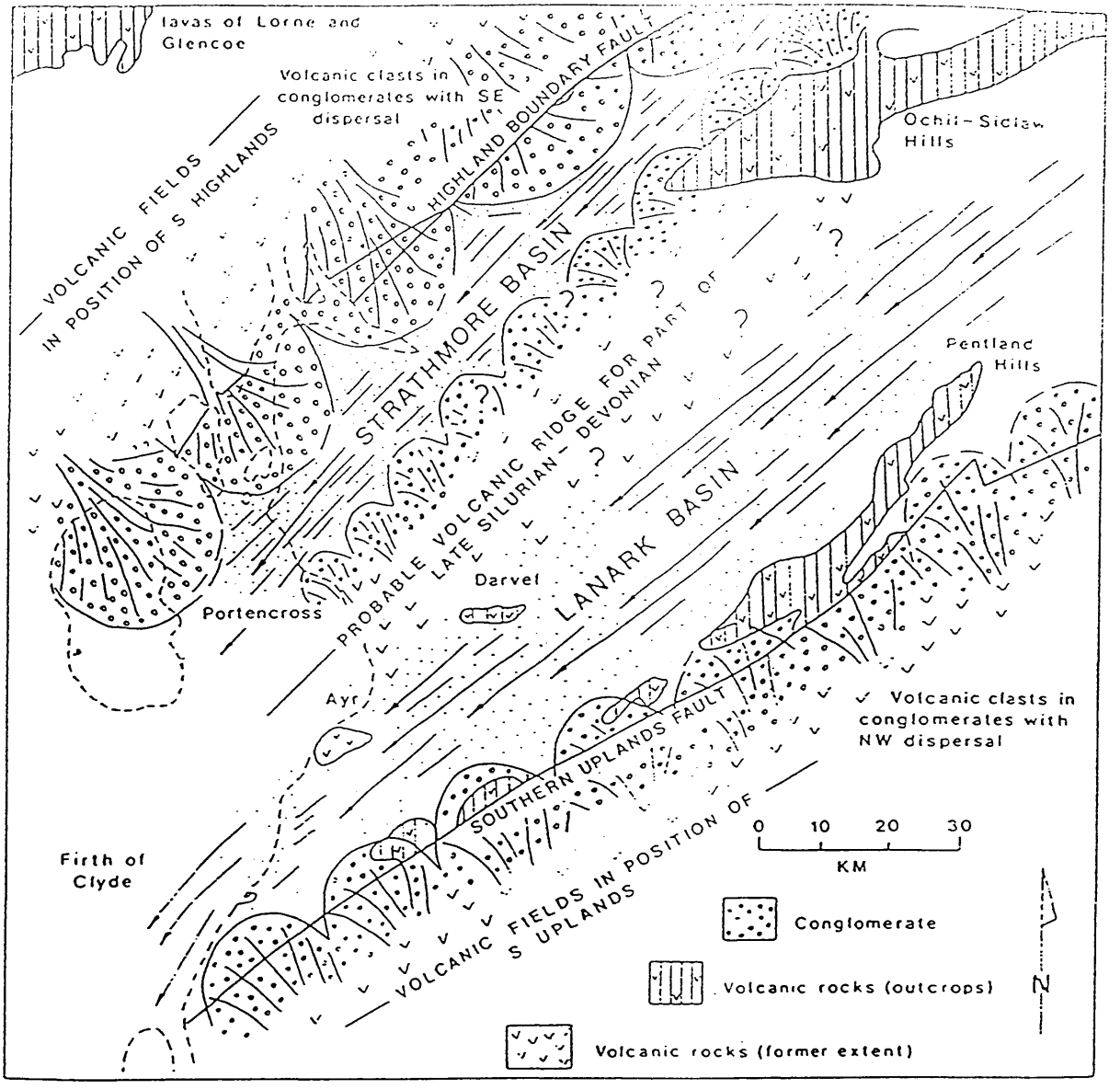

Fig. 1.5 Palaeogeography of the Midland Valley during the late Silurian and early Devonian (after Bluck 1983).

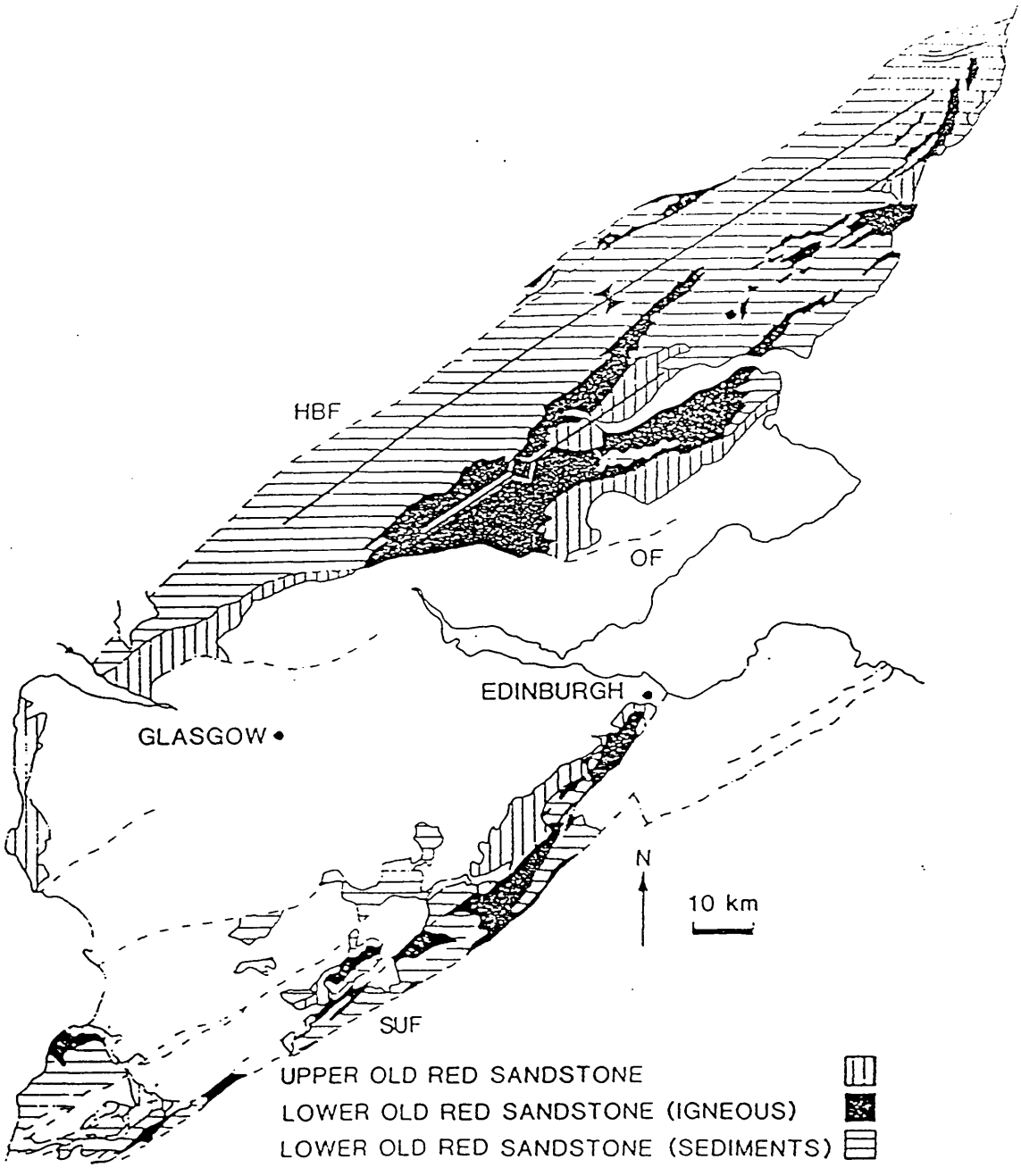

Fig. 1.6 Distribution of ORS strata in the Midland Valley of Scotland. (after Dentith 1987). Ochil Fault - OF

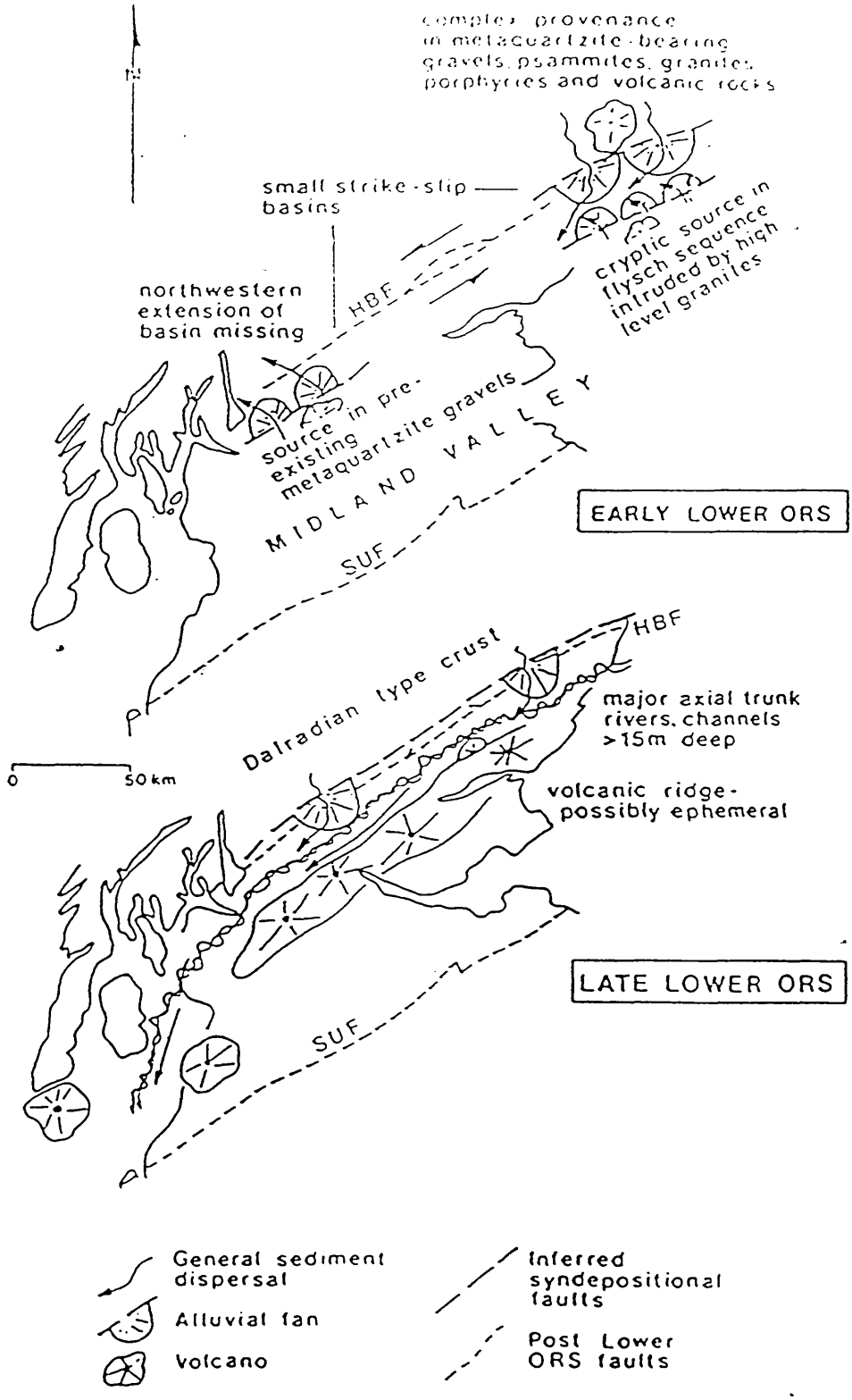

Fig. 1.7 Early and Late Lower ORS palaeogeographies for the northern Midland Valley (after Haughton 1989).

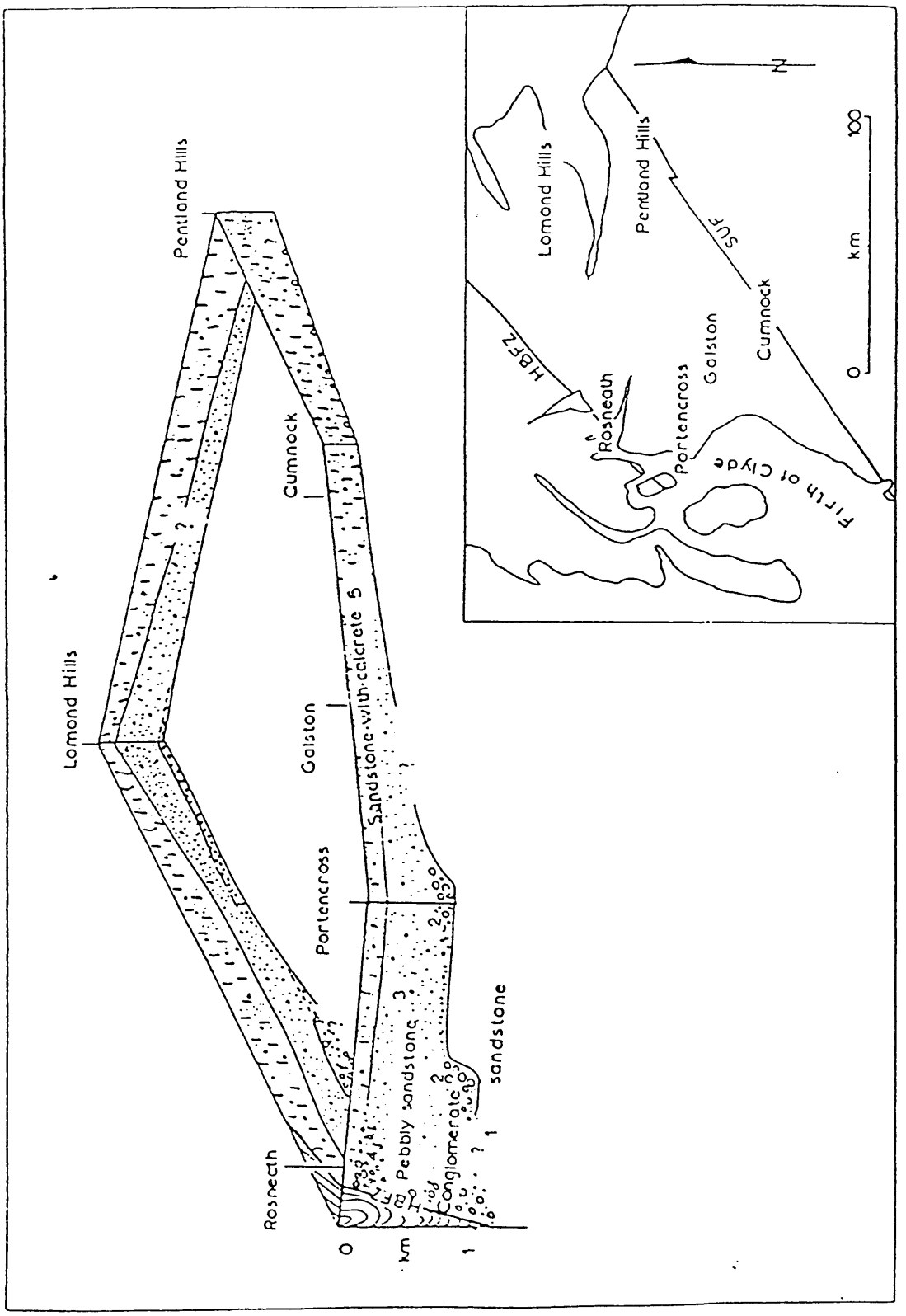

Fig. 1.8 Distribution of Upper Old Red Sandstone rocks in the Midland Valley (after Bluck 1978).

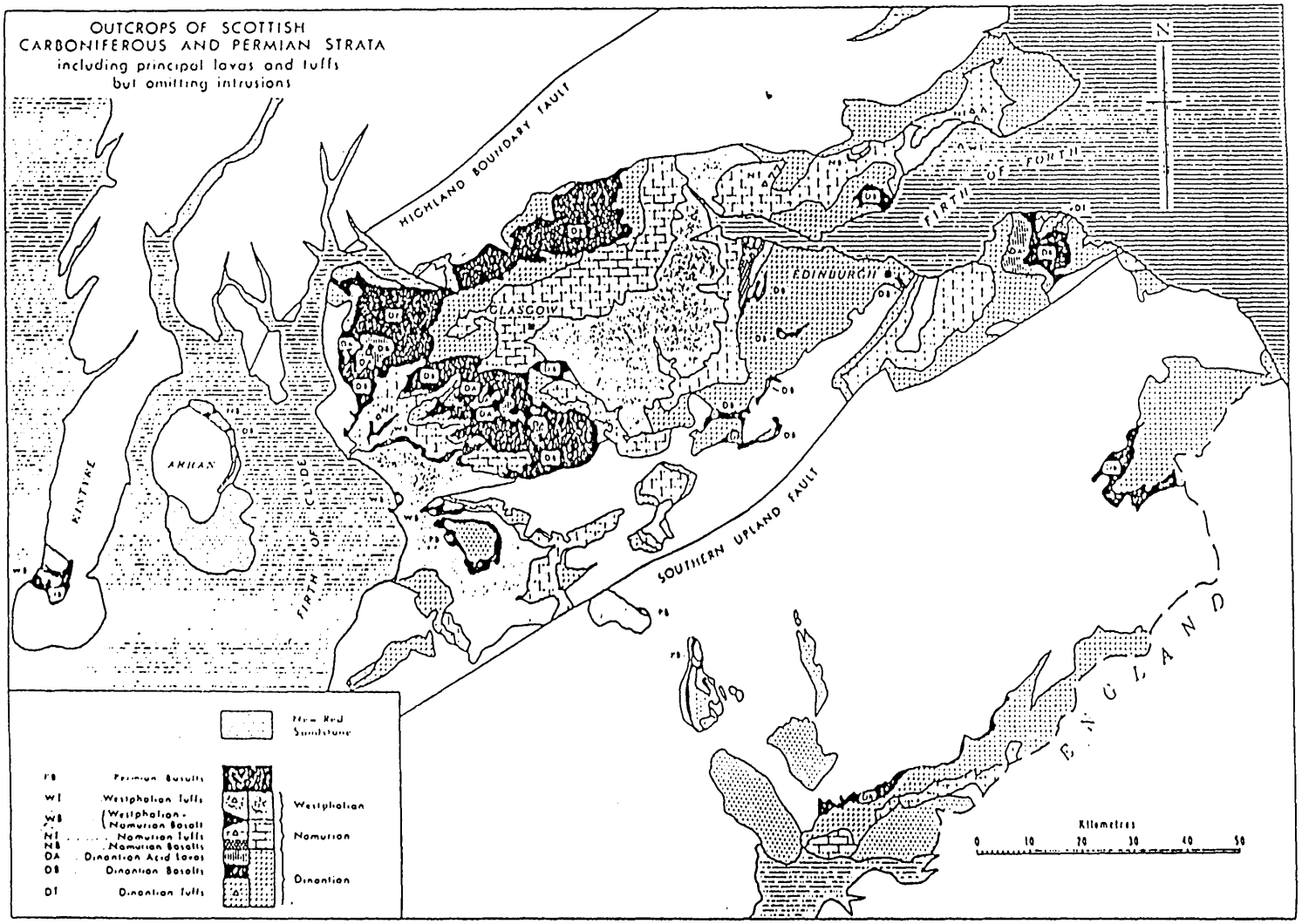

Fig. 1.9 Distribution of Permo-Carboniferous volcanic rocks in southern Scotland (after Francis 1983).

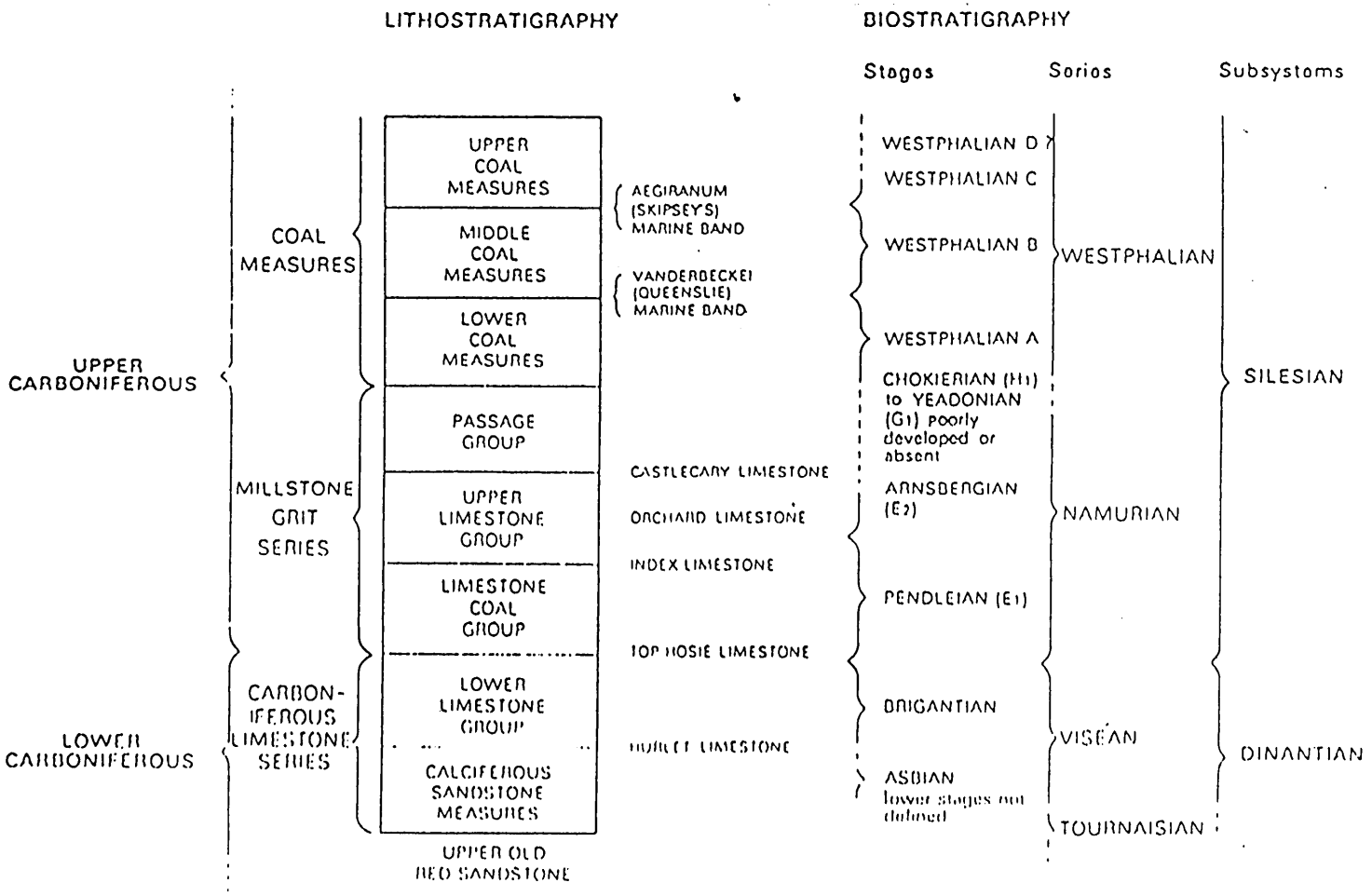

Fig. 1.10 Carboniferous stratigraphy of the Midland Valley of Scotland (after Cameron & Stephenson 1985).

Thickness of Carboniferous rocks in the western Midland Valley

Ballycastle	Machrihanish	Arran	South and central Ayrshire	North Ayrshire
		Coal Measures ?200–300 m (an attenuated sequence with no coals)	Barren Red Measures Volcanics (Stephanian) up to c. 205 m Sediments up to 550 m	Barren Red Measures up to 380 m (variable thickness)
	Lower and Middle Coal Measures c. 150 m	Passage Group c. 59 m (sandstones, marls and volcanics, cut out northwards)	Lower and Middle Coal Measures 427 m at Dalmellington	Lower and Middle Coal Measures 150–220 m
Namurian c. 100 m	Passage Group c. 137 m (lavas with sedimentary intercalations)	Carboniferous Limestone Series c. 138 m	Passage Group up to 128 m (entirely sedimentary sequence)	Passage Group Upper sedimentary Group thin and variable Volcanics up to 150 m Lower Sedimentary Group thin and variable
Lower Carboniferous c. 540 m (arenaceous with coals and marine bands)	Upper Limestone Group	Calciferous Sandstone Series thickness unknown	Upper Limestone Group c. 215 m	Upper Limestone Group 90 m+
	Limestone Coal Group 77 m (with good coals)		Limestone Coal Group c. 60 m	Limestone Coal Group 150 m+
	No Calciferous Sandstone sediments recognised but an unknown thickness of lavas is present		Lower Limestone Group up to 30 m	Lower Limestone Group up to 60 m
			Calciferous Sandstone Series 490 m (max.) Upper Group Cementstone Group Shale Subgroup Cornstone Beds Basal Sandstones	Calciferous Sandstone Series Upper Sedimentary Group up to 45 m Clyde Plateau Lavas Cementstone Group

Fig. 1.11 Thickness of Carboniferous rocks in the western Midland Valley (after McLean & Deegan 1978).

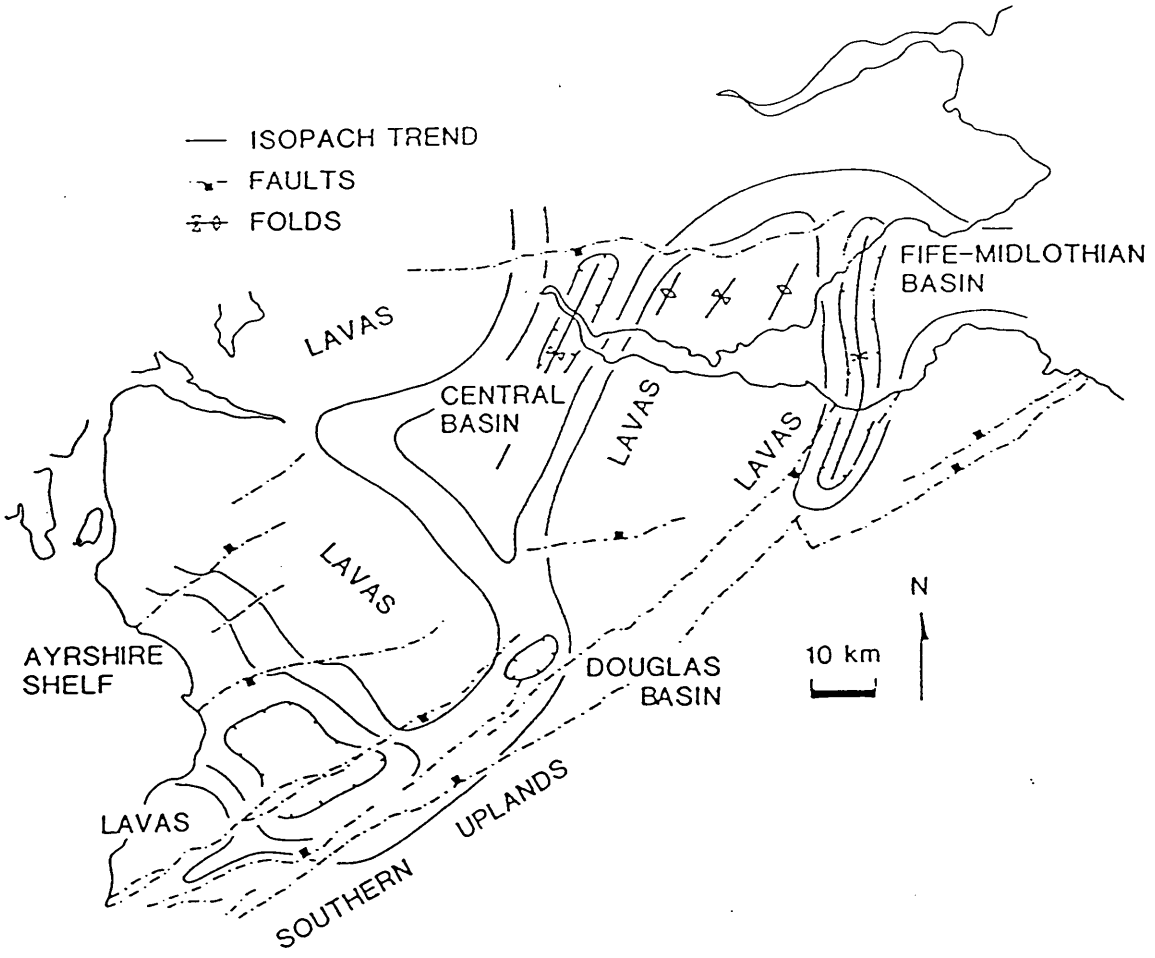

Fig. 1.12 Controls on sedimentation within the Midland Valley of Scotland. Ticks are downthrown side of faults (after Dentith 1987).

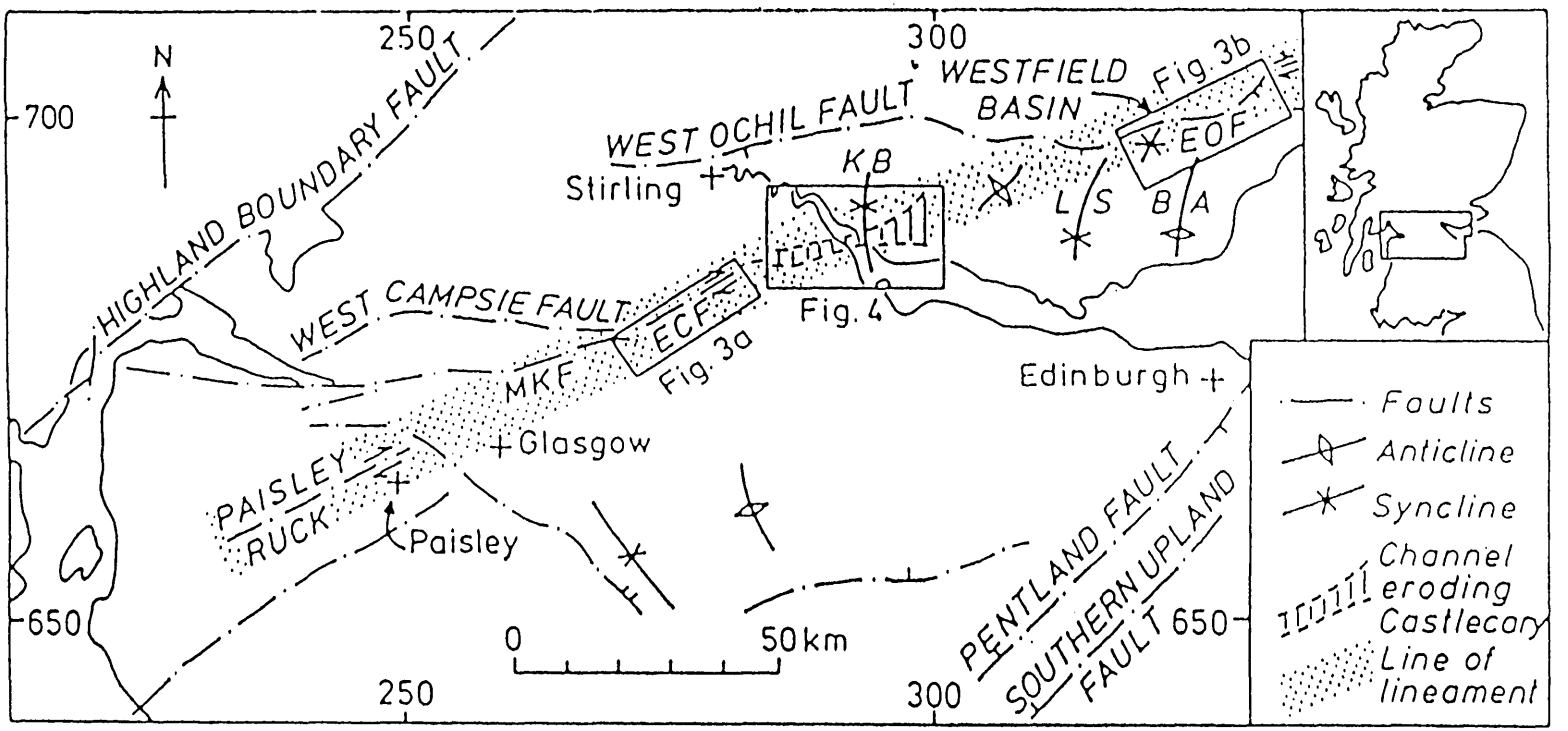

Fig. 1.13 Sketch map of part of the Midland Valley, showing selected major surface structures (after Read 1989).

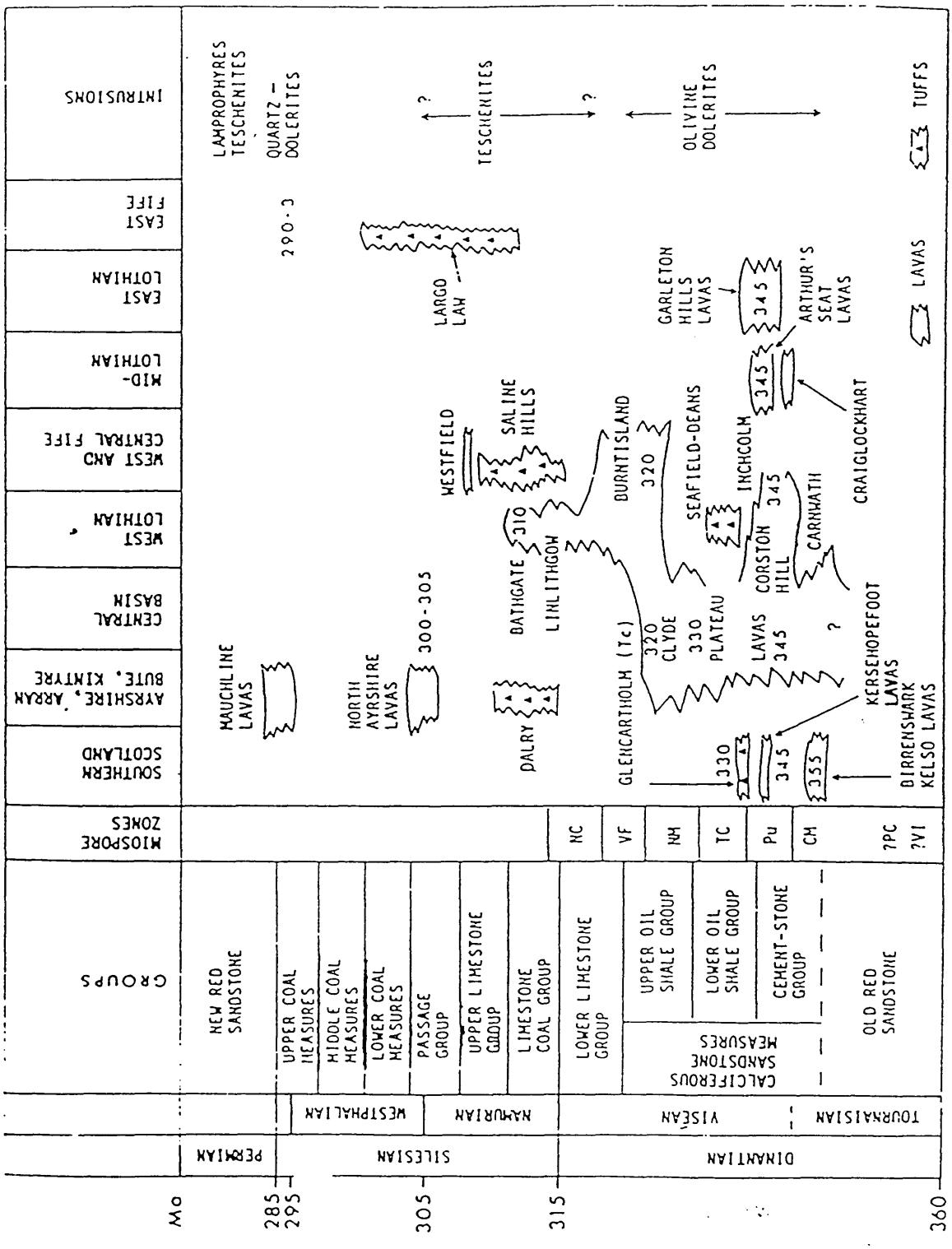

Fig. 1.14 Summary of the distribution of ages and lateral extent of Carboniferous lavas in the Midland Valley (after Francis 1983).

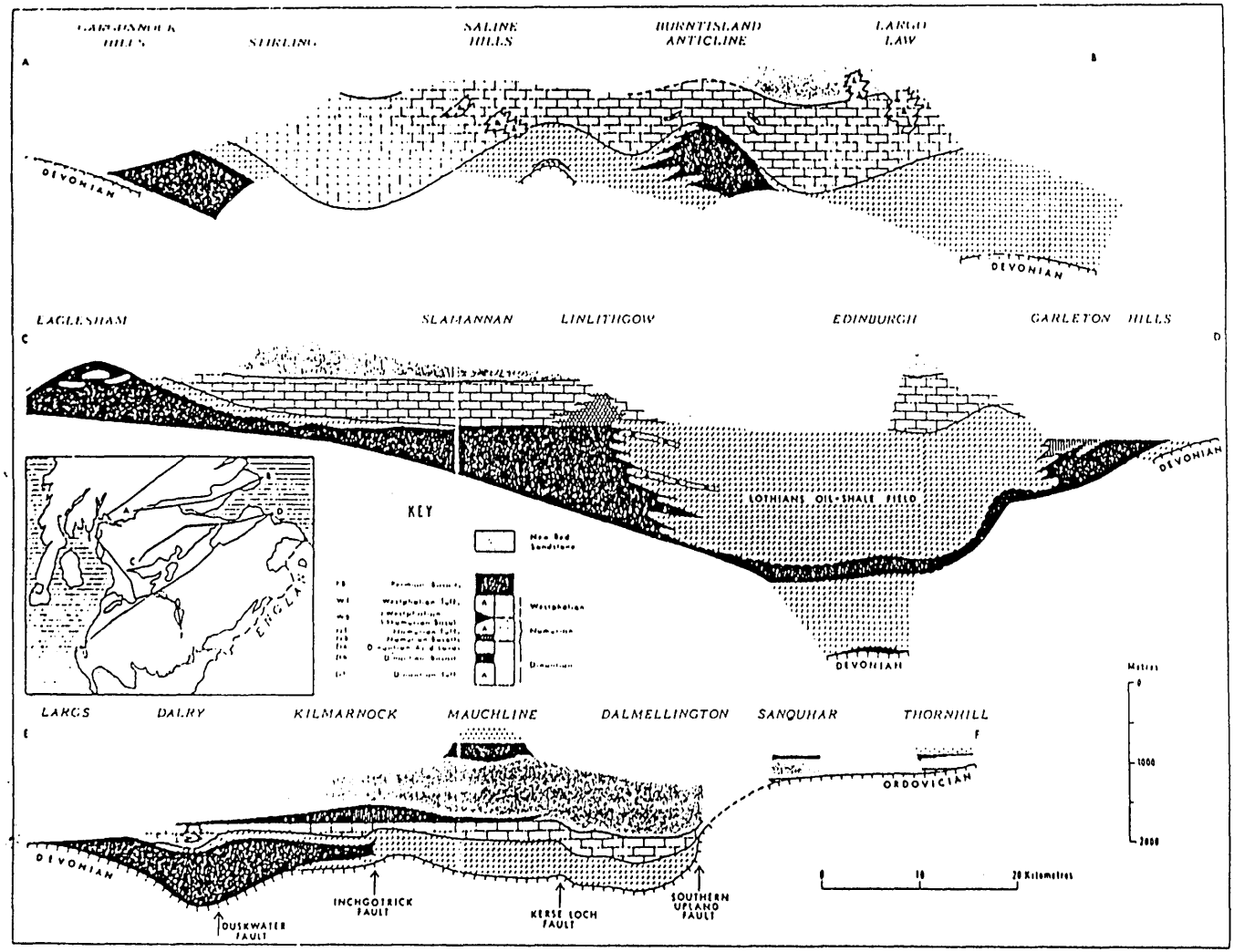

Fig. 1.15 Horizontal sections across the Midland Valley to show the stratigraphical position of the principal lavas and tuffs (after Francis 1983).

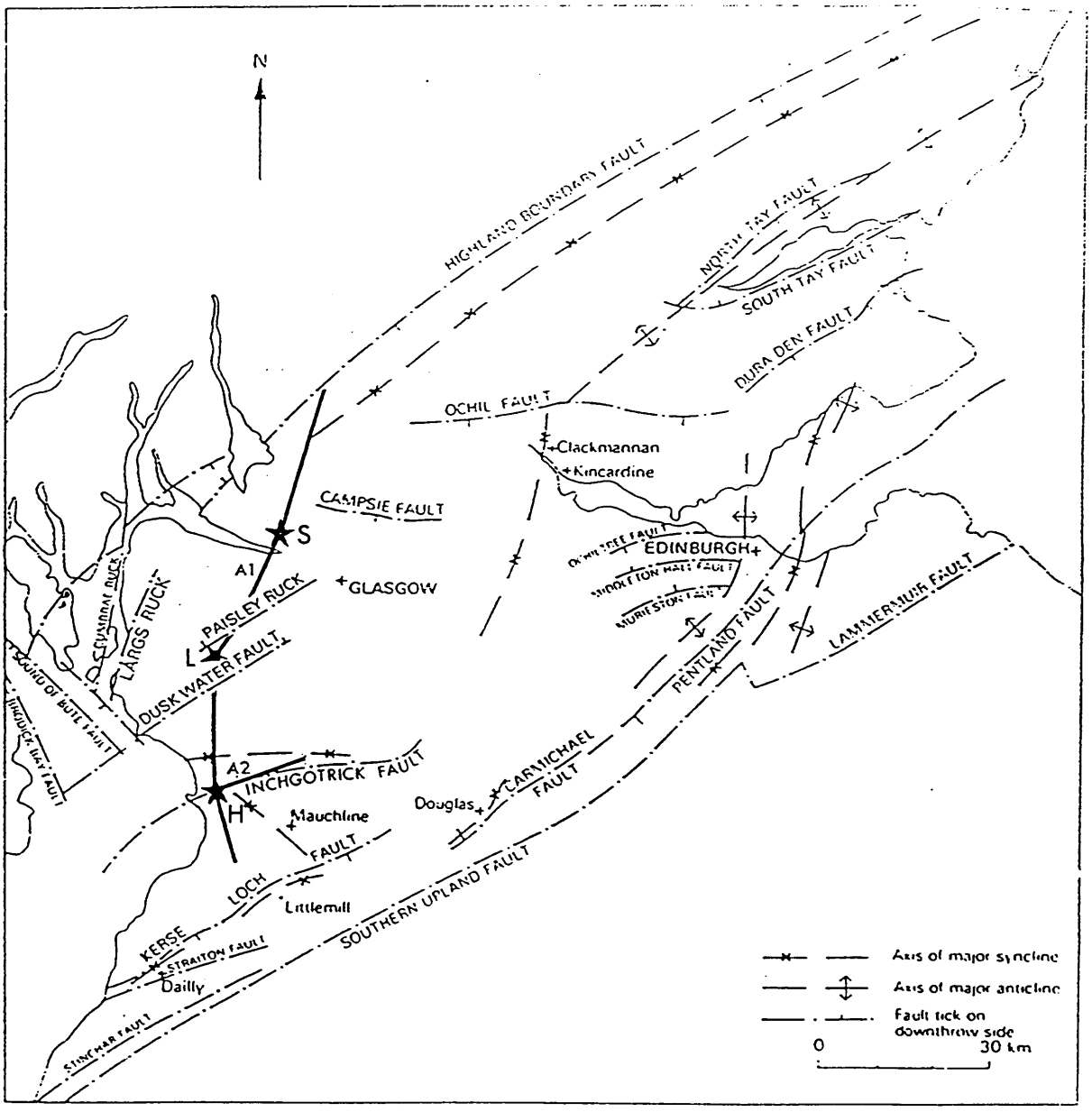

Fig. 1.16 Principal faults and folds in the Midland Valley (after Cameron & Stephenson 1985), showing the seismic profiles of this study. A star indicates a shotpoint used in this study. H = Hillhouse, L = Loanhead, S = Sheephill.

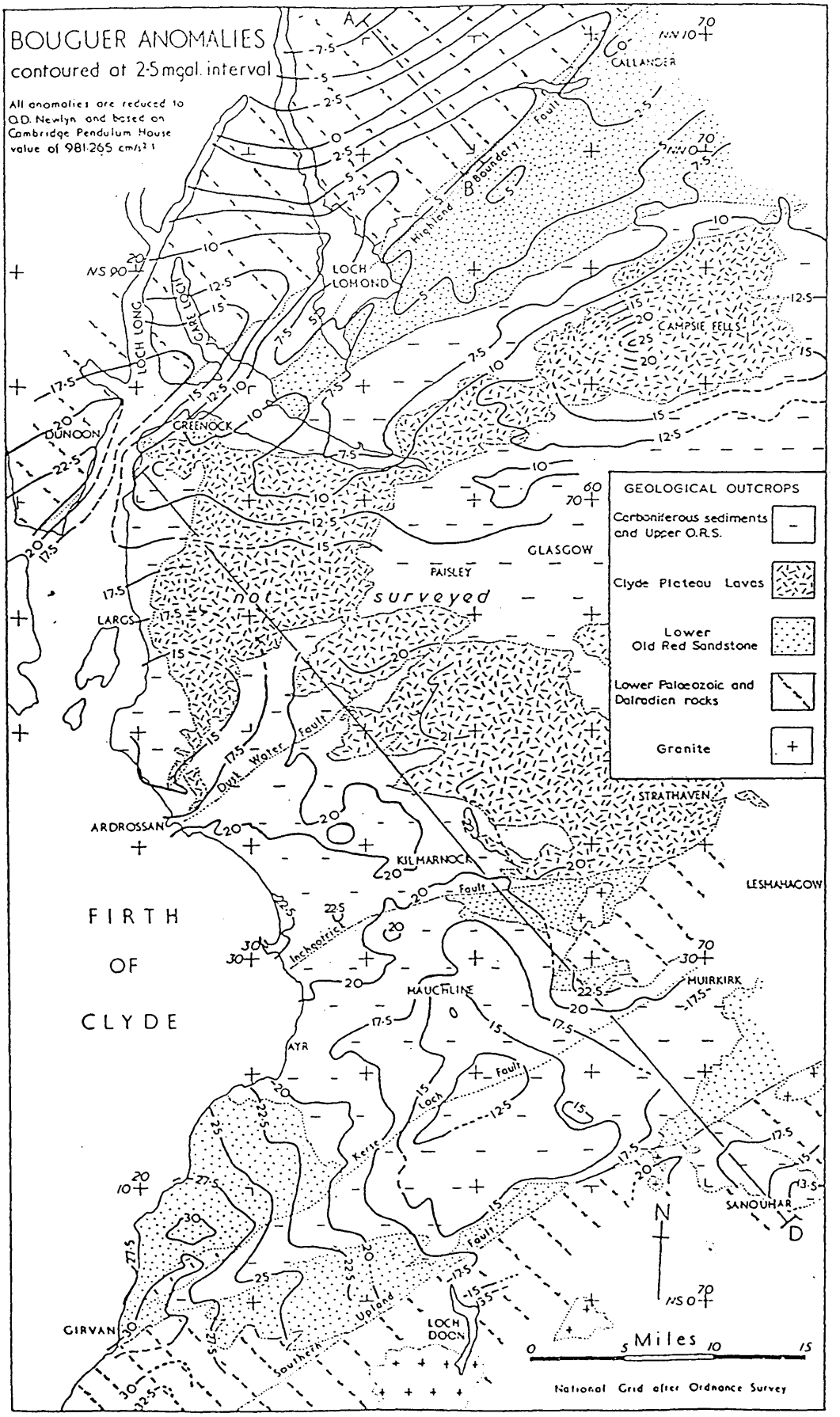

Fig. 2.1 Bouguer anomalies map of the western Midland Valley (after McLean and Qureshi, 1966).

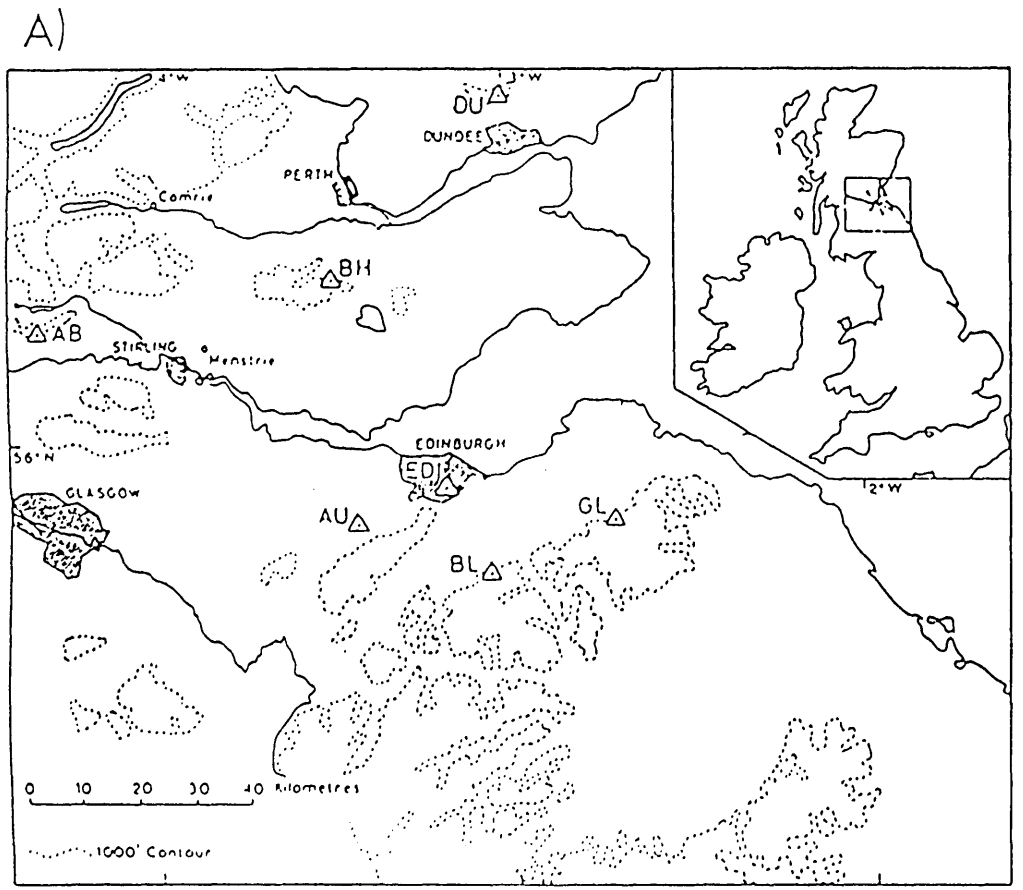

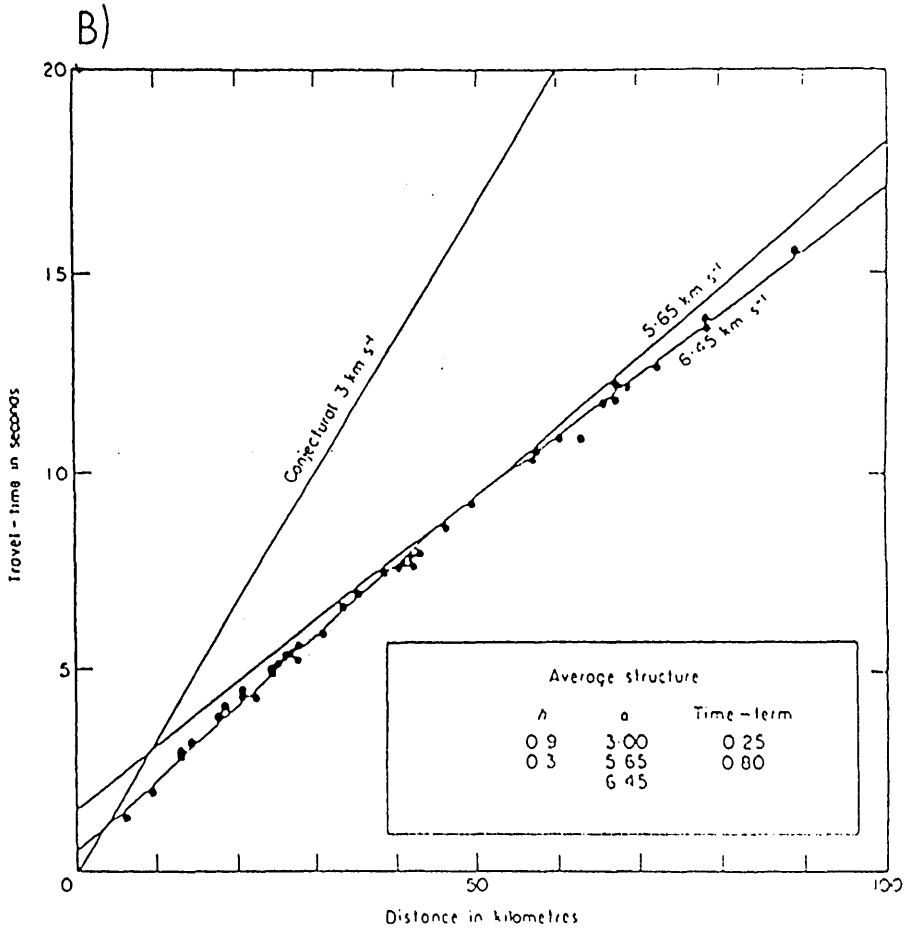

Fig. 2.2 LOWNET: A) Location of seismic arrays. AB-Aberfoyle, AU-Auchinoon Hill, BH-Black Hill, BL-Broad Law, DU-Craigowl Hill, Dundee, EDI-Royal Observatory Edinburgh, GL - Gala Law. B) Travel-time data and interpretation (after Crampin *et al.* 1970).

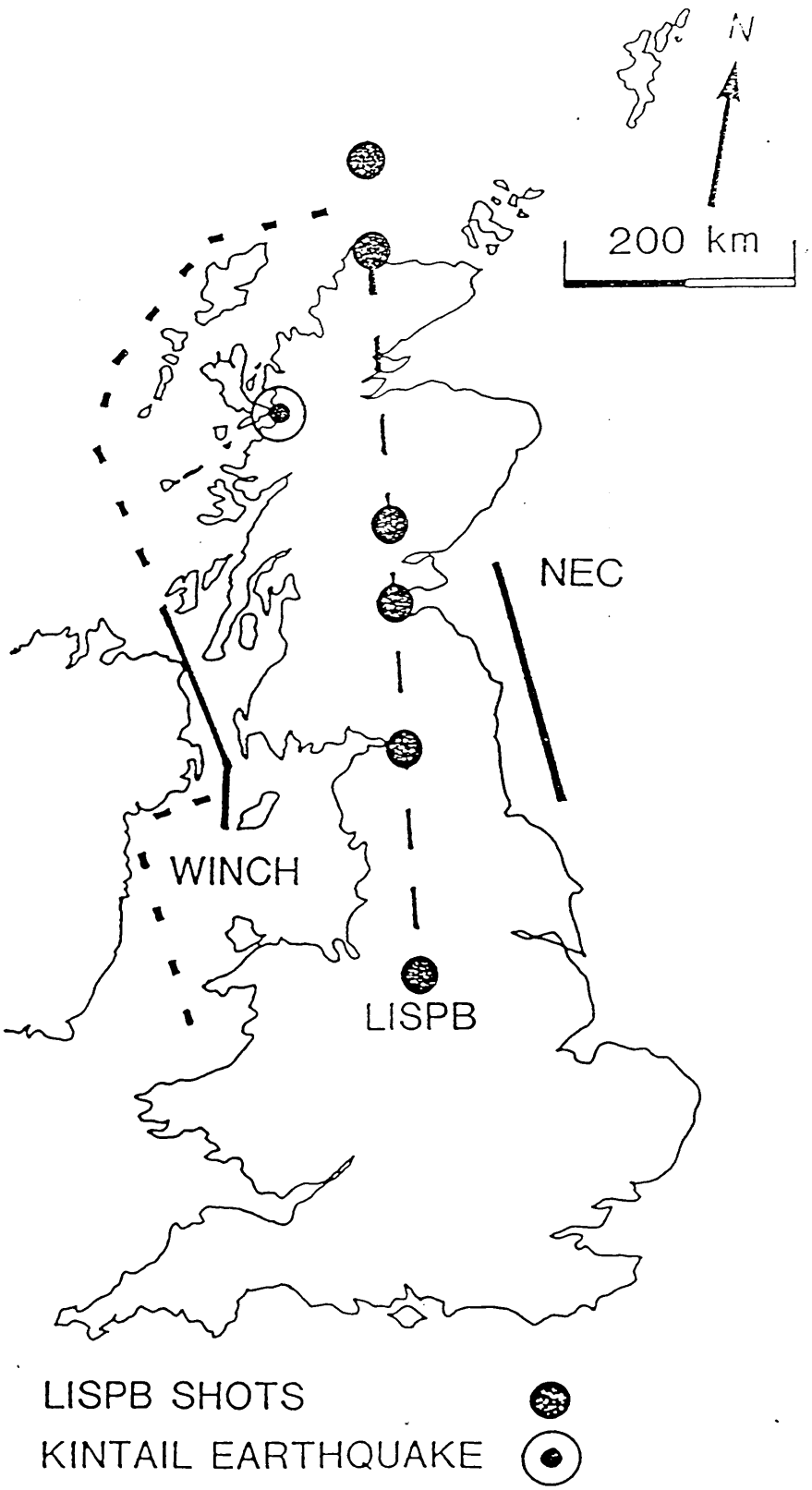

Fig. 2.3 Location map for deep seismic lines crossing the Midland Valley. The section of the WINCH line drawn solid is shown in Fig. 2.8.

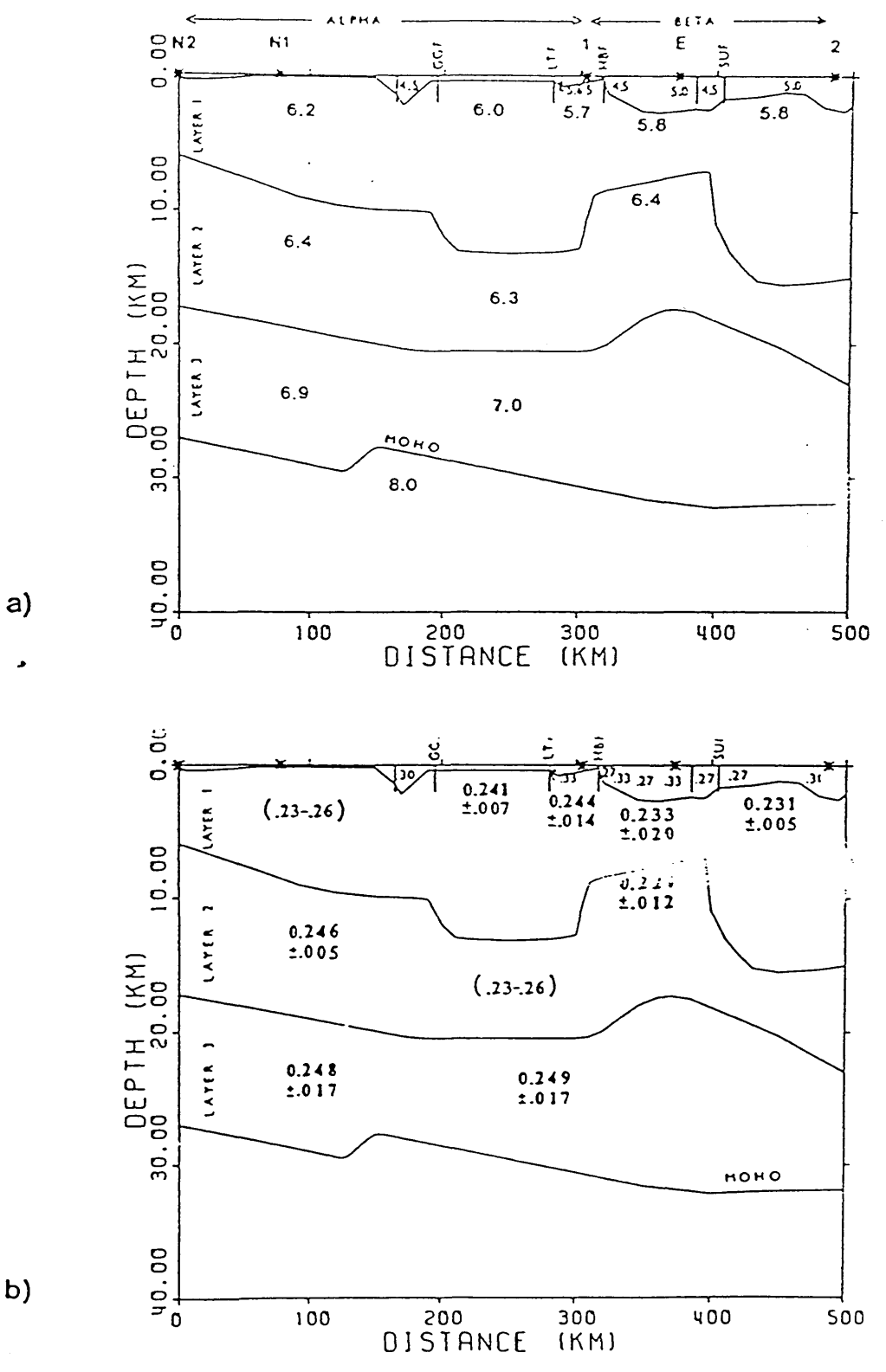

Fig. 2.4 Crustal structure of northern Britain from the LISPB study (after Assumpcao & Bamford 1978).

a) P-wave structure.

b) Poisson's ratio structure using the ts/tp method.

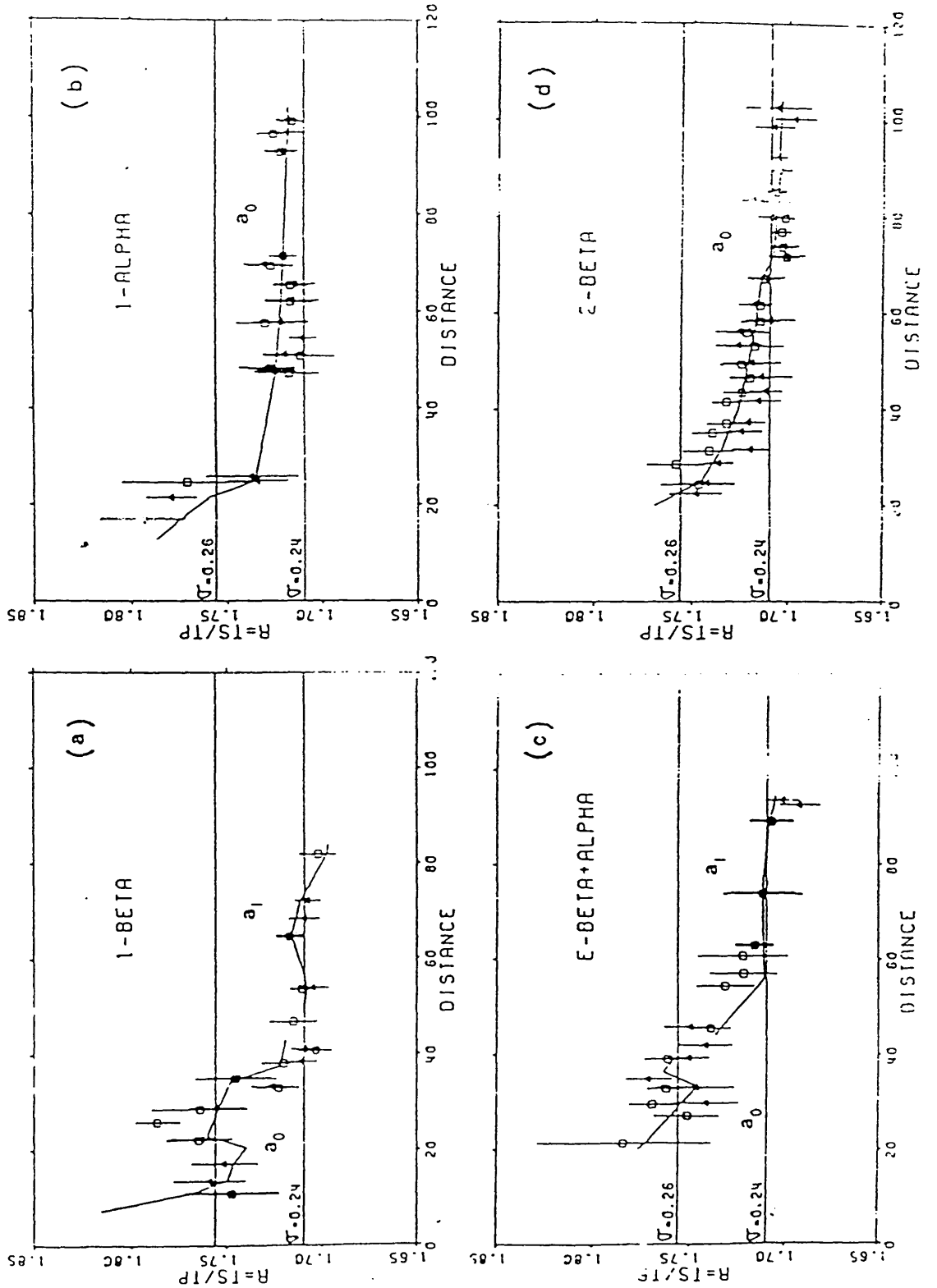

Fig. 2.5 ts/tp ratio data from LISPB. Diagrams a & c give a reversed coverage across the Midland Valley (after Assumpcao & Bamford 1978).

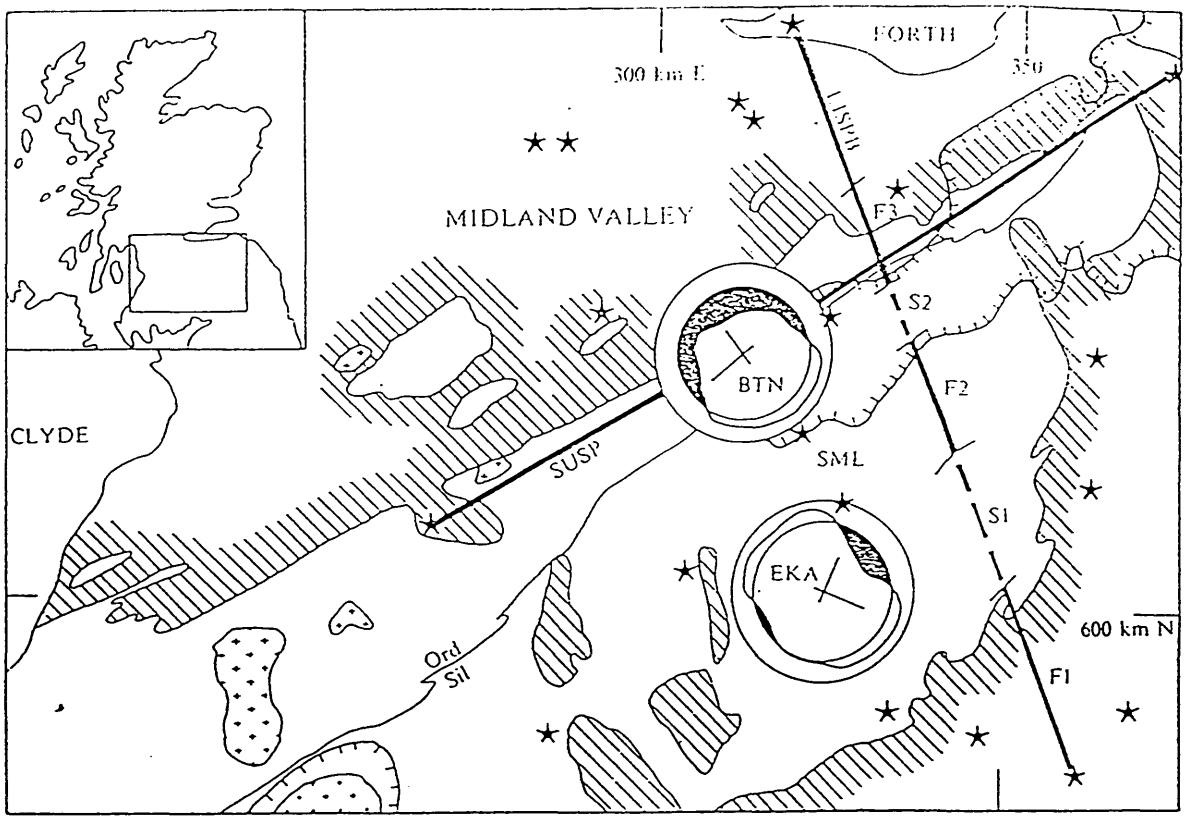

LOWER PALAEOZOIC

GRANITE

SEISMIC EVENTS

NEGATIVE BOUGUER GRAVITY

Fig. 2.6 Location of previous seismic work in southern Scotland. On LISPB F1-3 and S1-2 locate high and low velocity blocks. BTN-Broughton seismic array, EKA-Eskdalemuir seismic array, SML-Saint Mary's Loch, SUSP-Southern Uplands Seismic Profile. Polar plots are of apparent velocity versus direction to source with scale rings at 5.5 km/s (outer) and 6.0 km/s (inner), so that the black area defines the sector in which velocity is greater than 6 km/s.

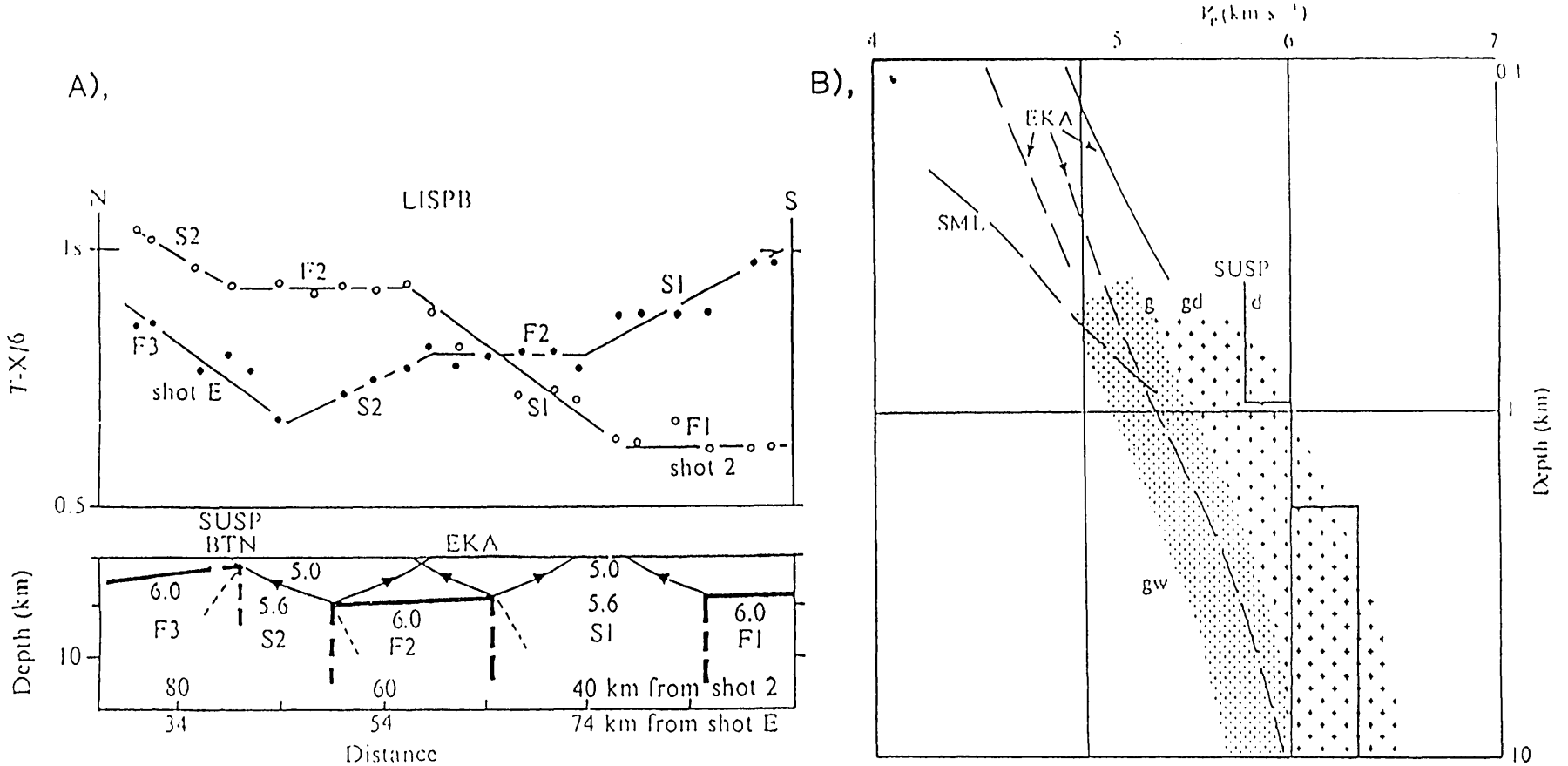

Fig. 2.7 A) LISPB time - distance data from the Southern Uplands, reduction velocity is 6.0 km/s. Structural model shows velocity distribution containing fast (F) and slow (S) blocks which give rise to the corresponding segments on the time - distance plot. B) Velocity-depth plot for the Southern Uplands. Solid lines show along-strike. velocities and dashed lines across-strike velocities. EKA -Eskdalemuir seismic array, SML is an array study at Saint Mary's Loch in the S2 slow block. Dotted area (gw) represents the velocity field for Lower Palaeozoic greywackes. Plusses indicate velocity field for plutonic rocks, g - granite, gd - granodiorite, d - diorite. SUSP - Southern Uplands Seismic Profile, (after Hall *et al.* 1983).

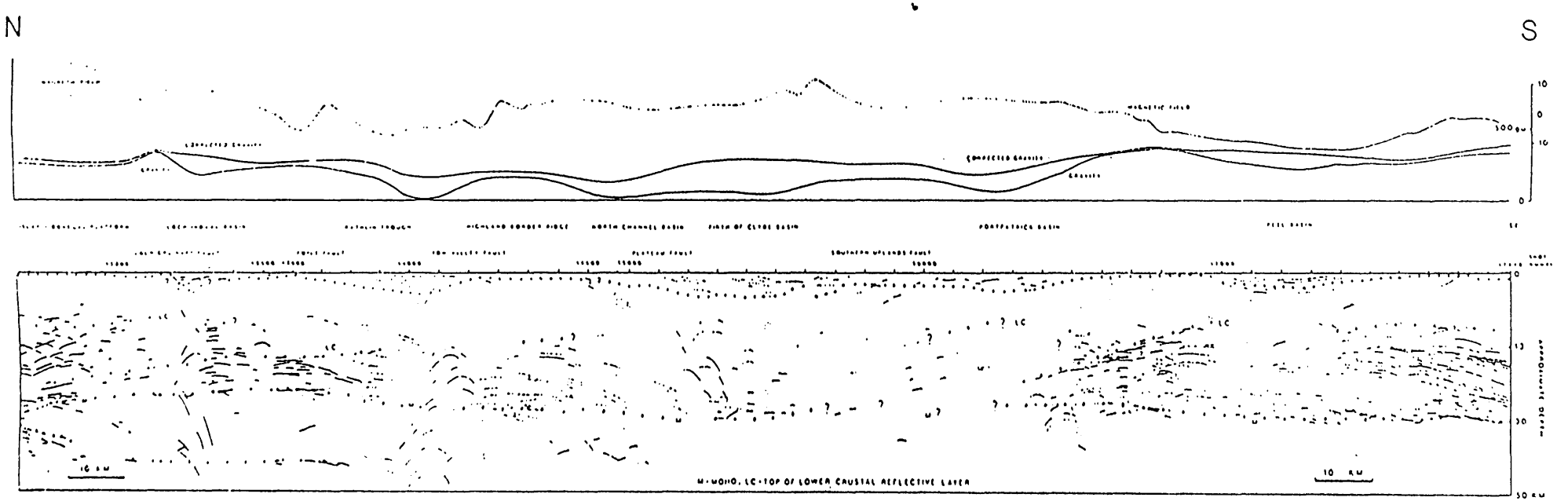

Fig. 2.8 Line drawing of WINCH section shown in Fig. 2.3. The magnetic and Bouguer gravity fields with corrected gravity, obtained by one-dimensional correction for the thickness of sedimentary rocks above basement, are shown (after Hall *et al.* 1984).

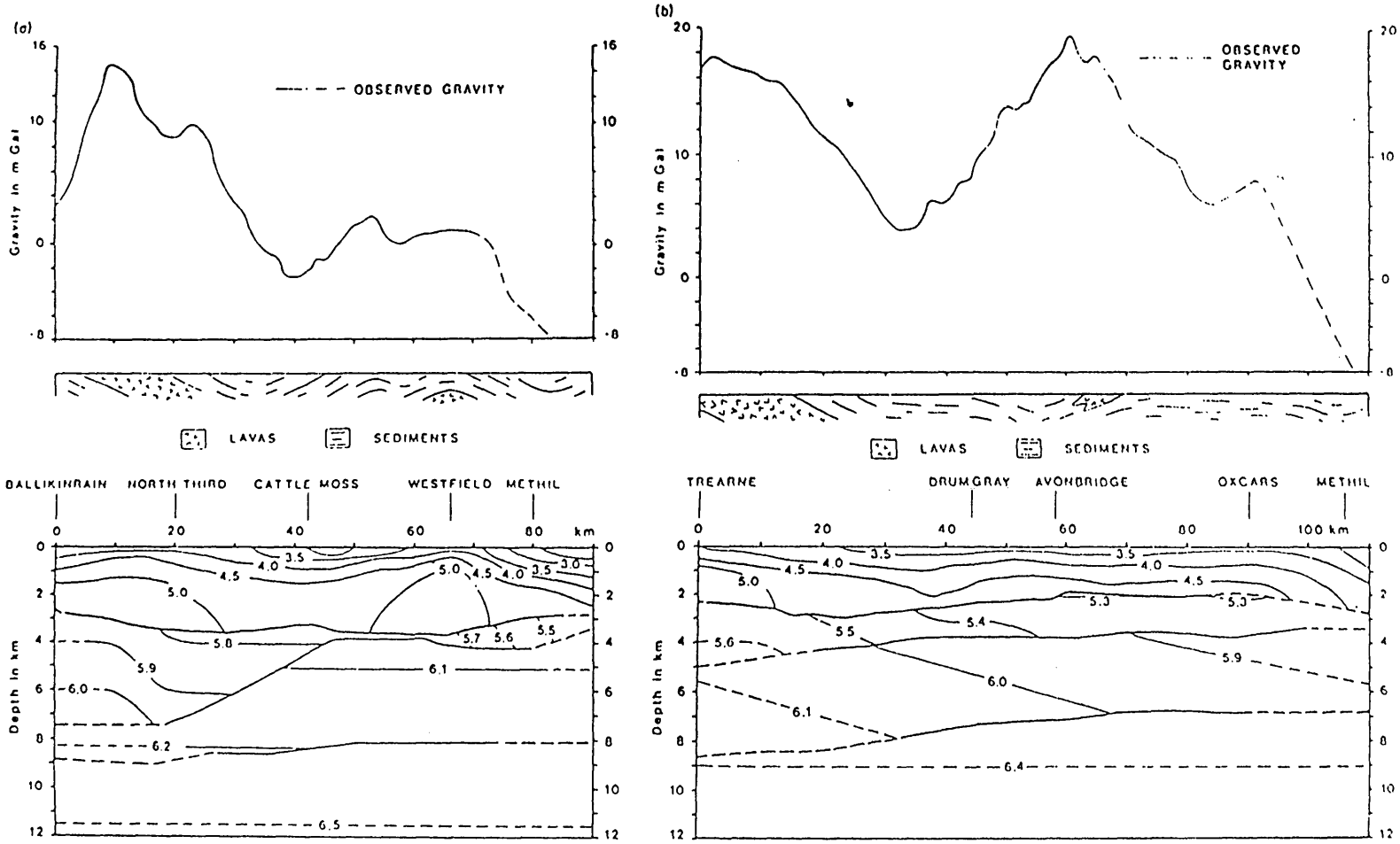

Fig. 2.9 Ray-tracing models and gravity profiles of (a) MAVIS North line and (b) South line. Interfaces shown by thick lines. Seismic velocity contours are in km/s. The schematic geological sections are based upon the surface geology along the profiles. (after Conway *et al.* 1987).

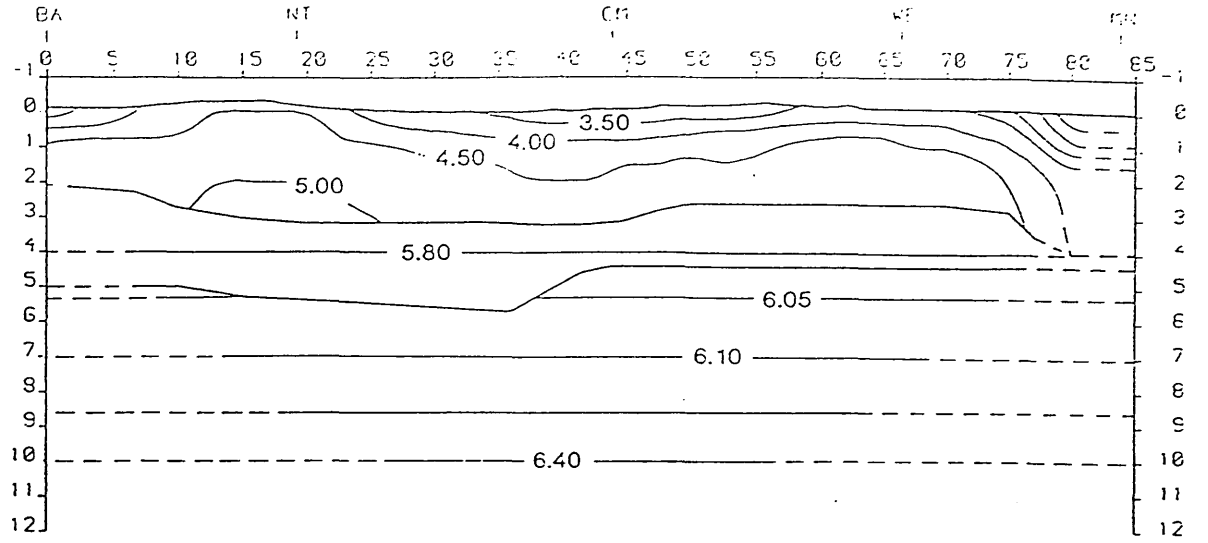

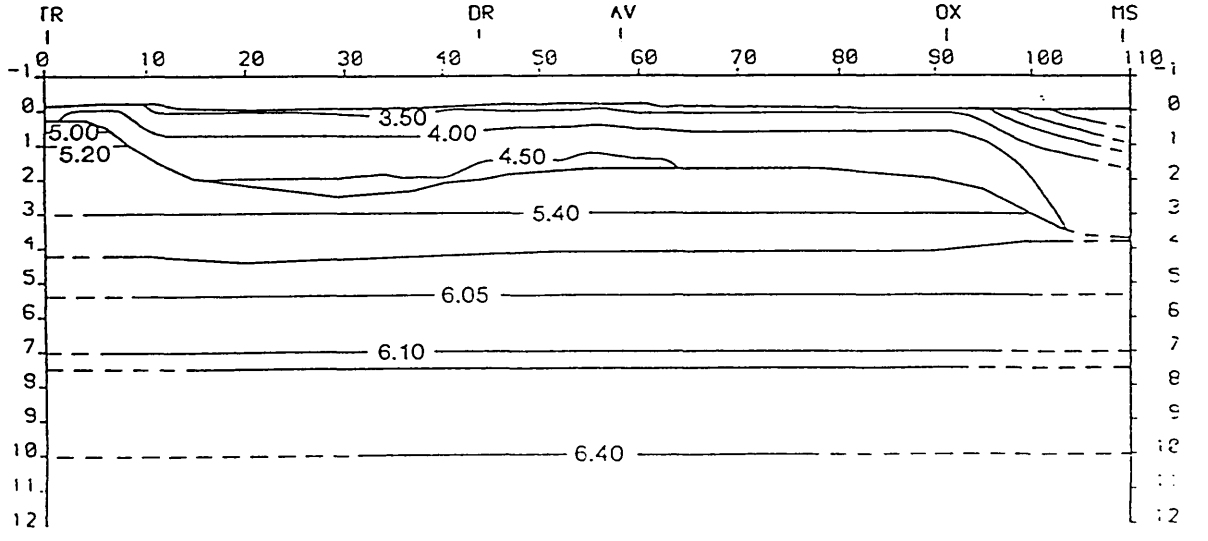

Fig. 2.10 Final ray-traced models of MAVIS profiles. Interfaces shown by thick lines, seismic velocity contours (in km/s) by thin lines. Scales are in km (after Dentith 1987).

A, MAVIS I north line : BA - Ballikinrain, NT - North Third, CM - Cattlemoss, WE - Westfield, MN - Methil.

B, MAVIS I south line : TR - Trearne, DR - Drumgray, AV - Avonbridge, OX - Oxcars, MS - Methil.

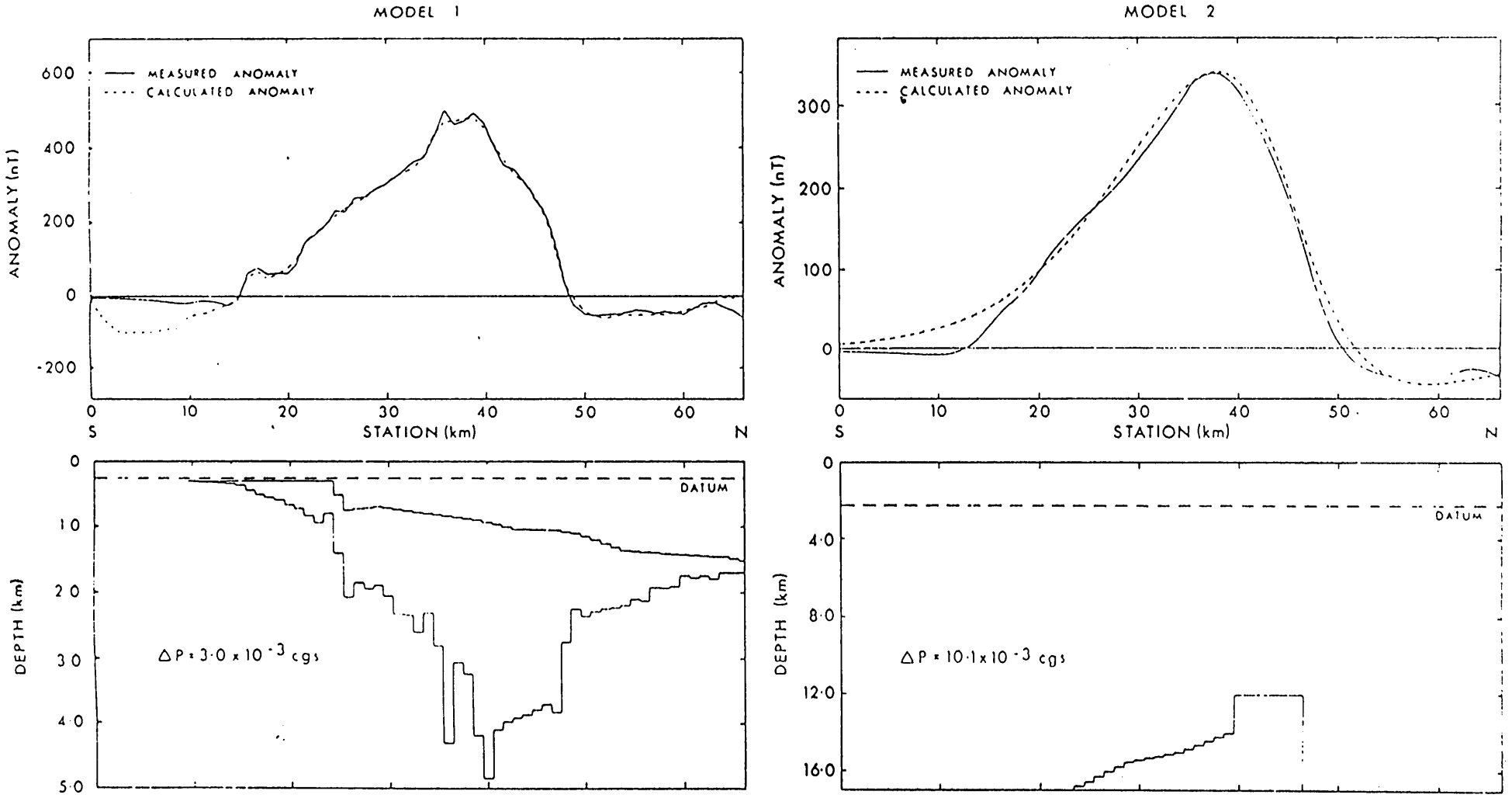

Fig. 2.11 Alternative models of the Bathgate magnetic anomaly (after Hossain 1976).

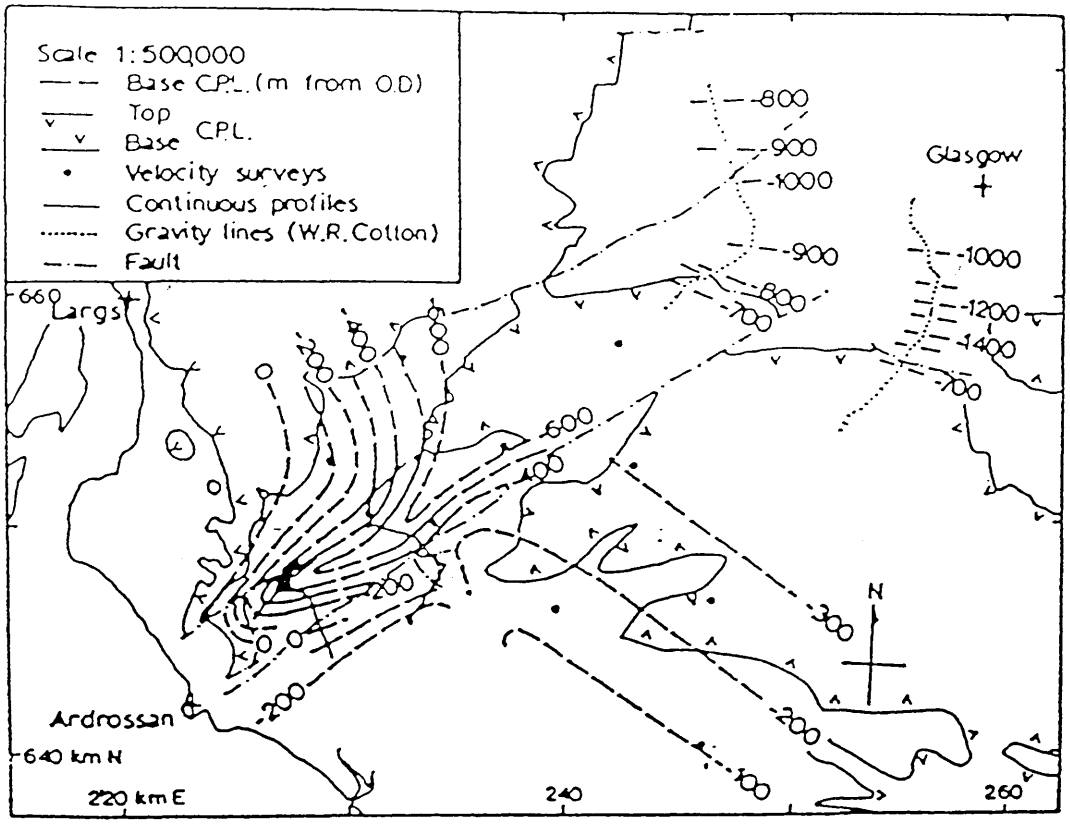

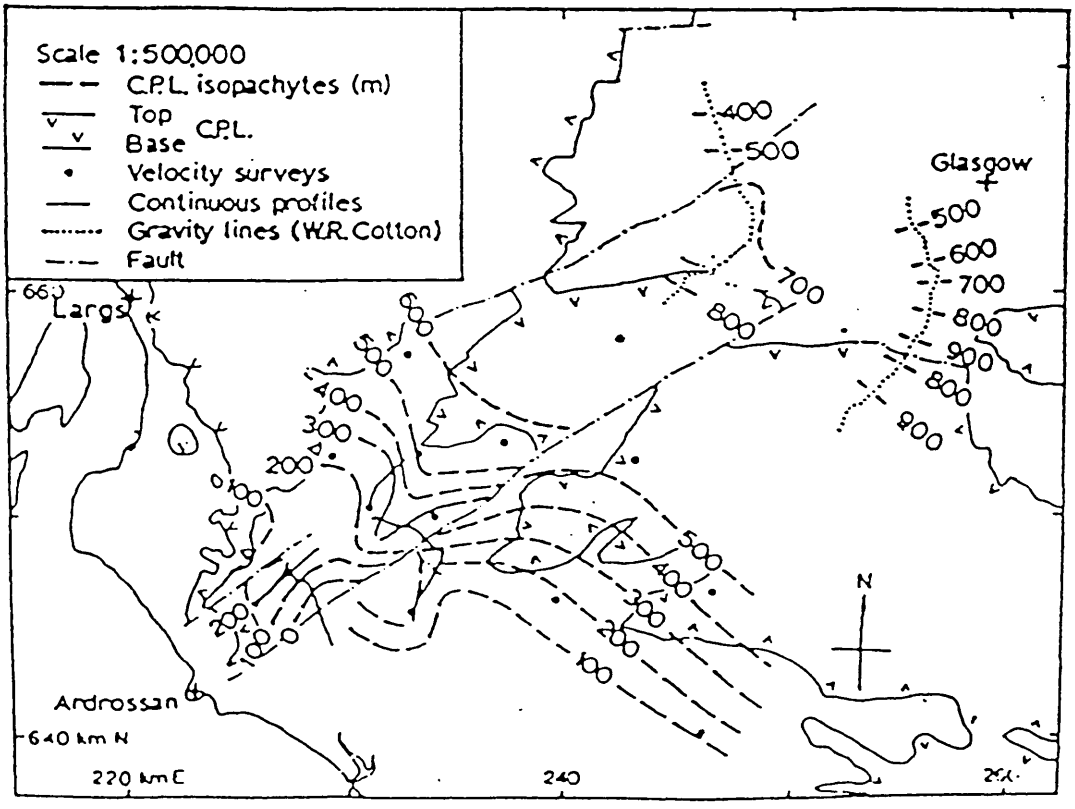

Fig. 2.12 Contour and isopach maps of the Clyde Plateau Lavas (after Hall 1974).

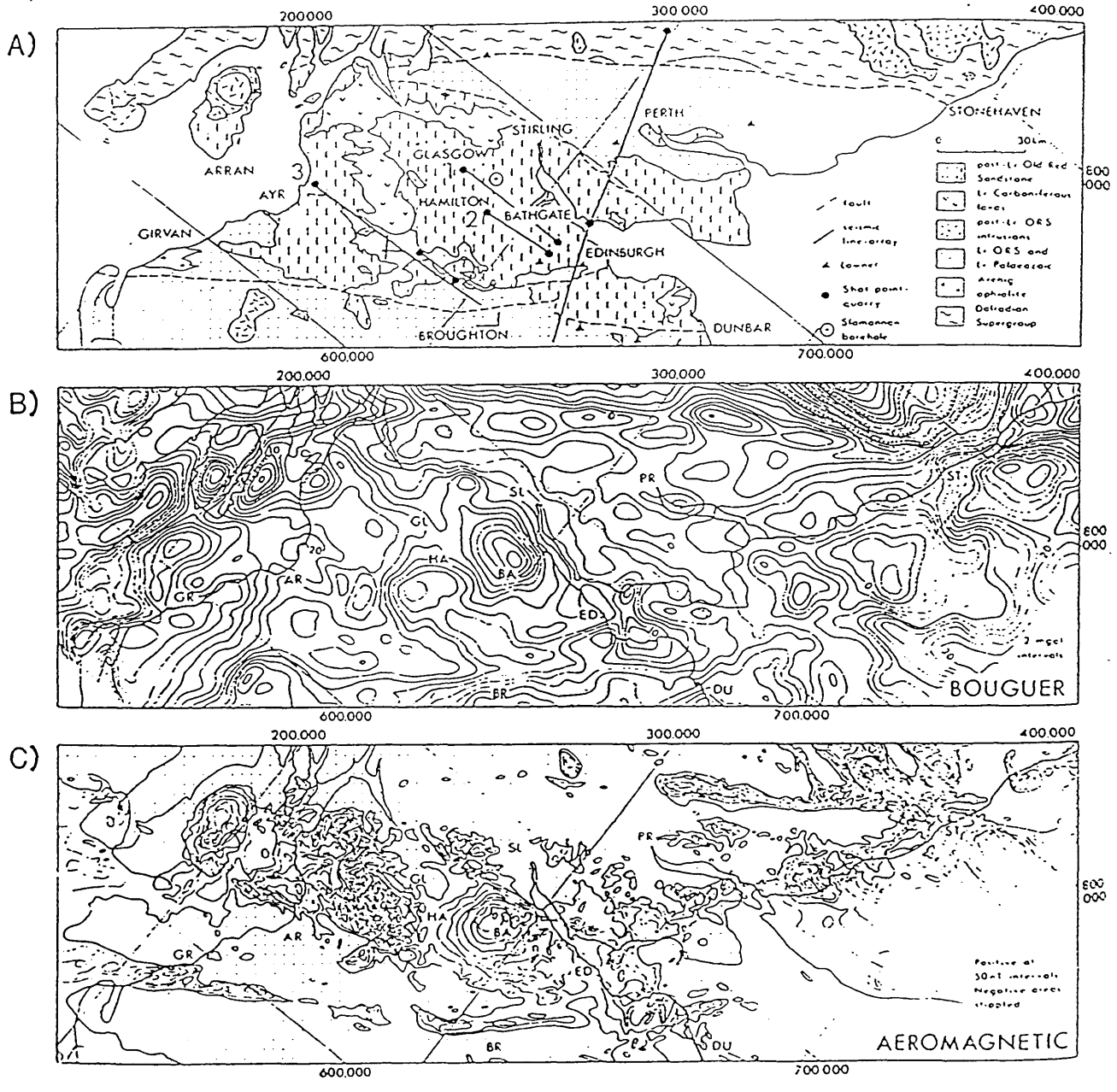

Fig. 2.13 A) Simplified geological map of the Midland Valley. Numbers refer to seismic lines. B) Bouguer gravity map of the Midland Valley (redrawn from Hussain & Hipkin 1981). Locality names abbreviated from (A). C) Aeromagnetic map of the Midland Valley (redrawn from I.G.S. 1972). Locality names abbreviated from (A). Negative contours omitted. (after Davidson *et al.* 1984).

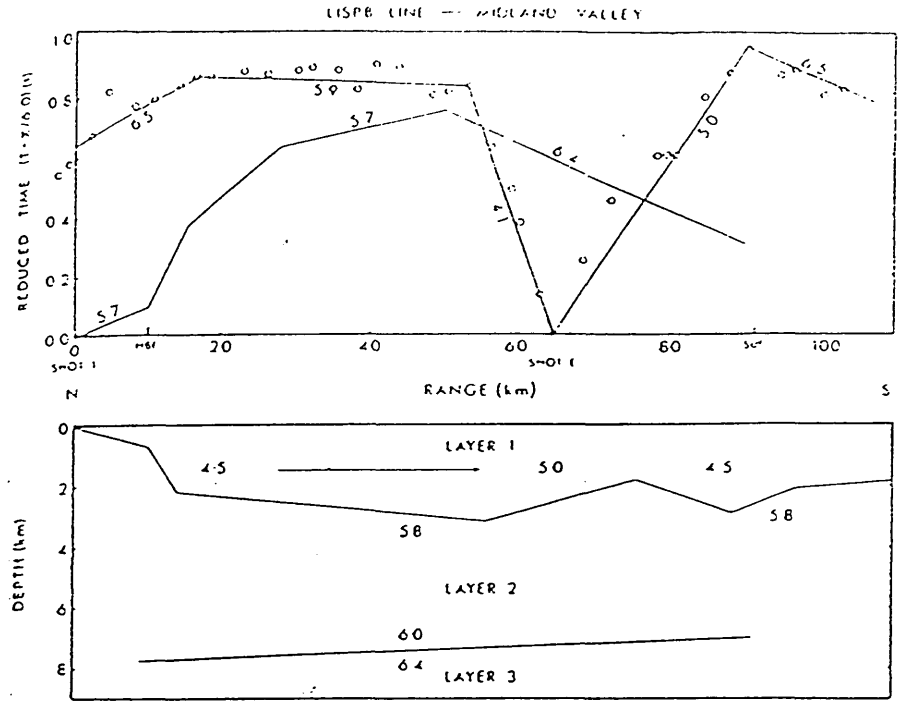

Fig. 2.14 The LISPB model across the Midland Valley with time - distance data interpretation (after Davidson *et al.* 1984).

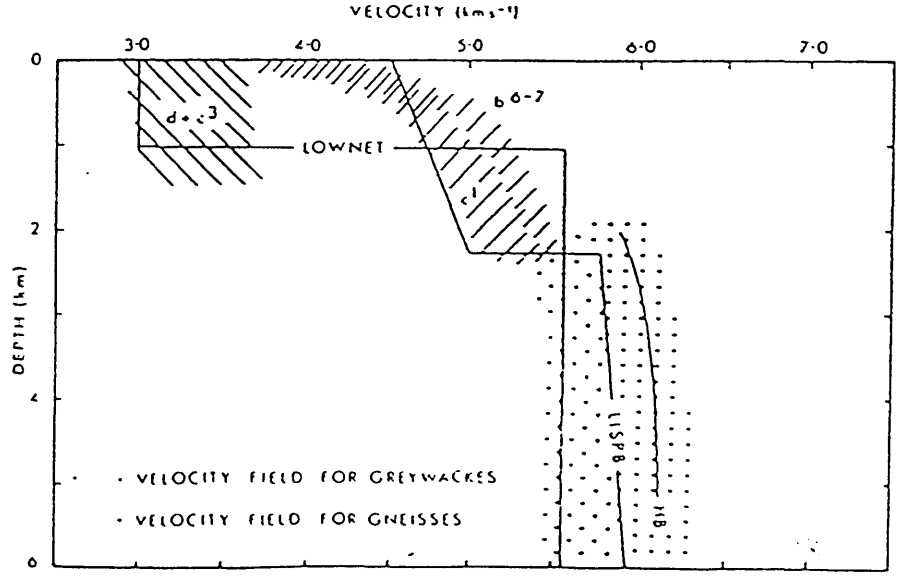

Fig. 2.15 Velocity - depth plot for Midland Valley lithologies. The velocity - depth models of LISPB and LOWNET are shown for comparison: d - Carboniferous, c3 - Upper ORS, c1 - Lower ORS, b6-7 - Silurian. HB is velocity of basement refractor (after Davidson *et al.* 1984).

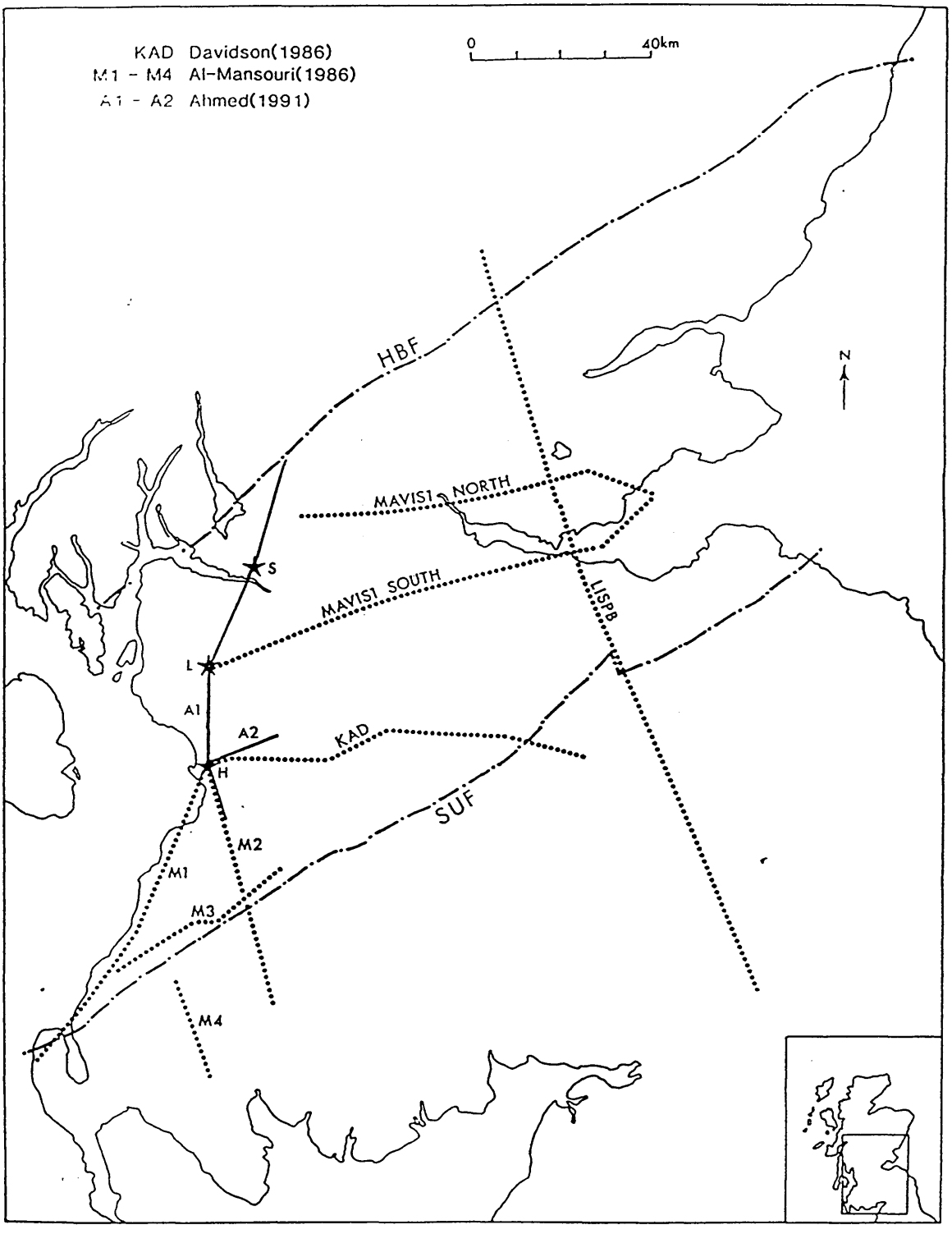

Fig. 3.1a Location map of the seismic profile (solid) recorded in this study, and previous profiles (dotted), HBF=Highland Boundary Fault, SUF=Southern Uplands Fault. A star indicates a shotpoint used in this study. H = Hillhouse, L = Loanhead, S = Sheephill.

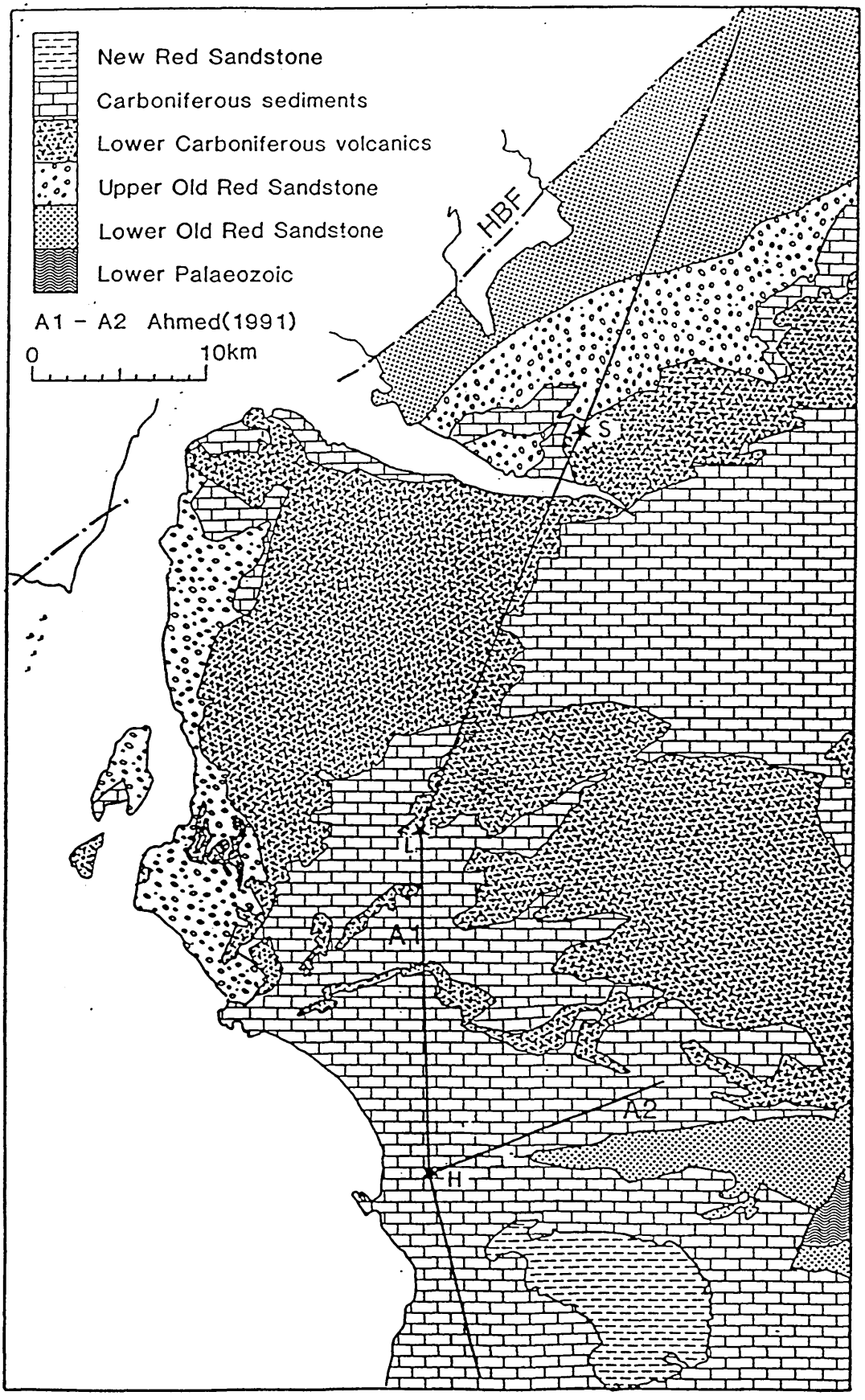

Fig. 3.1b Detailed geological map of the study area. Seismic shot points shown by star, H= Hillhouse, L= Loanhead, S= Sheephill. Refer to Fig. 1.16 for the names of principal faults within the Western Midland Valley. HBF= Highland Boundary Fault.

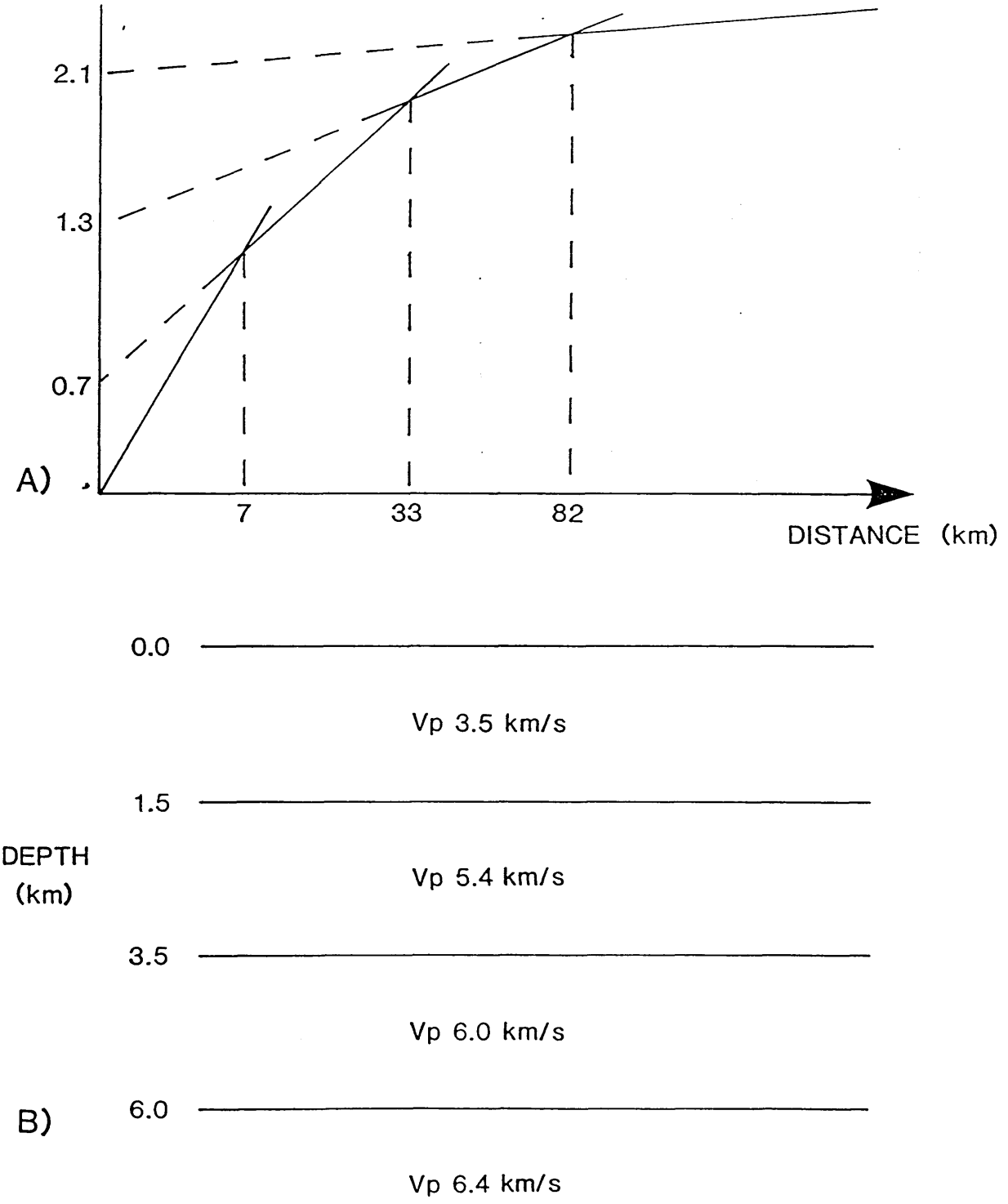

Fig. 3.2 General upper crustal model assumed in the planning of this project, A), time- distance graph B), crustal model (after Dentith 1987).

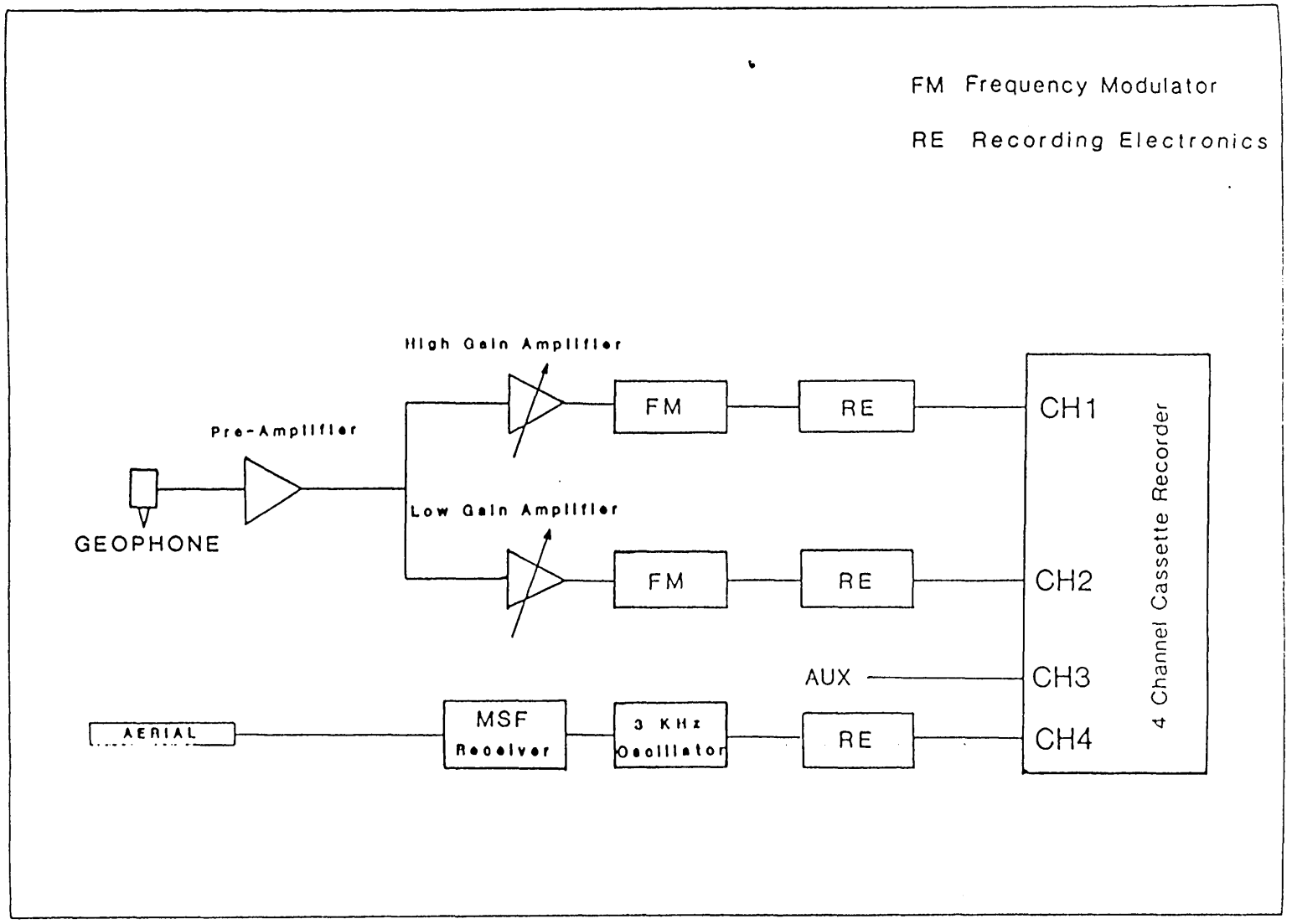

Fig. 3.3 Block diagram showing the recording arrangement of the Glasgow FM "Mark2" recorder system.

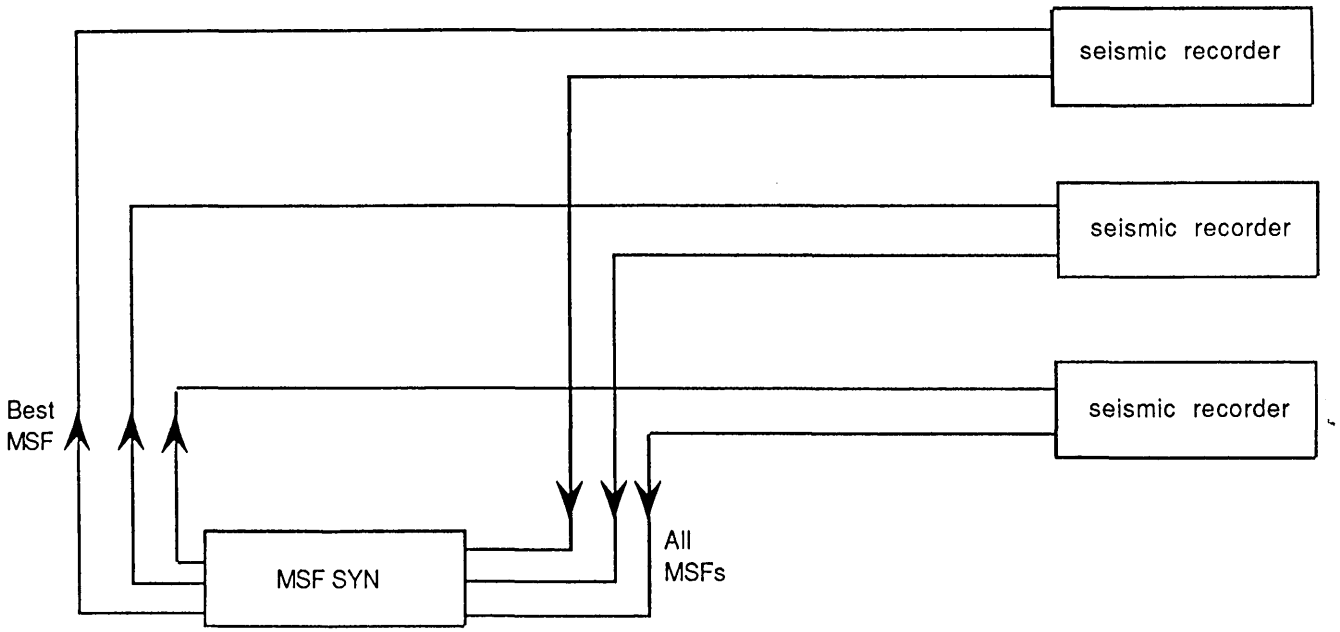

Fig 3.4 Block diagram of the MSF SYN device

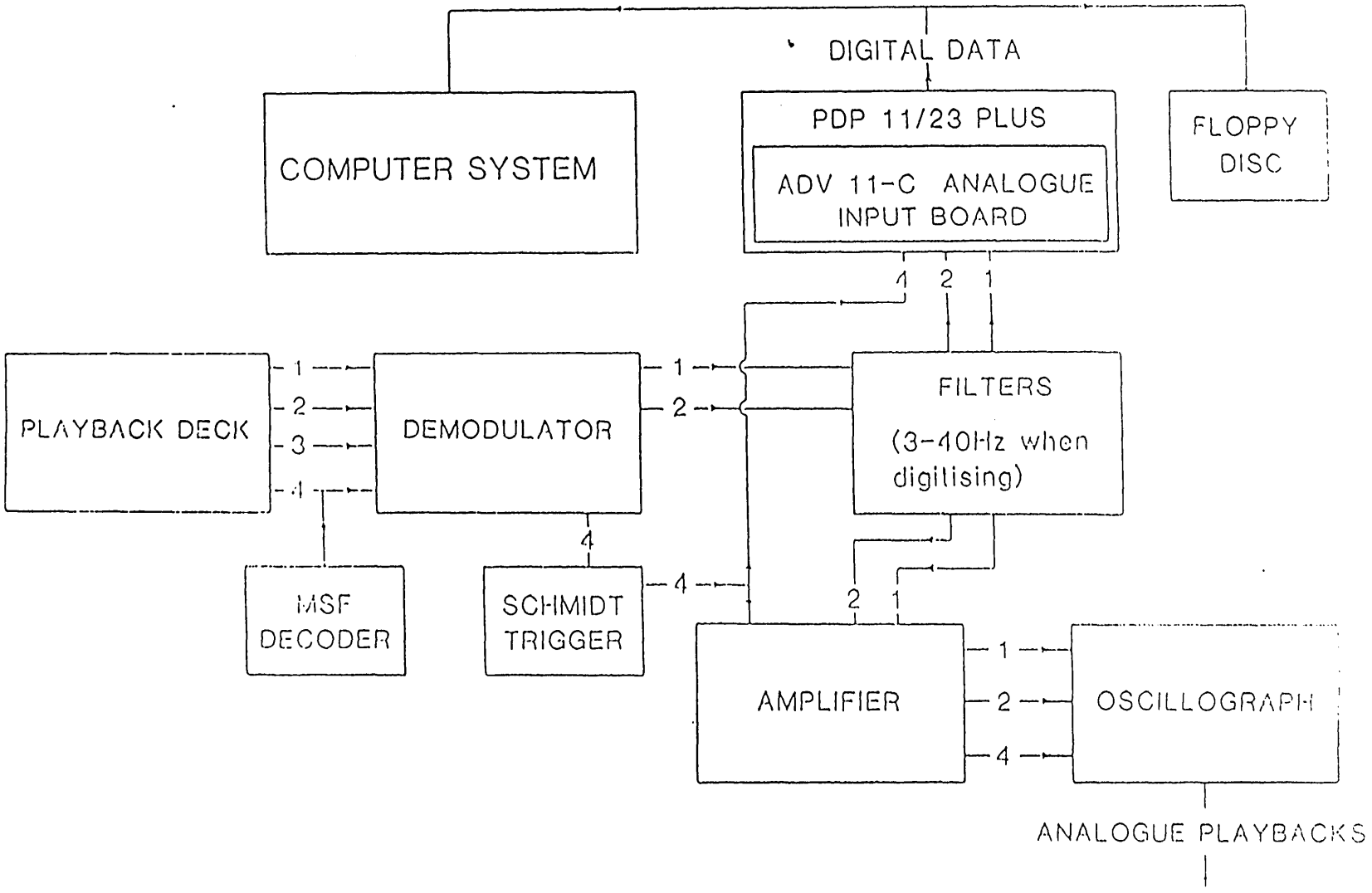

Fig. 3.5 Schematic diagram of Glasgow playback and digitising system.

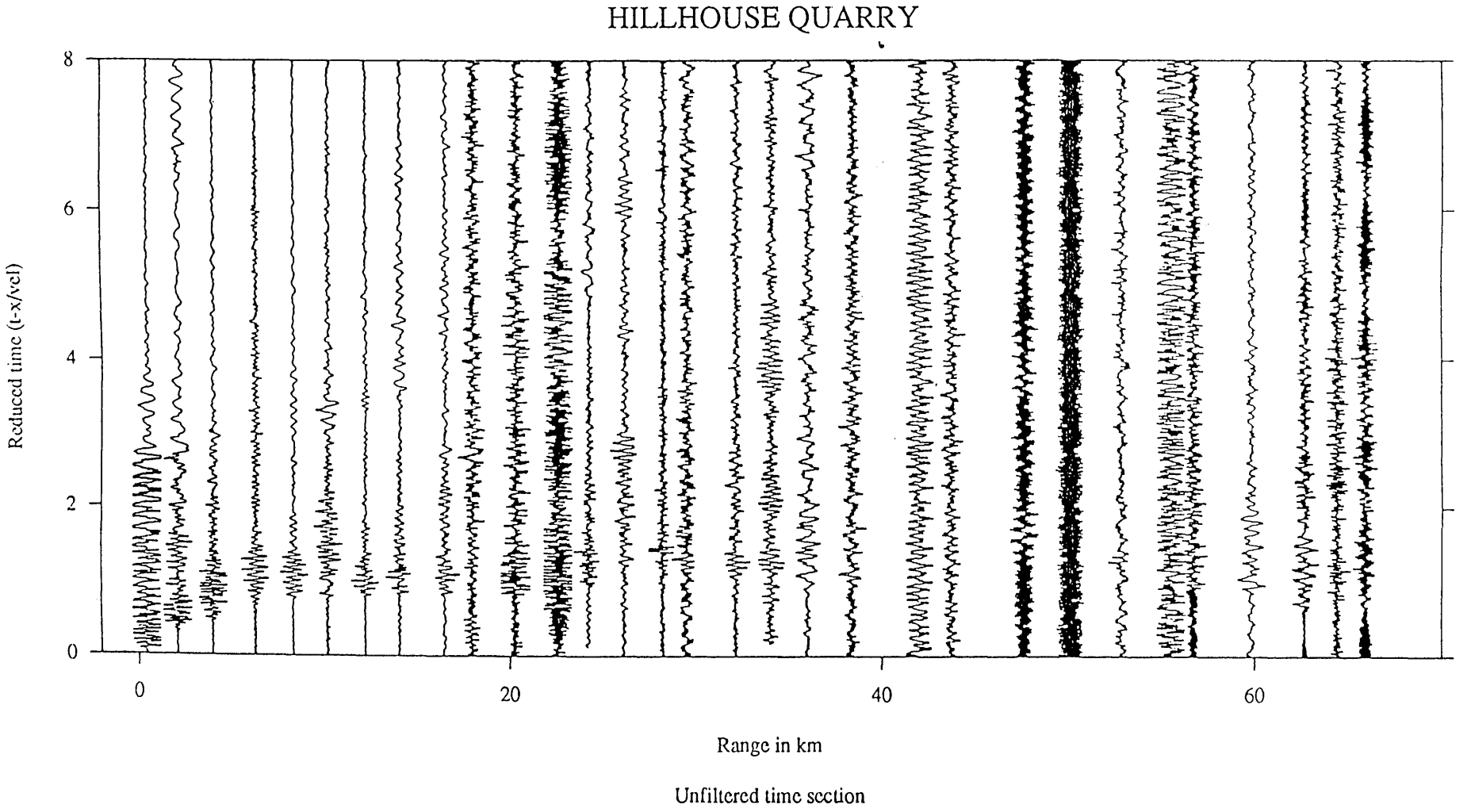

Fig. 3.6 Unfiltered vertical component data from Hillhouse Quarry along the main seismic line, reduction velocity 6.0 km/s.

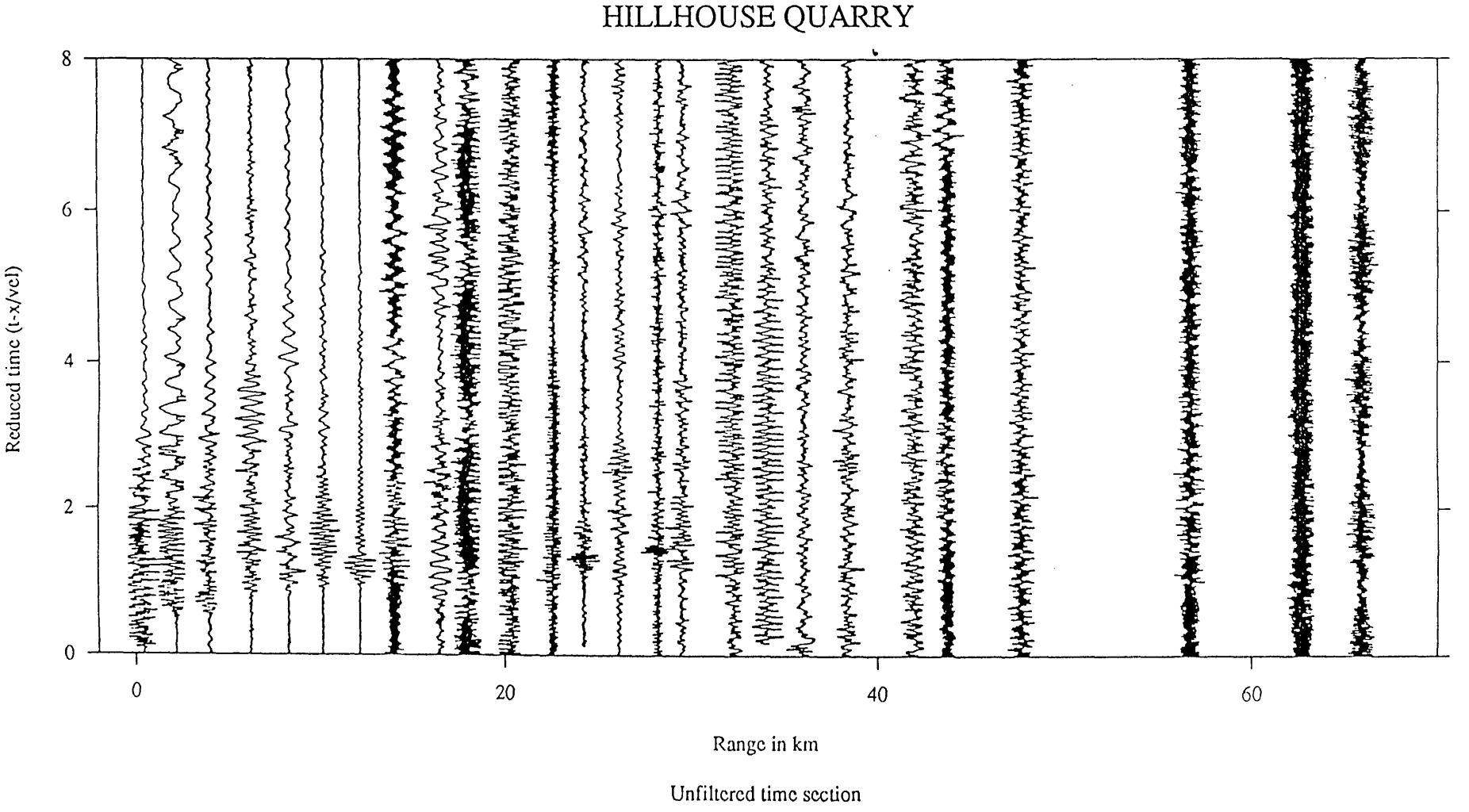

Fig. 3.7 Unfiltered radial component data from Hillhouse Quarry along the main seismic line, reduction velocity 6.0 km/s.

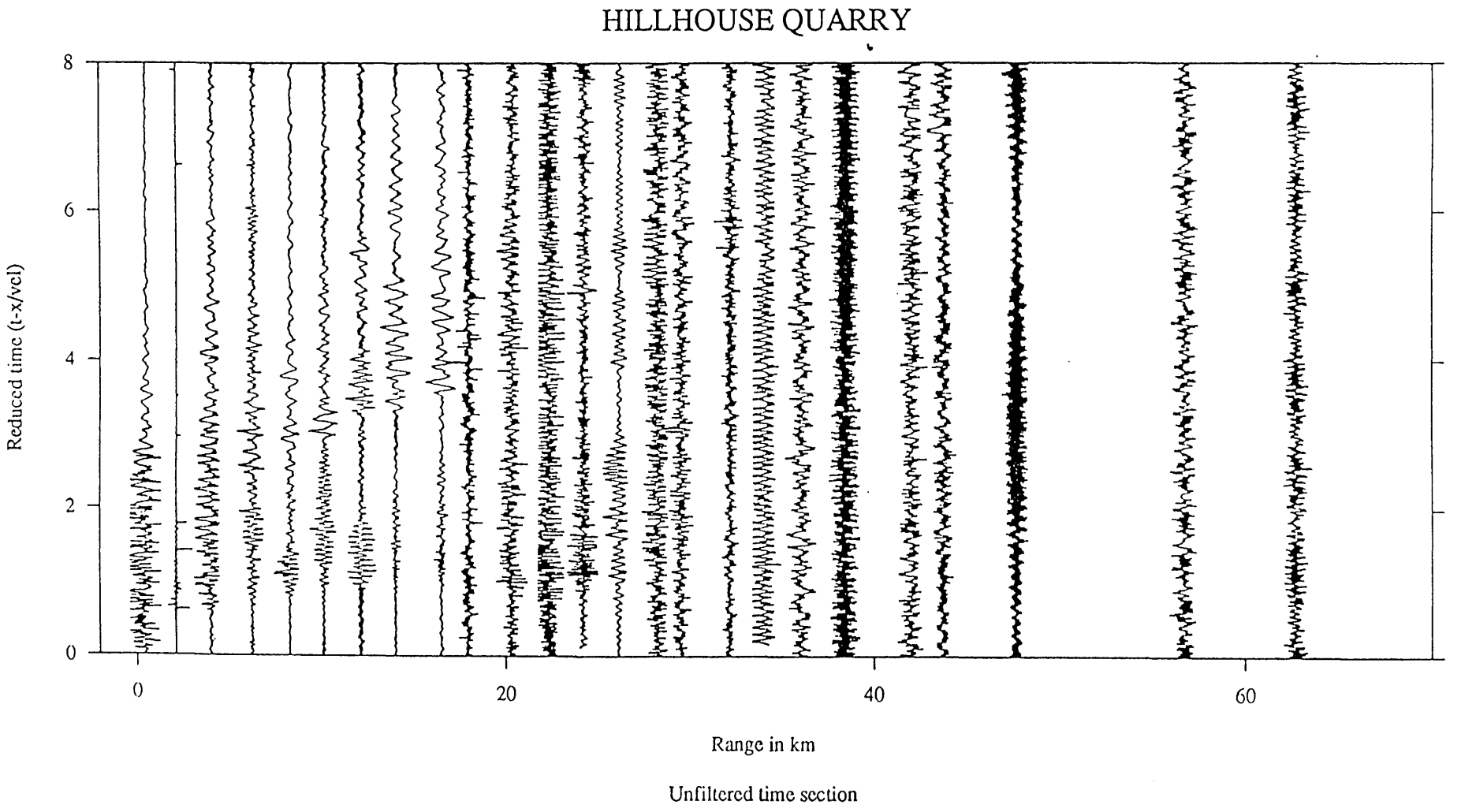

Fig. 3.8 Unfiltered transverse component data from Hillhouse Quarry along the main seismic line, reduction velocity 6.0 km/s.

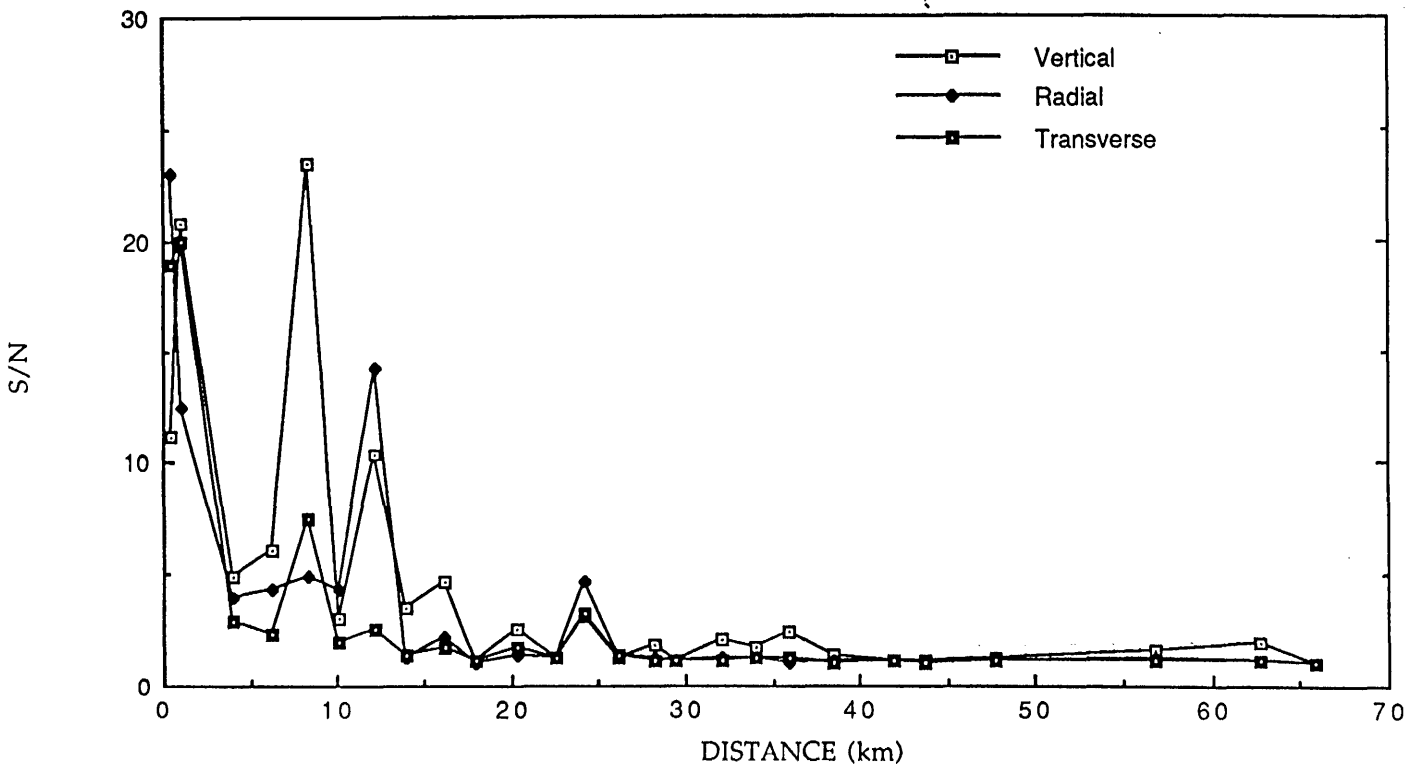

Fig. 3.9 Signal to noise ratio relation with offset;
Hillhouse shot

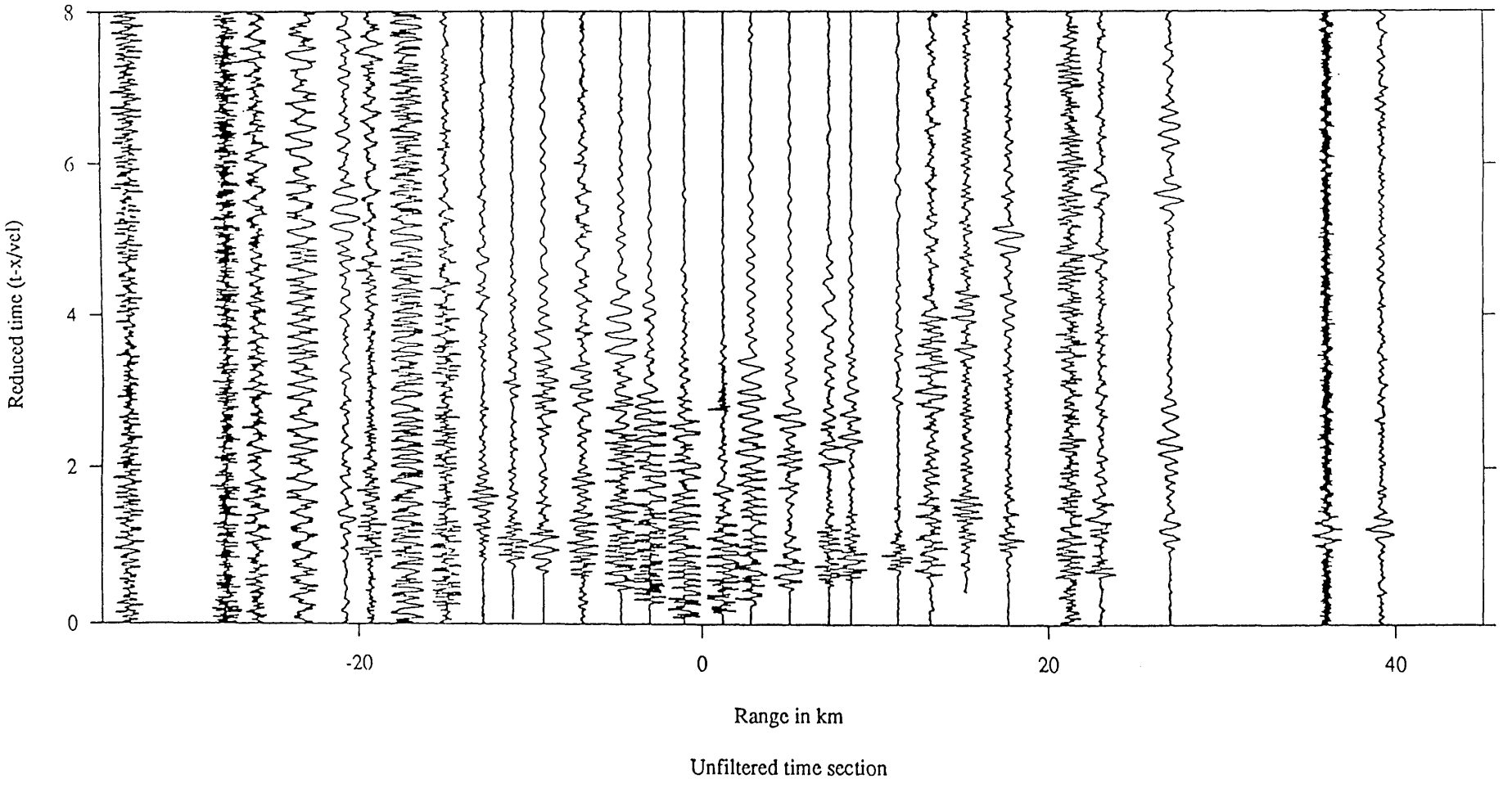

Fig. 3.10 Unfiltered vertical component data from Loanhead Quarry, reduction velocity 6.0 km/s.

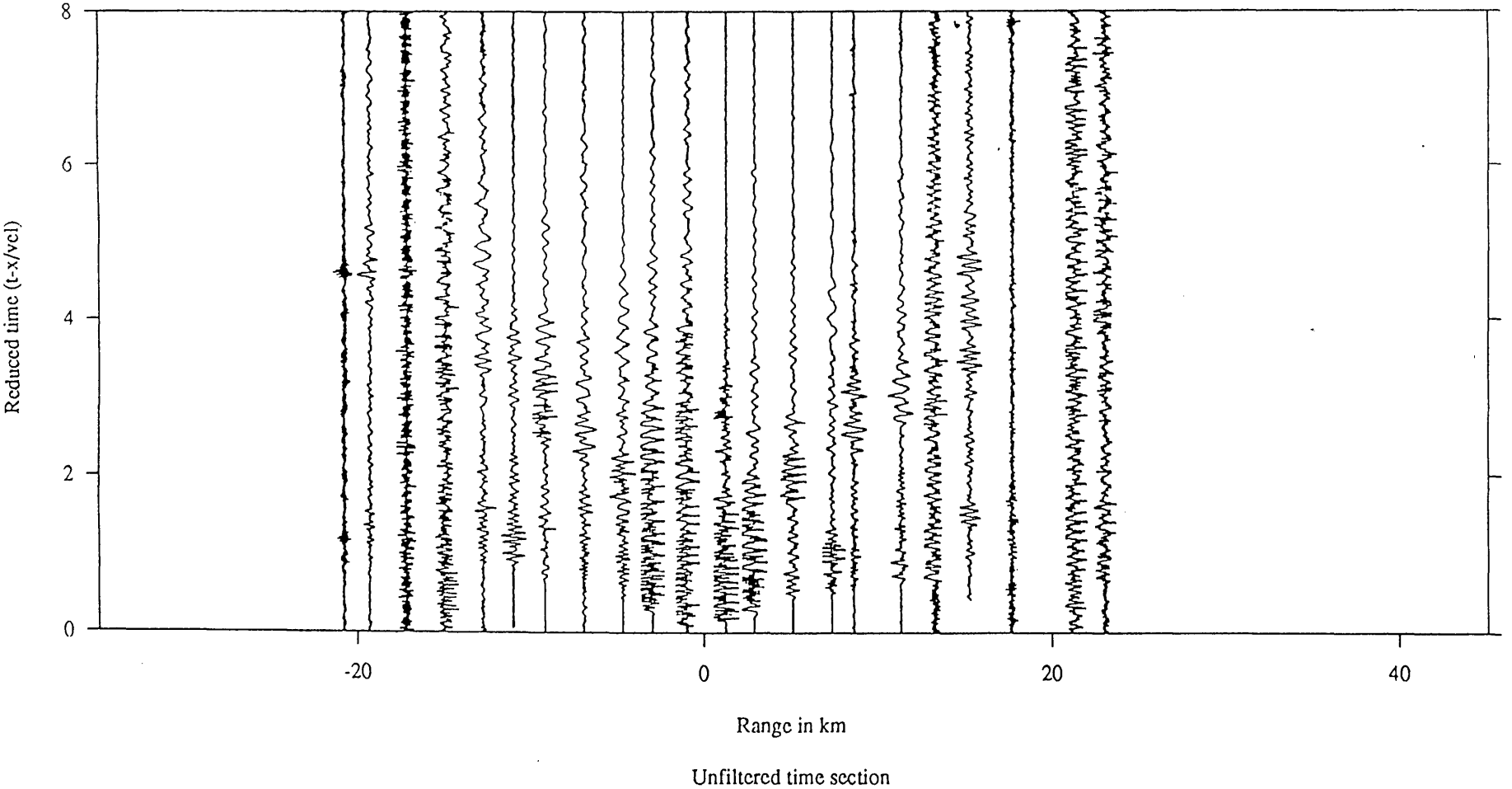

Fig. 3.11 Unfiltered radial component data from Loanhead Quarry, reduction velocity 6.0 km/s.

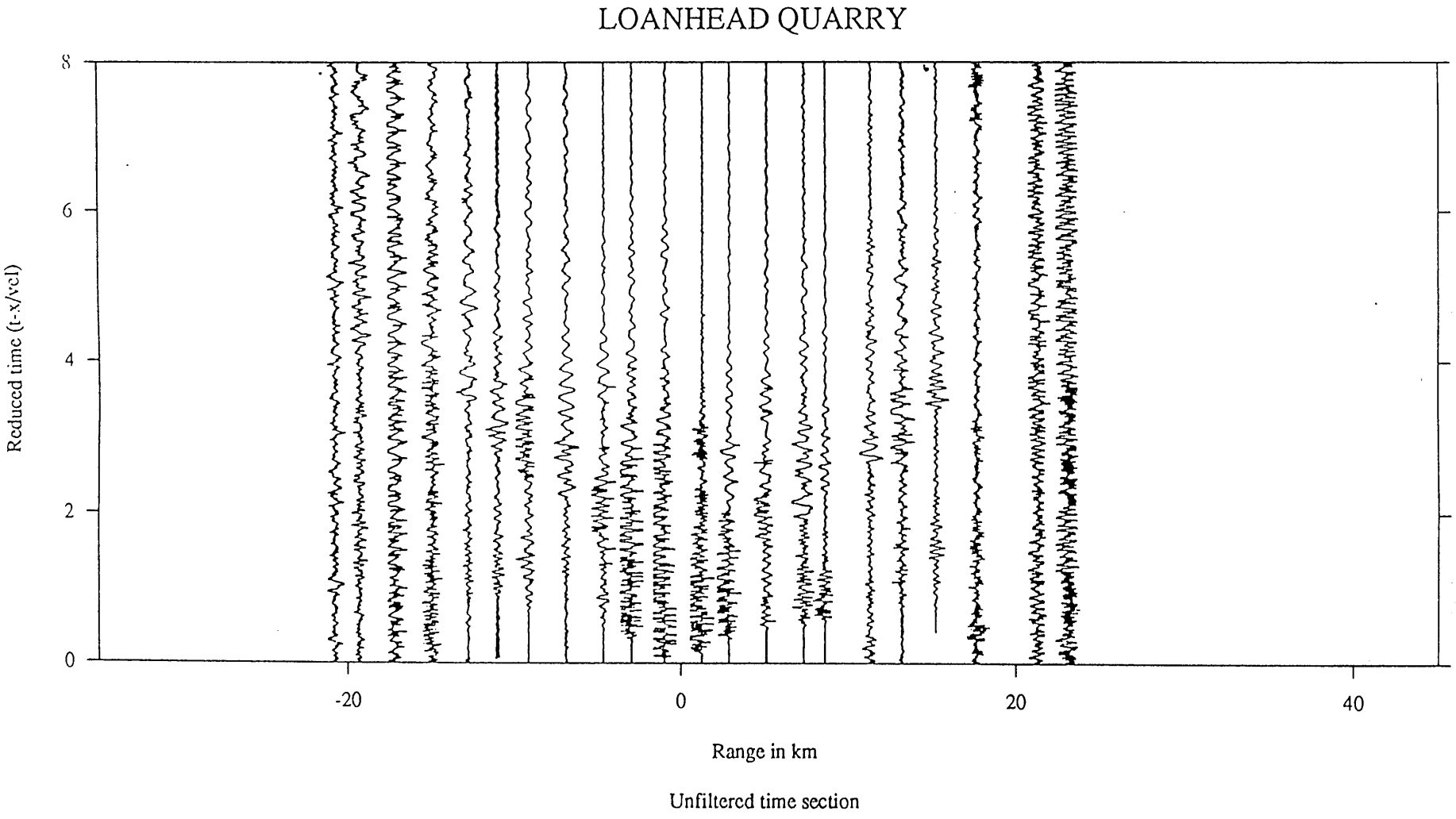

Fig. 3.12 Unfiltered transverse component data from Loanhead Quarry, reduction velocity 6.0 km/s.

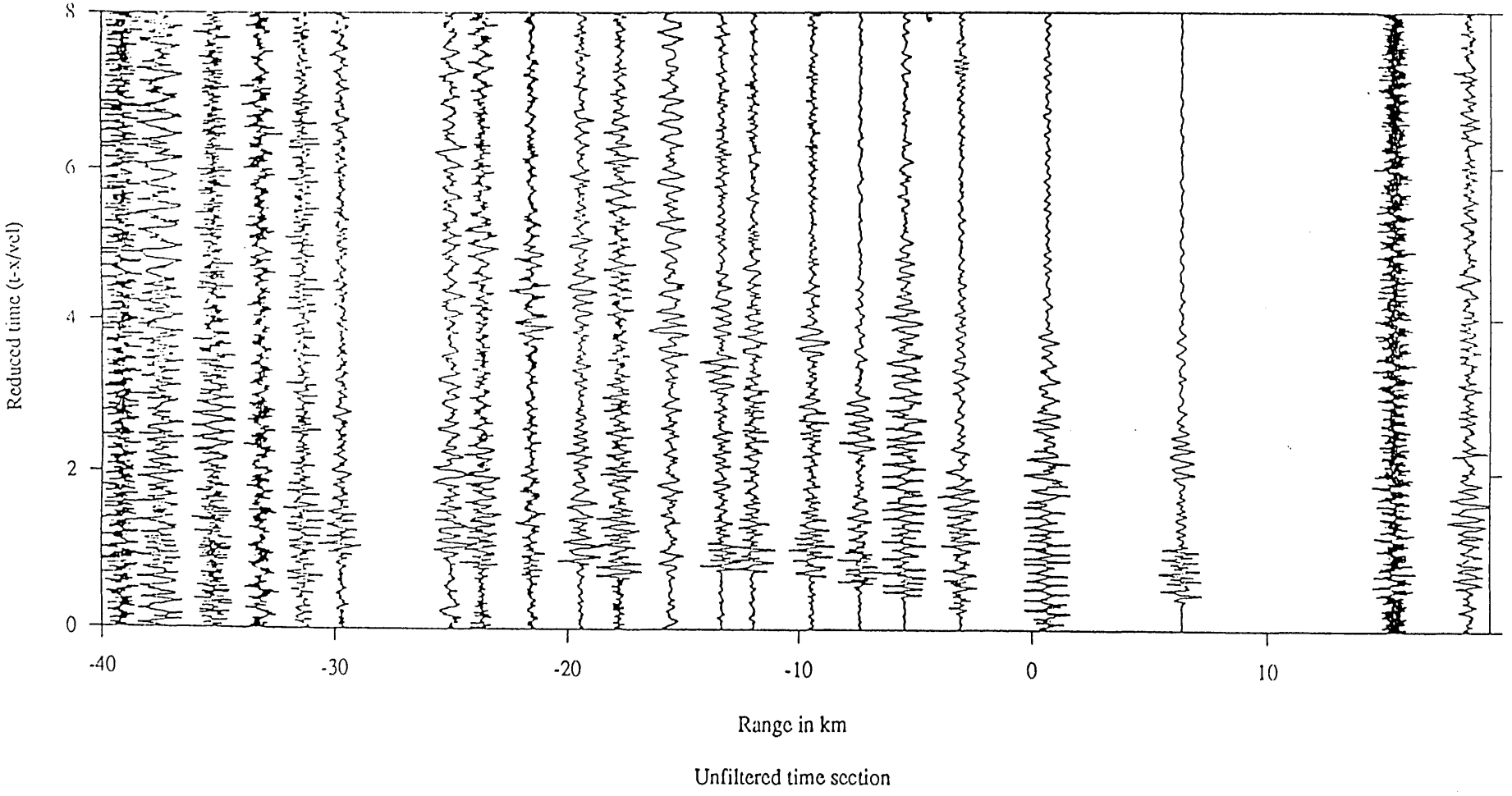

Fig. 3.13 Unfiltered vertical component data from Sheephill Quarry, reduction velocity 6.0 km/s.

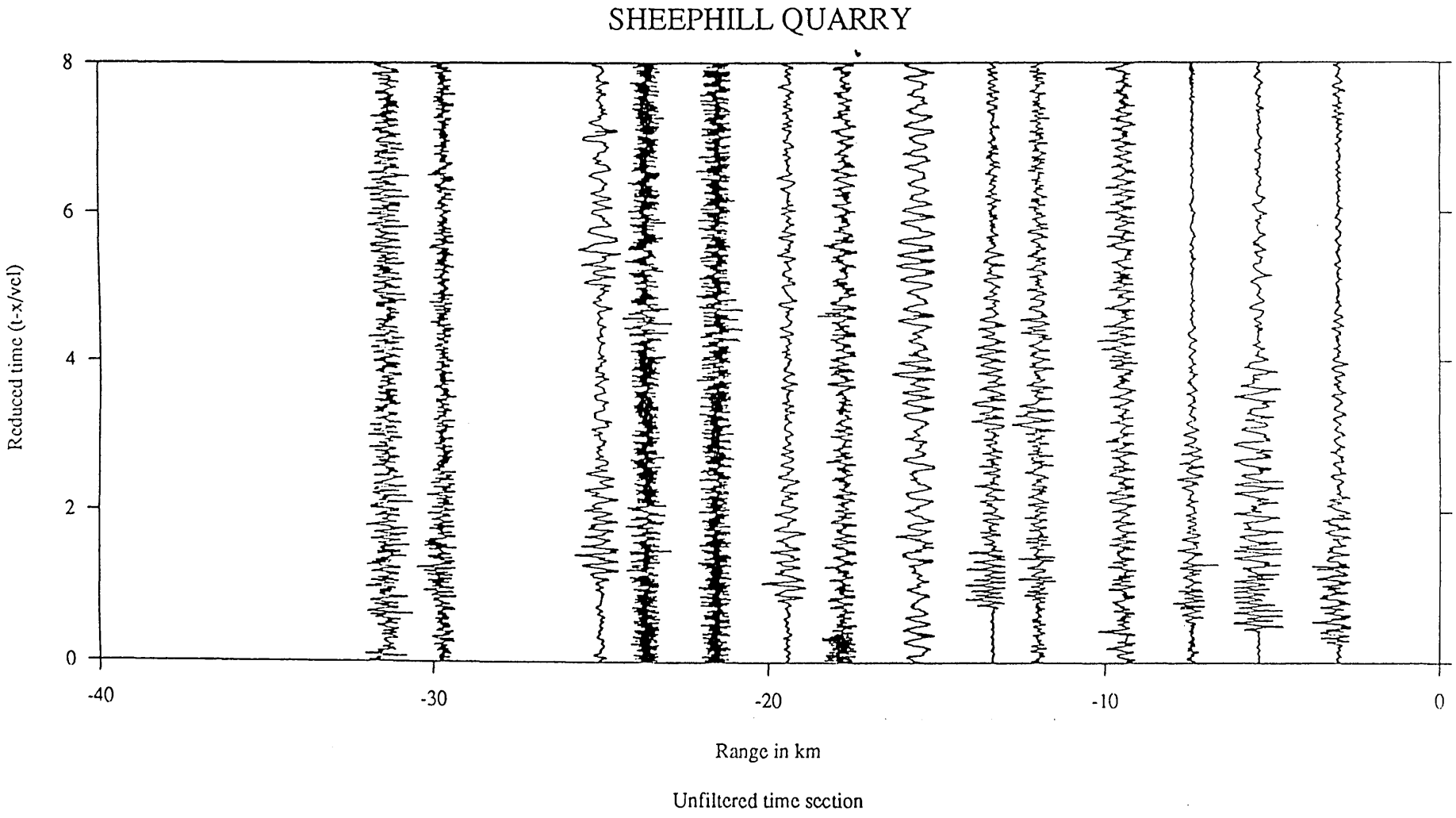

Fig. 3.14 Unfiltered radial component data from Sheephill Quarry, reduction velocity 6.0 km/s.

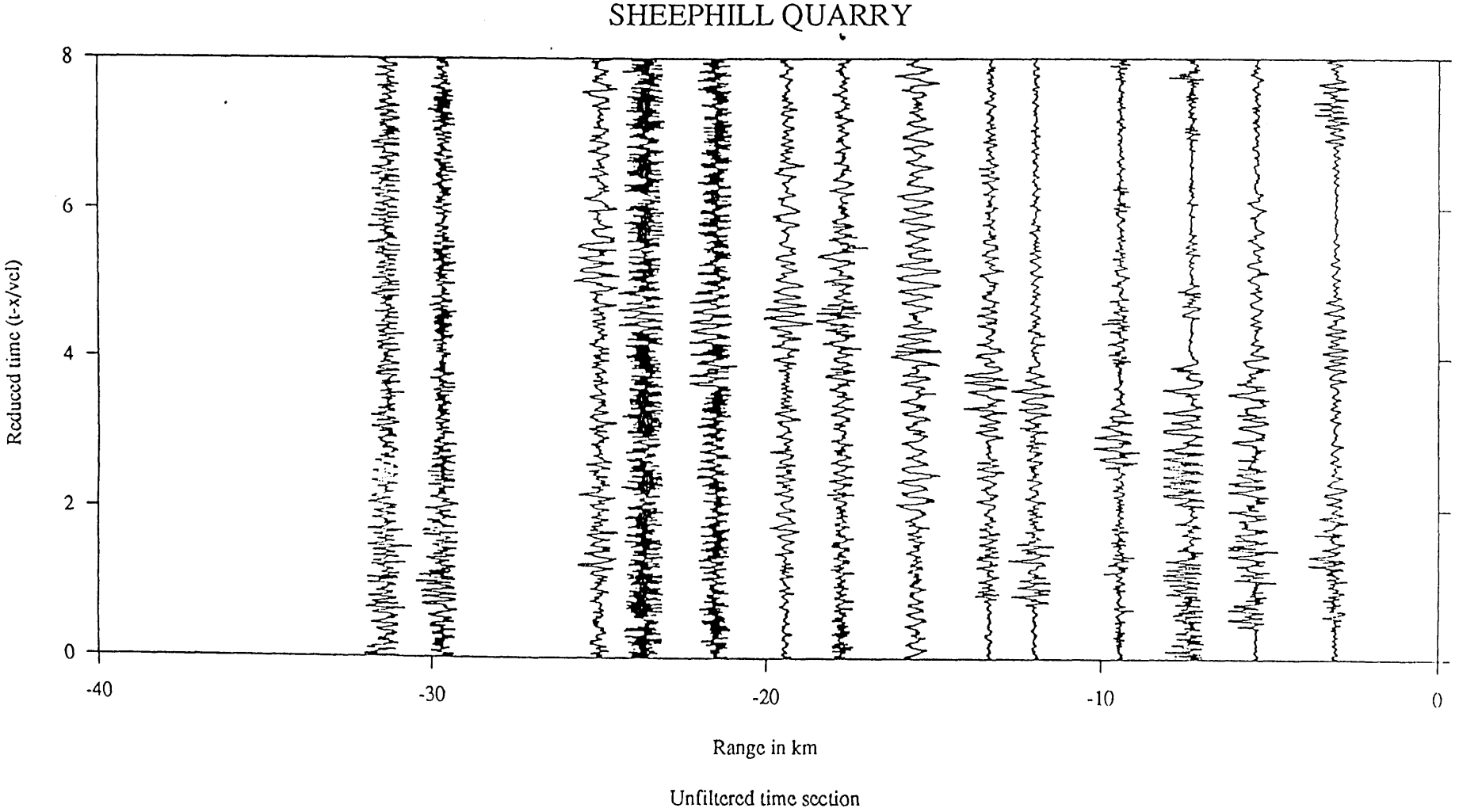

Fig. 3.15 Unfiltered transverse component data from Sheephill Quarry, reduction velocity 6.0 km/s.

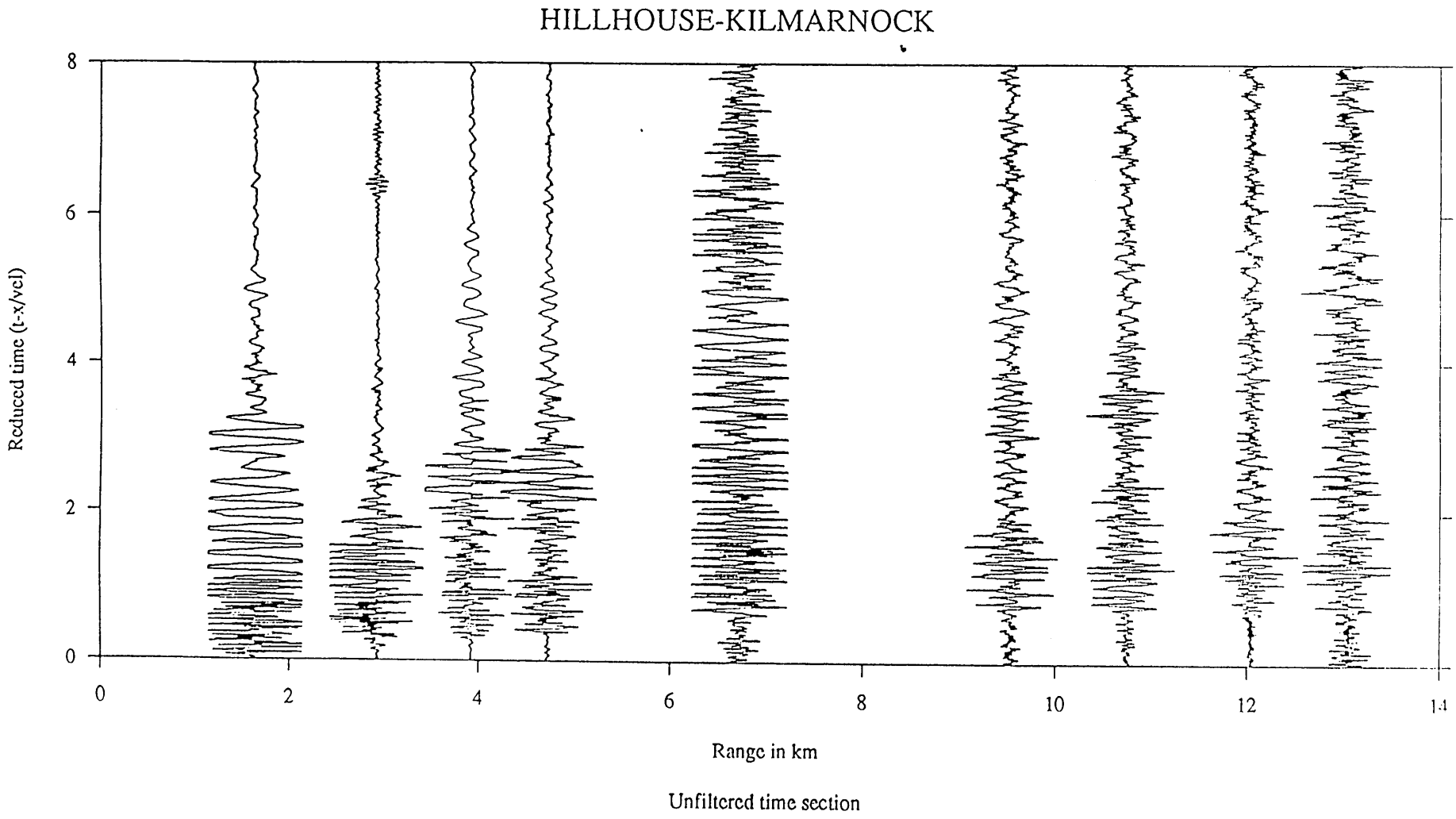

Fig. 3.16 Unfiltered vertical component data from Hillhouse along the Hillhouse Kilmarnock profile, reduction velocity 6.0 km/s.

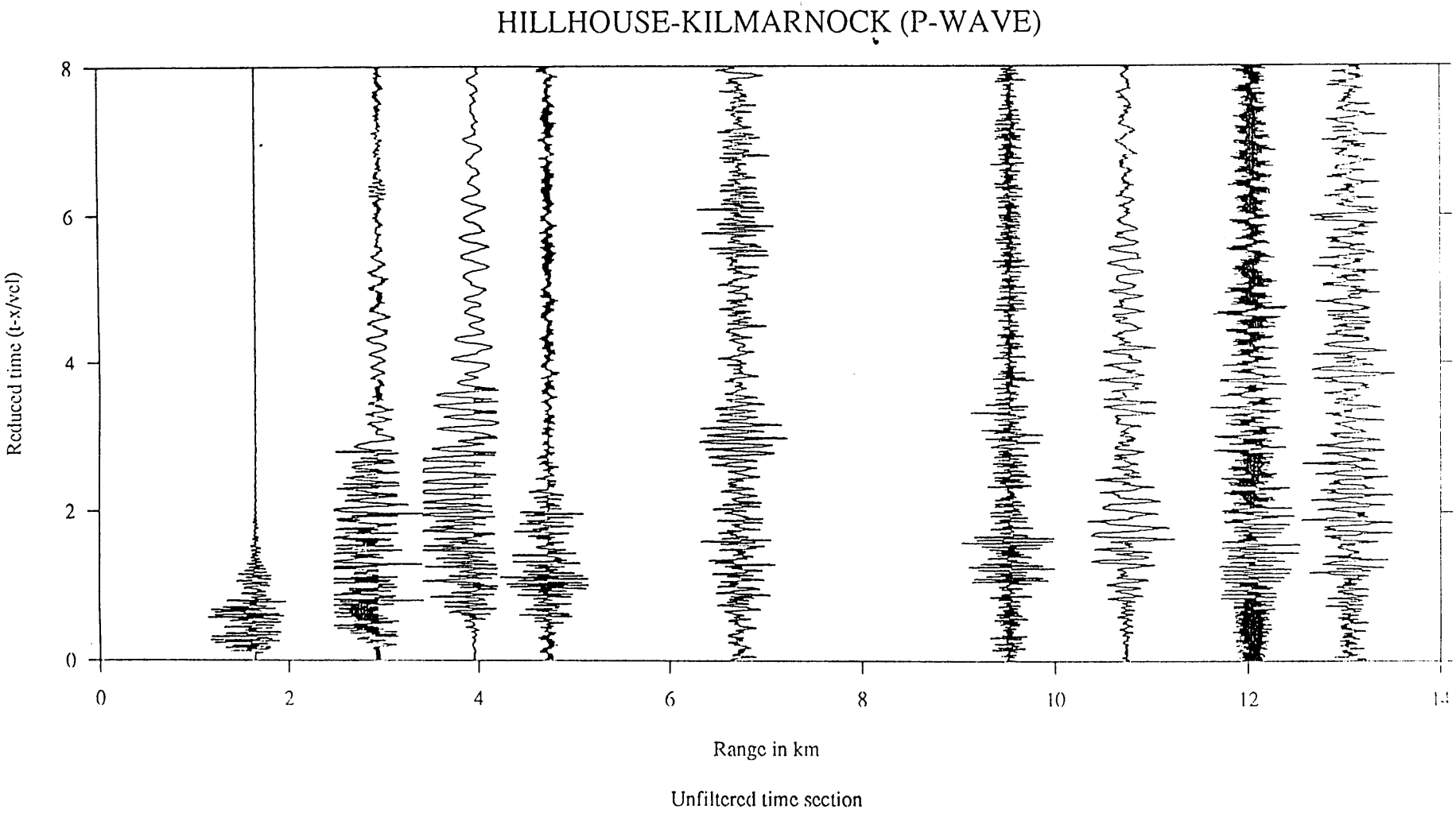

Fig. 3.17 Unfiltered radial component data from Hillhouse along the Hillhouse-Kilmarnock profile, reduction velocity 6.0 km/s.

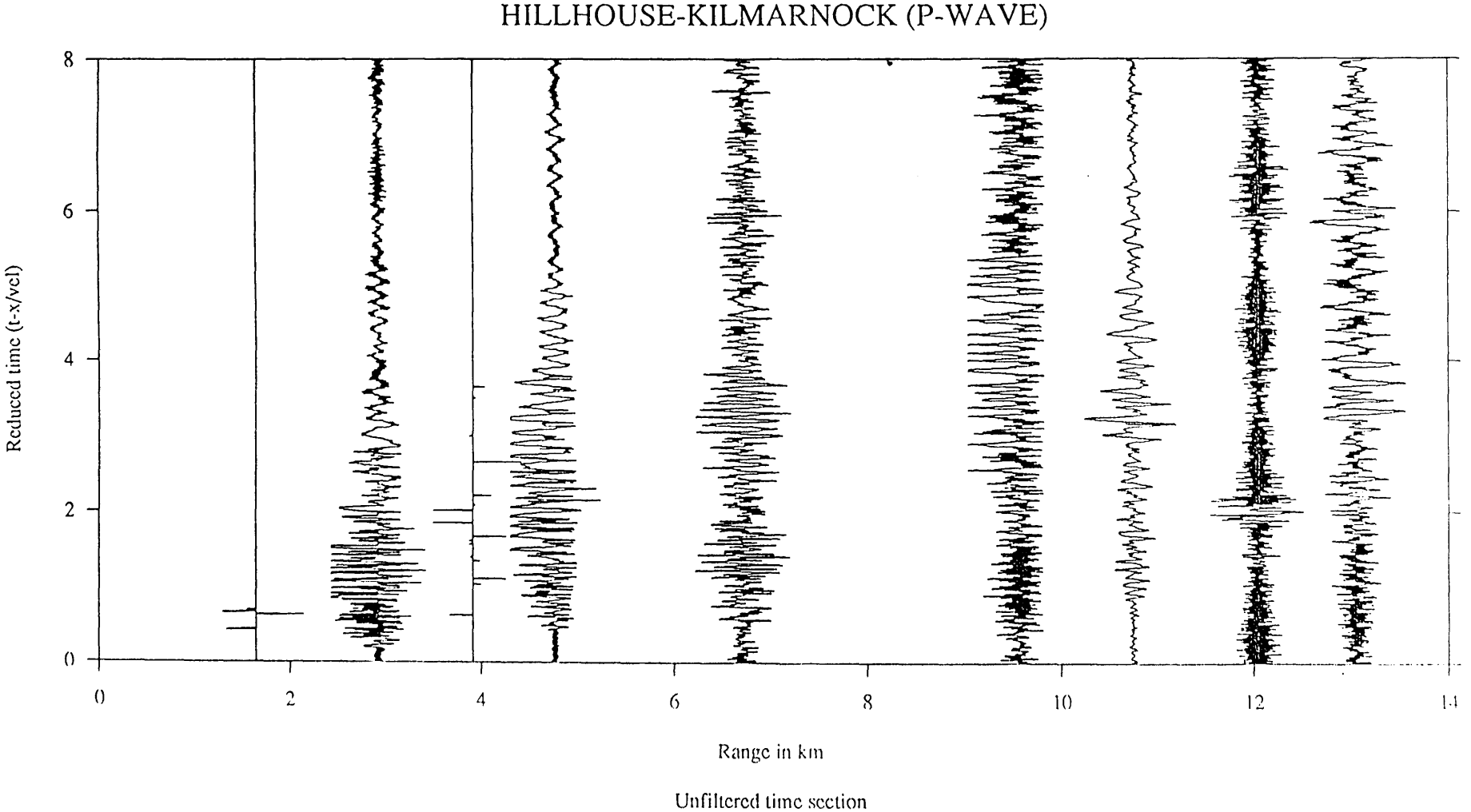

Fig. 3.18 Unfiltered transverse component data from Hillhouse along the Hillhouse-Kilmarnock profile, reduction velocity 6.0 km/s.

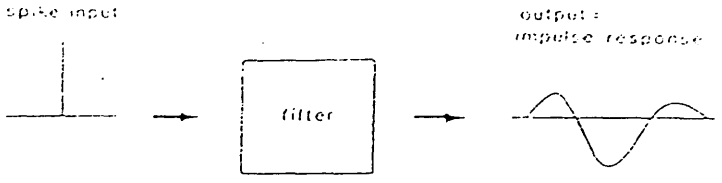

Fig. 3.19 The impulse response of a filter (after Keary & Brooks 1984).

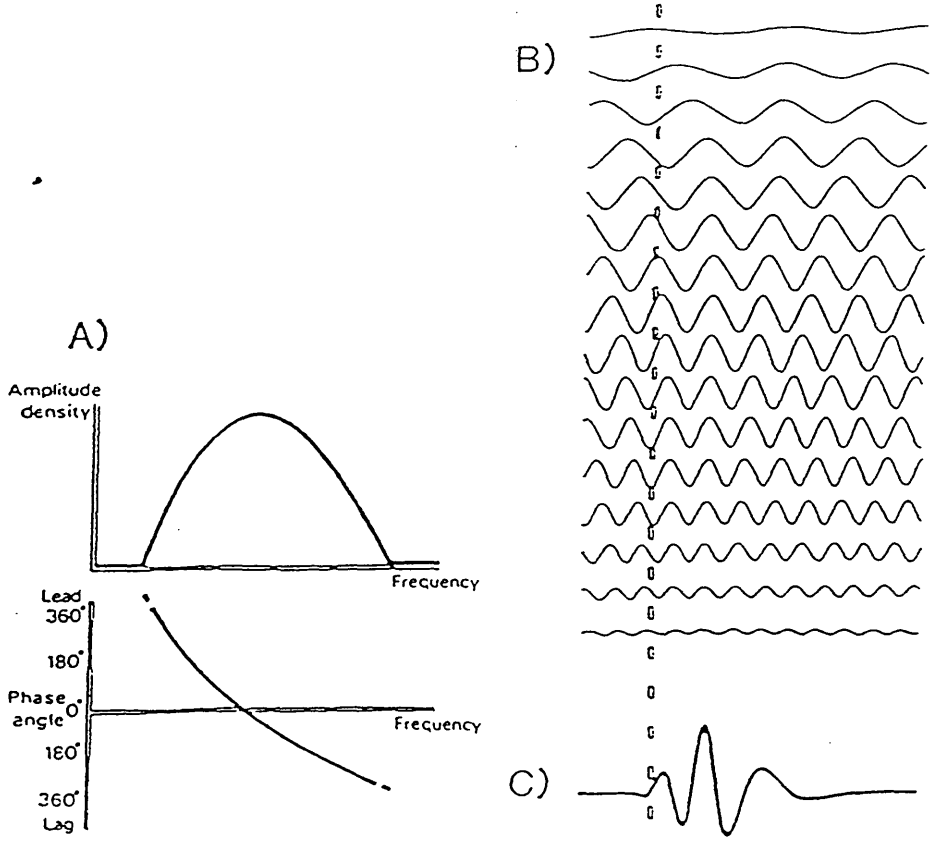

Fig. 3.20 Fourier representation of seismic waveform; A) , amplitude and phase spectra. B), sinusoidal waves having amplitudes and time shifts corresponding to the spectra in (A). C), synthesis of the waveform by summation of the waves in (B). (after Dentith 1987).

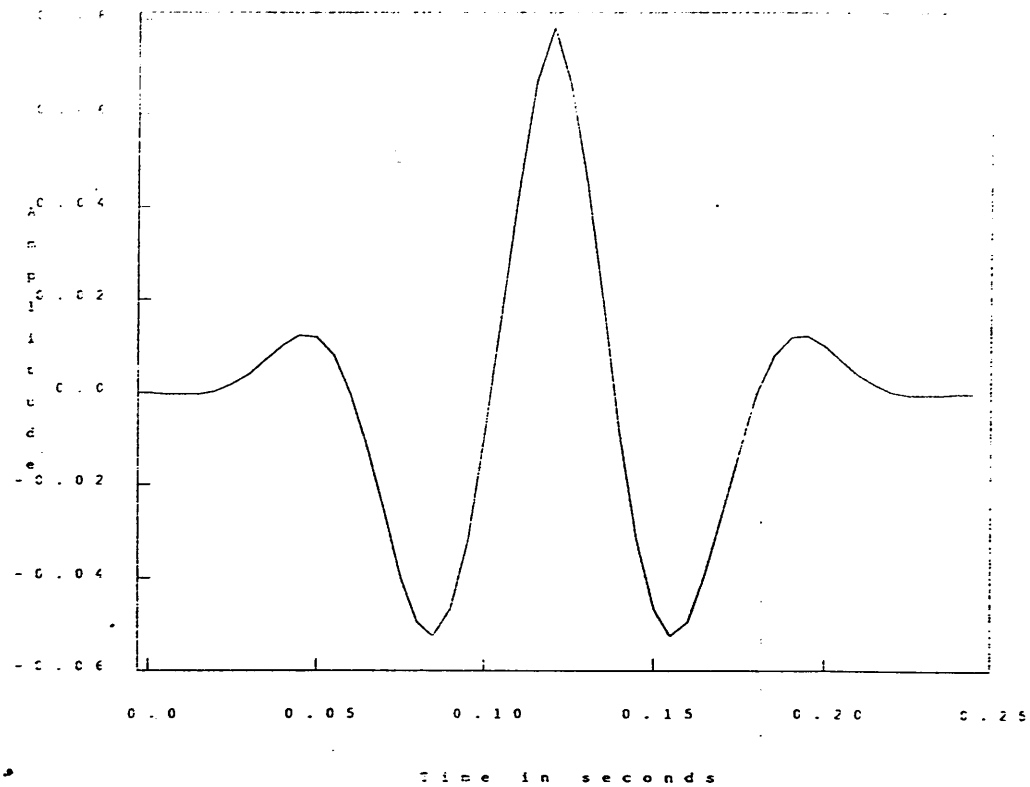

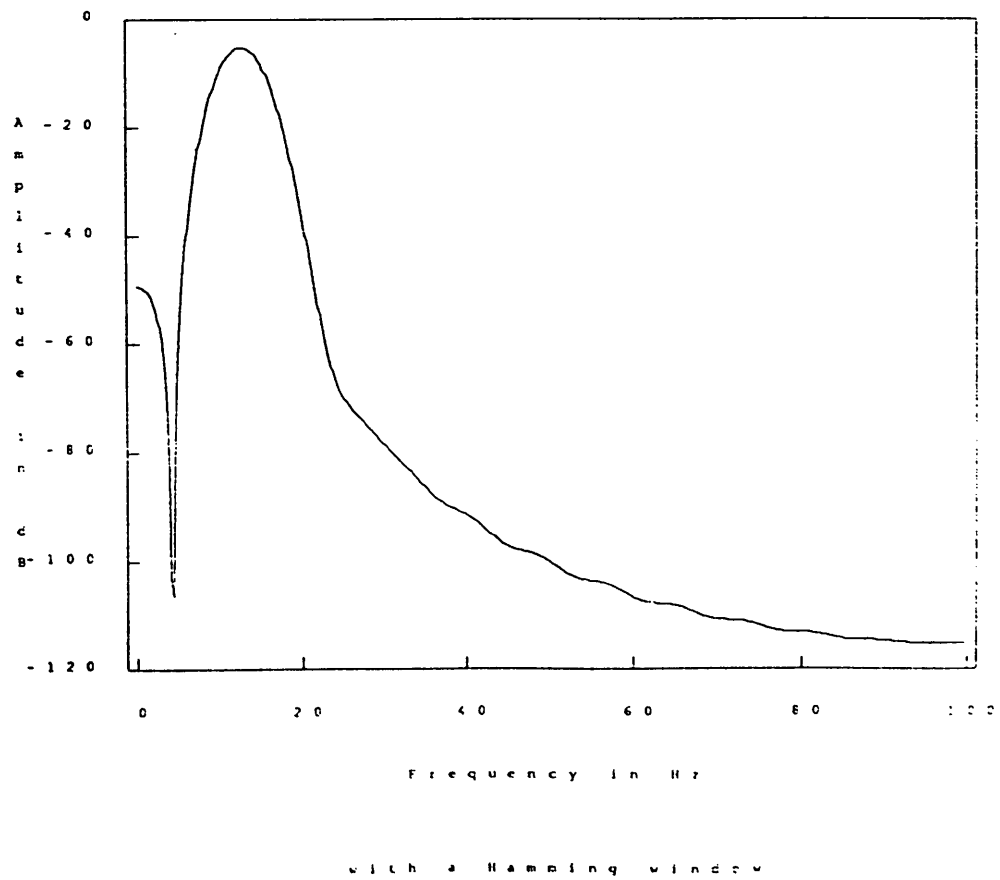

Fig. 3.21a Impulse and frequency response for a zero phase 8-16 Hz band-pass filter.

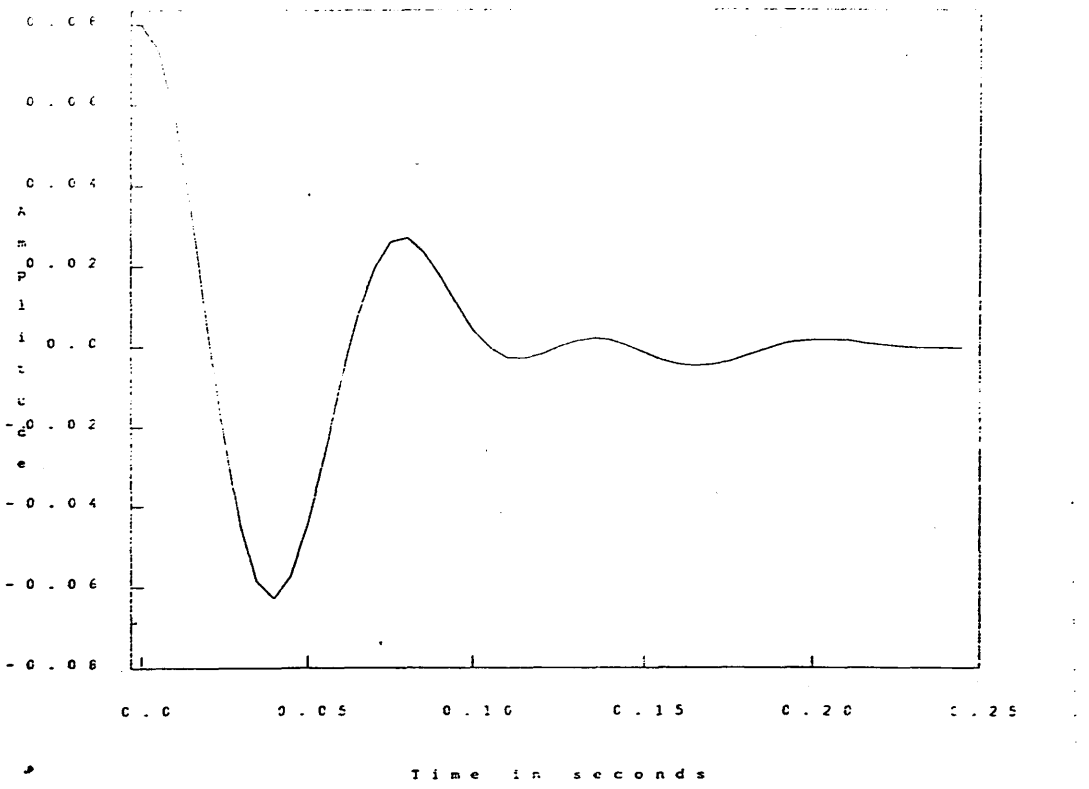

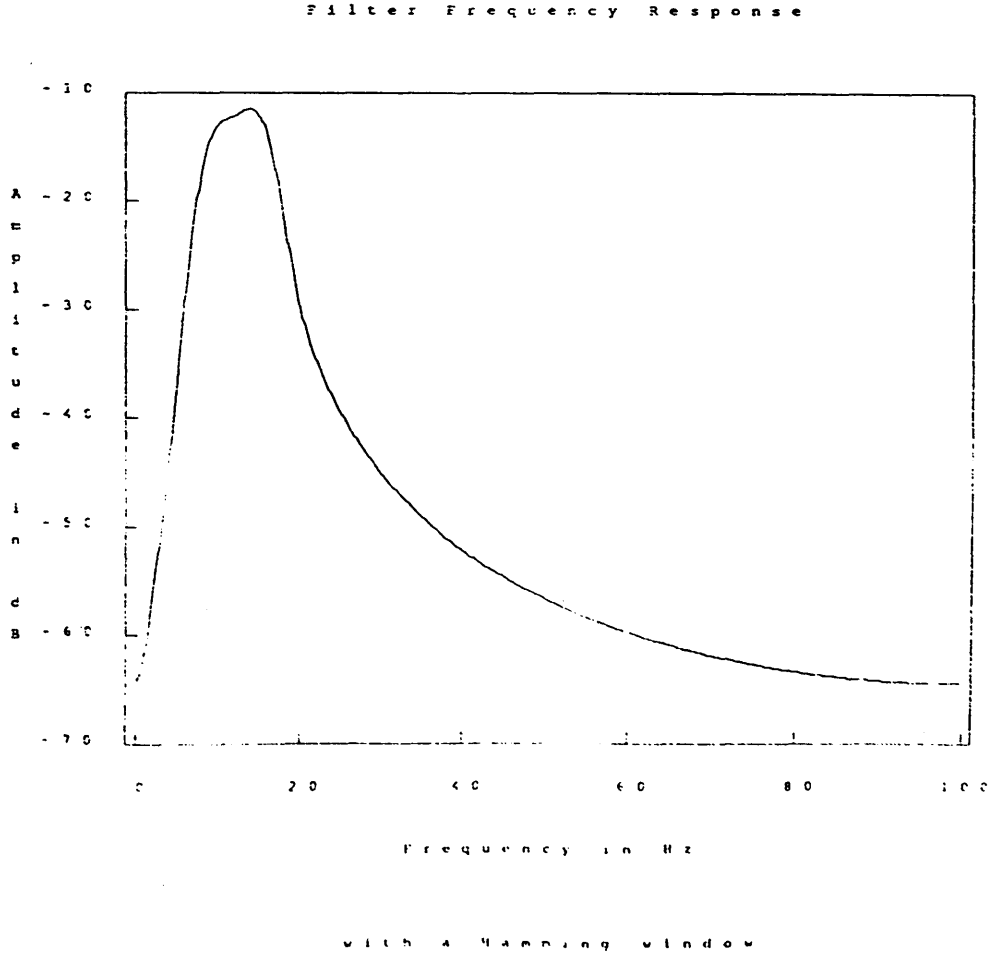

Fig. 3.21b Impulse and frequency response for a minimum phase 8-16 Hz band-pass filter.

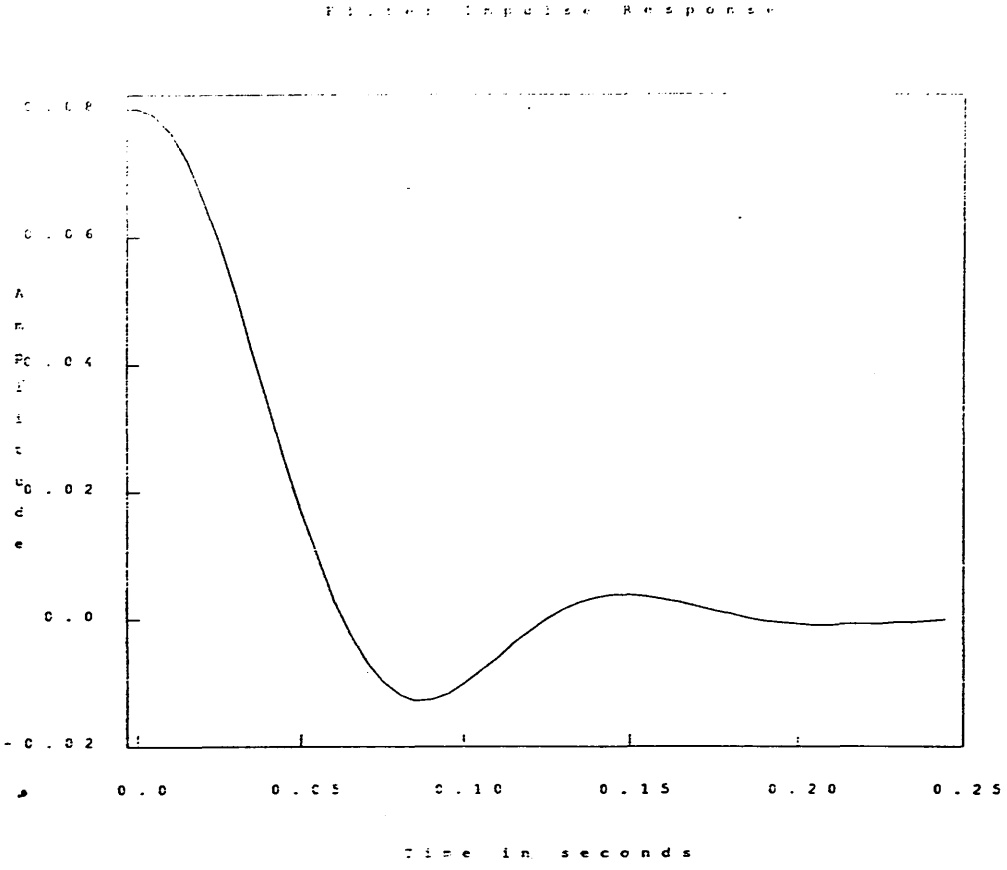

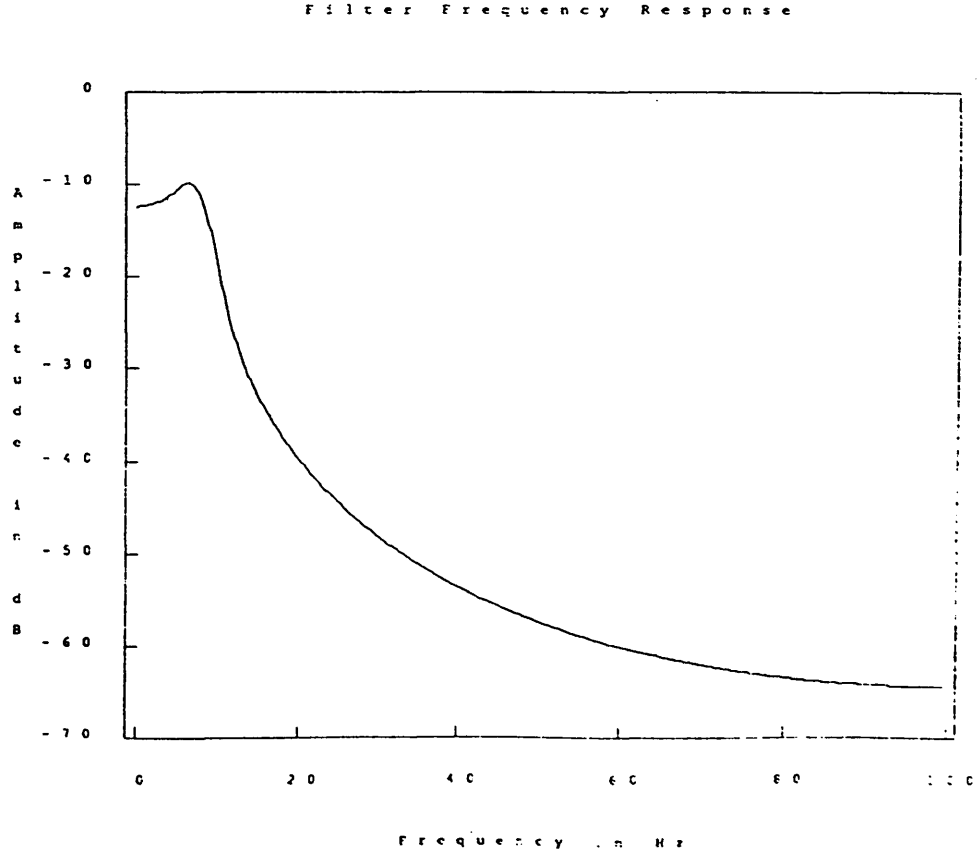

Minimum-phase, lowpass filter 8.0Hz and length 0.2
with a Hamming window

Fig. 3.22a Impulse and frequency response for a zero phase 8 Hz low-pass filter

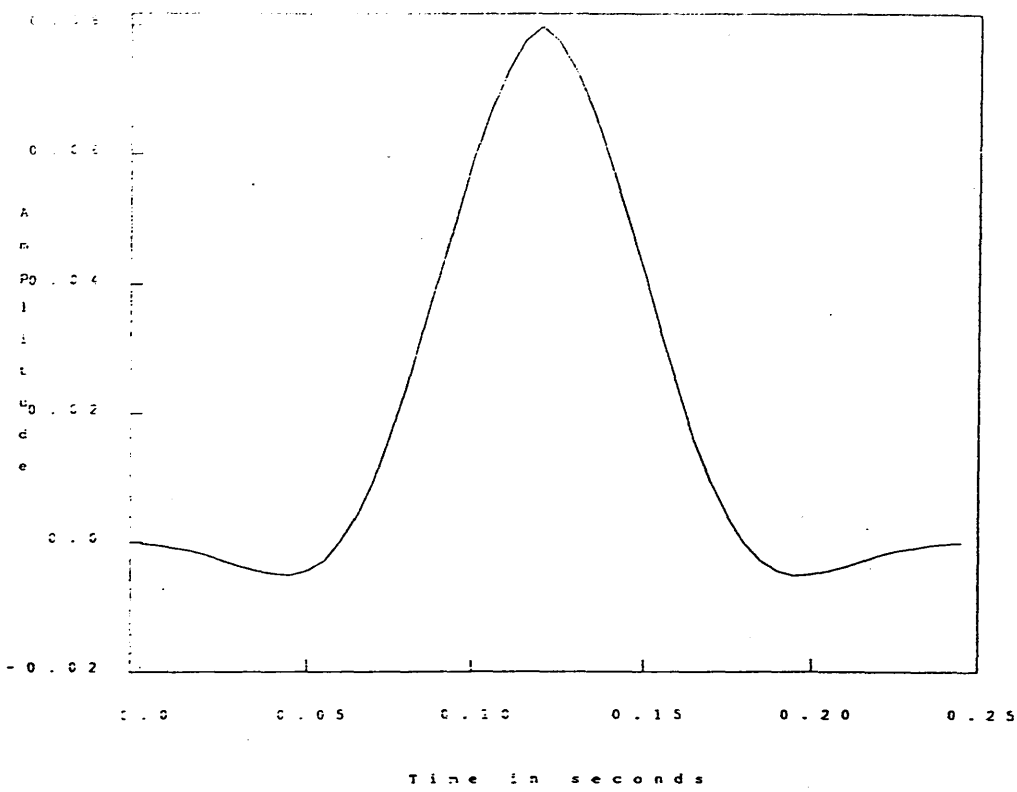

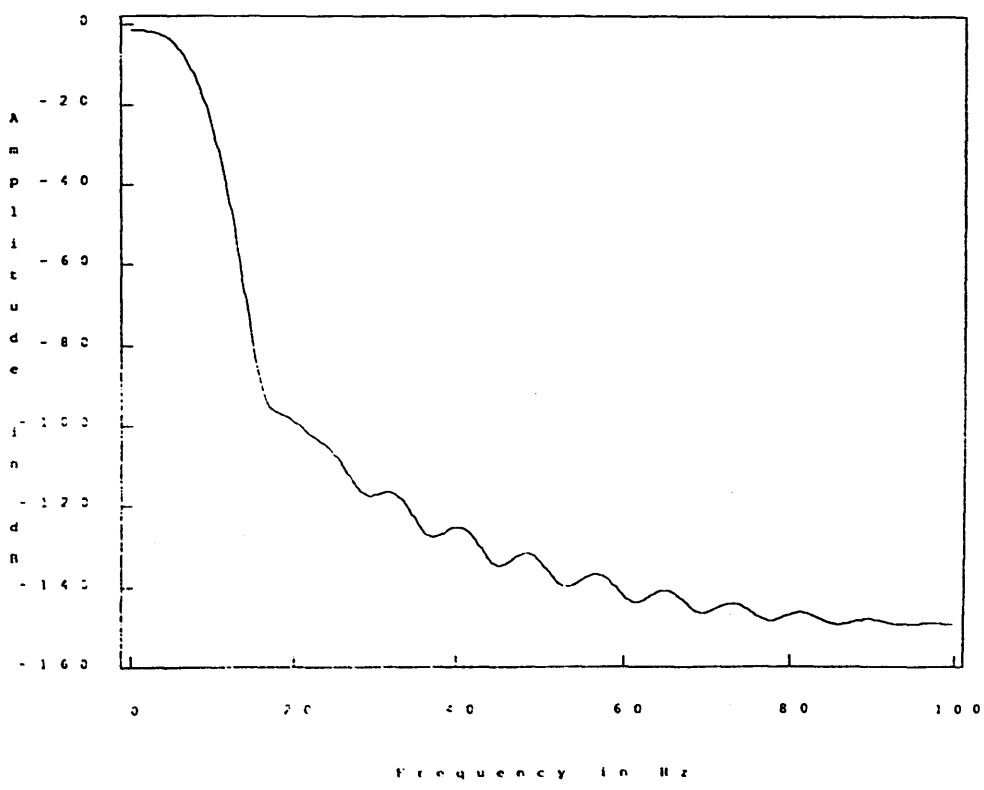

Fig. 3.22b Impulse and frequency response for a minimum phase 8 Hz low-pass filter.

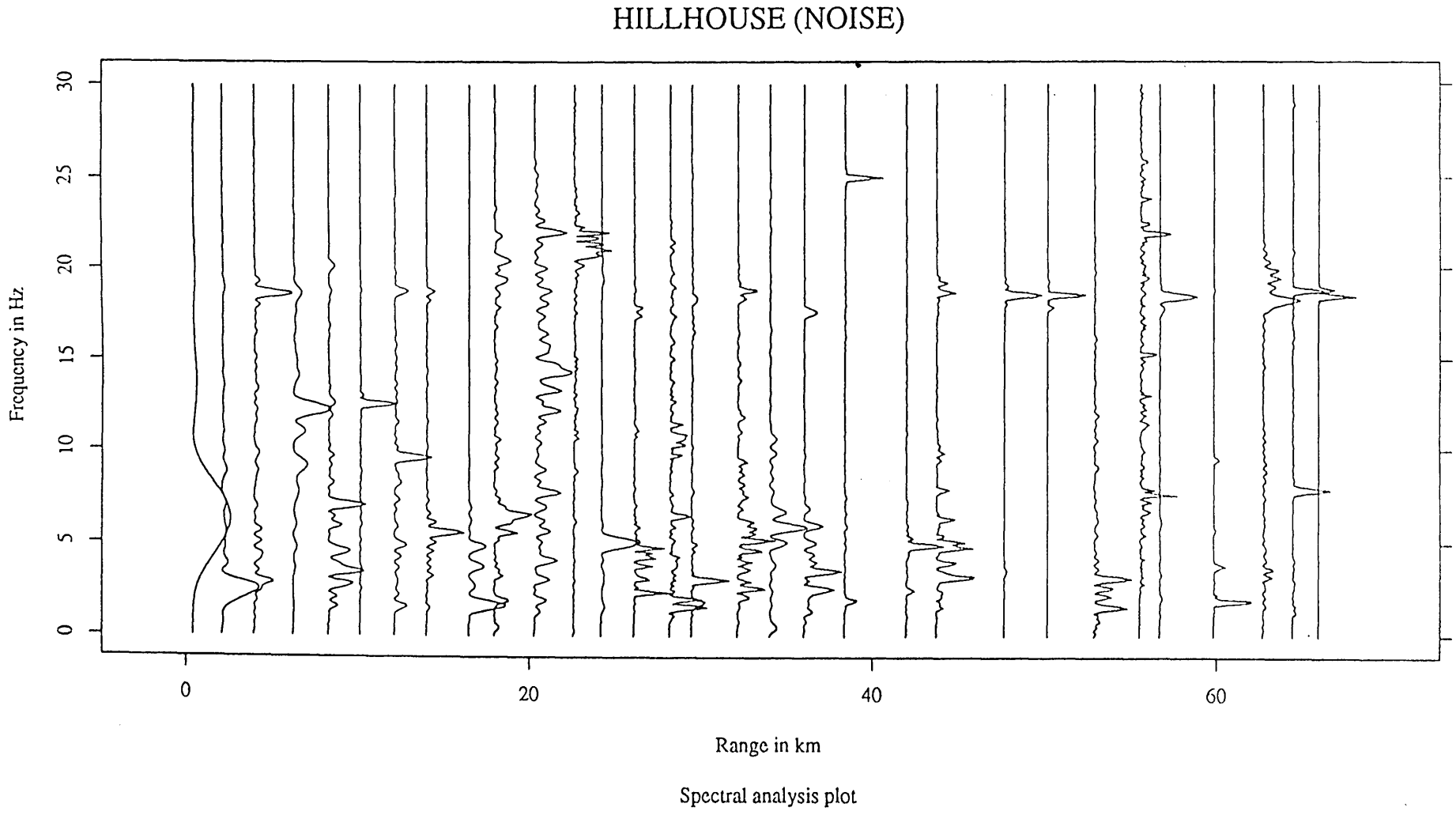

Fig. 3.23 Noise spectral analysis along the main profile.

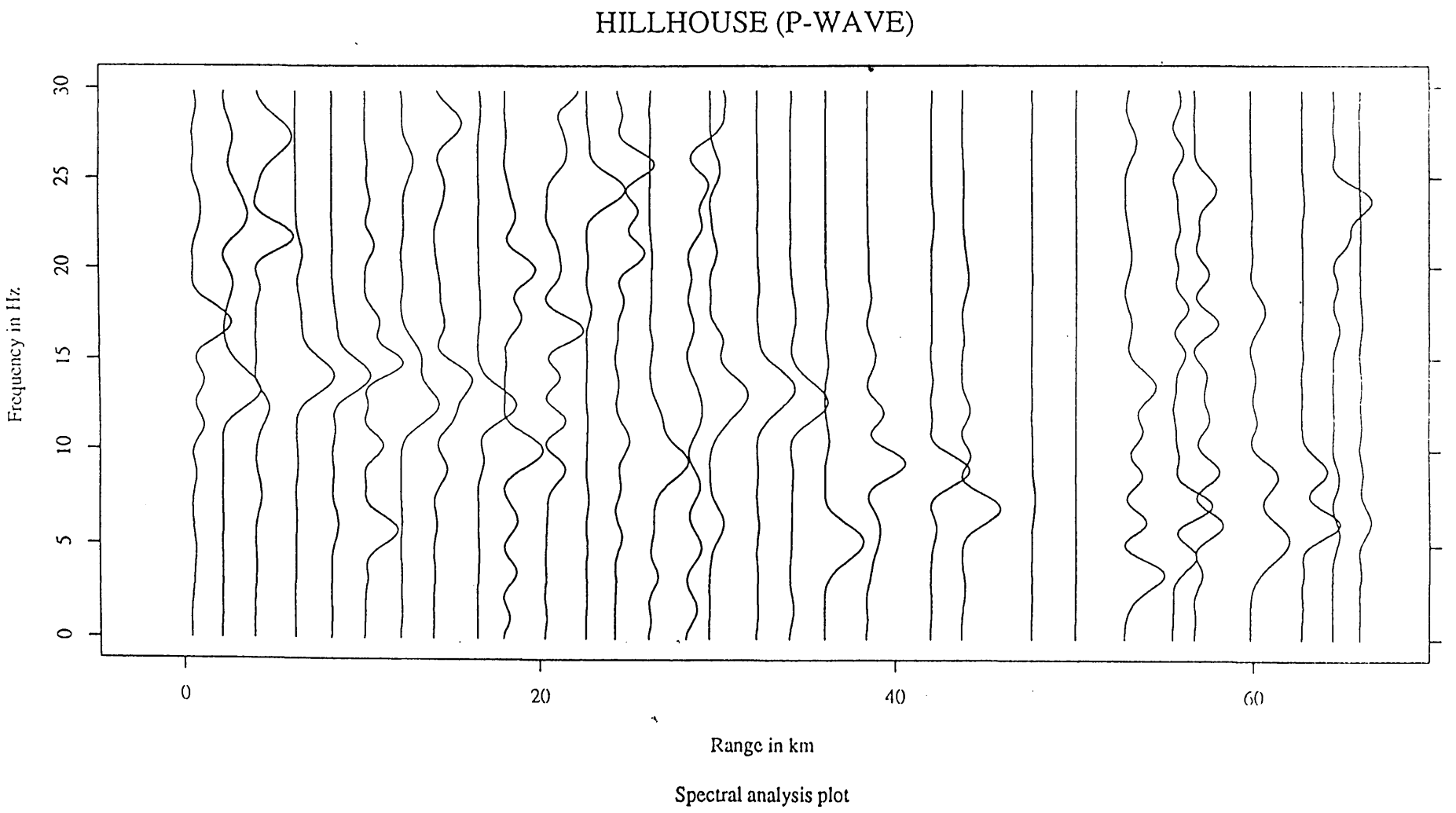

Fig. 3.24 P-wave spectral analysis for Hillhouse (main line) vertical component data.

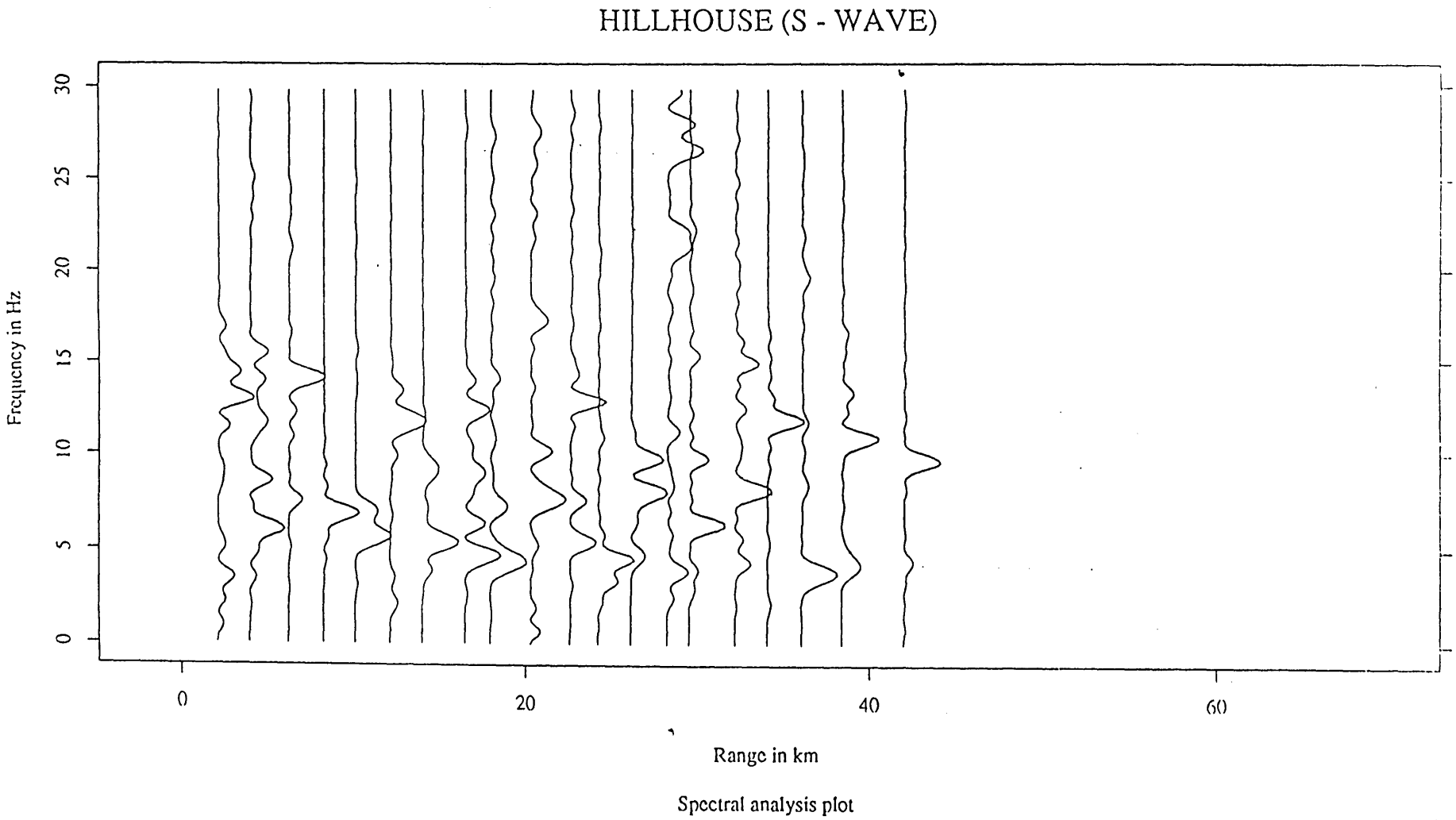

Fig. 3.25 S-wave spectral analysis for Hillhouse (main line) vertical component data.

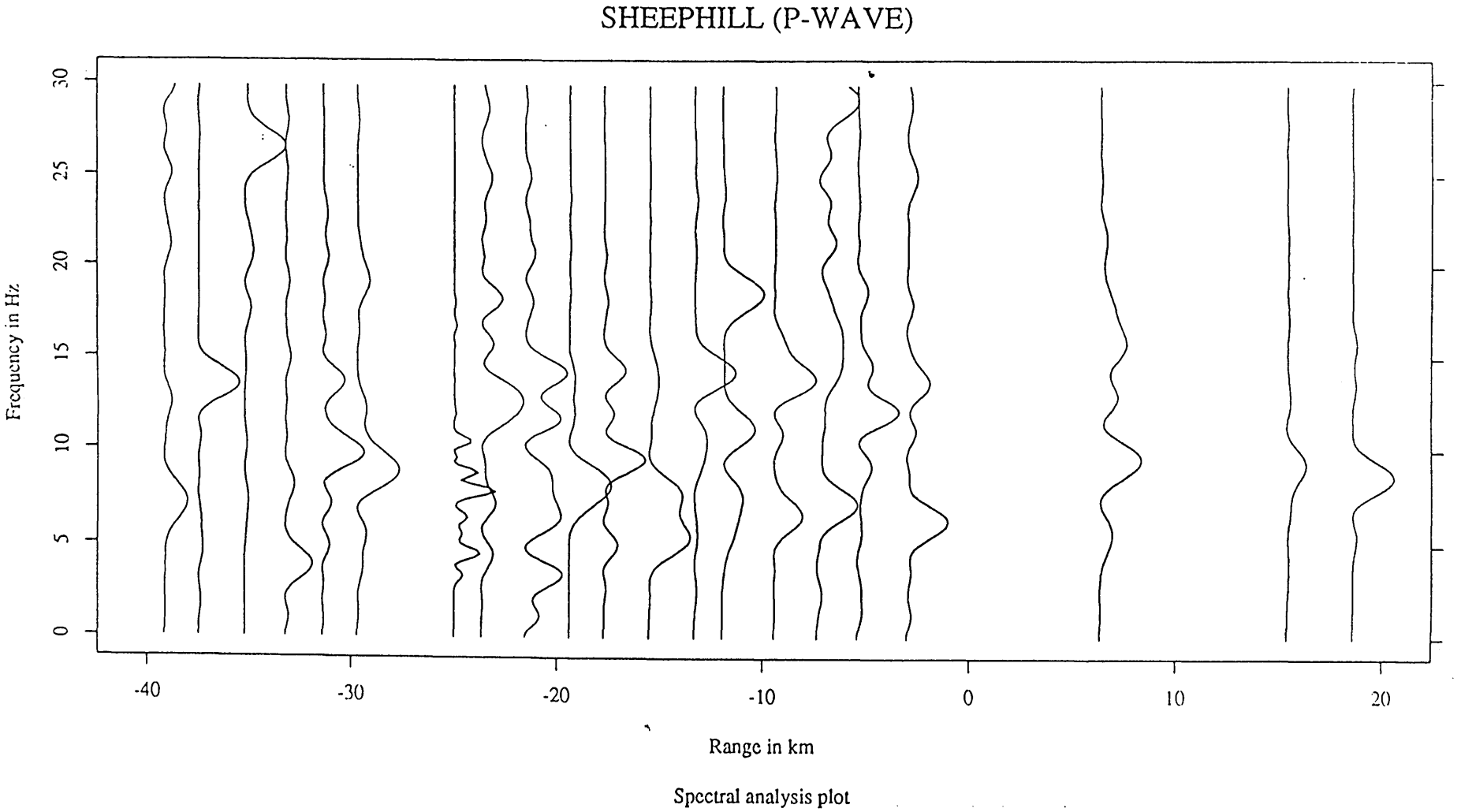

Fig. 3.26 P-wave spectral analysis for Sheephill (main line) vertical component data.

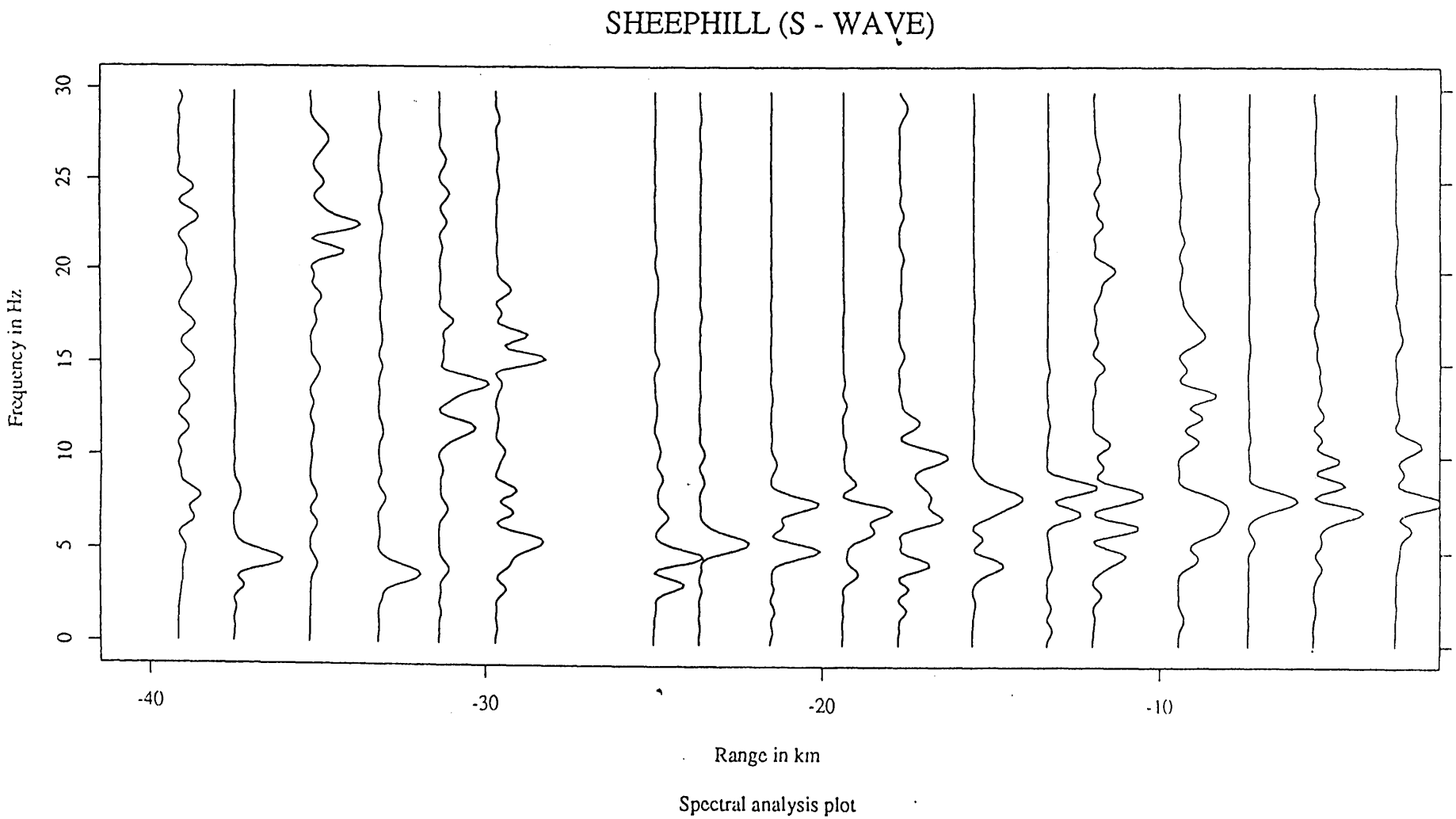

Fig. 3.27 S-wave spectral analysis for Sheephill (main line) vertical component data.

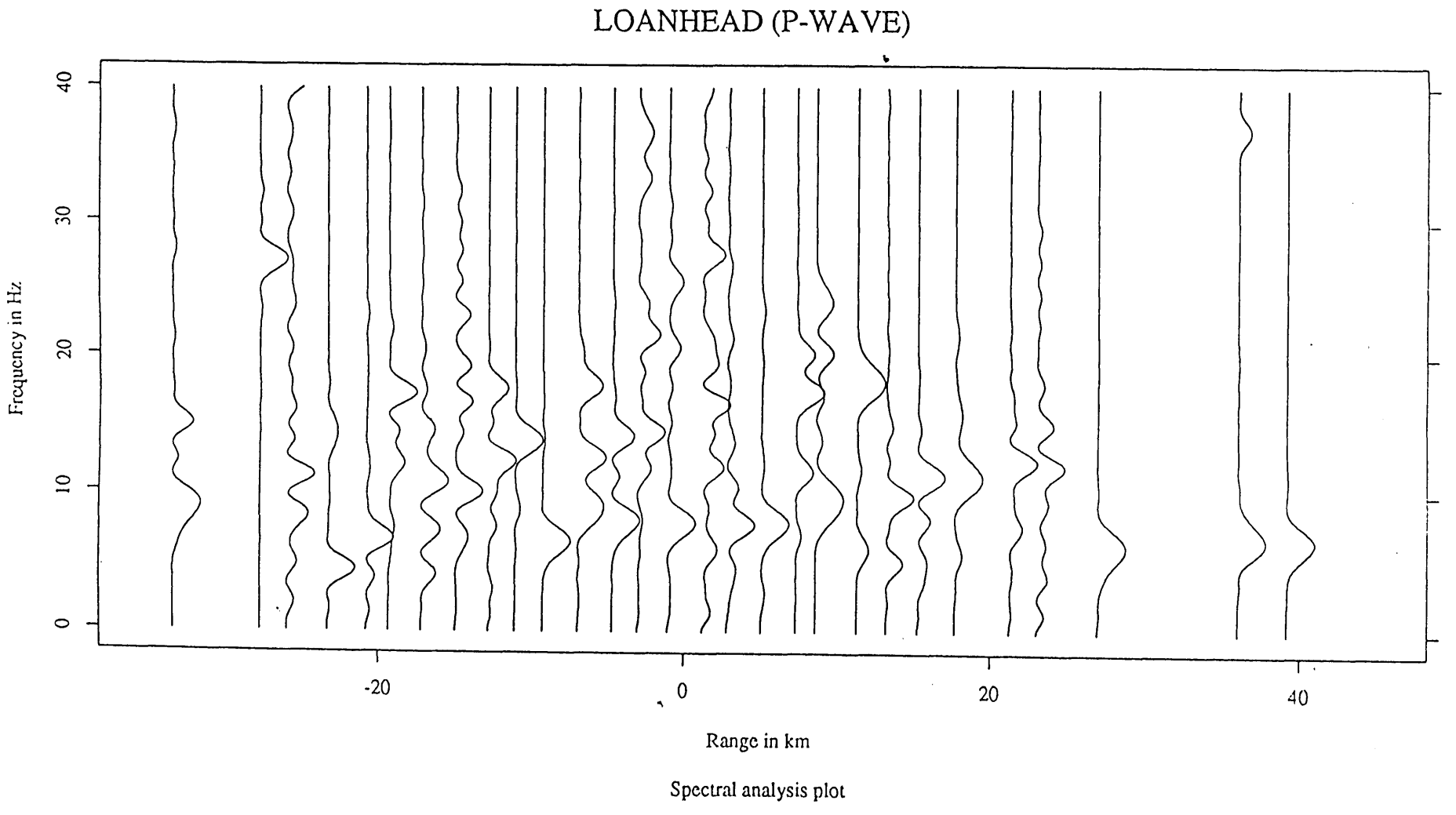

Fig. 3.28 P-wave spectral analysis for Loanhead (main line) vertical component data.

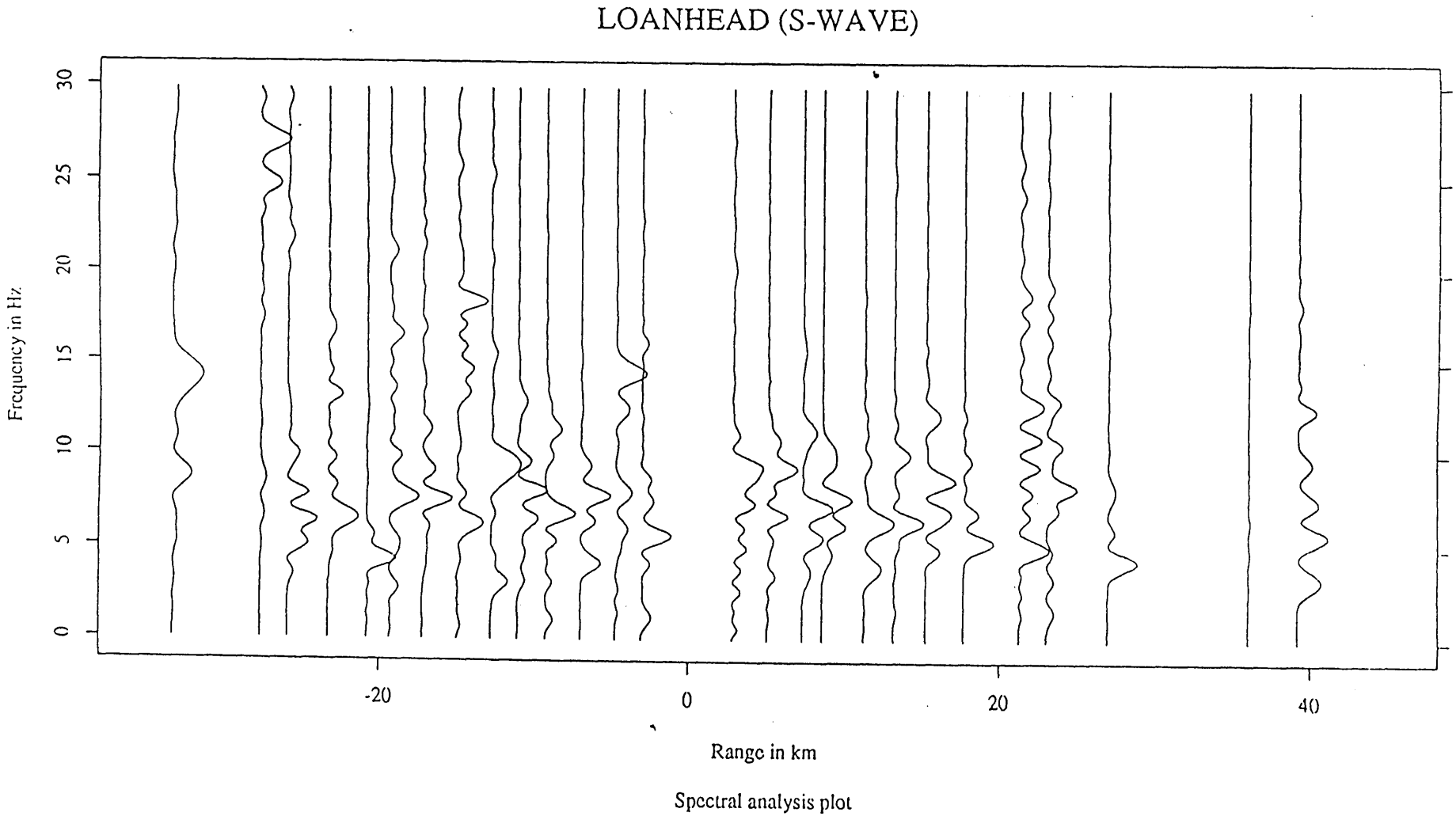

Fig. 3.29 S-wave spectral analysis for Loanhead (main line) vertical component data.

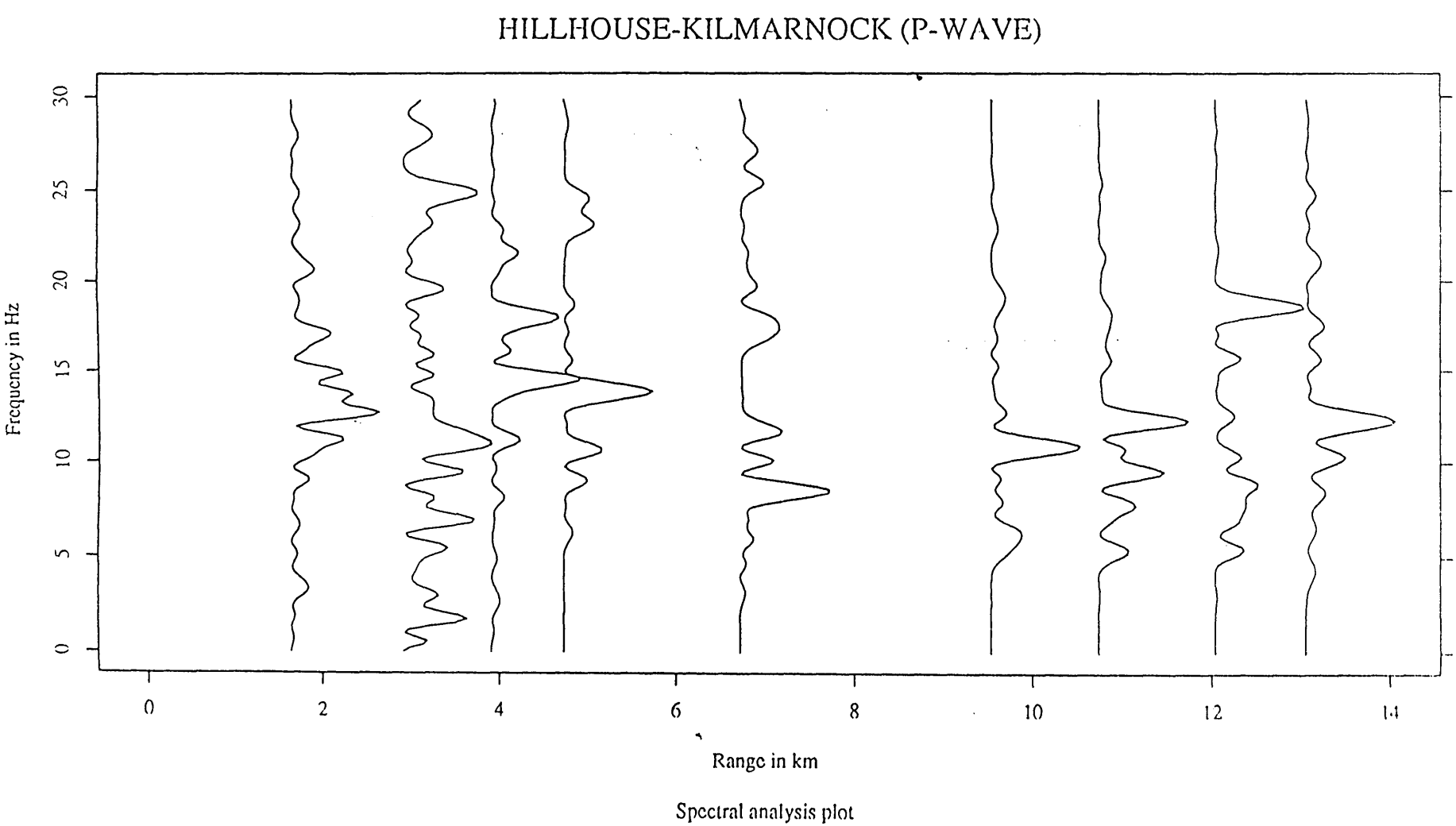

Fig. 3.30 P-wave spectral analysis (vertical component) for the Hillhouse-Kilmarnock line.

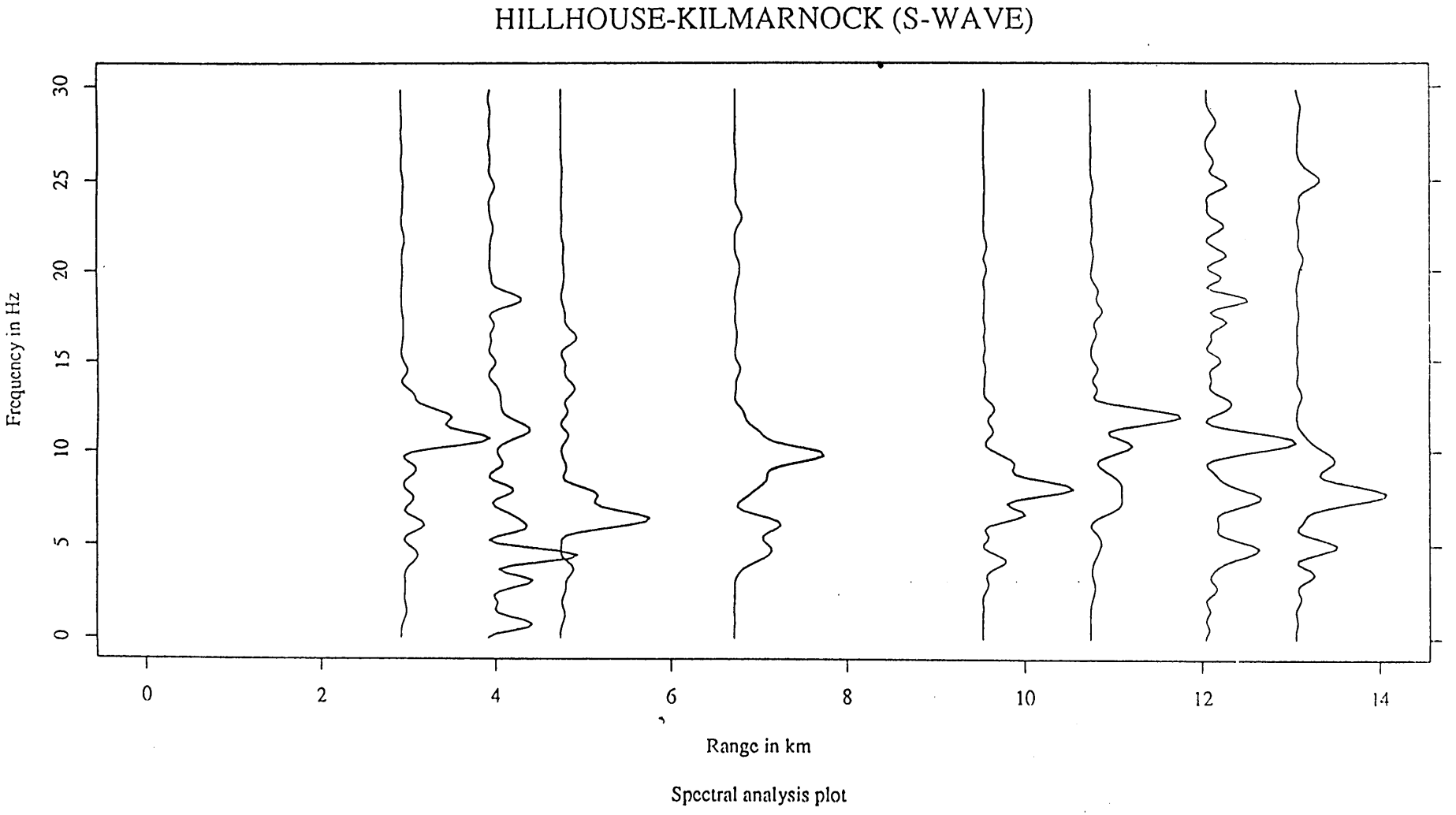

Fig. 3.31 S-wave spectral analysis (vertical component) for the Hillhouse- Kilmarnock line.

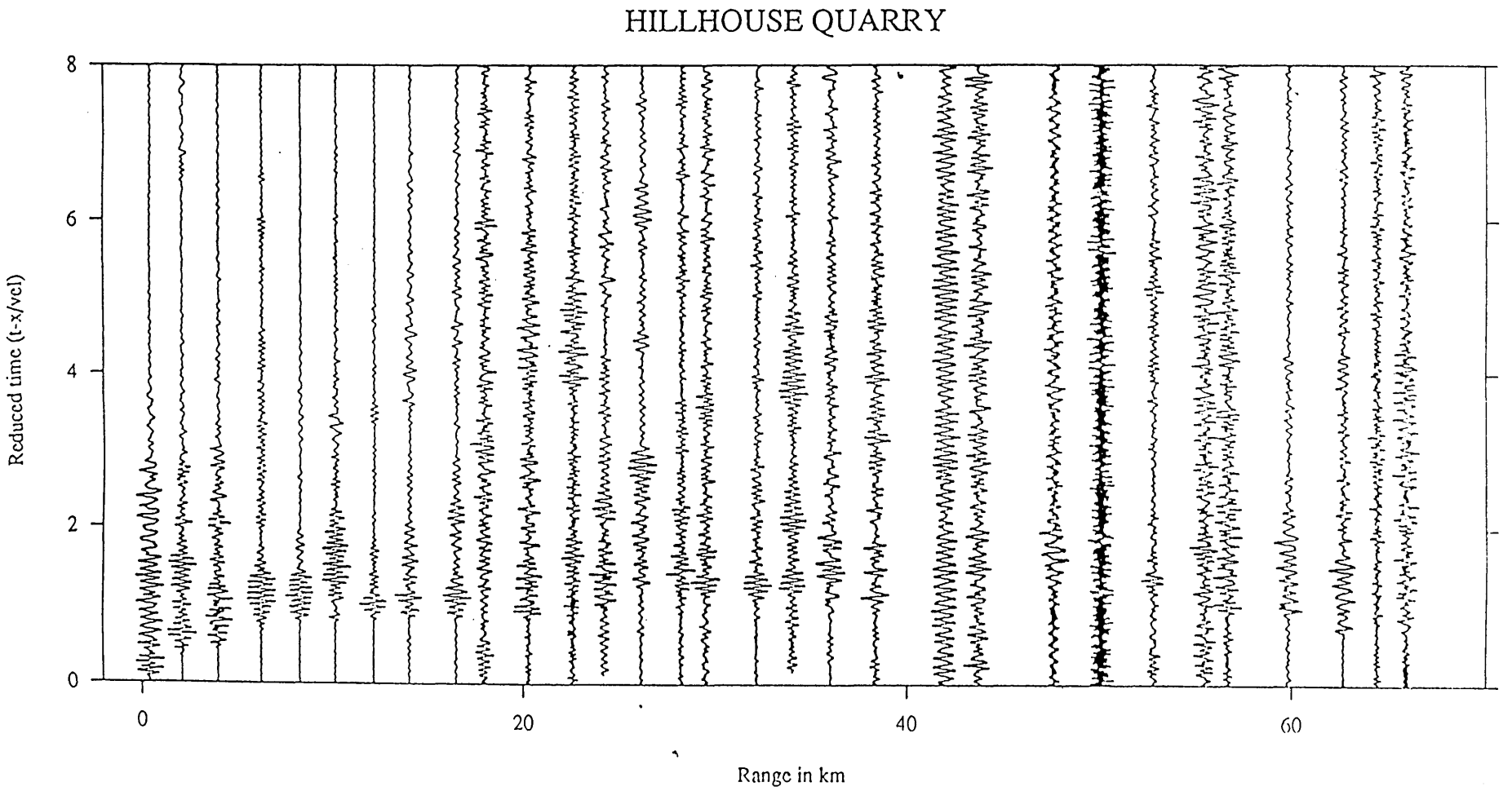

Fig. 3.32 Hillhouse (main line) vertical component data filtered with a minimum-phase, band-pass 8.0-16.0 Hz filter with a 0.25 s Hamming window. Reduction velocity 6.0 km/s.

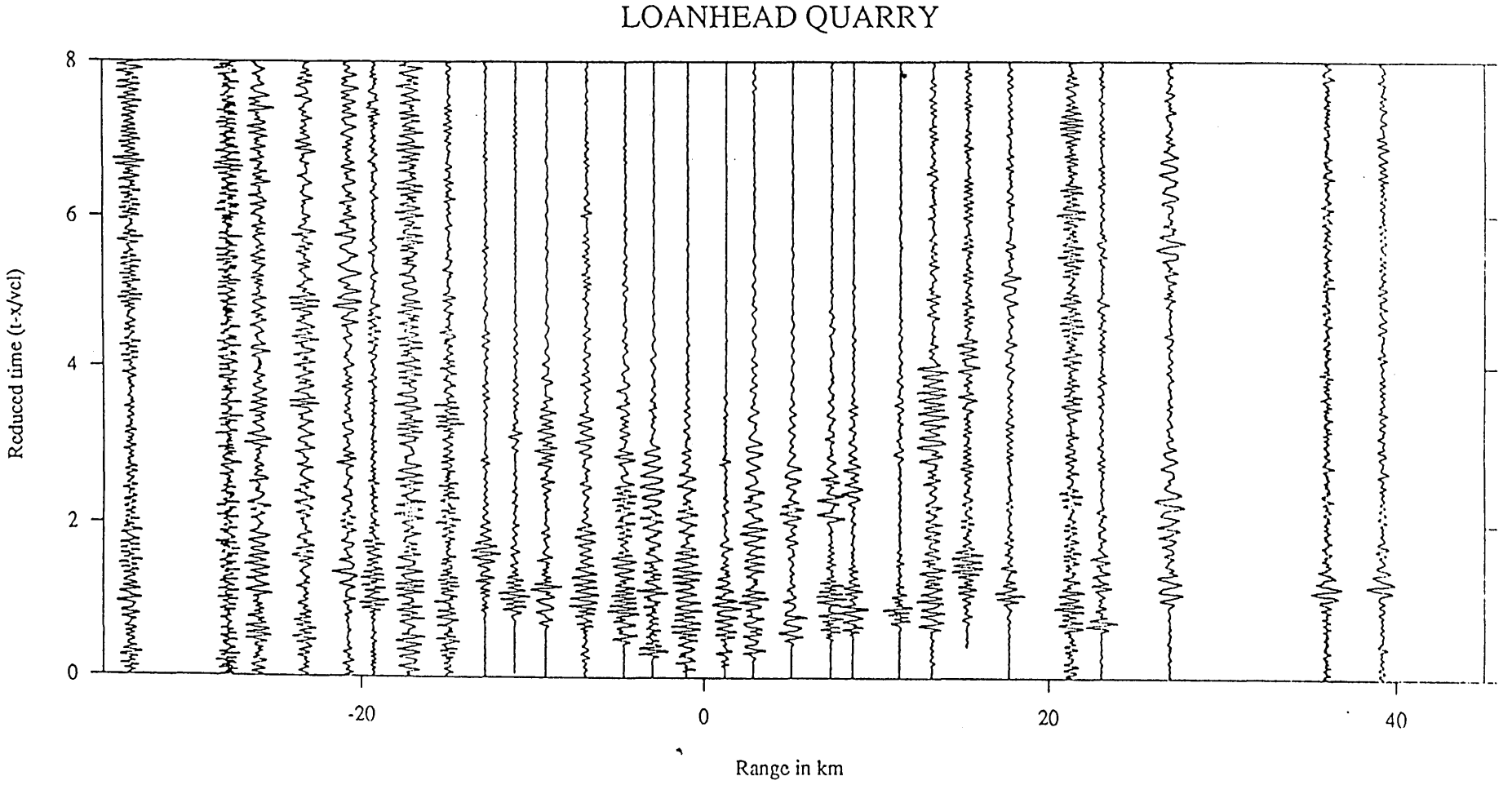

Fig. 3.33 Loanhead vertical component data filtered with a minimum-phase, band-pass 8.0-16.0 Hz filter with a 0.25 s Hamming window. Reduction velocity 6.0 km/s.

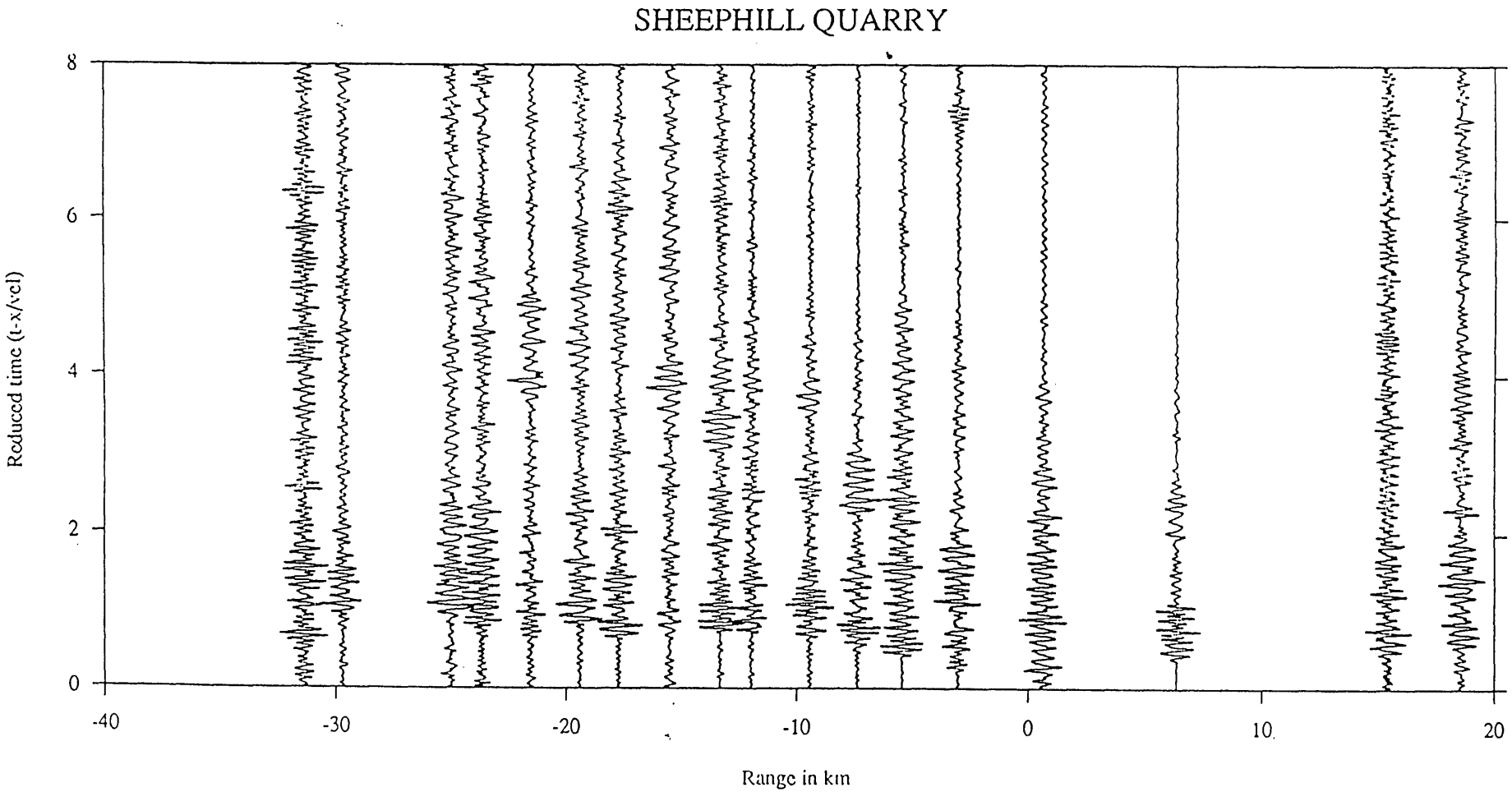

Fig. 3.34 Sheephill vertical component data filtered with a minimum-phase, band-pass 8.0-16.0 Hz filter with a 0.25 s Hamming window. Reduction velocity 6.0 km/s.

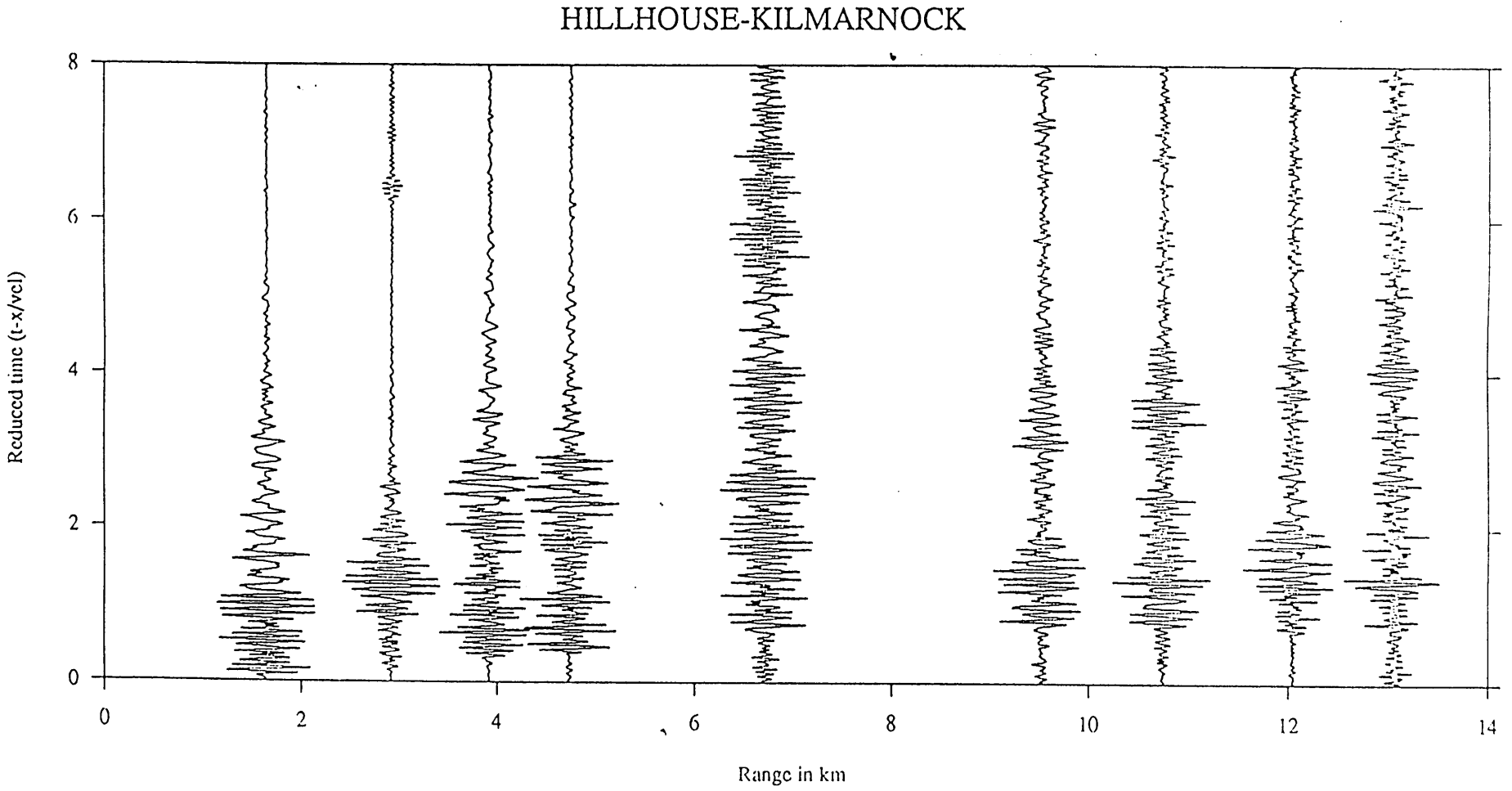

Fig. 3.35 Hillhouse-Kilmarnock line vertical component data filtered with a minimum-phase, band-pass 8.0-16.0 Hz filter with a 0.25 s Hamming window. Reduction velocity 6.0 km/s.

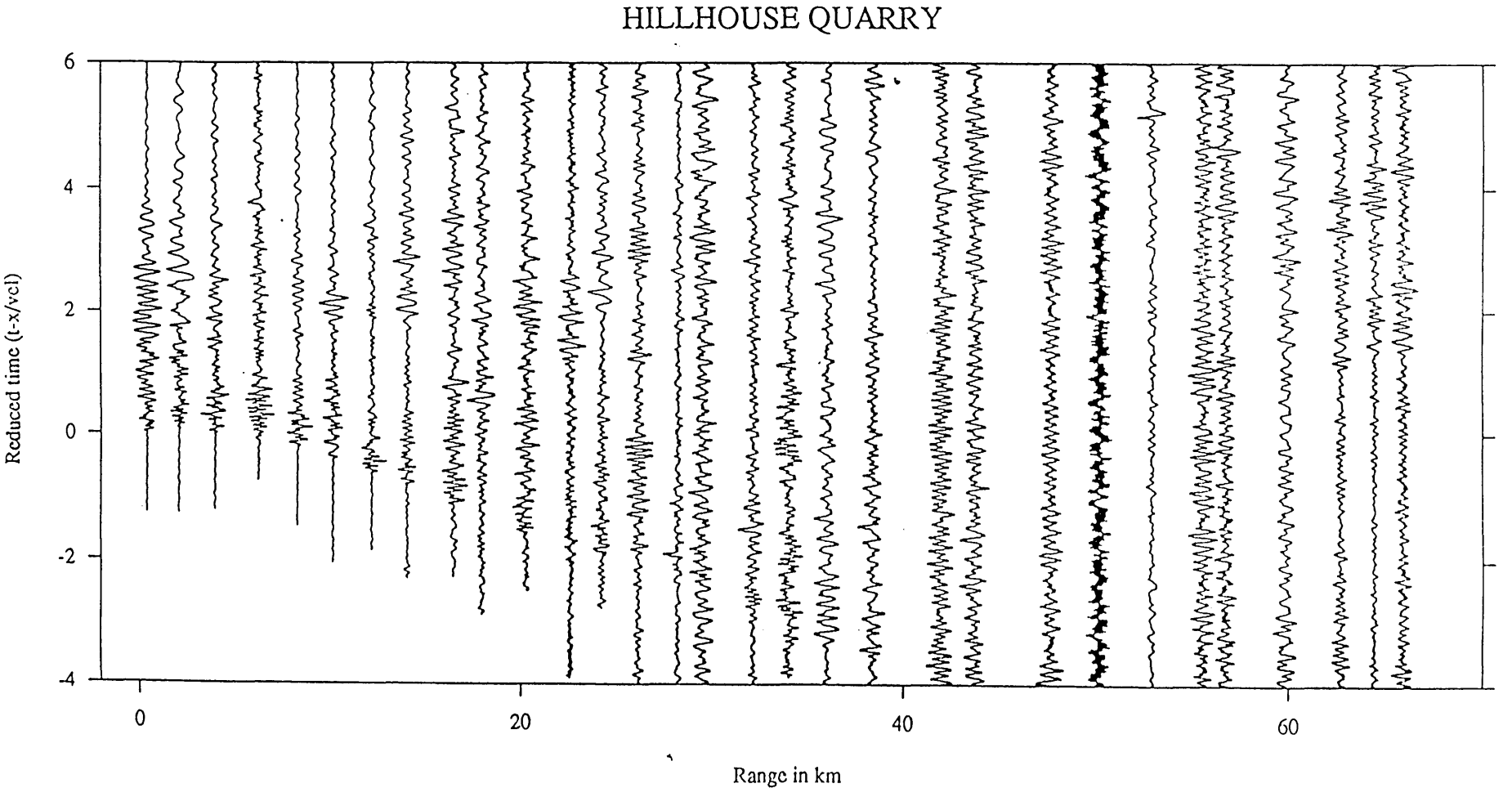

Fig. 3.36 Hillhouse (main line) vertical component data filtered with a minimum-phase, low-pass 8.0 Hz filter with a 0.25 s Hamming window. Reduction velocity 3.5 km/s.

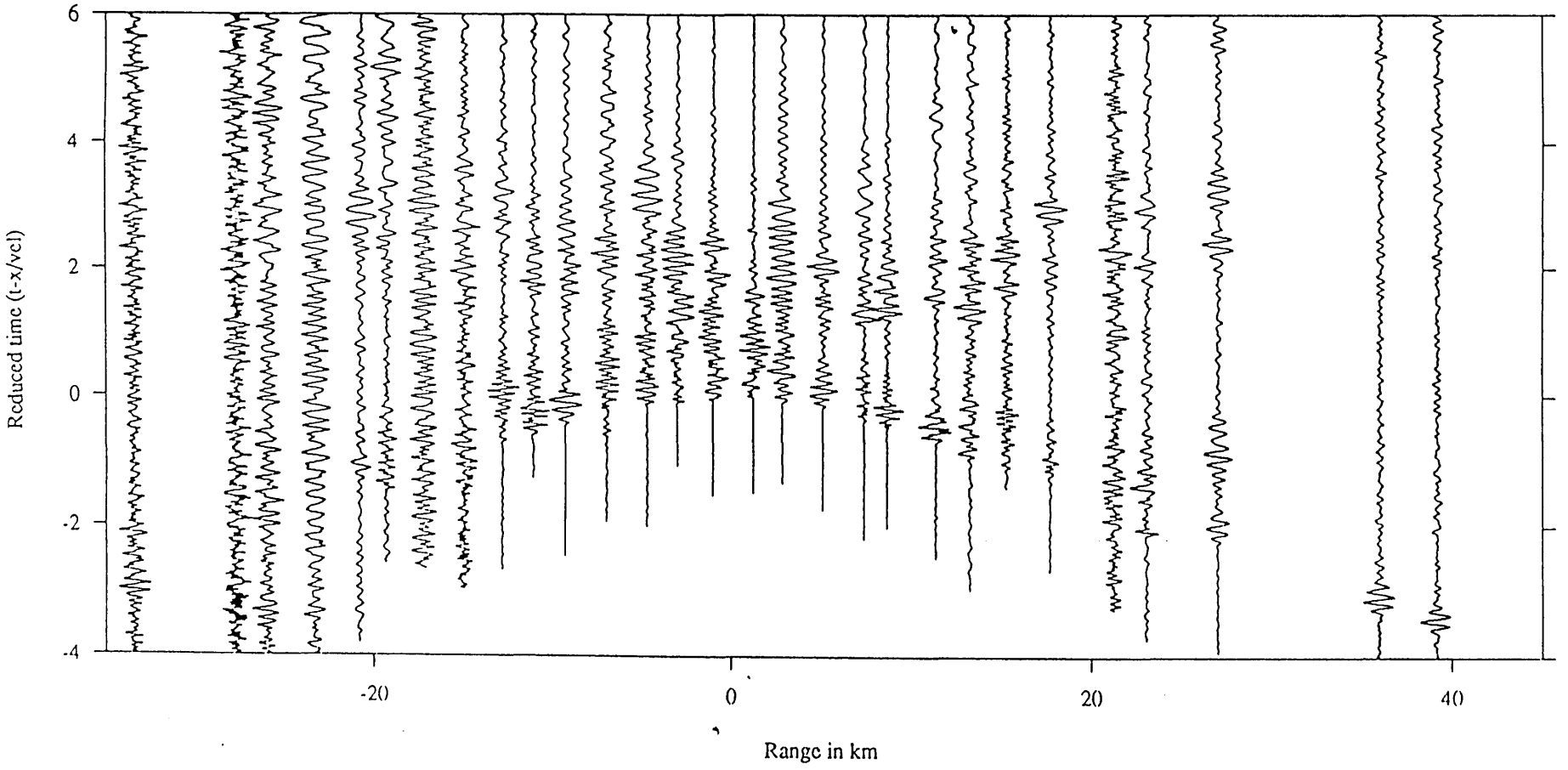

Fig. 3.37 Loanhead (main line) vertical component data filtered with a minimum-phase, low-pass 8.0 Hz filter with a 0.25 s Hamming window. Reduction velocity 3.5 km/s.

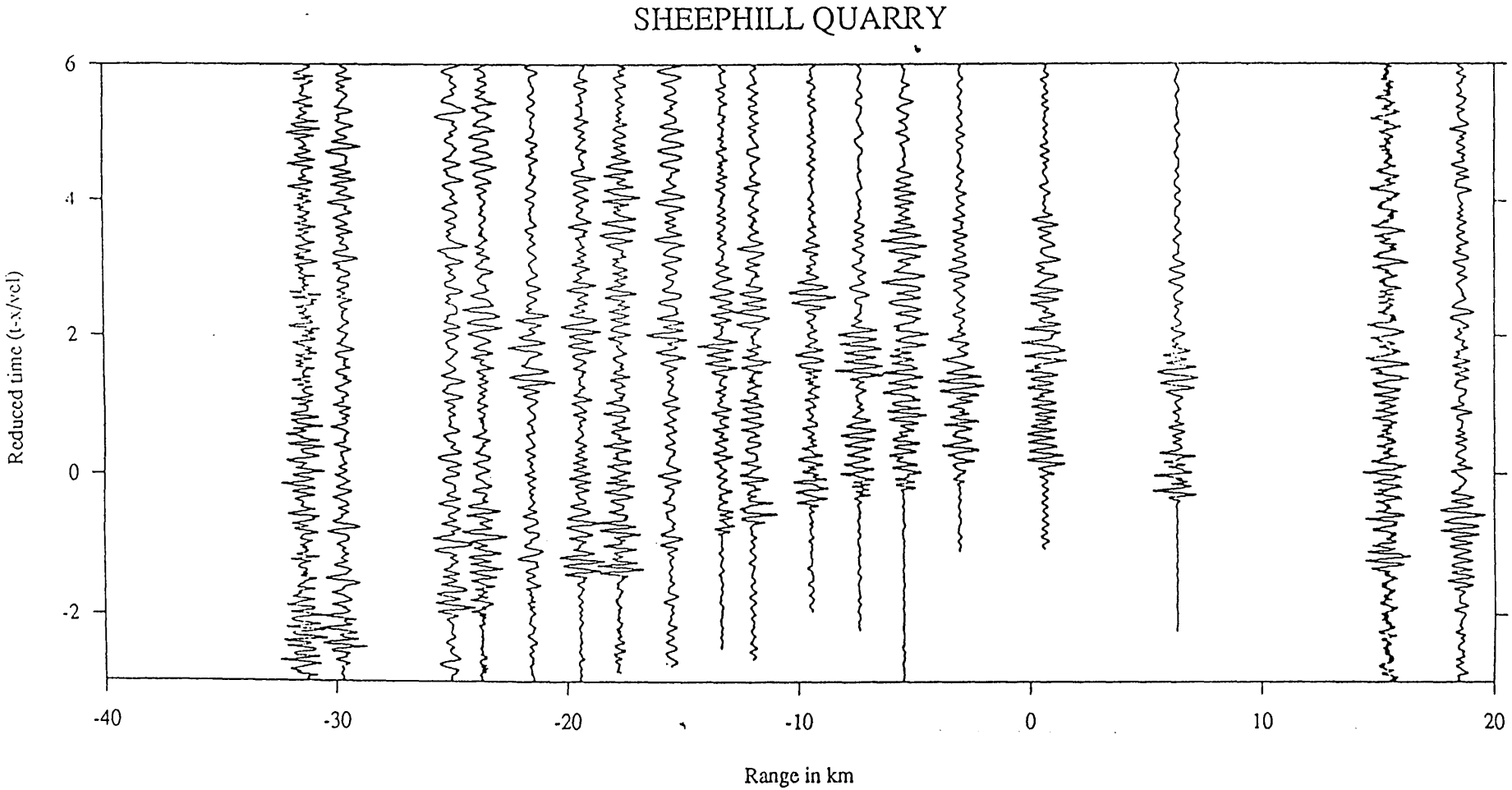

Fig. 3.38 Sheephill (main line) vertical component data filtered with a minimum-phase, low-pass 8.0 Hz filter with a 0.25 s Hamming window. Reduction velocity 3.5 km/s.

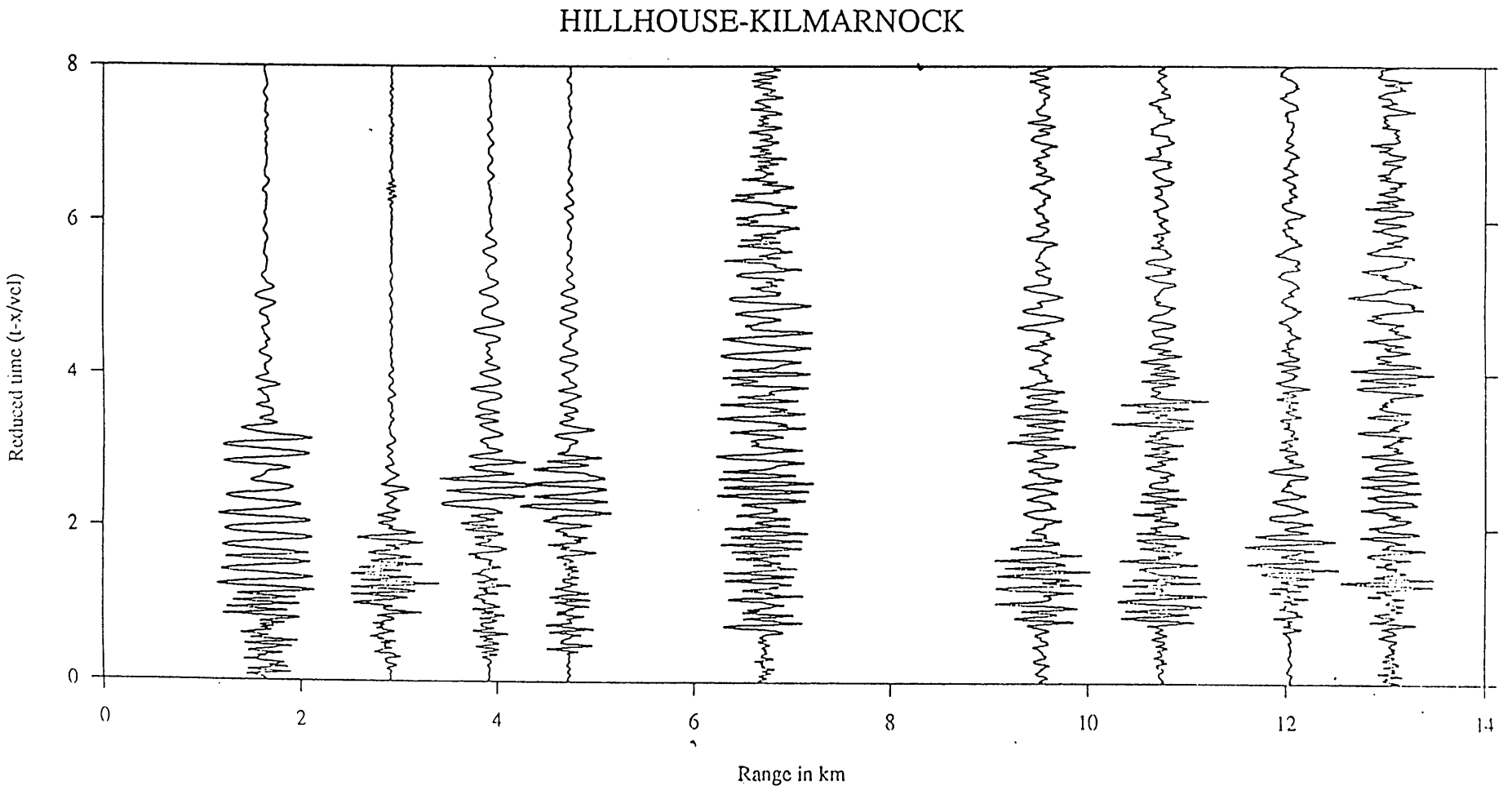

Fig. 3.39 Hillhouse-Kilmarnock line vertical component data filtered with a minimum-phase, low-pass 8.0 Hz filter with a 0.25 s Hamming window. Reduction velocity 6.0 km/s.

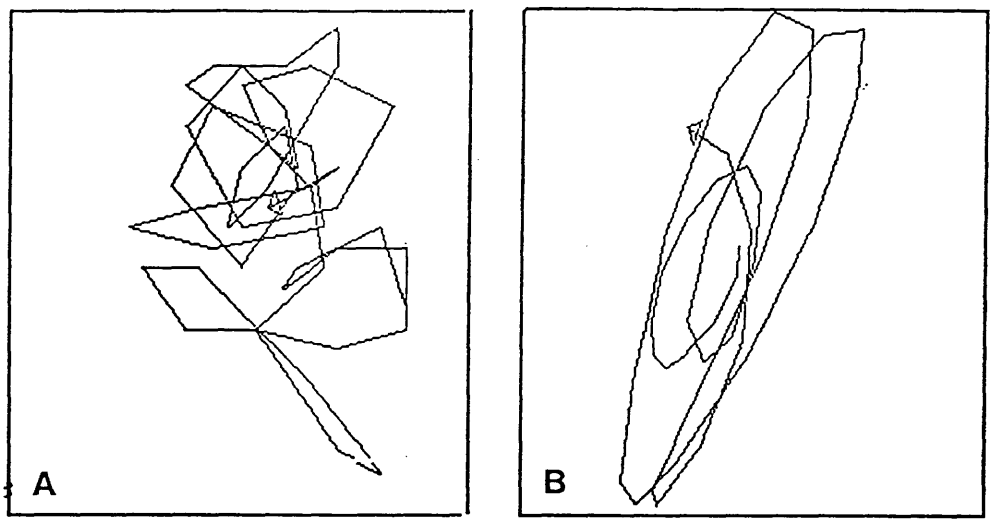

Fig. 3.40 The particle motion of (A) noise and (B) P-wave signal in vertical-radial plane.

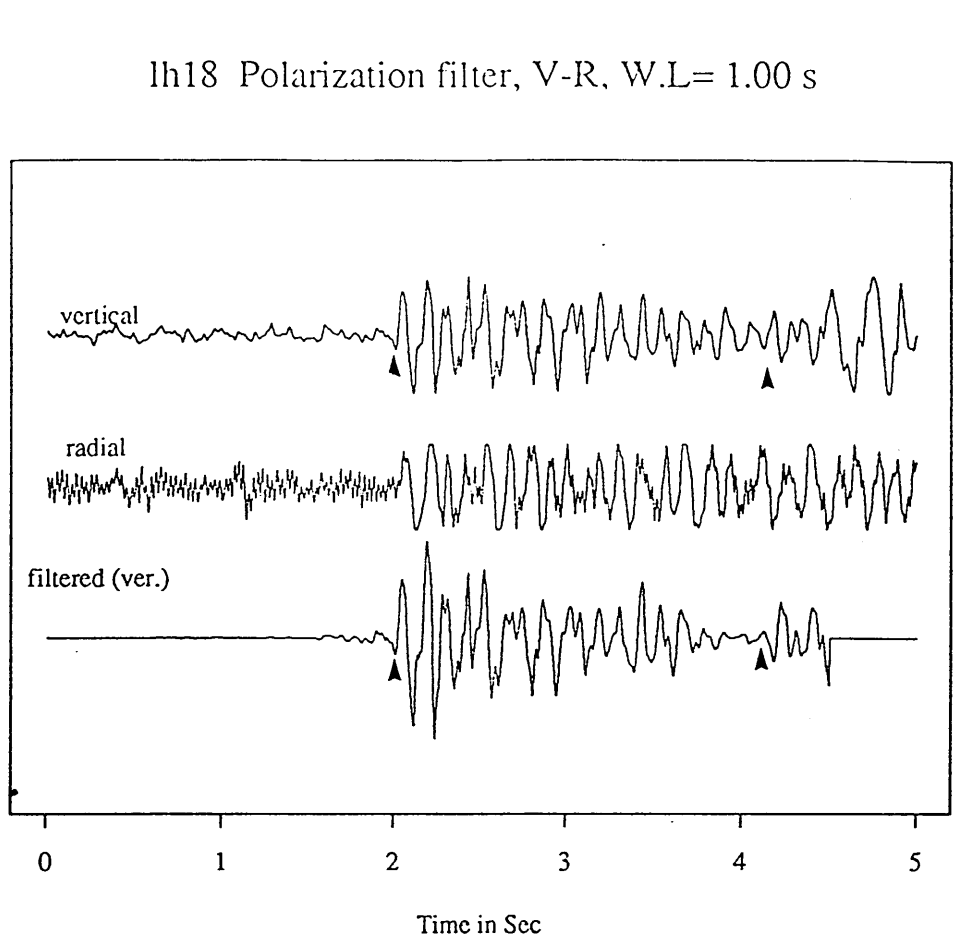

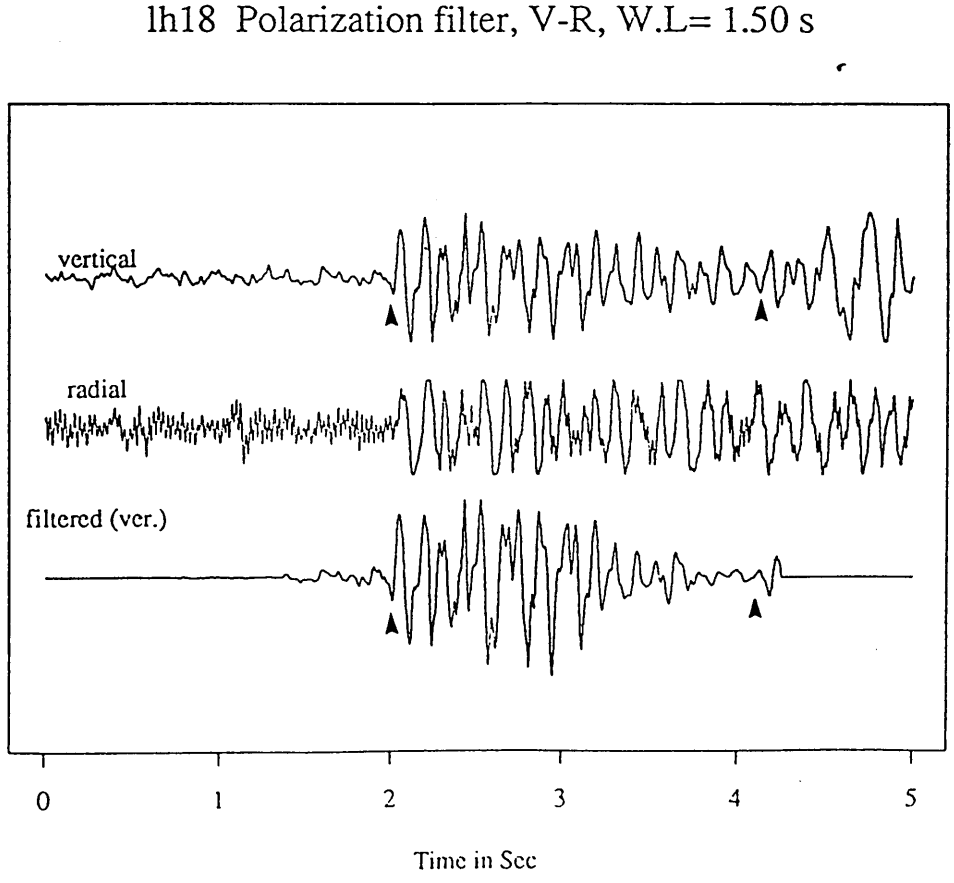

Fig. 3.41 Effect of window length on polarization filter, the arrows show the P & S-wave picking. (continued)

lh18 Polarization filter, V-R, W.L= 0.30 s

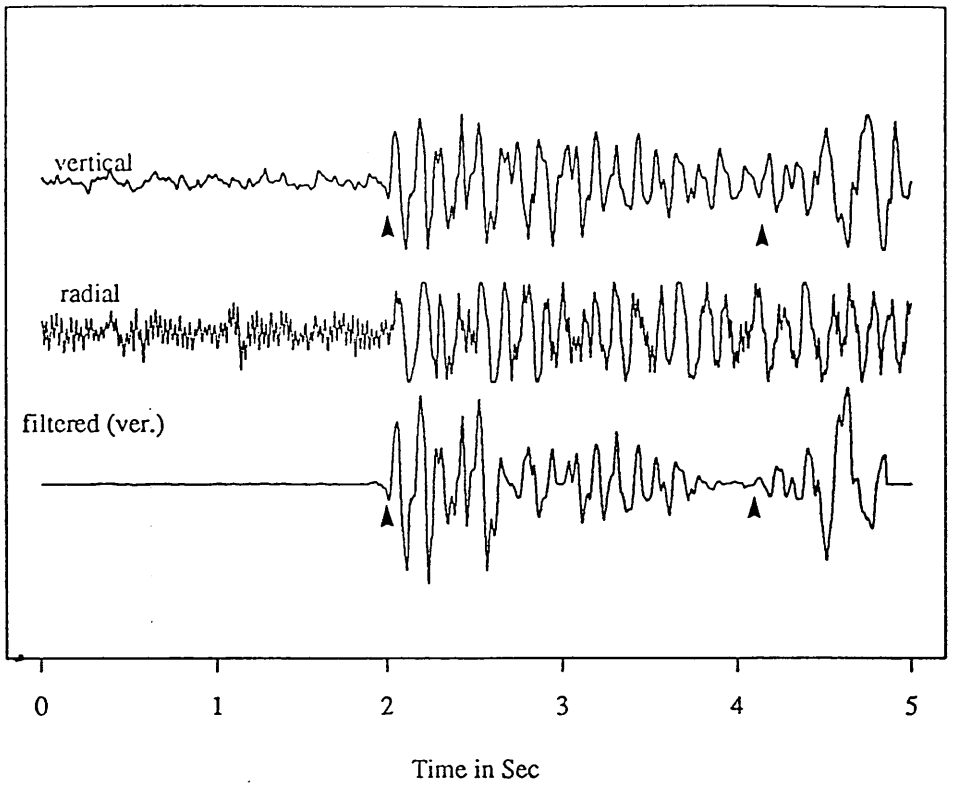

lh18 Polarization filter, V-R, W.L= 0.50 s

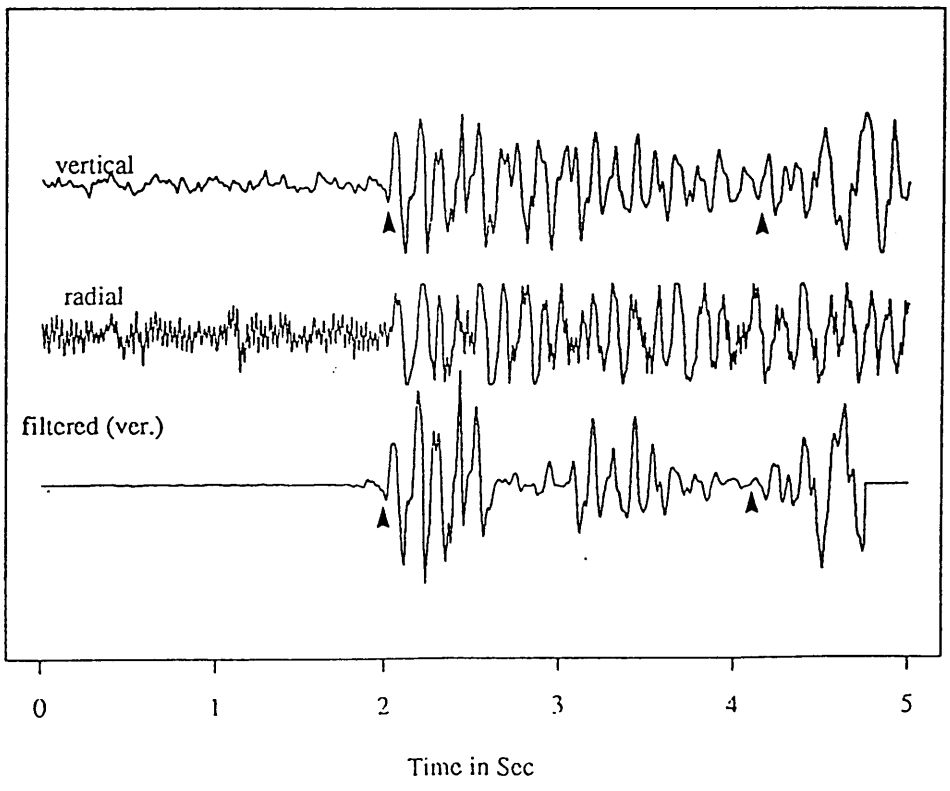

Fig. 3.41 Effect of window length on polarization filter, the arrows show the P & S-wave picking.

(continued)

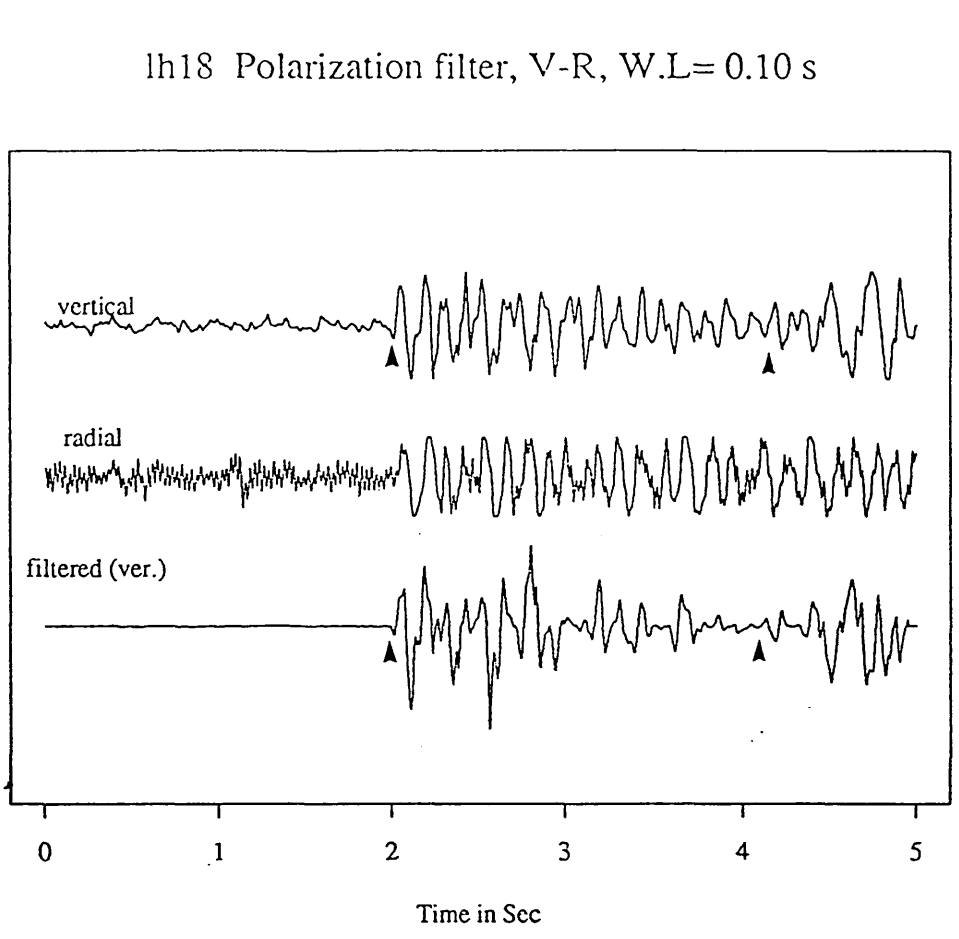

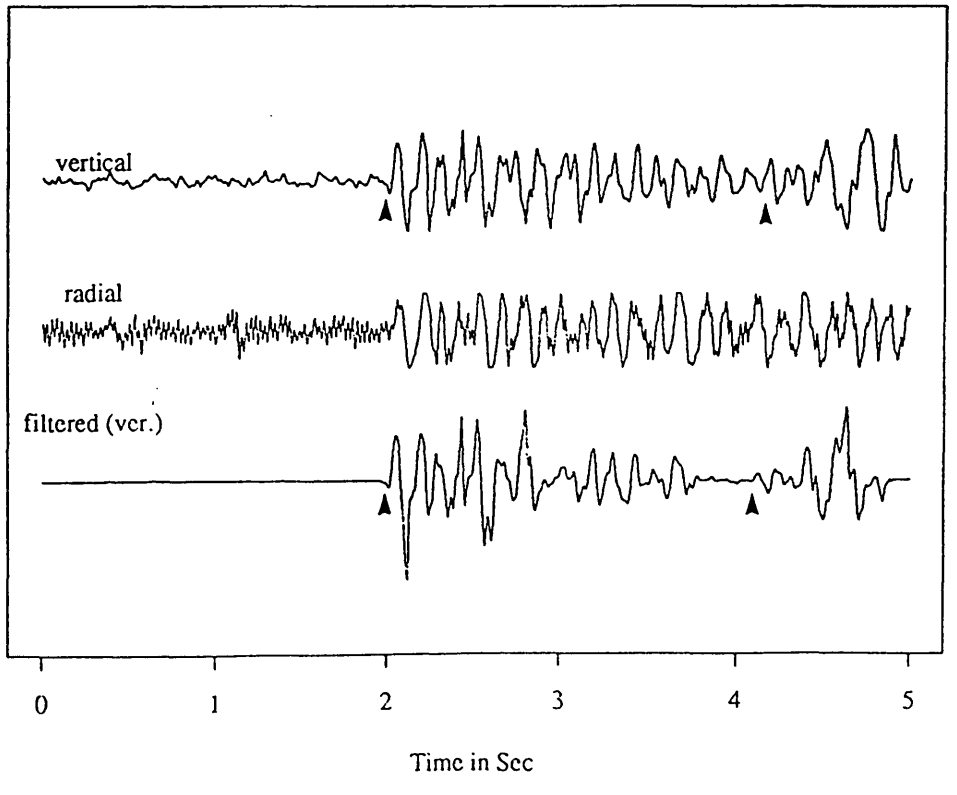

Fig. 3.41 Effect of window length on polarization filter, the arrows show the P & S-wave picking.

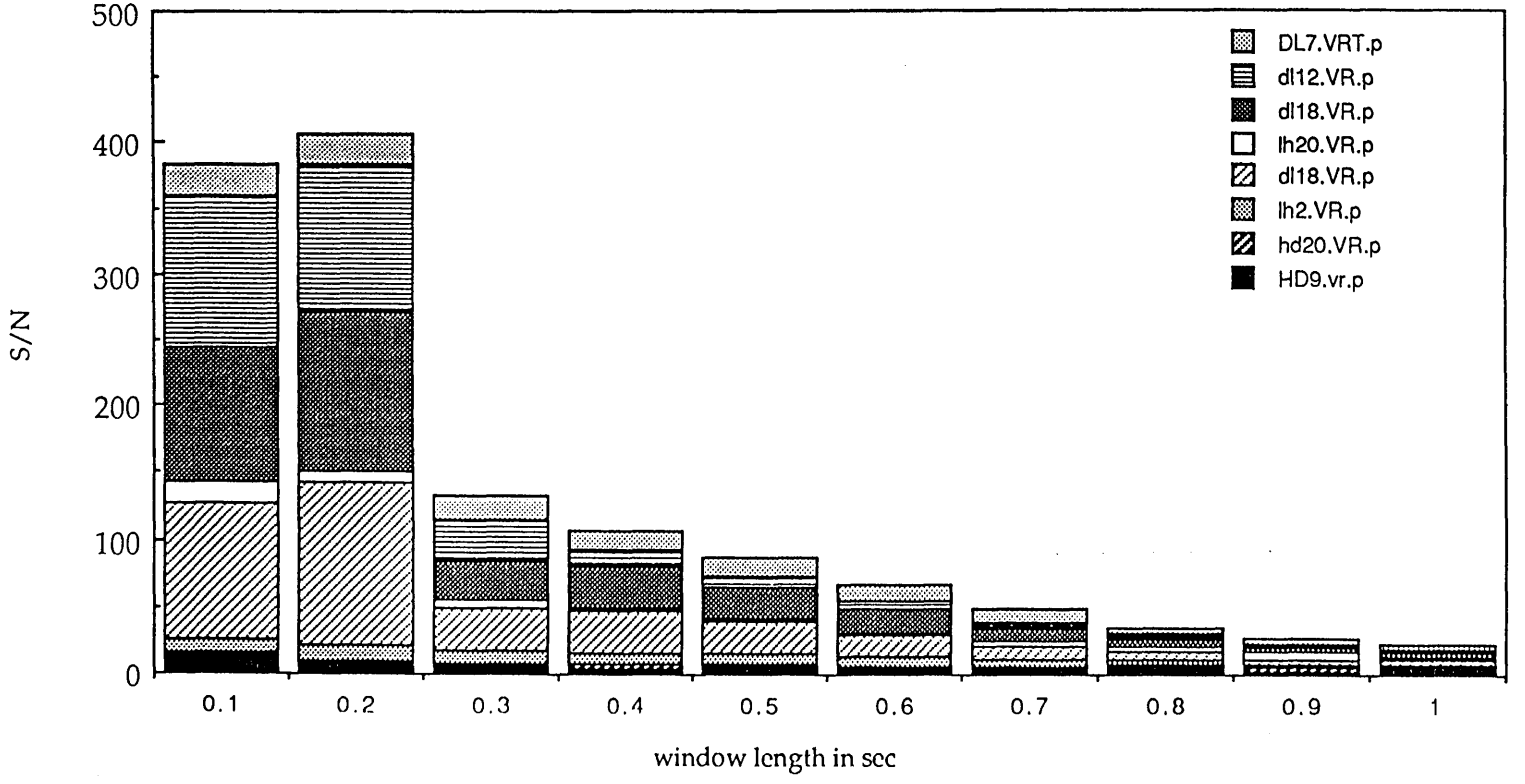

Fig. 3.42 Relation of S/N ratio with window length after applying the polarization filter

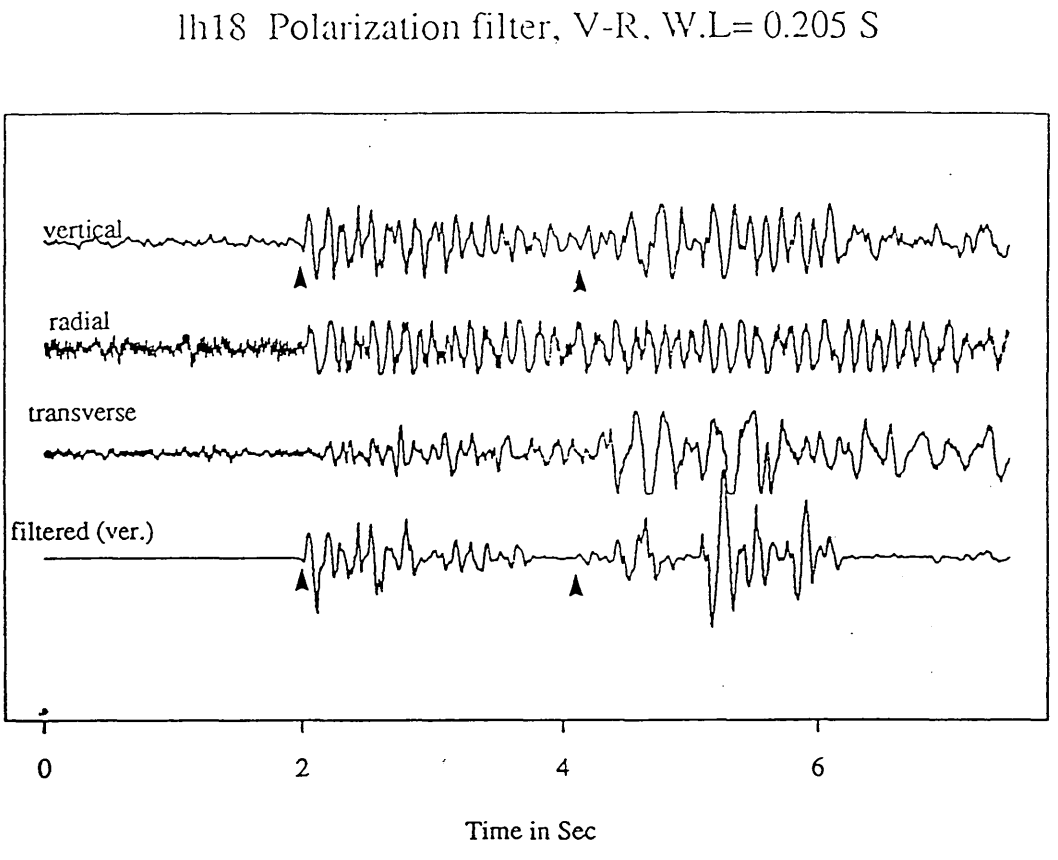

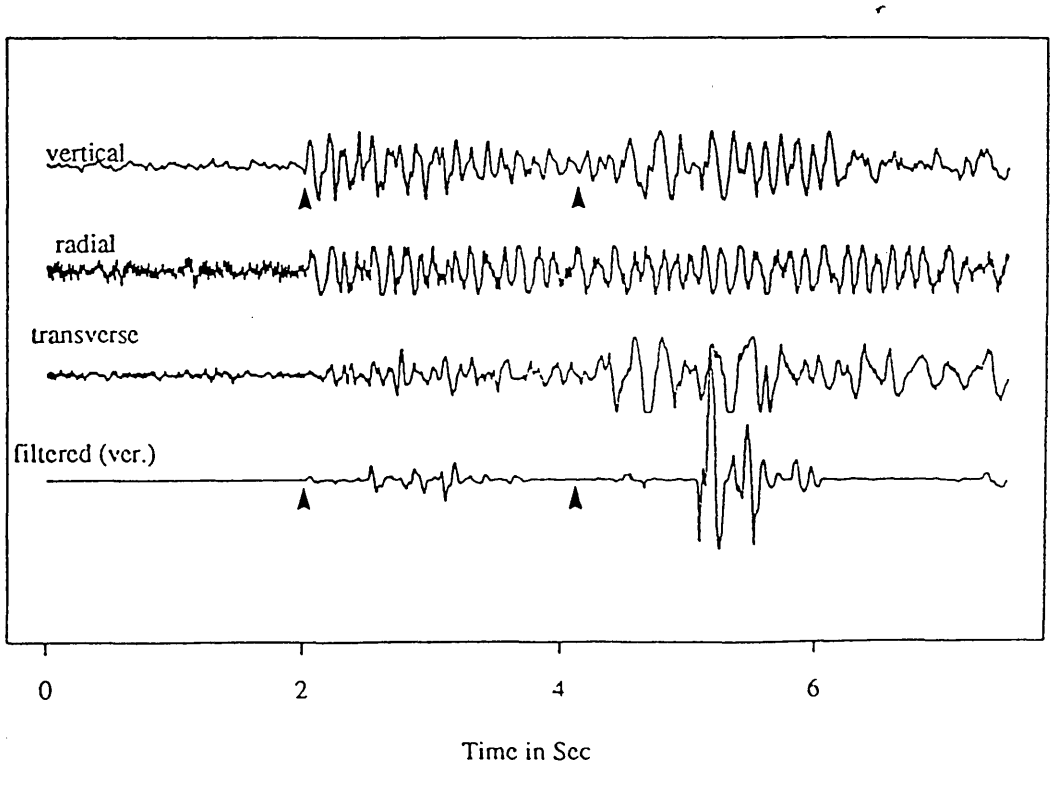

Fig. 3.43 Comparison between using two and three components in polarization filtering, the arrows show the P & S-wave picking.

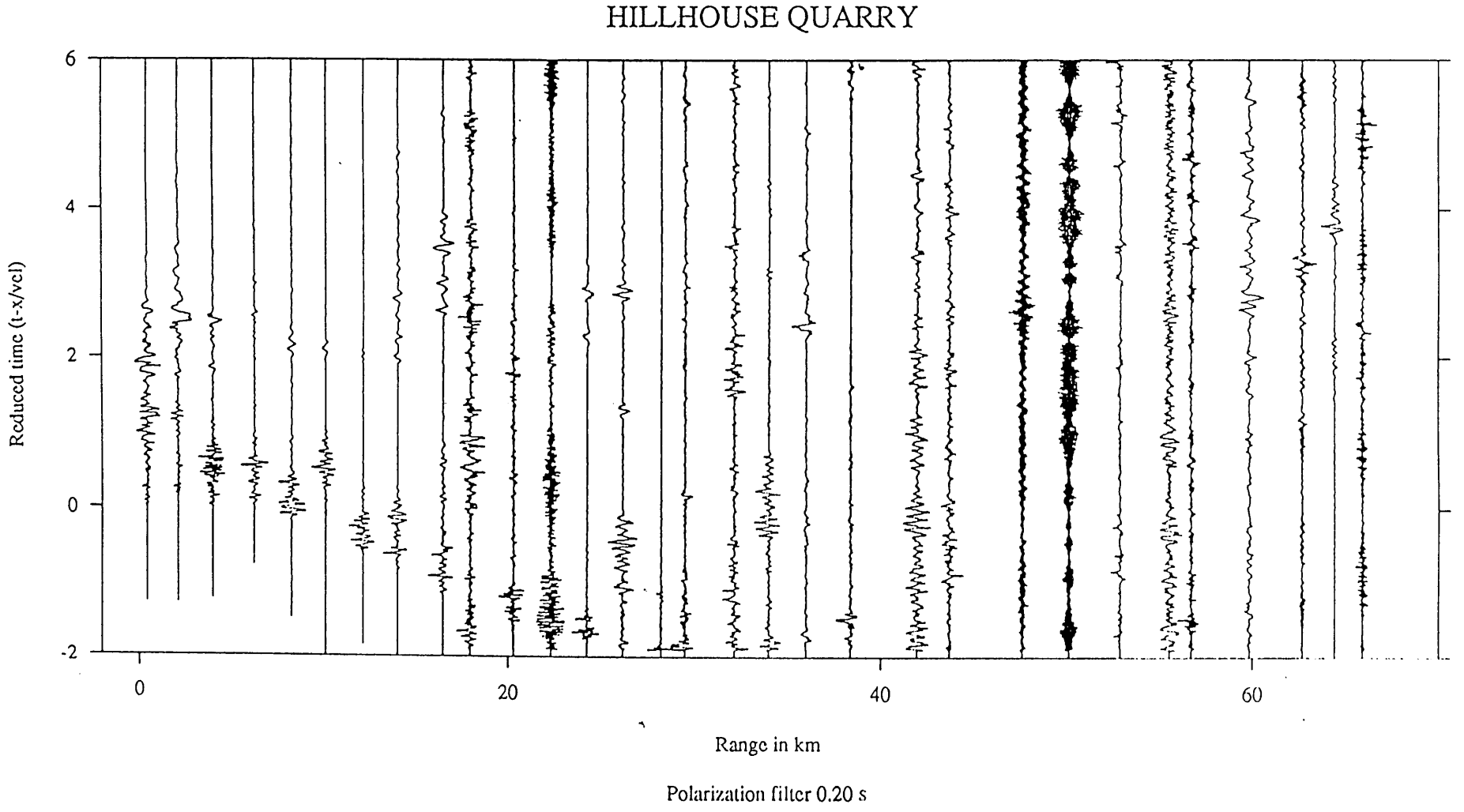

Fig. 3.44 Hillhouse (main line) vertical component data with polarization filtering, reduction velocity 3.5 km/s.

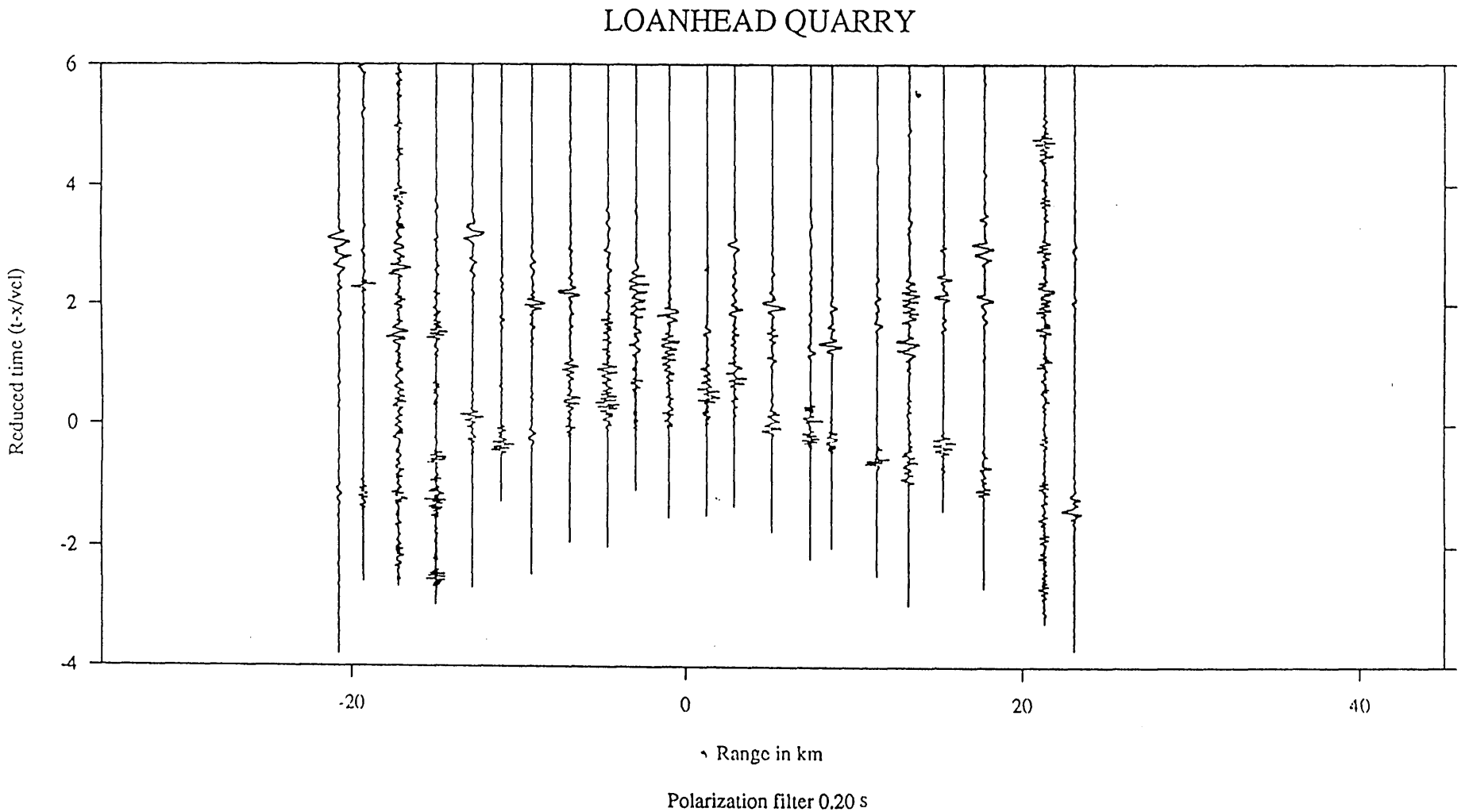

Fig. 3.45 Loanhead vertical component data with polarization filtering, reduction velocity 3.5 km/s.

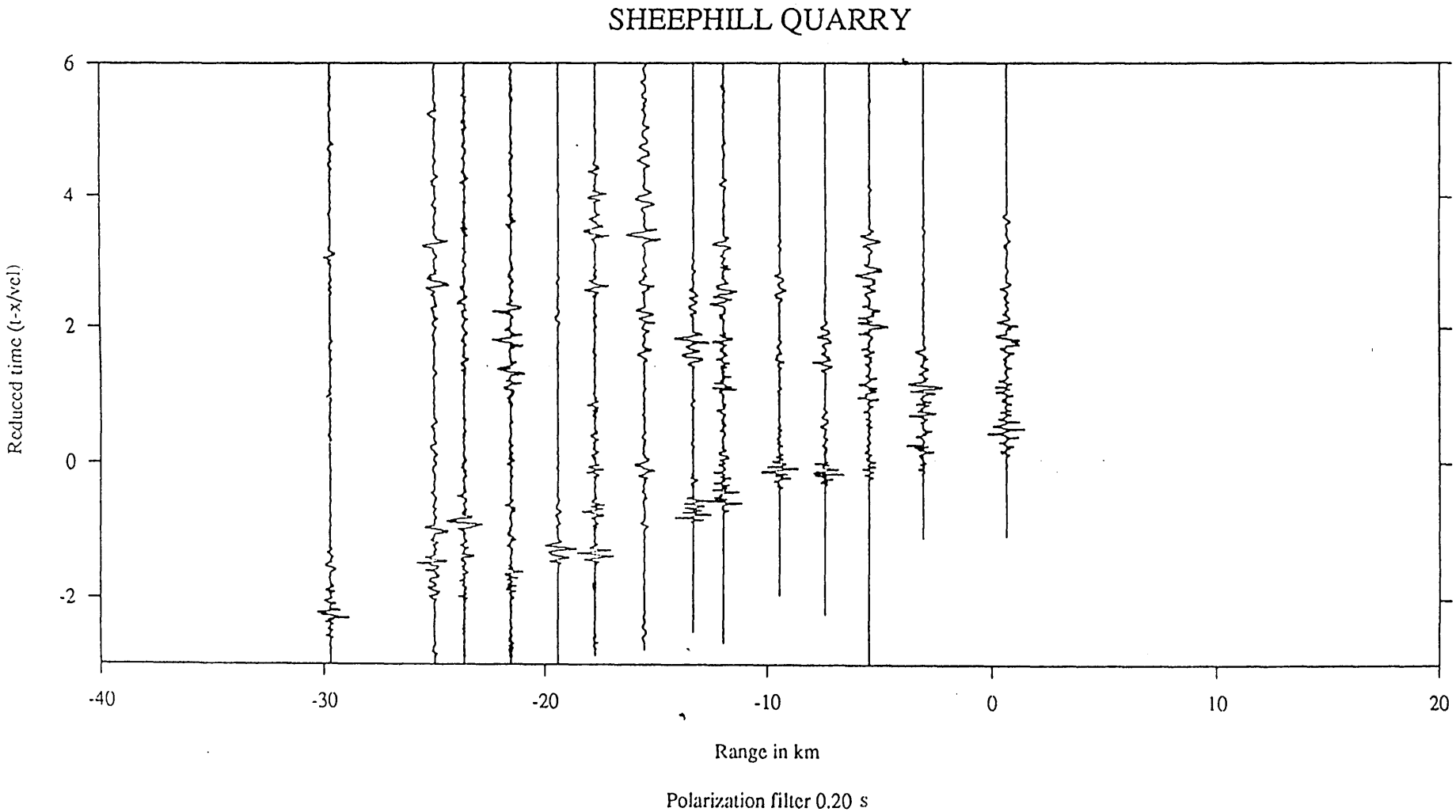

Fig. 3.46 Sheephill vertical component data with polarization filtering, reduction velocity 3.5 km/s.

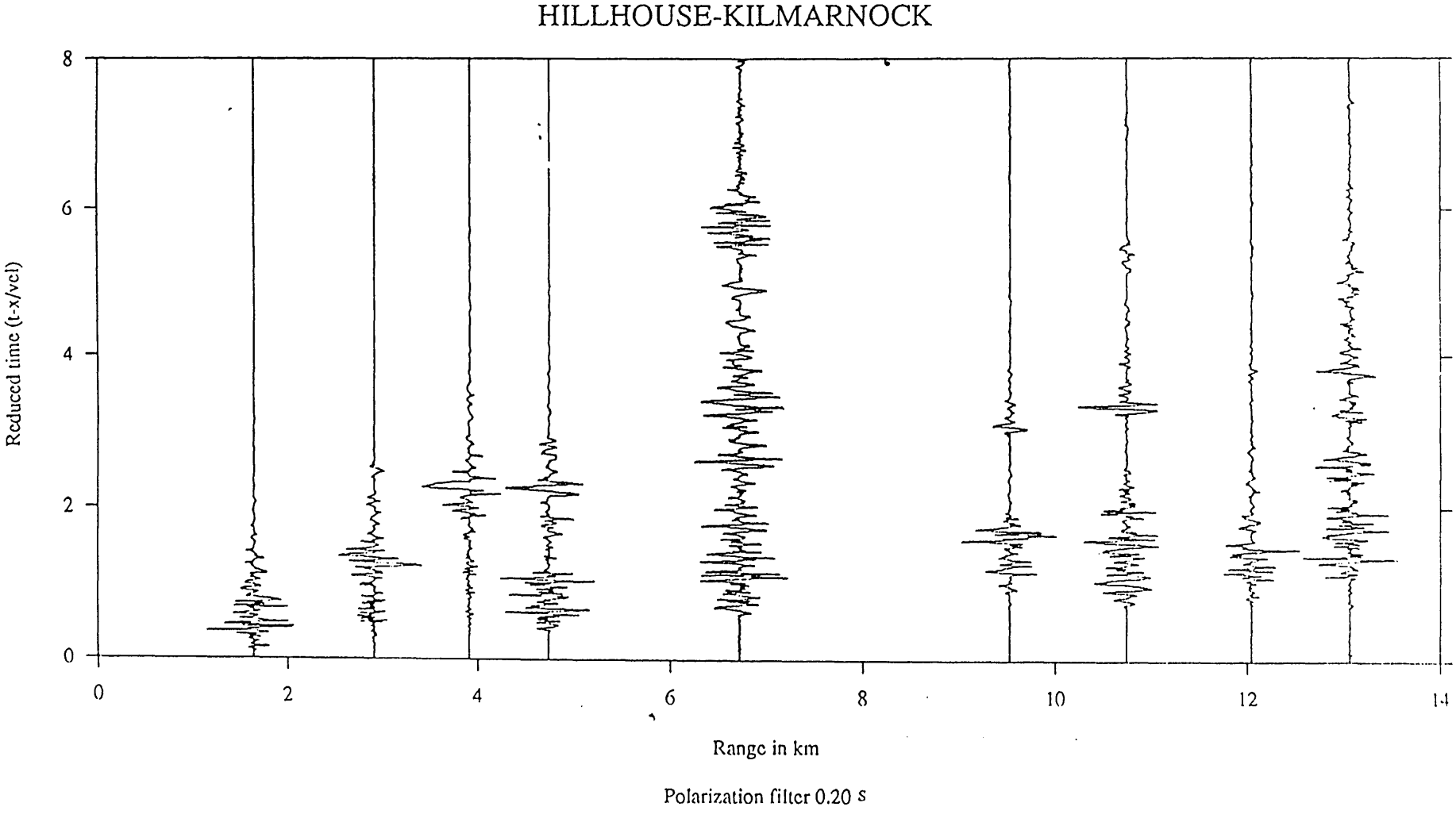

Fig. 3.47 Hillhouse-Kilmarnock line vertical component data with polarization filtering, reduction velocity 6.0 km/s.

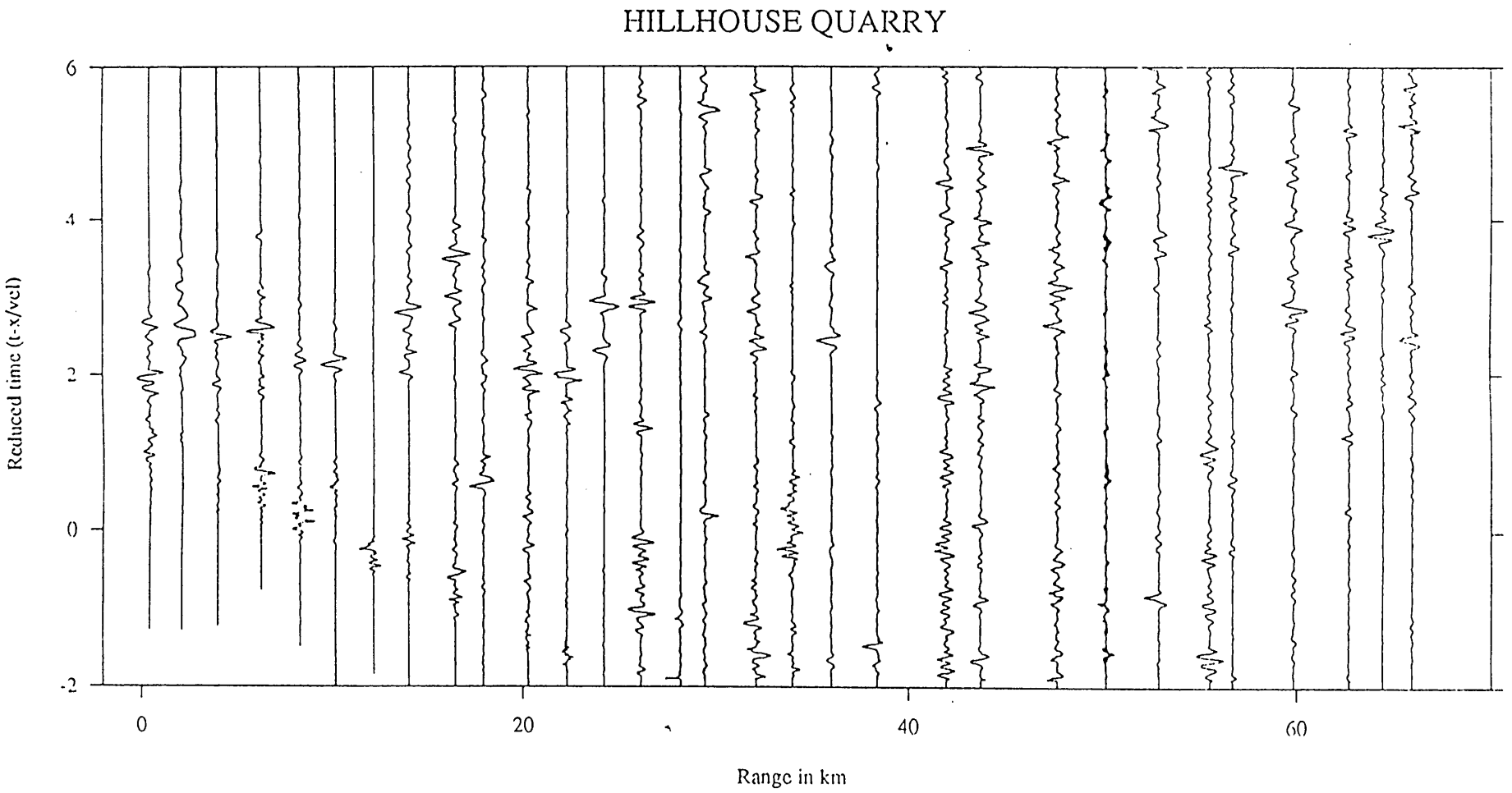

Fig. 3.48 Hillhouse (main line) vertical component data filtered with lowpass and polarization filter, reduction velocity 3.5 km/s. Filter parameters were: minimum-phase, lowpass 8.0 Hz frequency filter with a 0.25 s Hamming window; polarization filter window length 0.20 s.

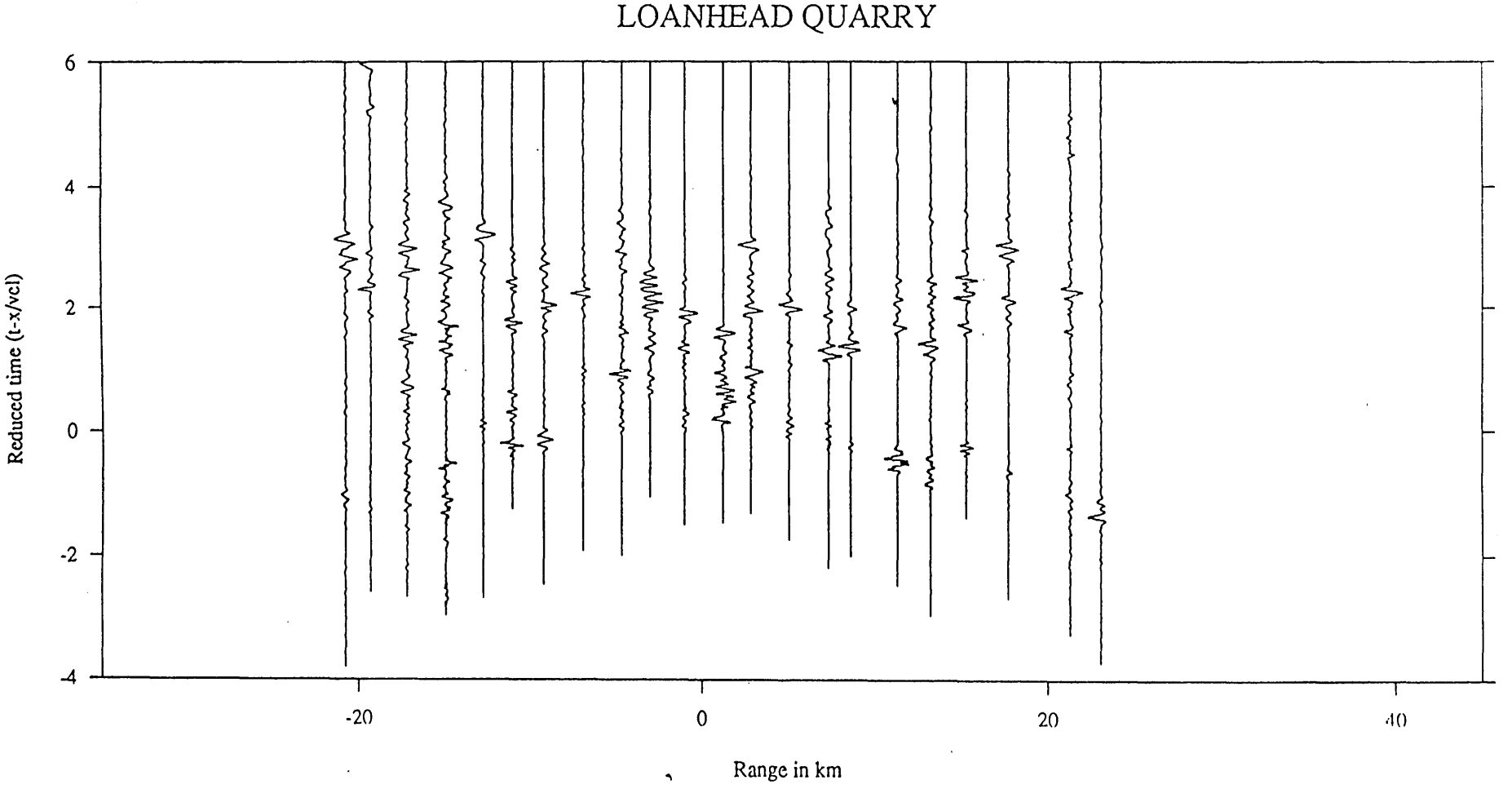

Fig. 3.49 Loanhead vertical componet data filtered with lowpass and polarization filter, reduction velocity 3.5 km/s. Filter parameters were: minimum-phase, lowpass 8.0 Hz frequency filter with a 0.25 s Hamming window; polarization filter window length 0.20 s.

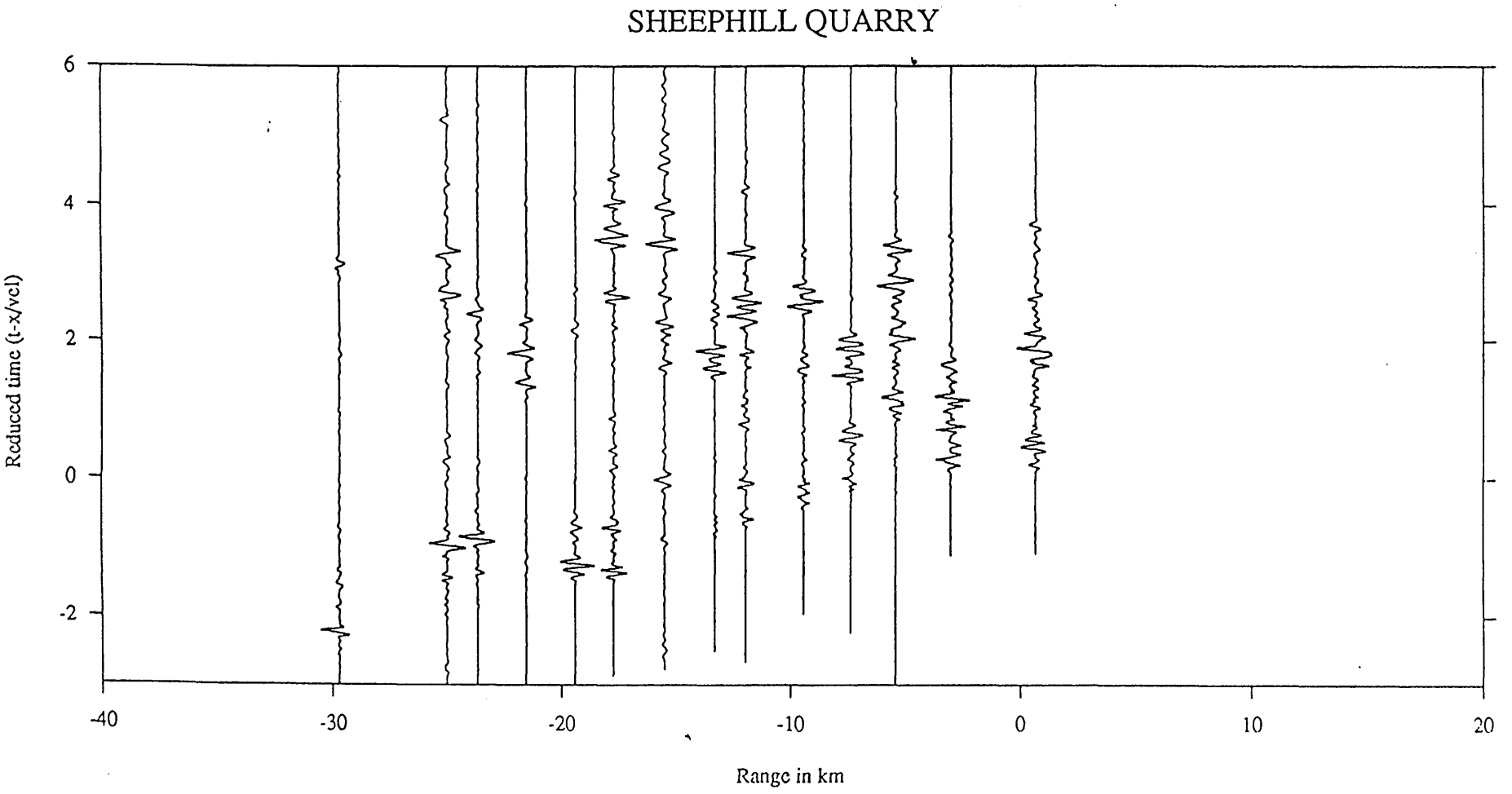

Fig. 3.50 Sheephill vertical component data filtered with lowpass and polarization filter, reduction velocity 3.5 km/s. Filter parameters were: minimum-phase, lowpass 8.0 Hz frequency filter with a 0.25 s Hamming window; polarization filter window length 0.20 s.

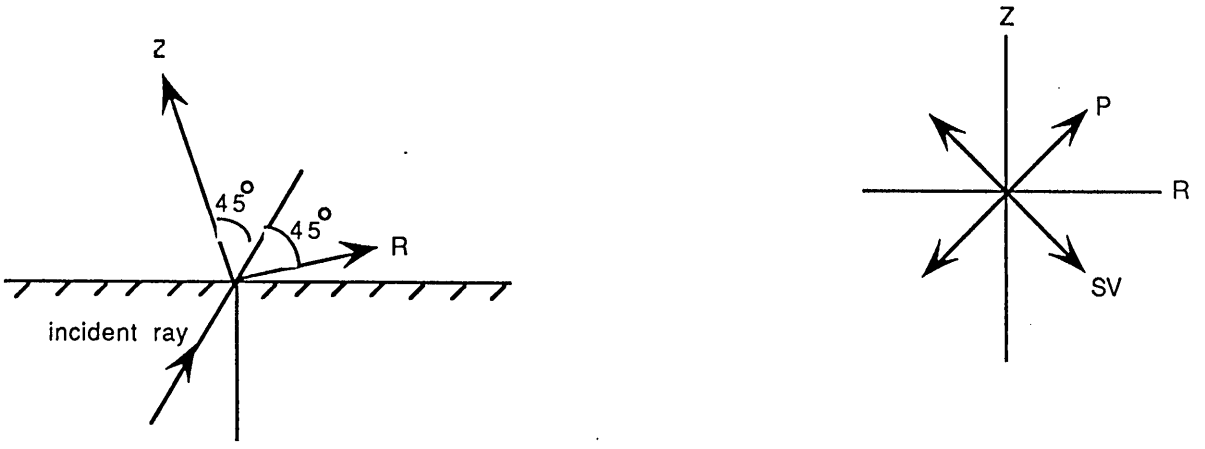

Fig 3.51 Rotation required to get Z' &R' components. The particle motion are of "incident" to be under "Rotation" P & SV waves

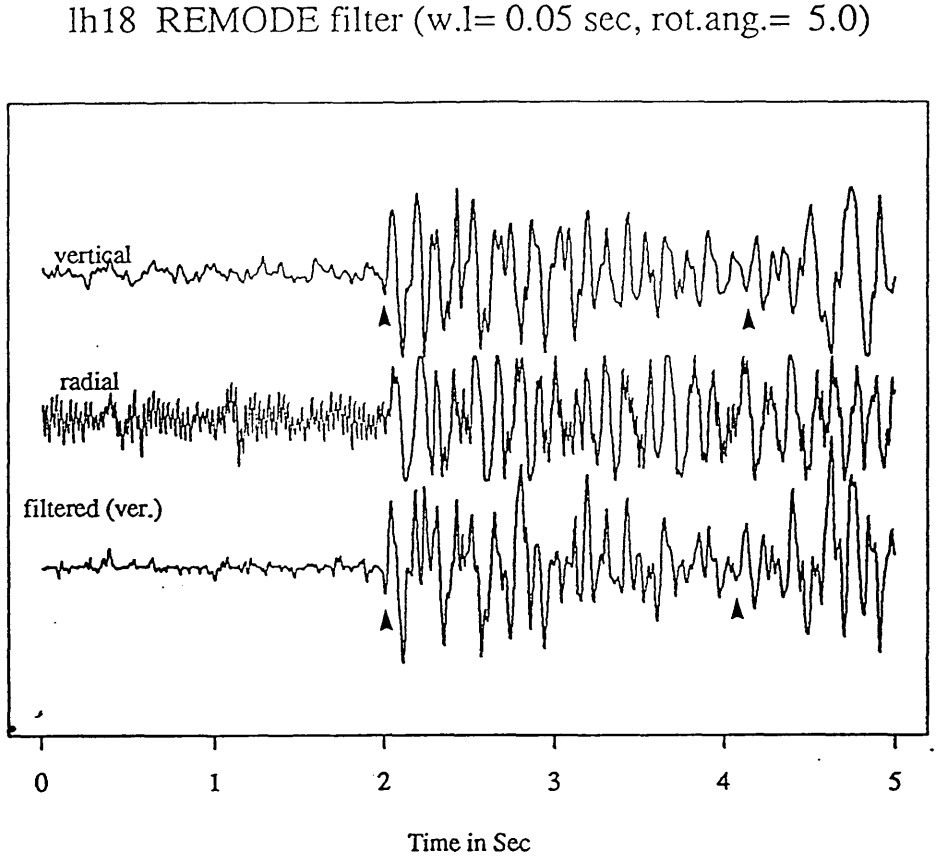

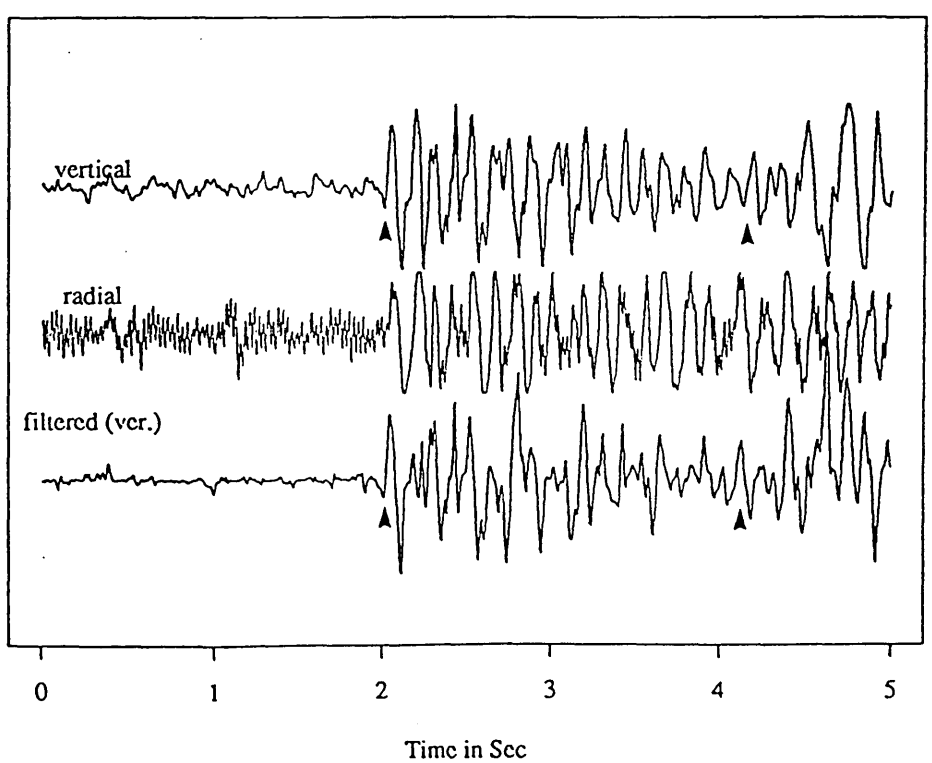

Fig. 3.52 Effect of window length on REMODE filter, the arrows show the P & S-wave picking.

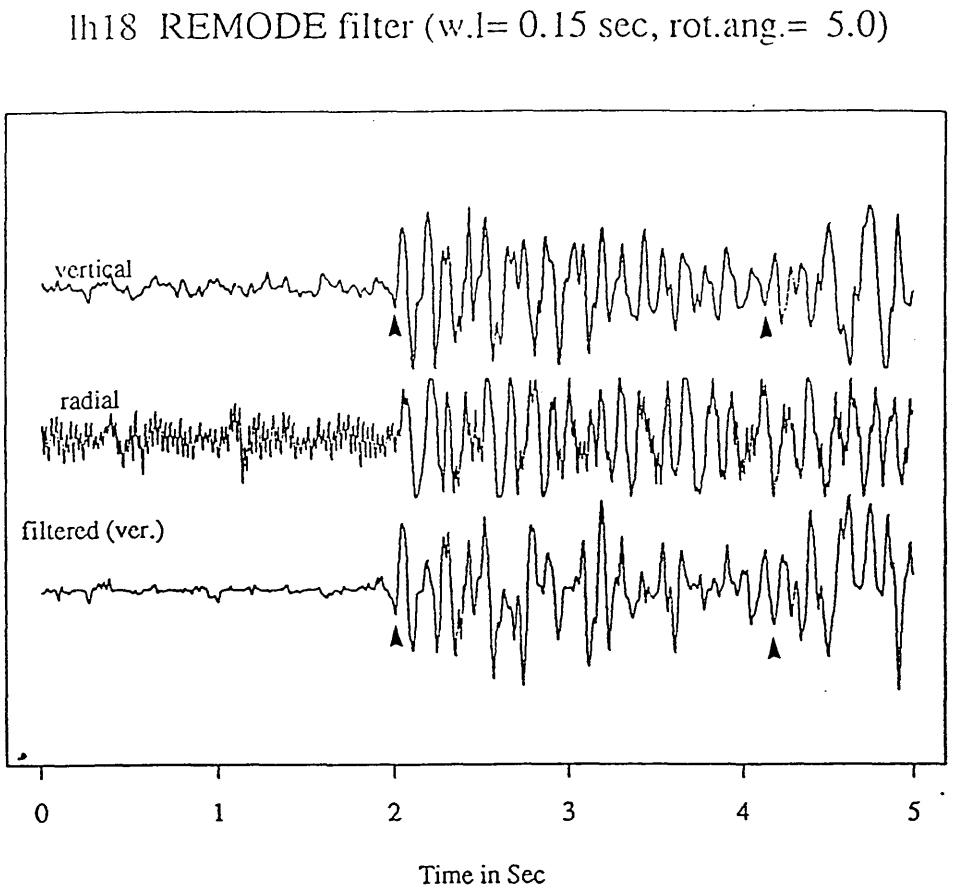

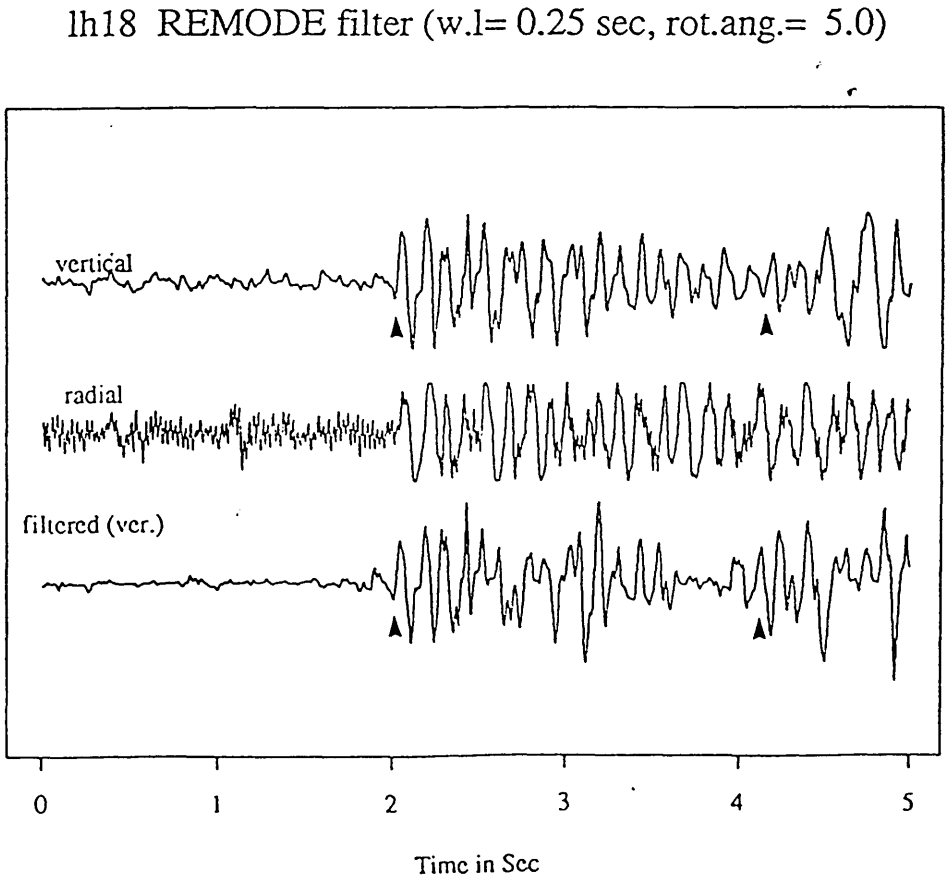

Fig. 3.52 Effect of window length on REMODE filter, the arrows show the P & S-wave picking.

(continued)

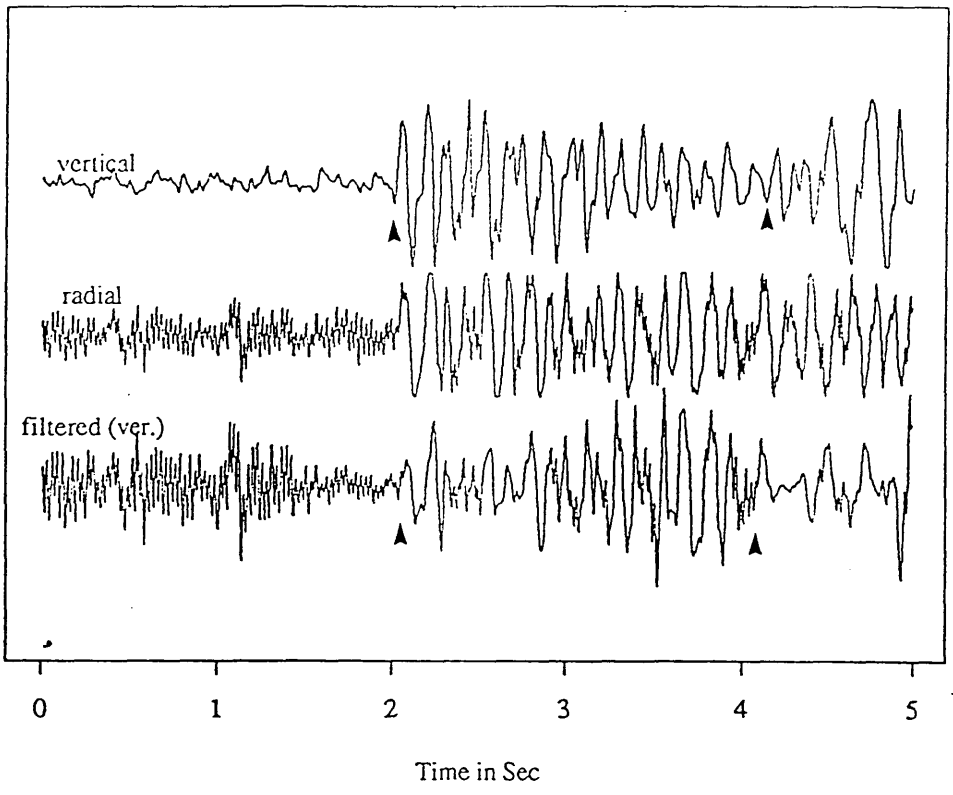

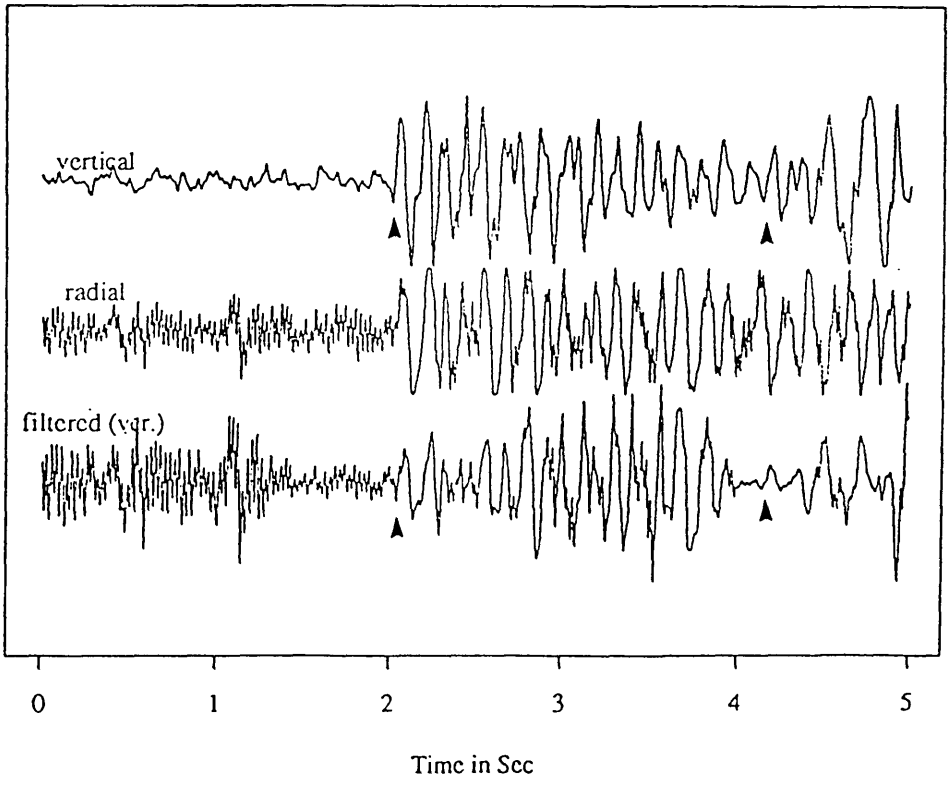

Fig. 3.52 Effect of window length on REMODE filter, the arrows show the P & S-wave picking.

(continued)

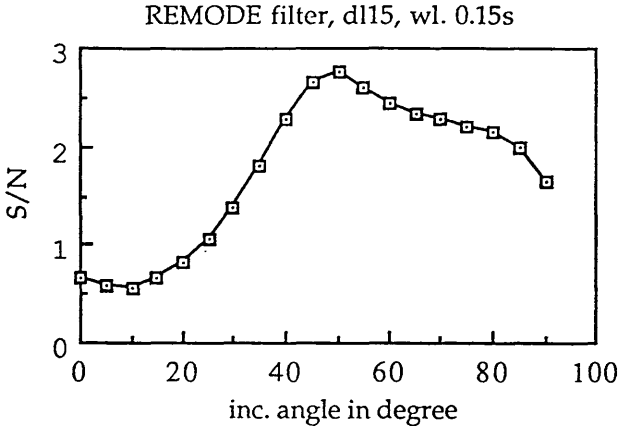

Fig. 3.53 Effect of the REMODE filter rotation angles on the S/N ratio

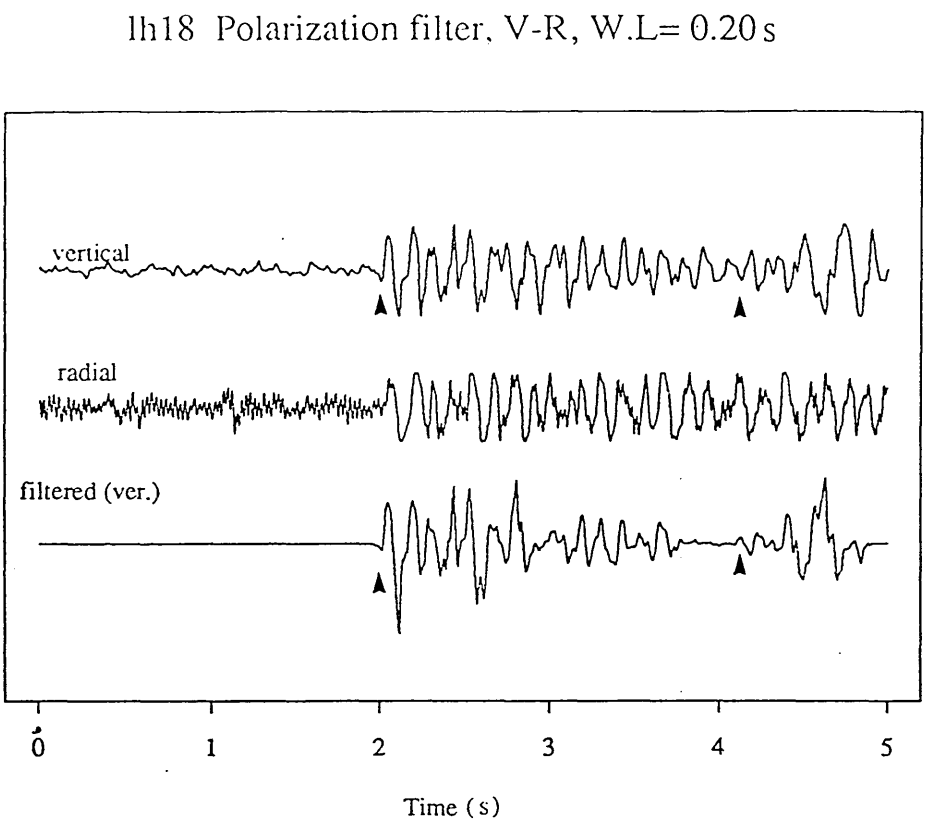

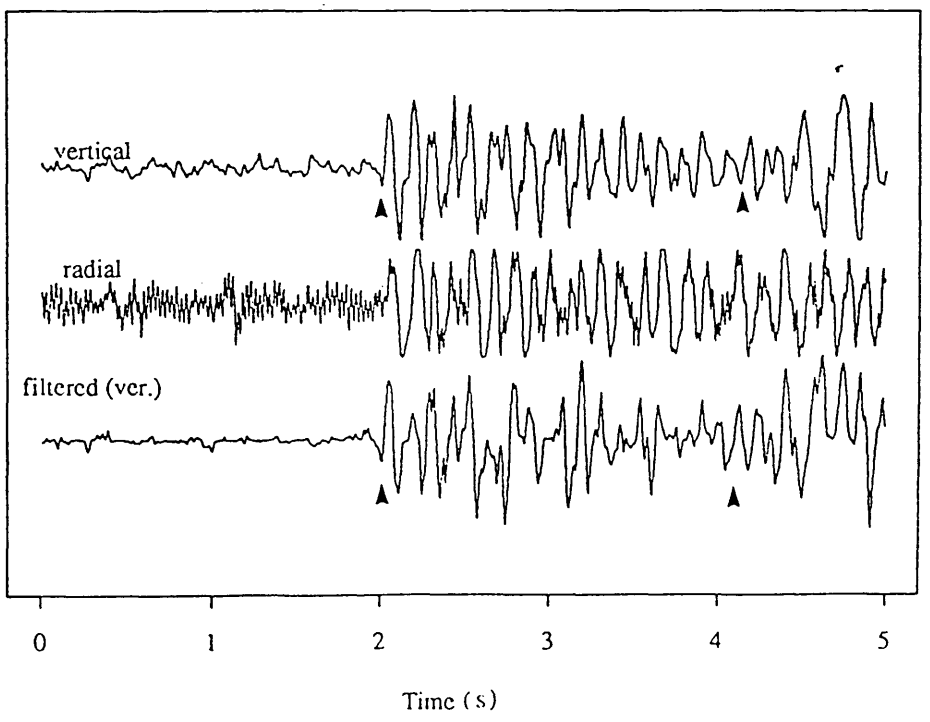

Fig. 3.54 Comparison of polarization and REMODE filtering.

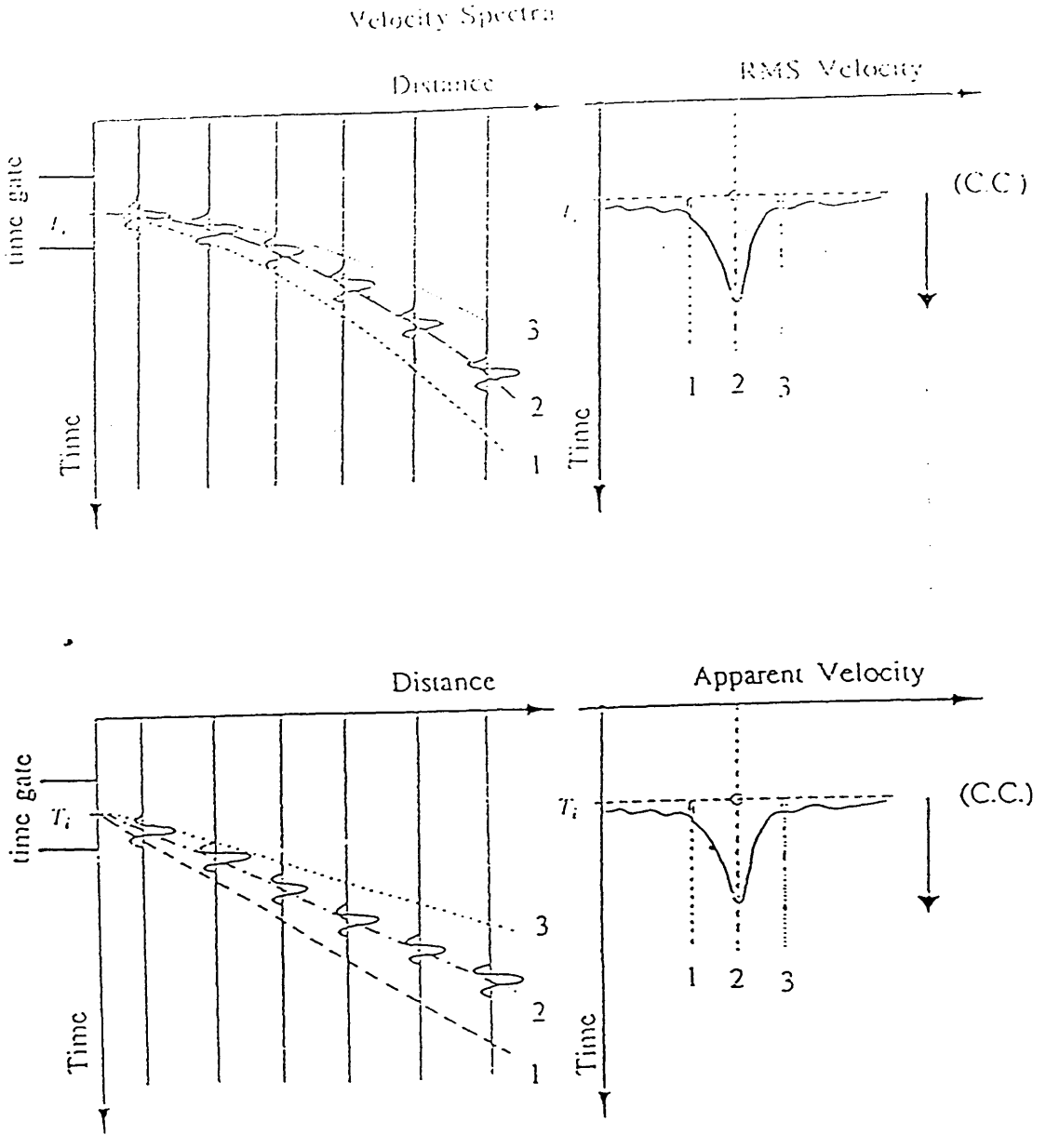

Fig. 3.55 Schematic velocity spectra for A) reflection data and B) refraction data (after Taner & Koehler and Said 1990).

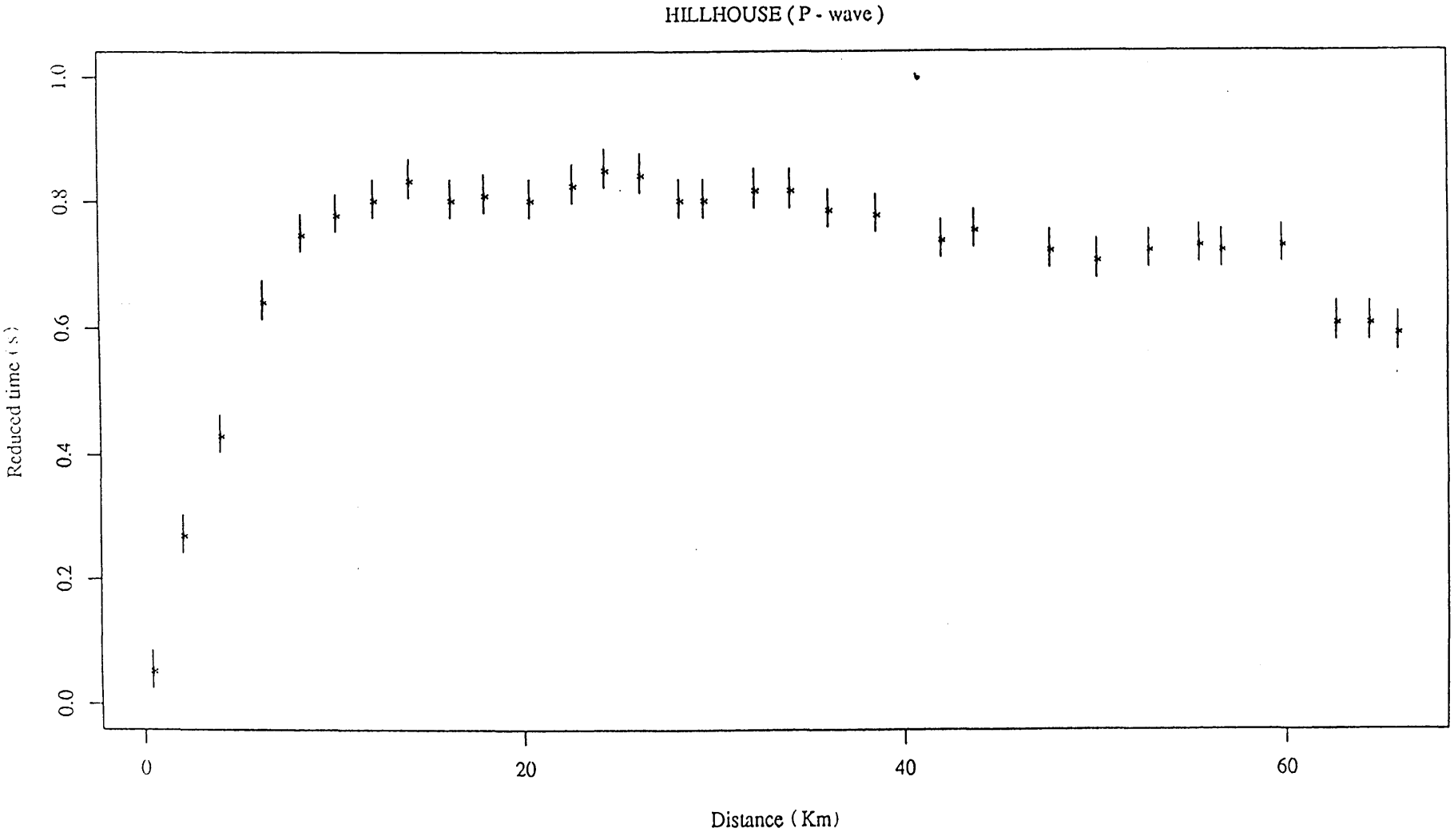

Fig. 3.56 P-wave time-distance data; Hillhouse (main line) with reduction velocity 6.0 km/s.

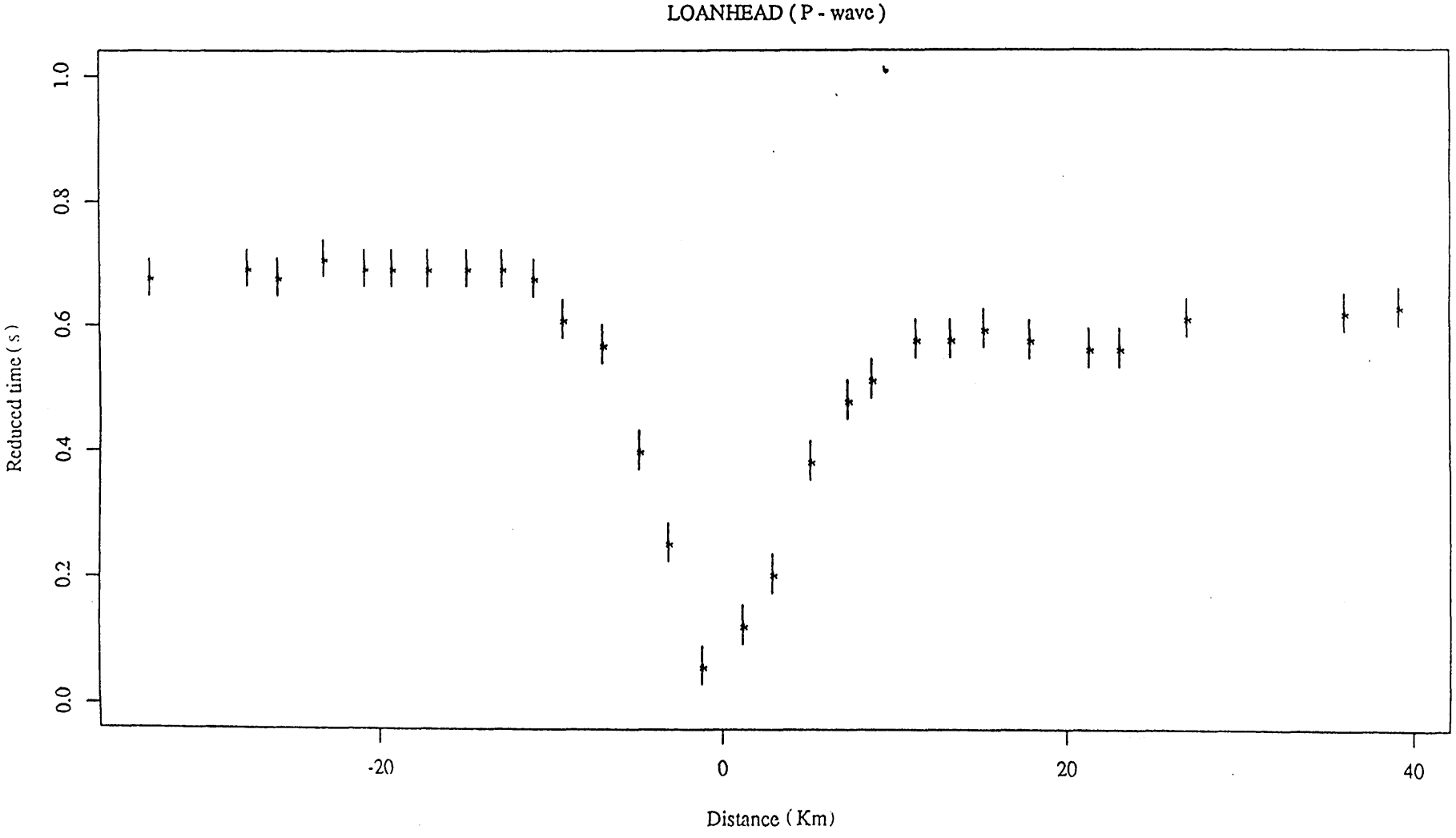

Fig. 3.57 P-wave time-distance data; Loanhead with reduction velocity 6.0 km/s.

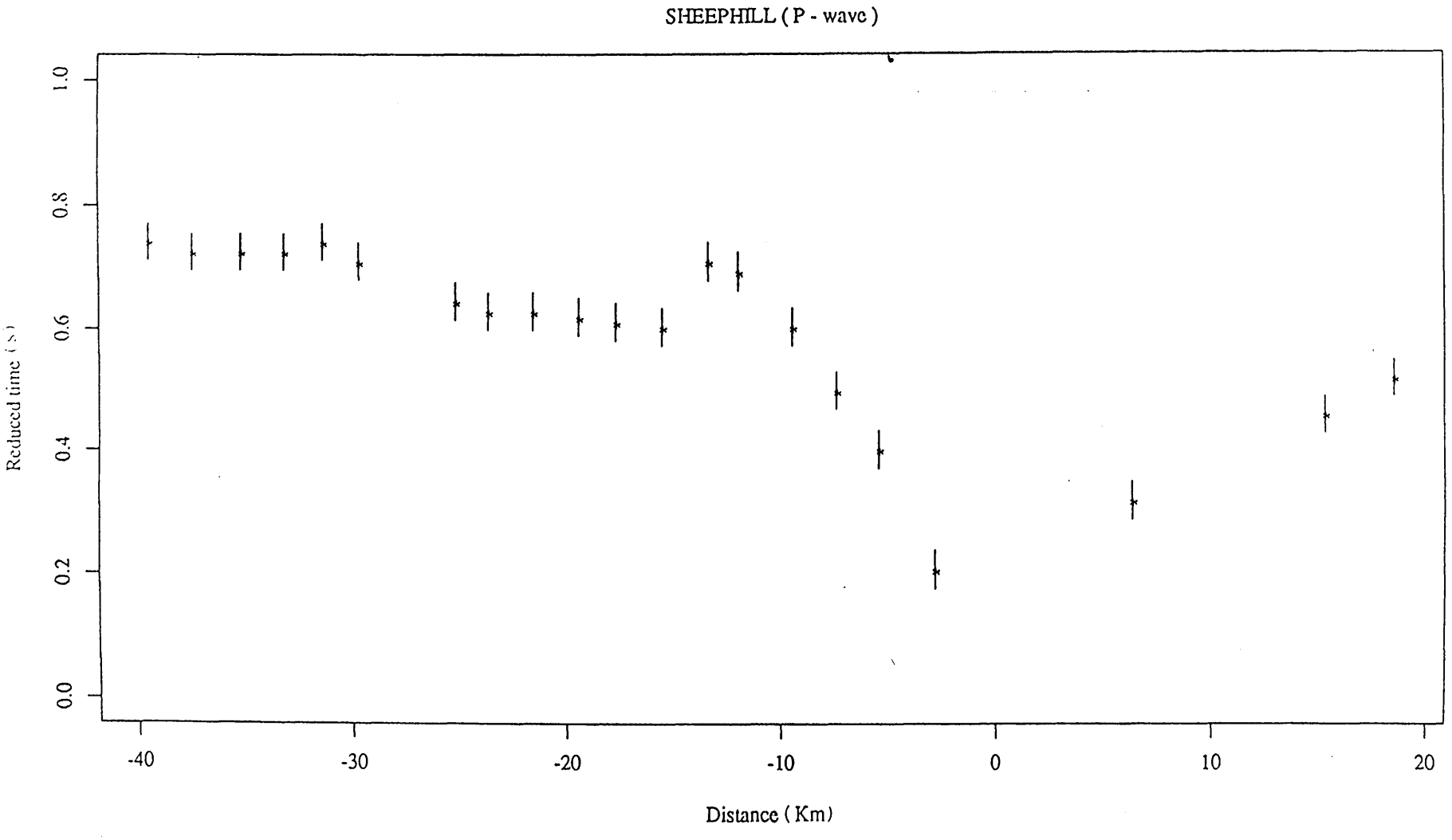

Fig. 3.58 P-wave time-distance data; Sheephill with reduction velocity 6.0 km/s.

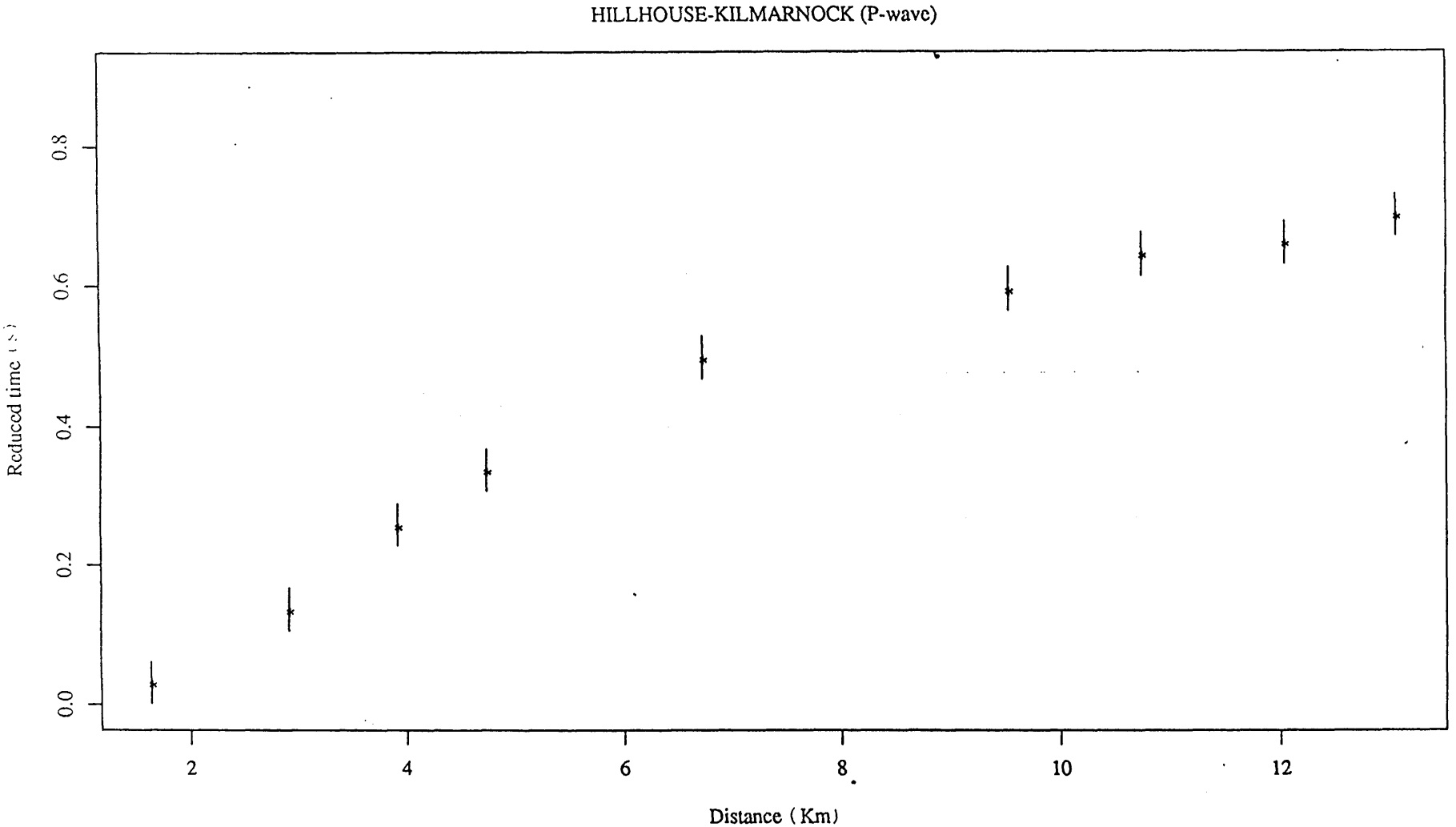

Fig. 3.59 P-wave time-distance data; Hillhouse-Kilmarnock line with reduction velocity 6.0 km/s.

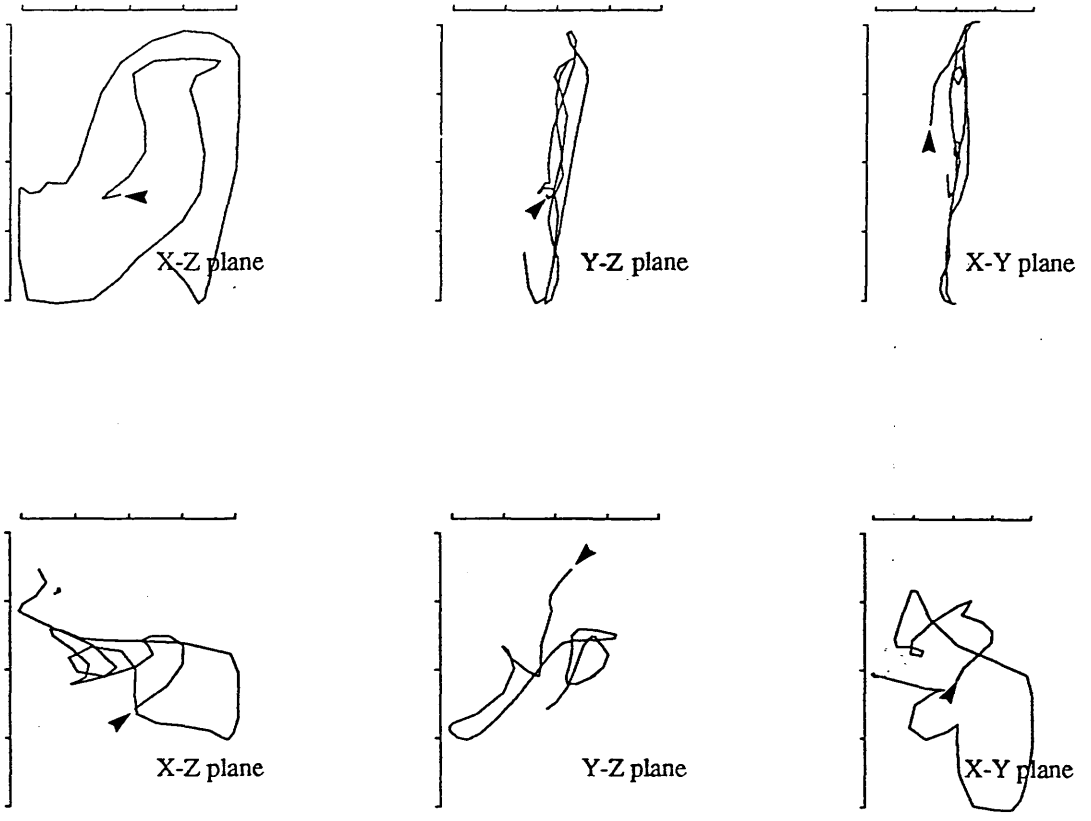

LOANHEAD QUARRY lh18.

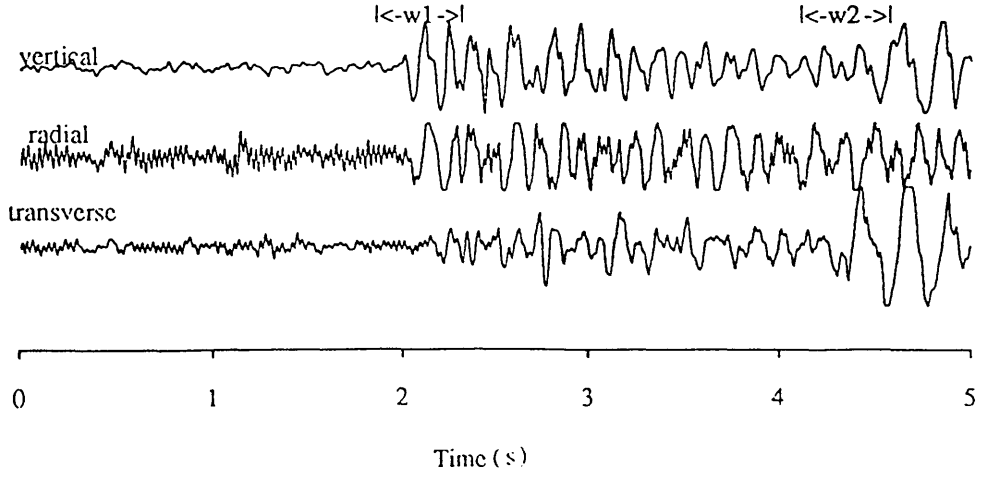

Fig. 3.60 P & S particle motions for recording at station lh18 from Loanhead.

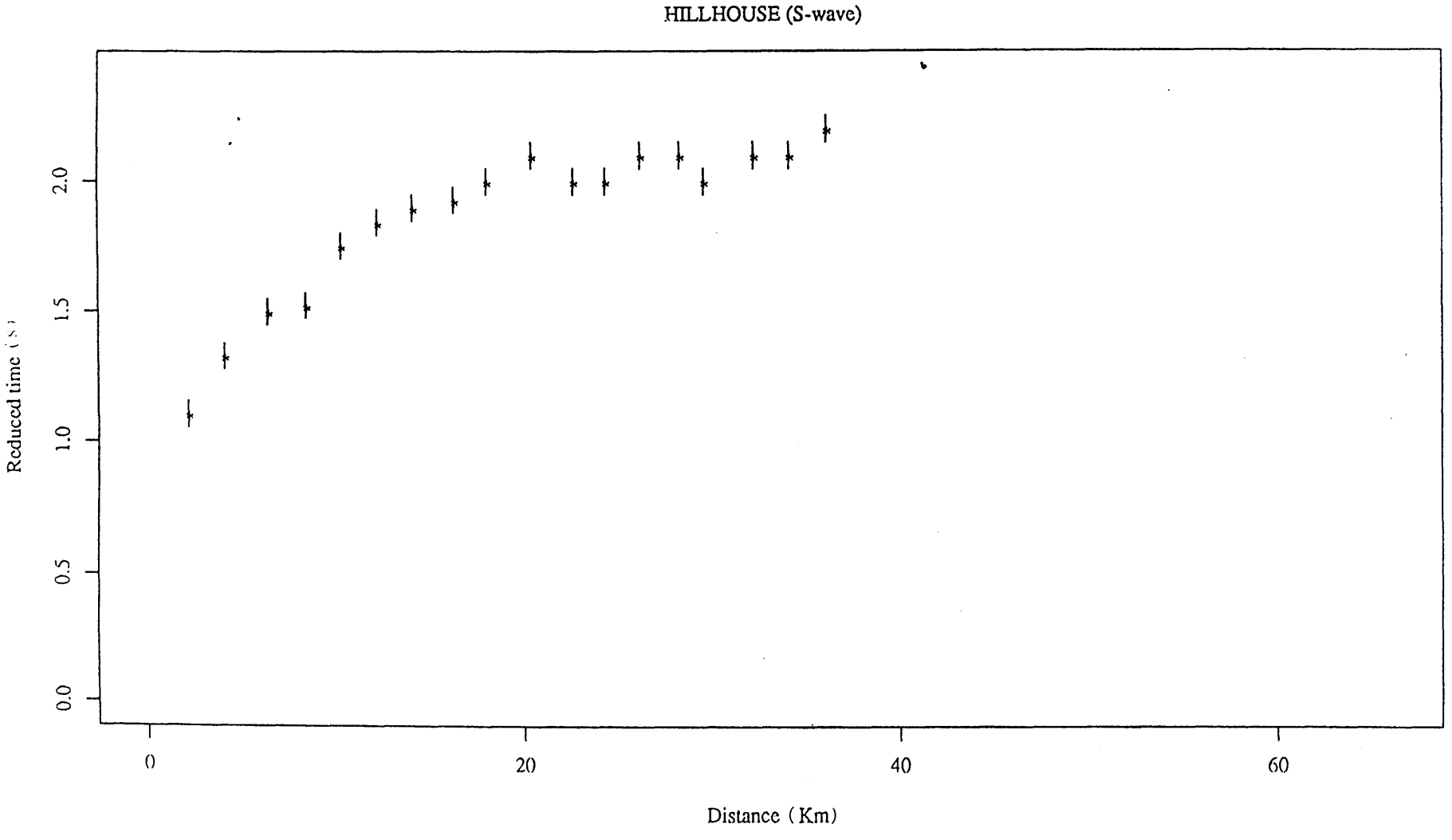

Fig. 3.61 S-wave time-distance data ; Hillhouse with reduction velocity of 3.5 km/s.

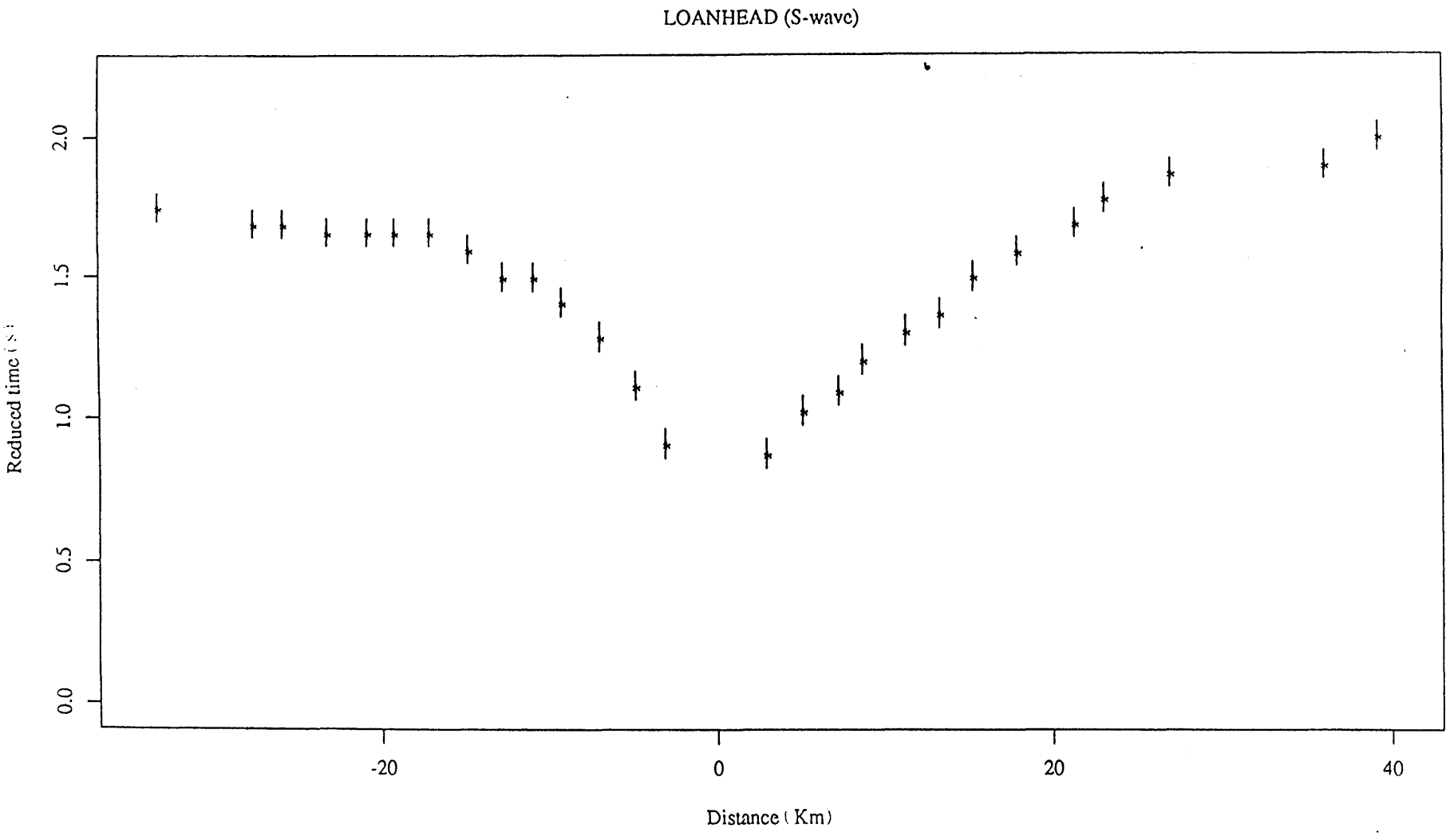

Fig. 3.62 S-wave time-distance data ; Loanhead with reduction velocity of 3.5 km/s.

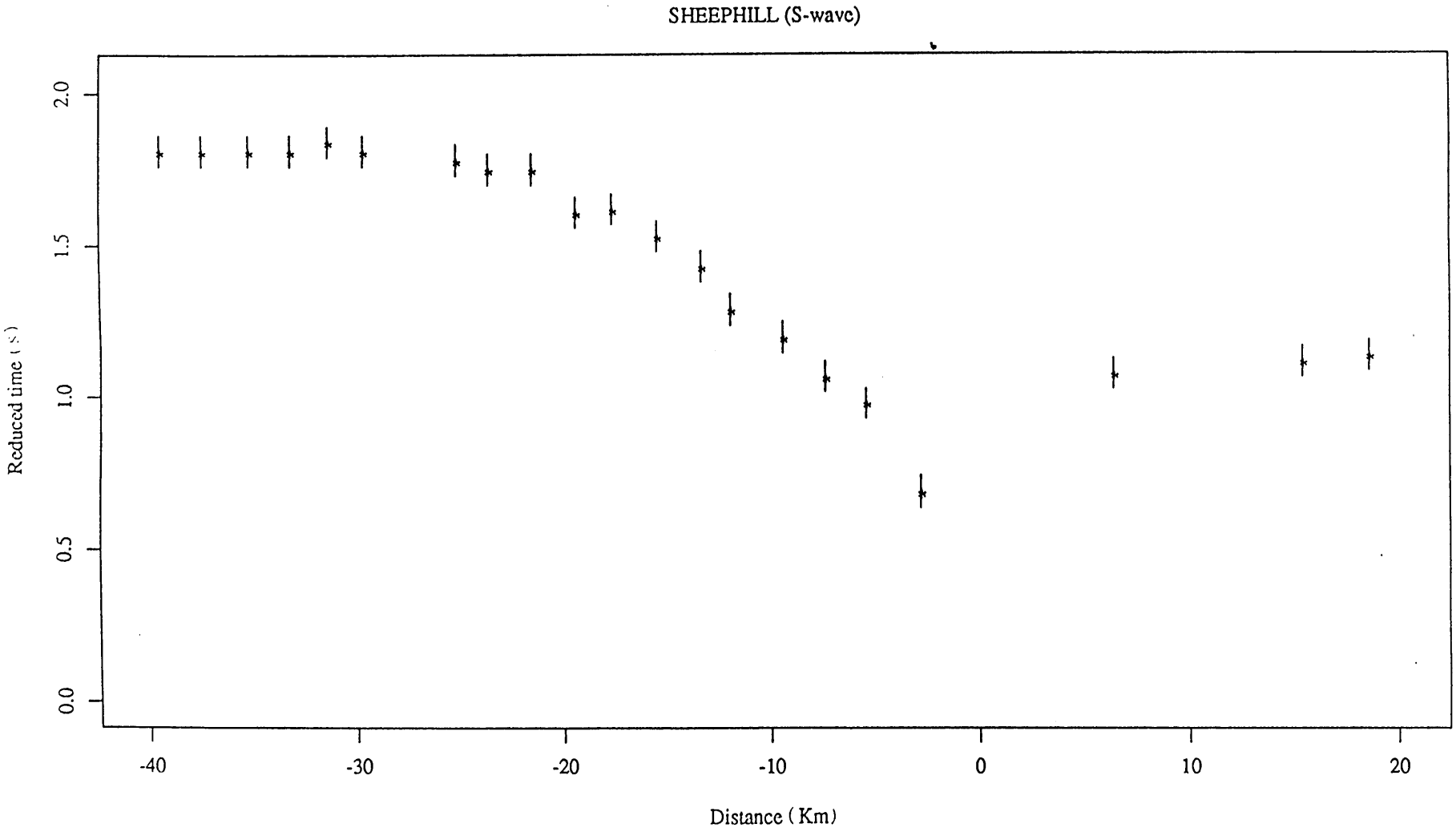

Fig. 3.63 S-wave time-distance data ; Sheephill with reduction velocity of 3.5 km/s.

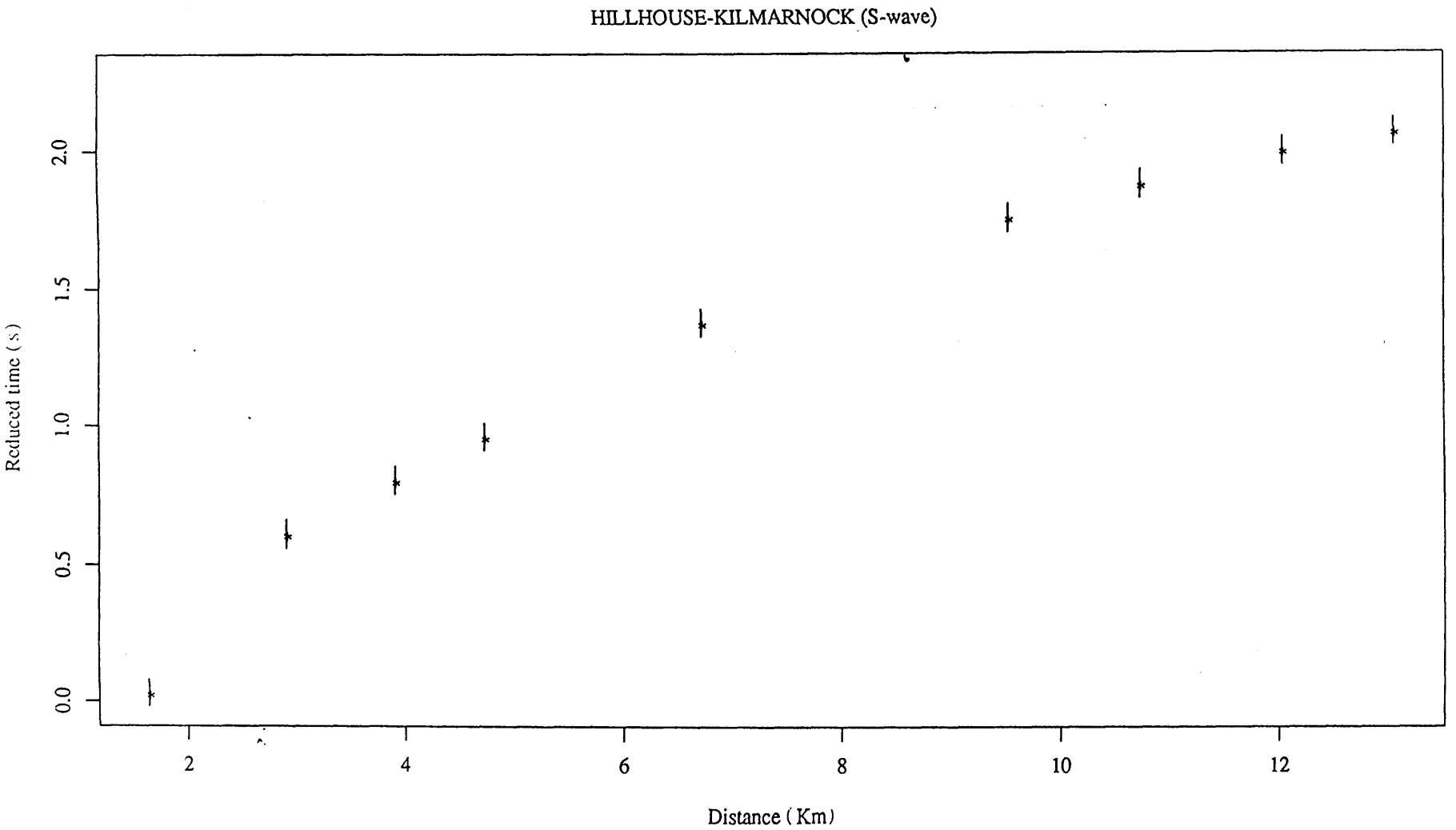

Fig. 3.64 S-wave time-distance data ; Hillhouse-kilmarnock line with reduction velocity of 3.5 km/s.

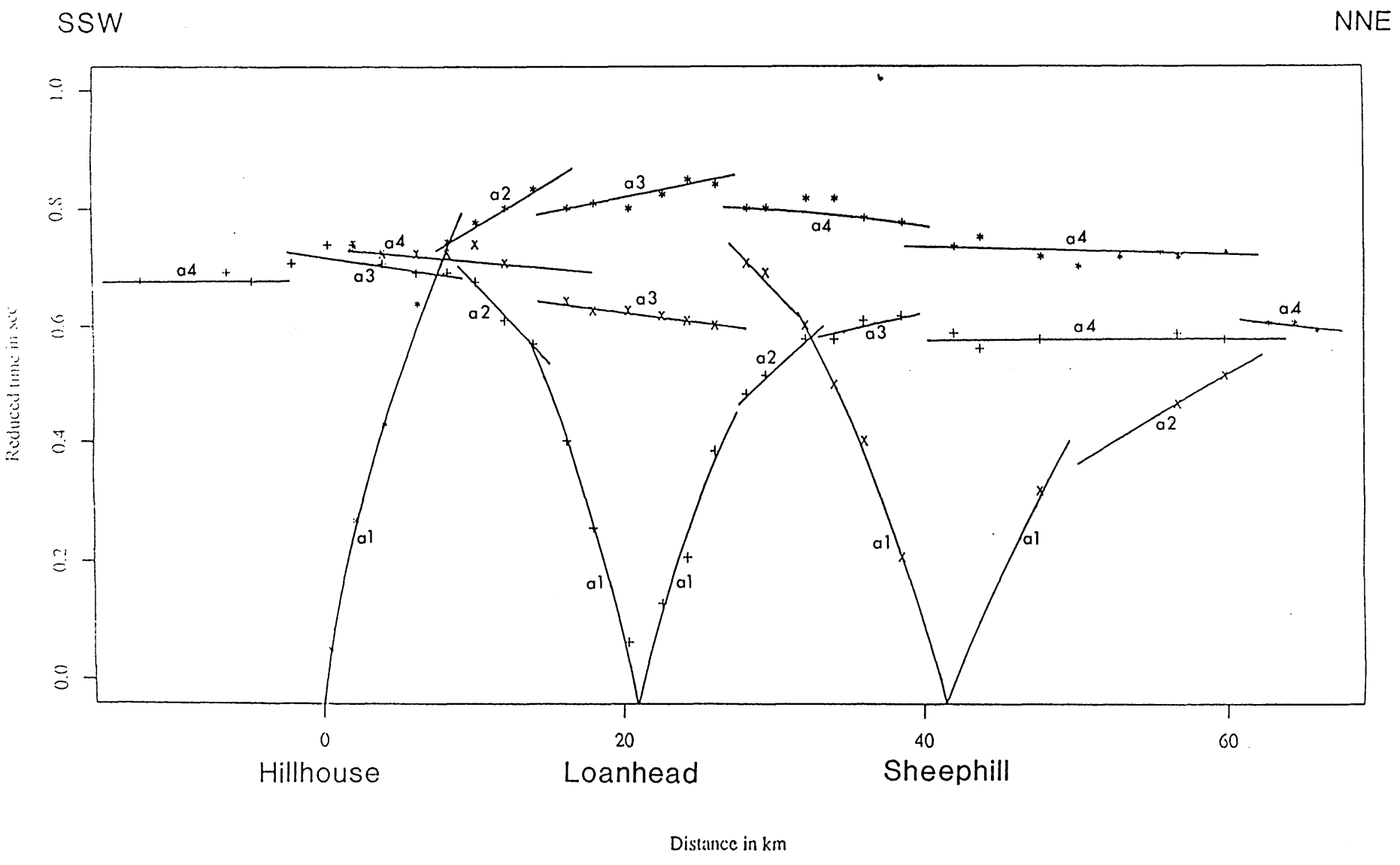

Fig. 4.1 P-wave time-distance graph (main line). A '*' denotes Hillhouse data, '+' Loanhead and 'x' Sheephill.

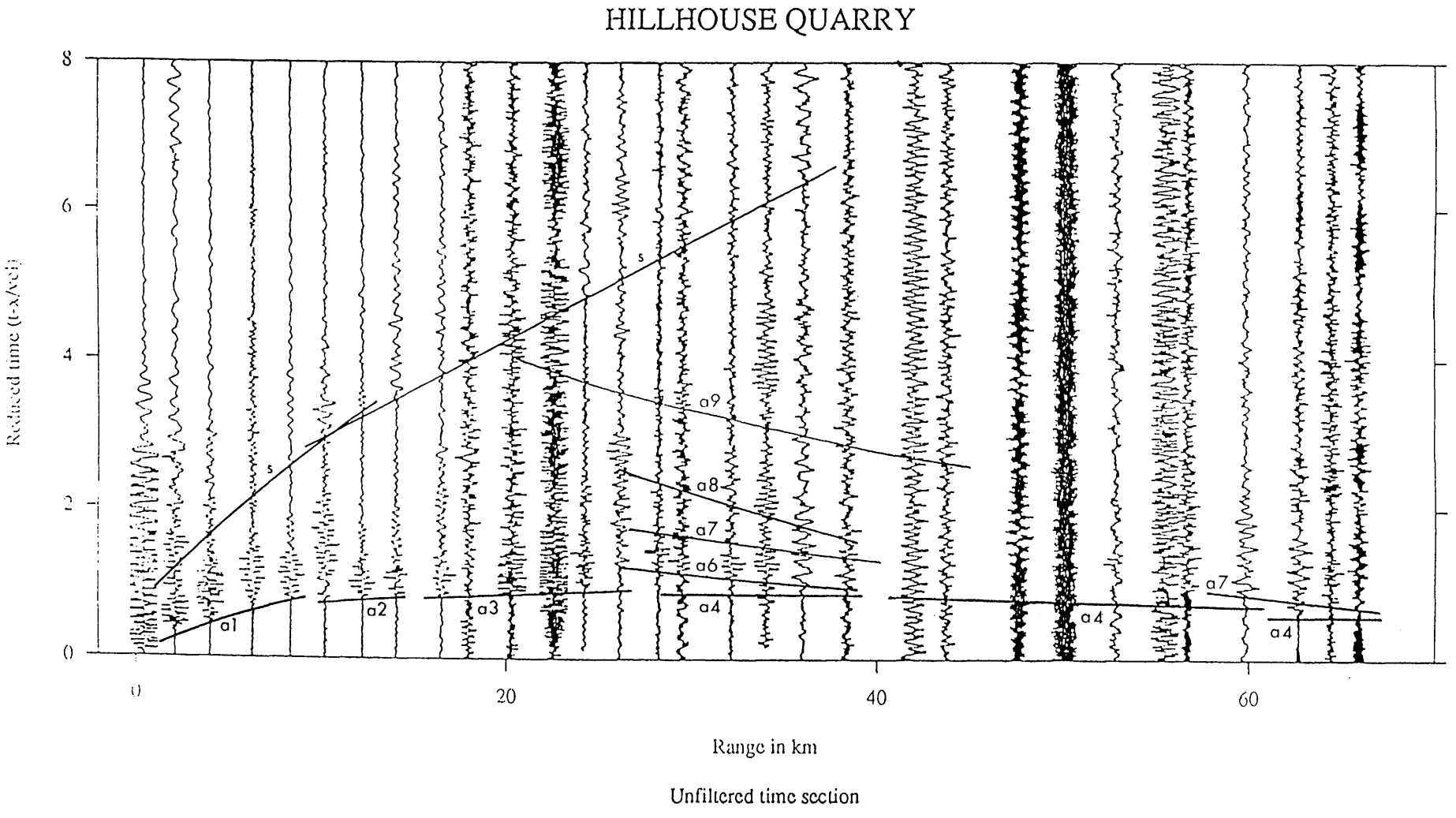

Fig. 4.2 Interpreted data; Hillhouse (main line) vertical component. Reduction velocity is 6 km/s.

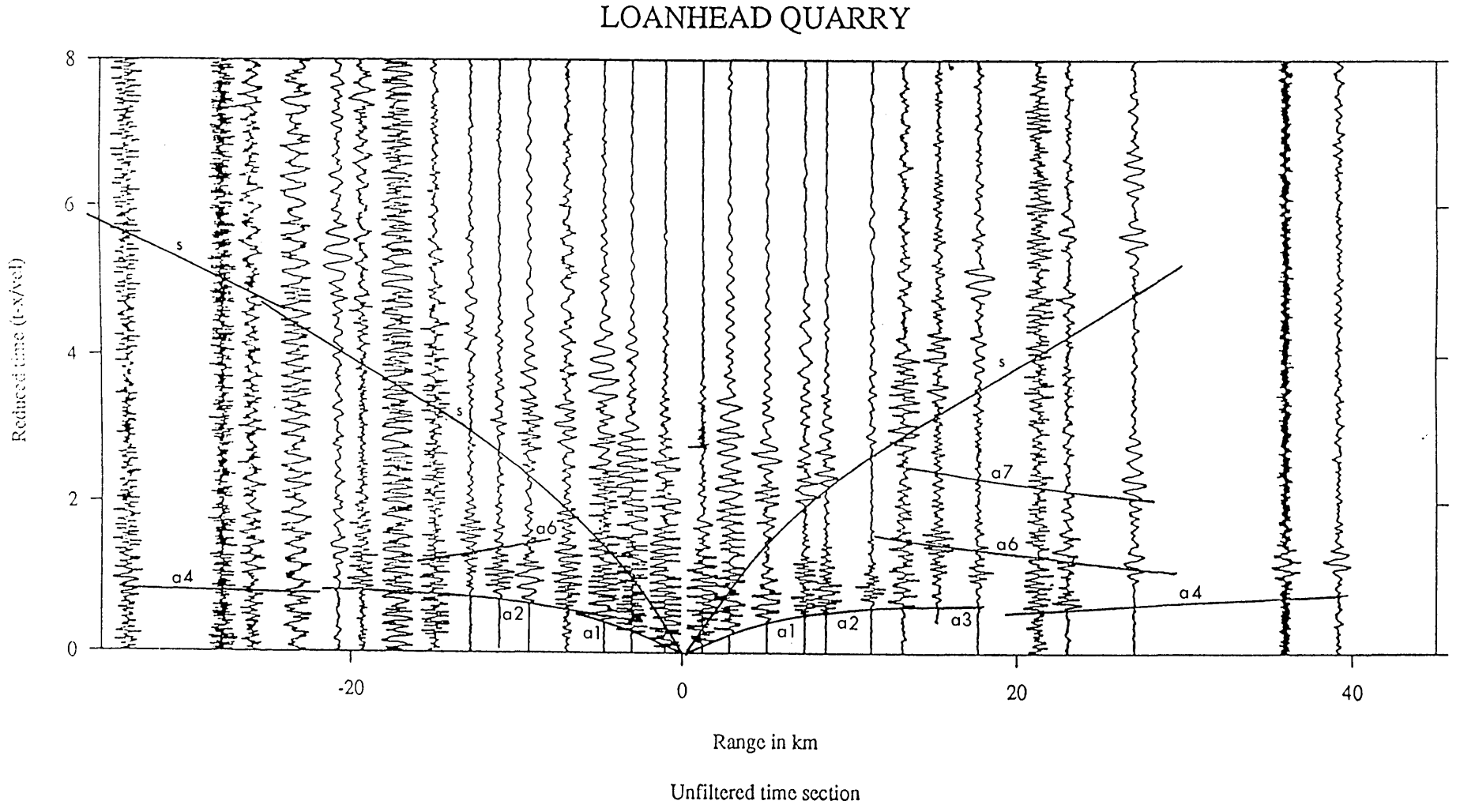

Fig. 4.3 Interpreted data; Loanhead vertical component. Reduction velocity is 6 km/s.

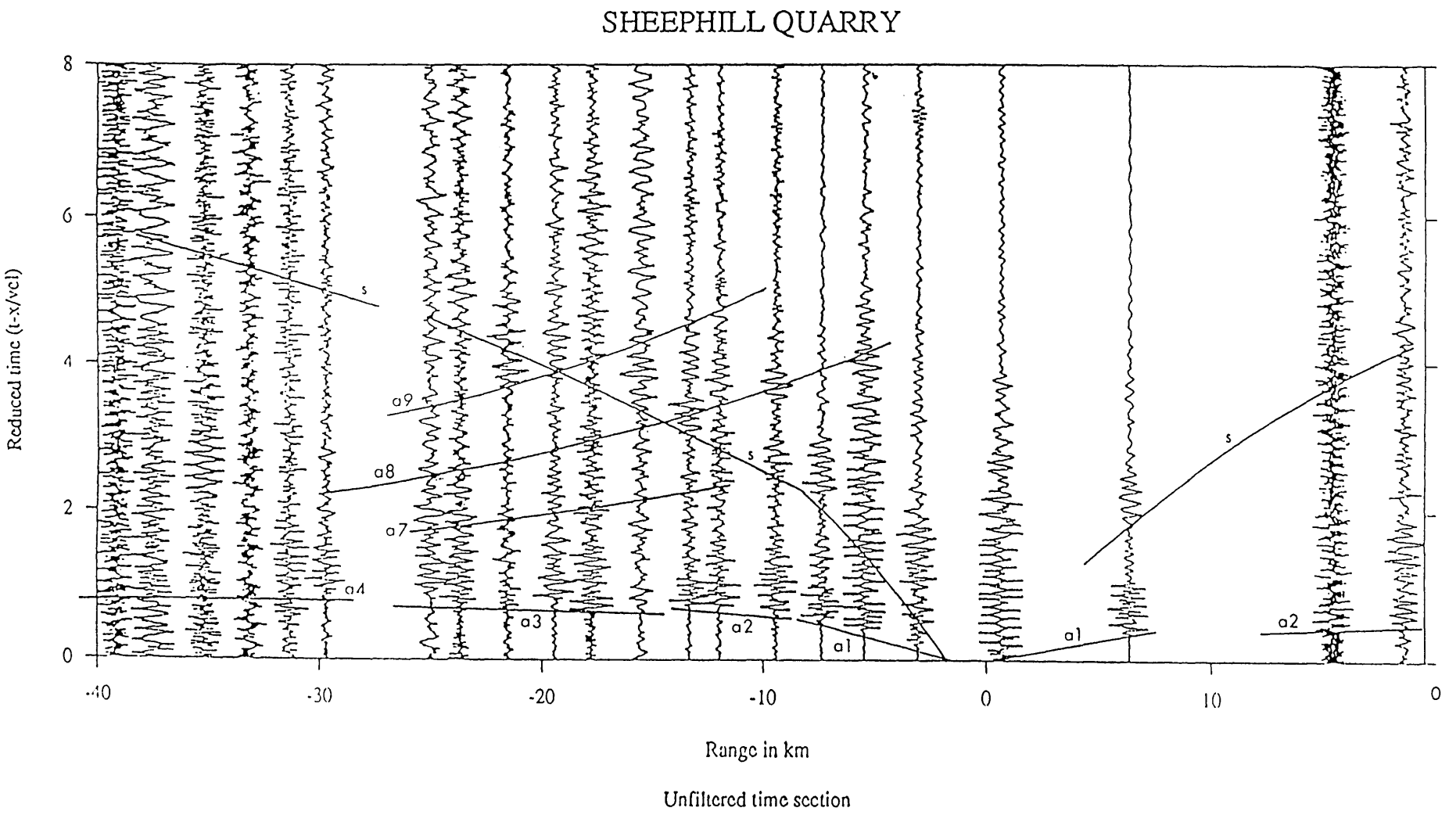

Fig. 4.4 Interpreted data; Sheephill vertical component. Reduction velocity is 6 km/s.

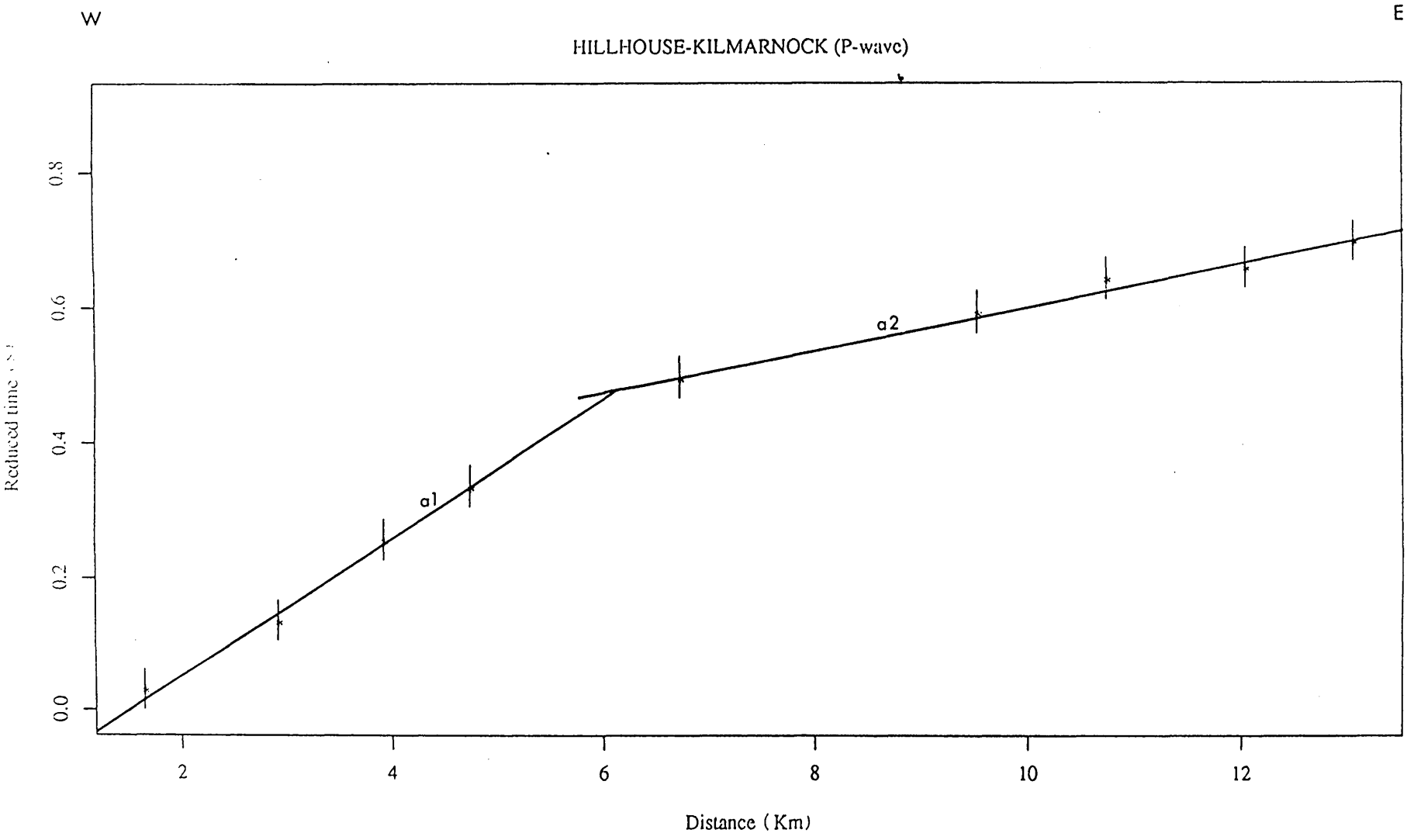

Fig. 4.5 P-wave time-distance graph (Hillhouse-Kilmarnock line).

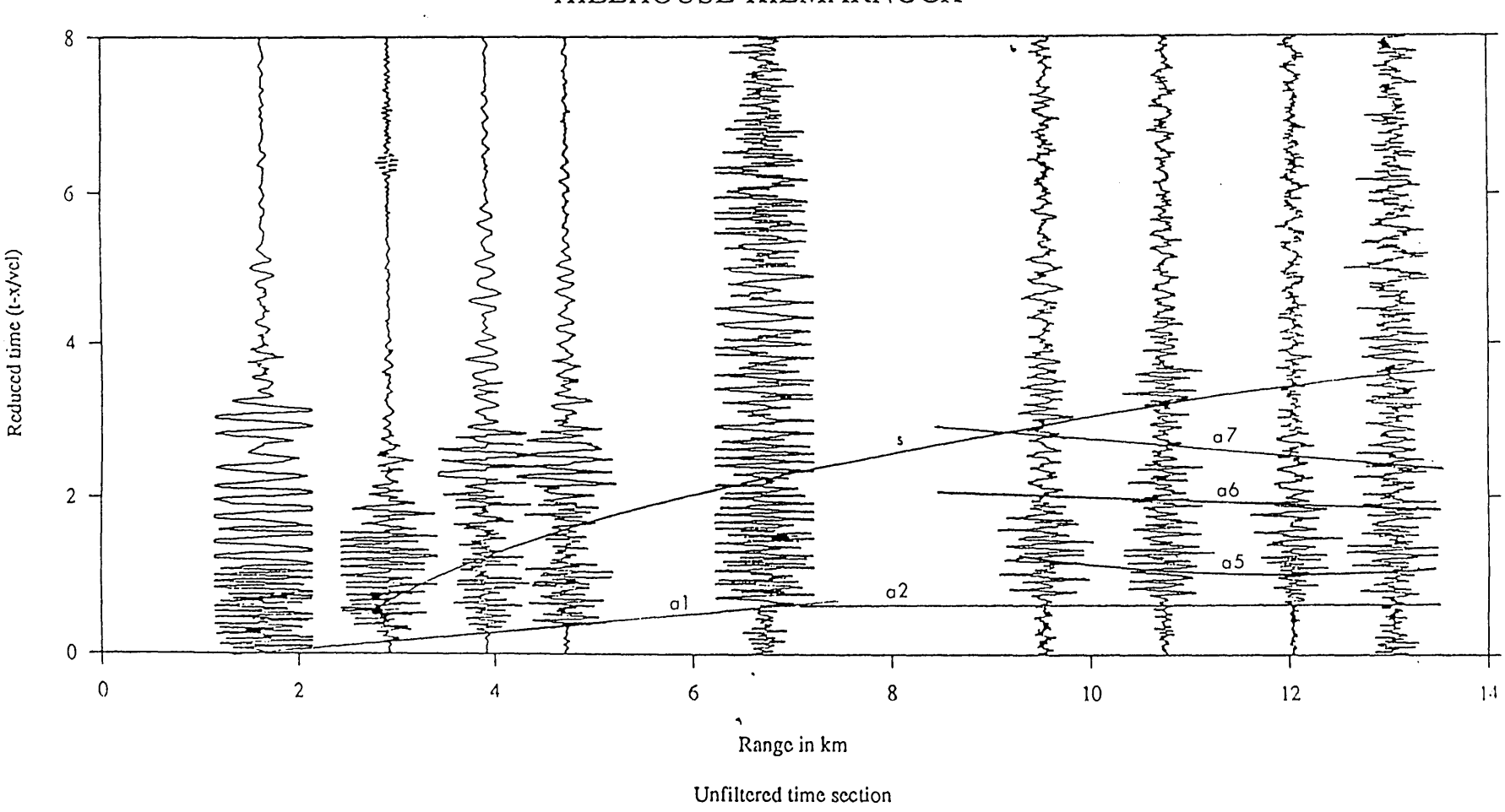

Fig. 4.6 Interpreted data; Hillhouse-Kilmarnock line (vertical component).
Reduction velocity 6.0 km/s.

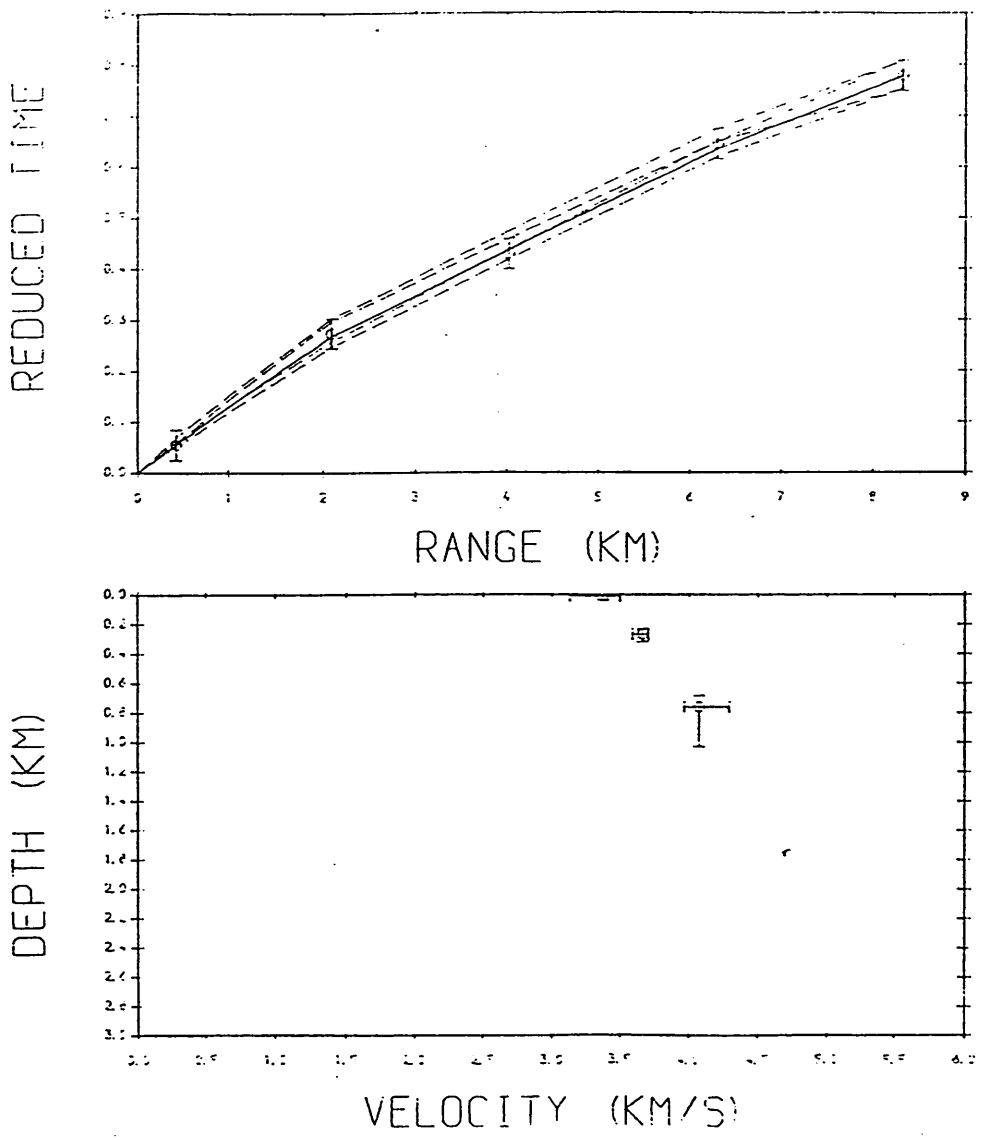

Fig. 4.7 WHB inversion method; Hillhouse main line (P-wave). Reducion velocity of top figure is 6.0 km/s.

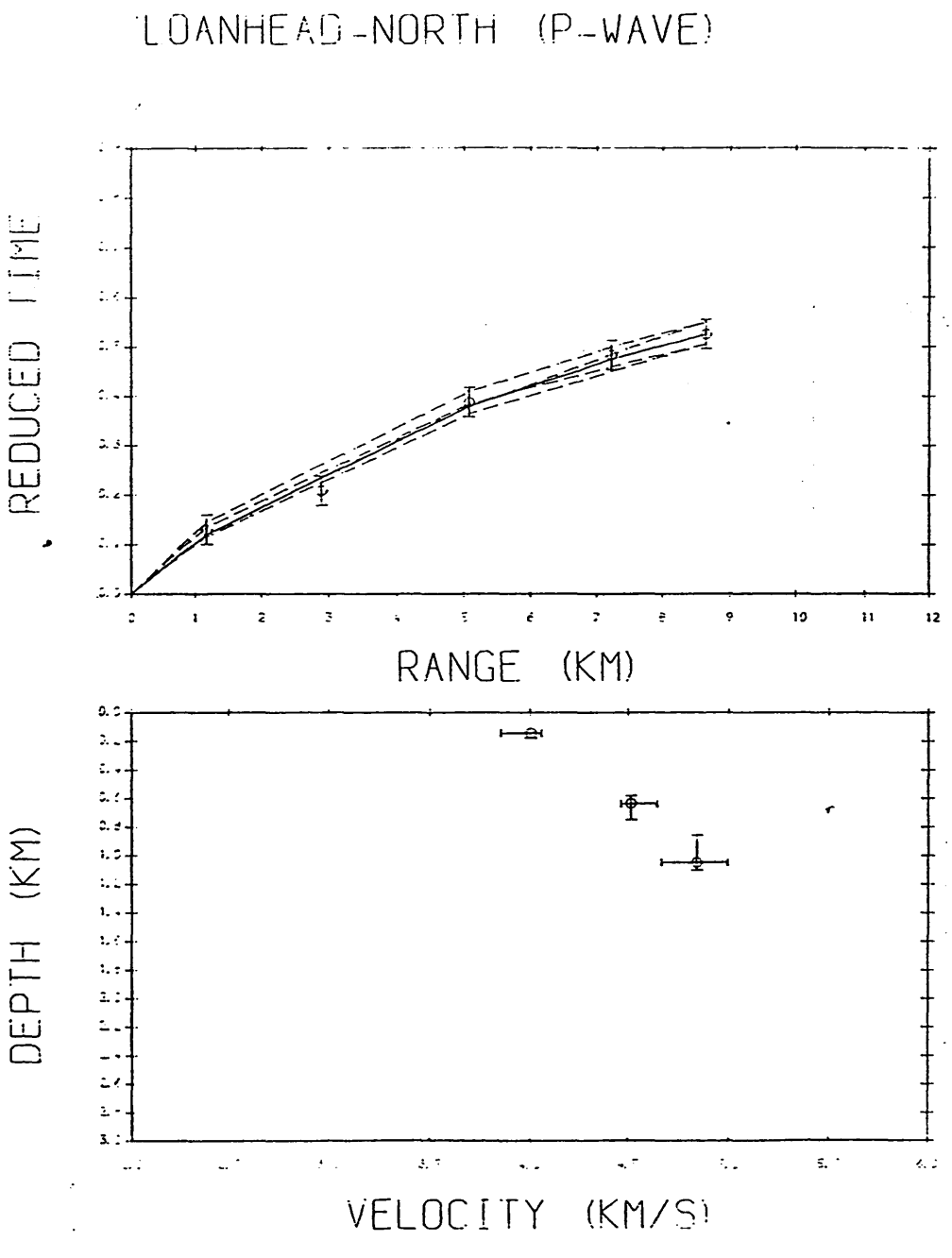

Fig. 4.8 WHB inversion method; Loanhead north (P-wave). Reducion velocity of top figure is 6.0 km/s.

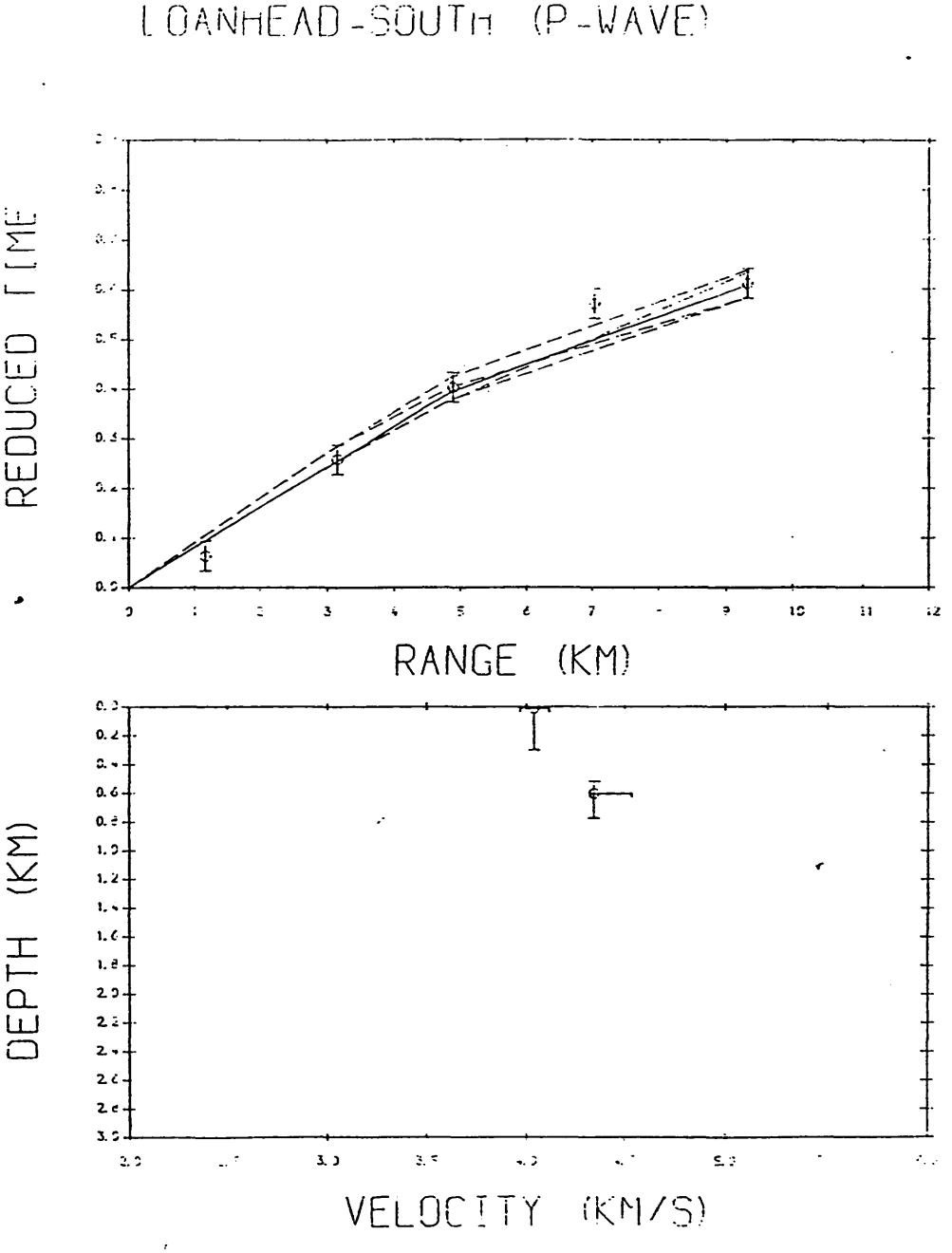

Fig. 4.9 WHB inversion method; Loanhead south (P-wave). Reducion velocity of top figure is 6.0 km/s.

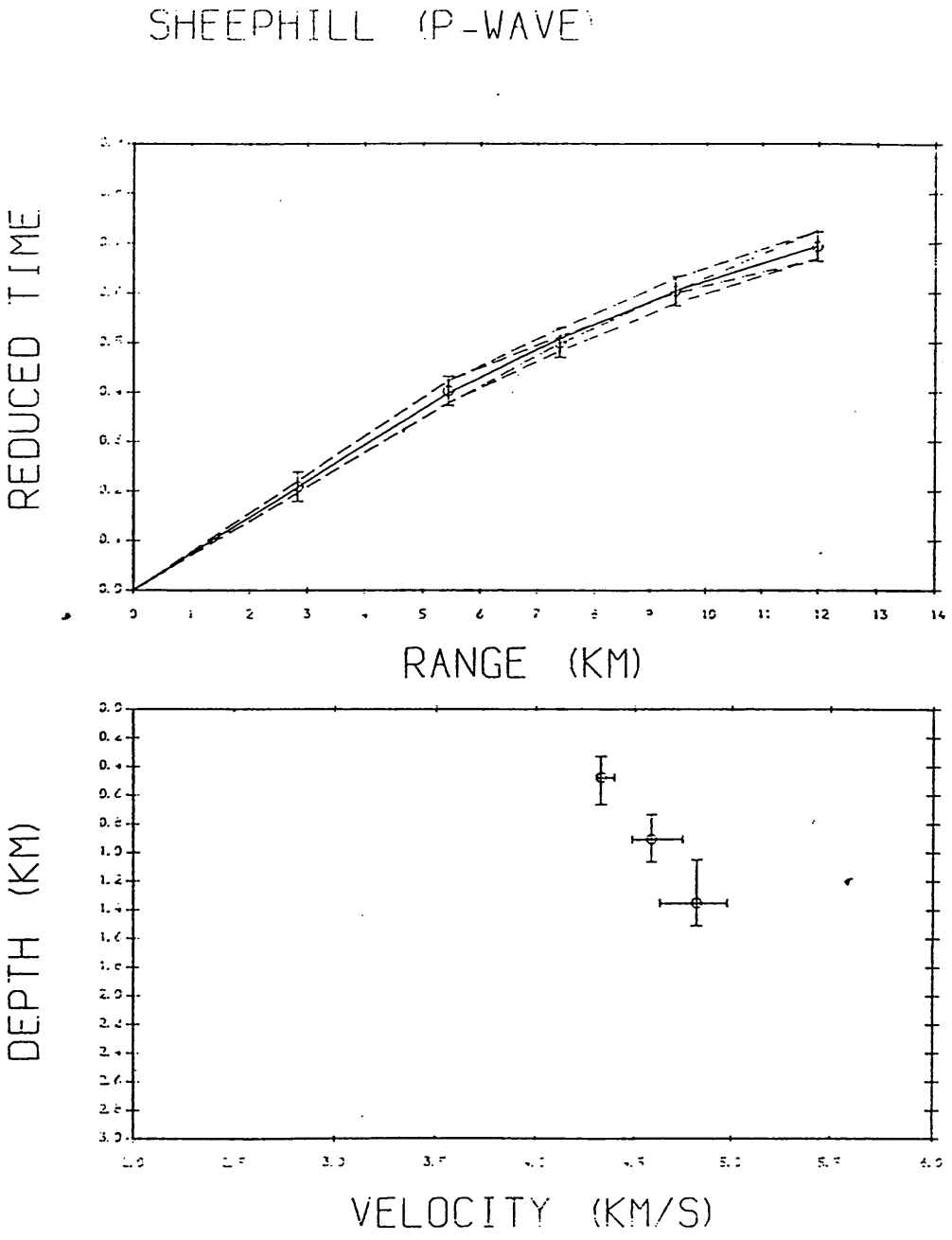

Fig. 4.10 WHB inversion method; Sheephill (P-wave). Reducion velocity of top figure is 6.0 km/s.

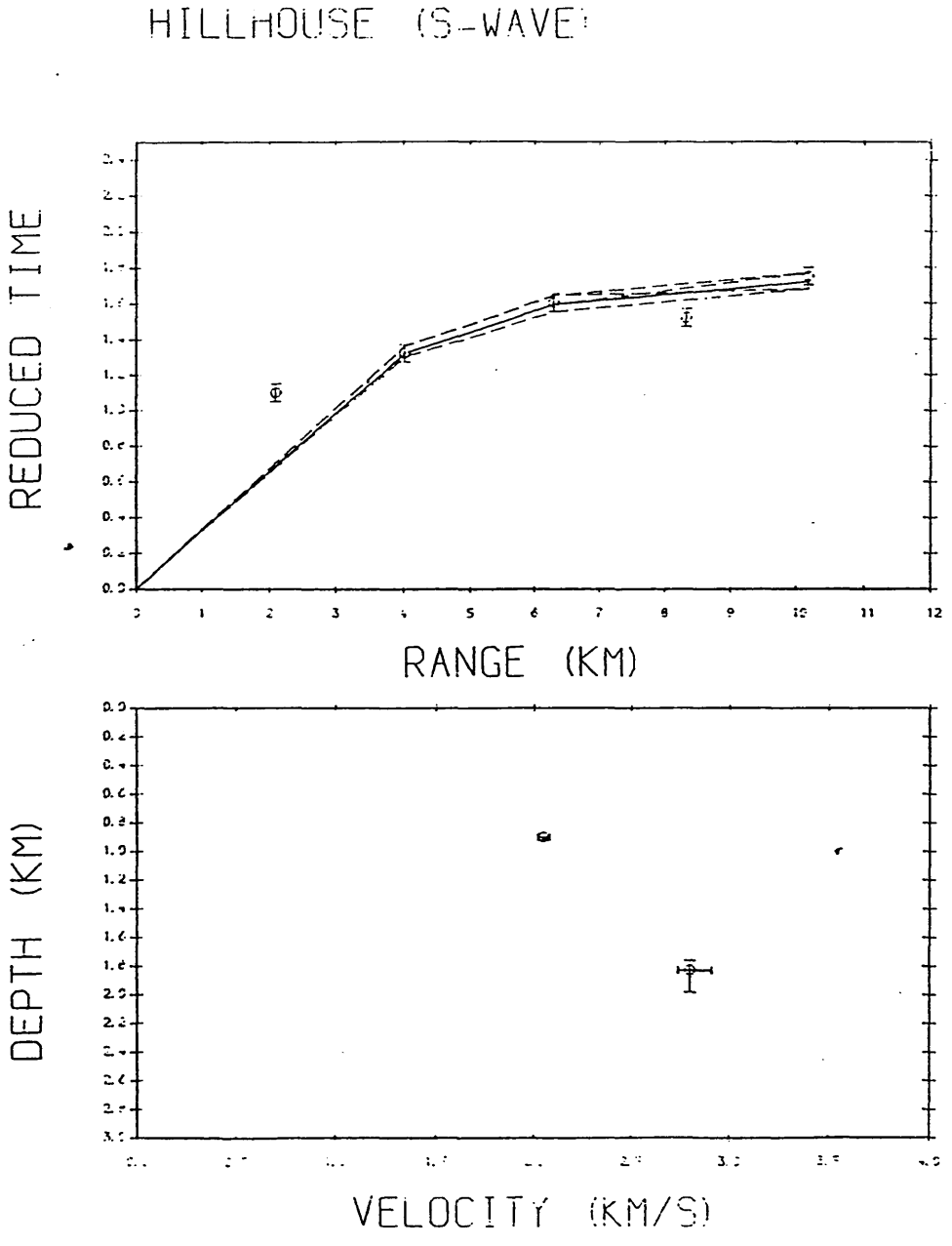

Fig. 4.11 WHB inversion method; Hillhouse main line (S-wave). Reducion velocity of top figure is 3.5 km/s.

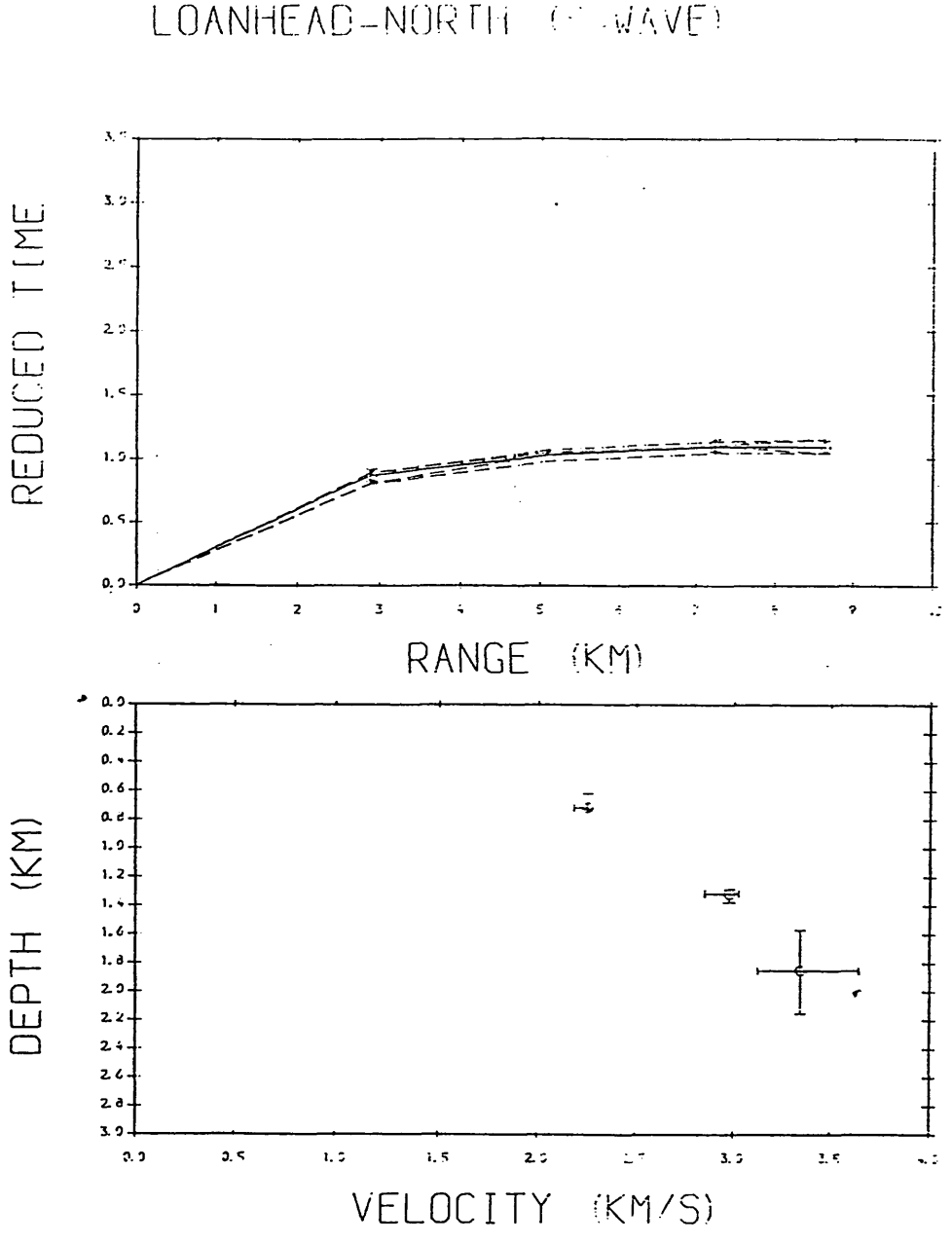

Fig. 4.12 WHB inversion method; Loanhead north (S-wave). Reducion velocity of top figure is 3.5 km/s.

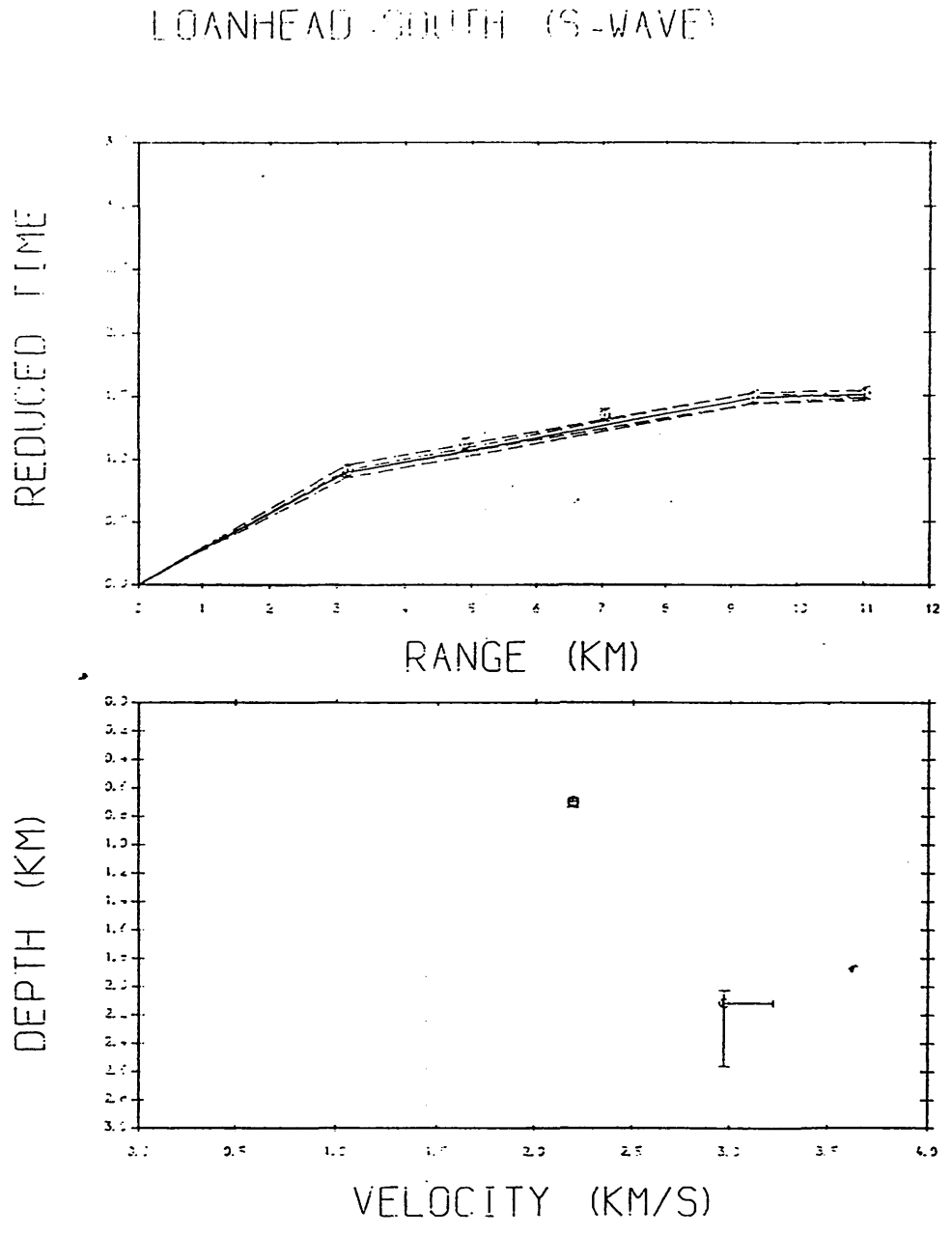

Fig. 4.13 WHB inversion method; Loanhead south (S-wave). Reducion velocity of top figure is 3.5 km/s.

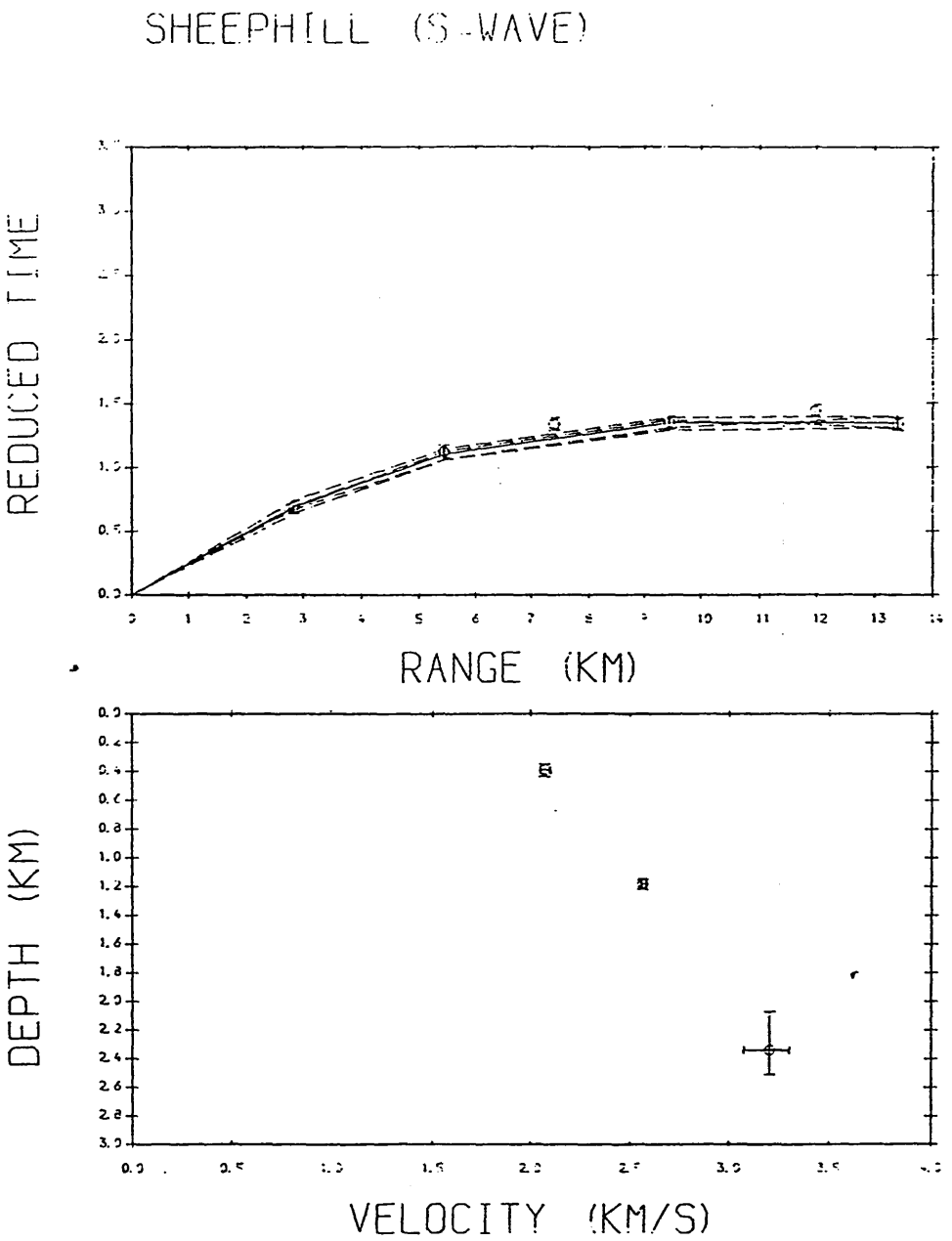

Fig. 4.14 WHB inversion method; Sheephill (S-wave). Reducion velocity of top figure is 3.5 km/s.

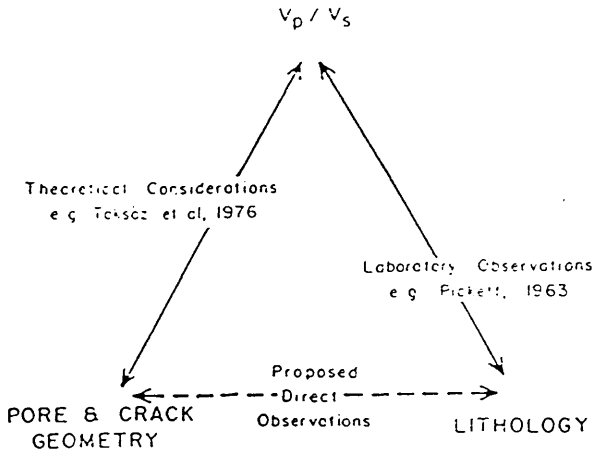

Fig. 4.15 Conceptual connection betwen sedimentary rock properties and the evidence supporting the connection (after Tatham 1984).

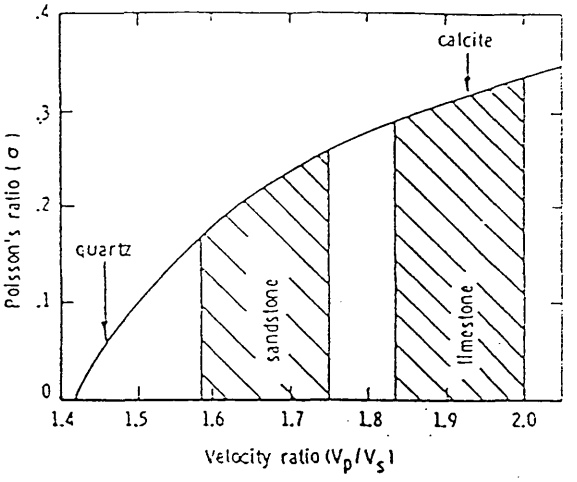

Fig. 4.16 Poisson's ratio versus velocity ratio graph (after Domenico 1984).

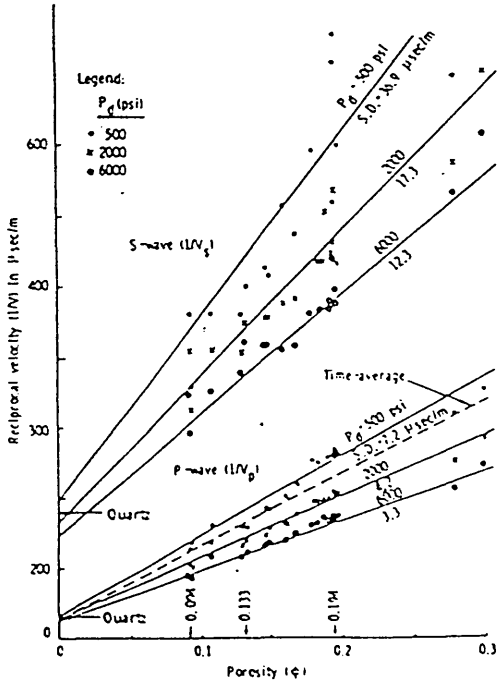

Fig. 4.17a Plot of measured reciprocal velocity versus porosity in sandstone (after Domenico 1984).

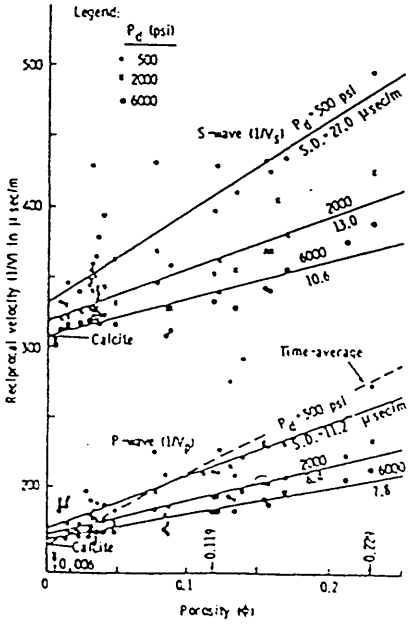

Fig. 4.17b Plot of measured reciprocal velocity versus porosity in limestone (after Domenico 1984).

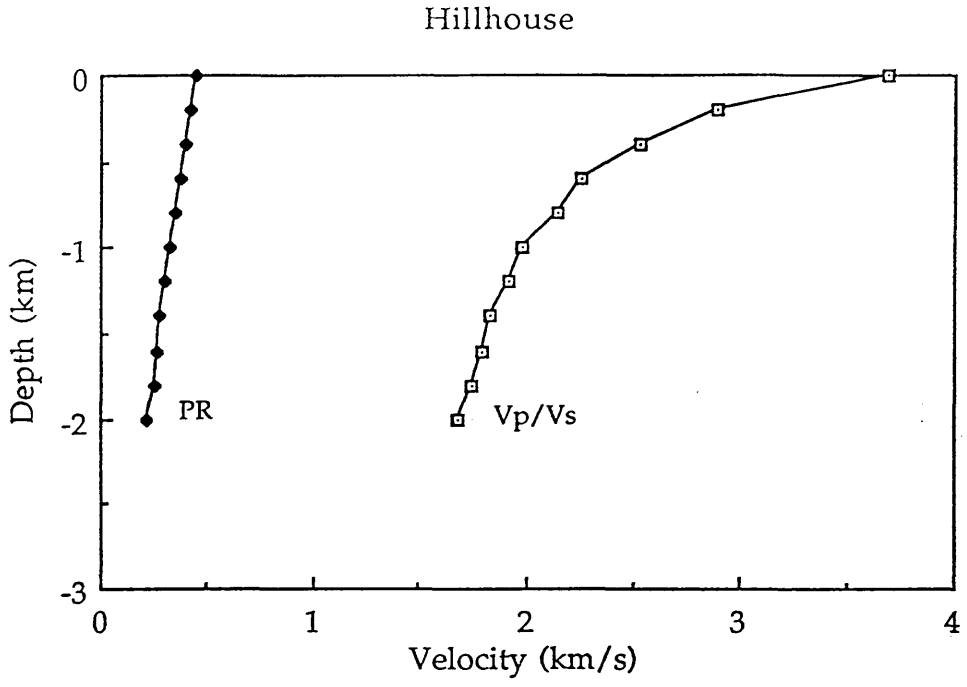

Fig. 4.18a Vp/Vs and Poisson's ratio for layer 1; Hillhouse (main line).

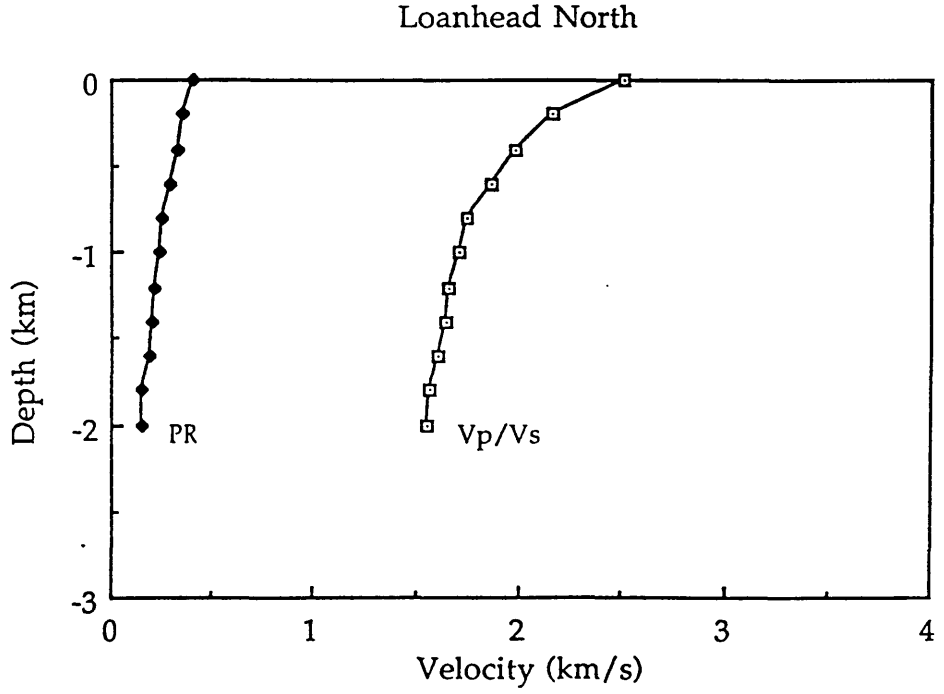

Fig. 4.18b Vp/Vs and Poisson's ratio for layer 1; Loanhead north.

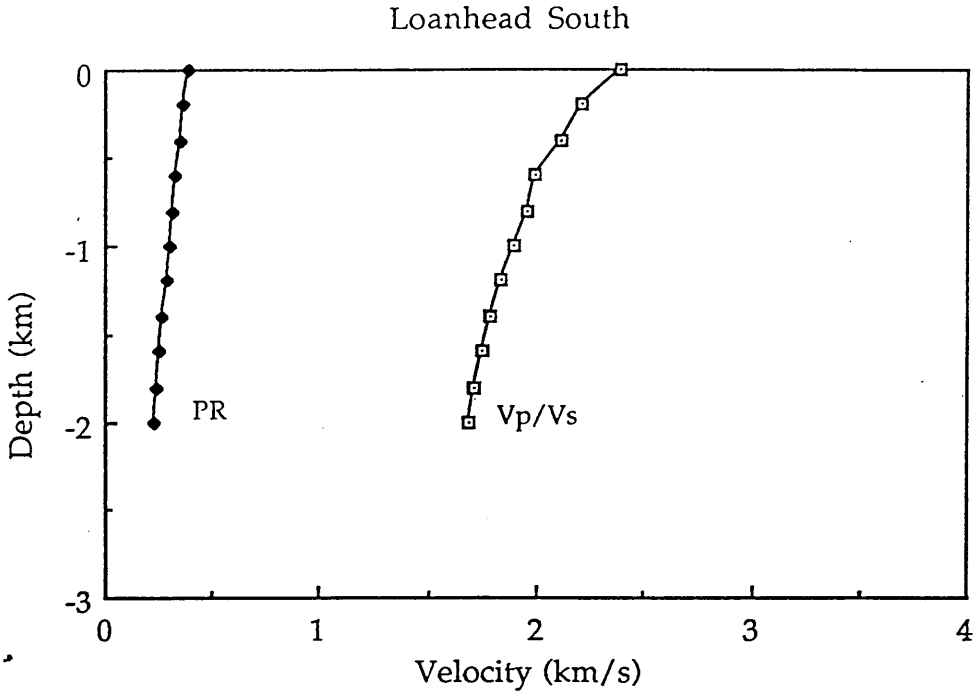

Fig. 4.18c Vp/Vs and Poisson's ratio for layer 1; Loanhead south.

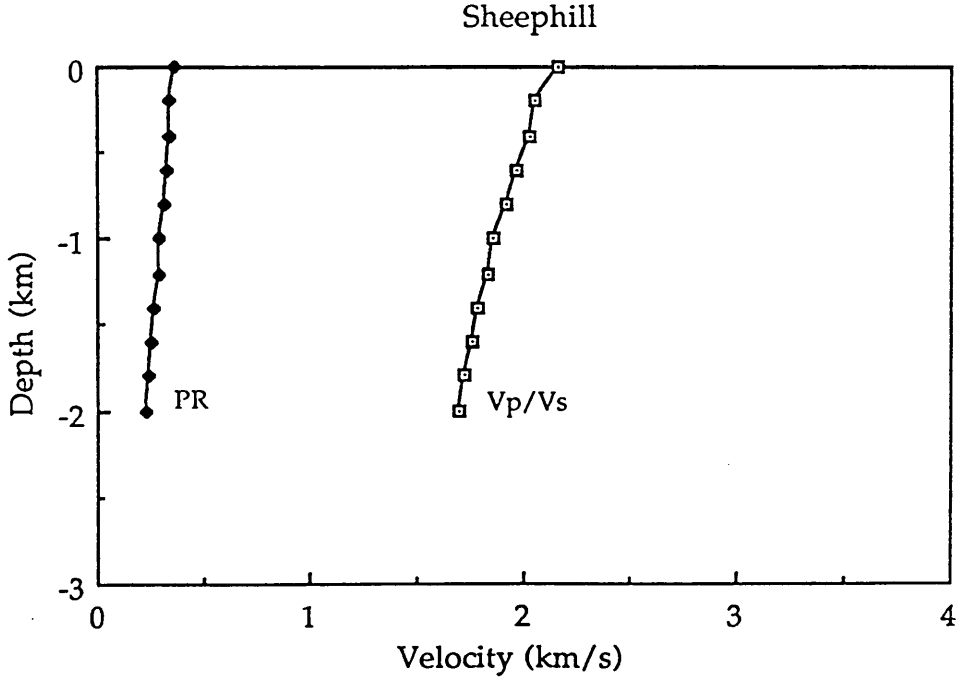

Fig. 4.18d Vp/Vs and Poisson's ratio for layer 1; Sheephill.

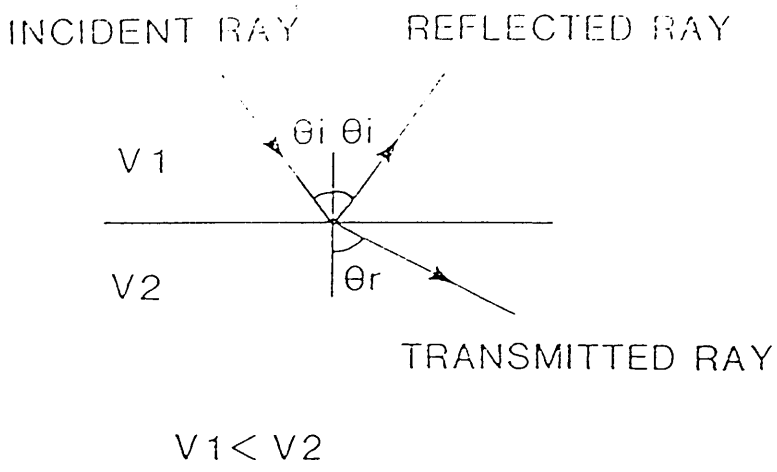

Fig. 4.19 Reflected and refracted rays.

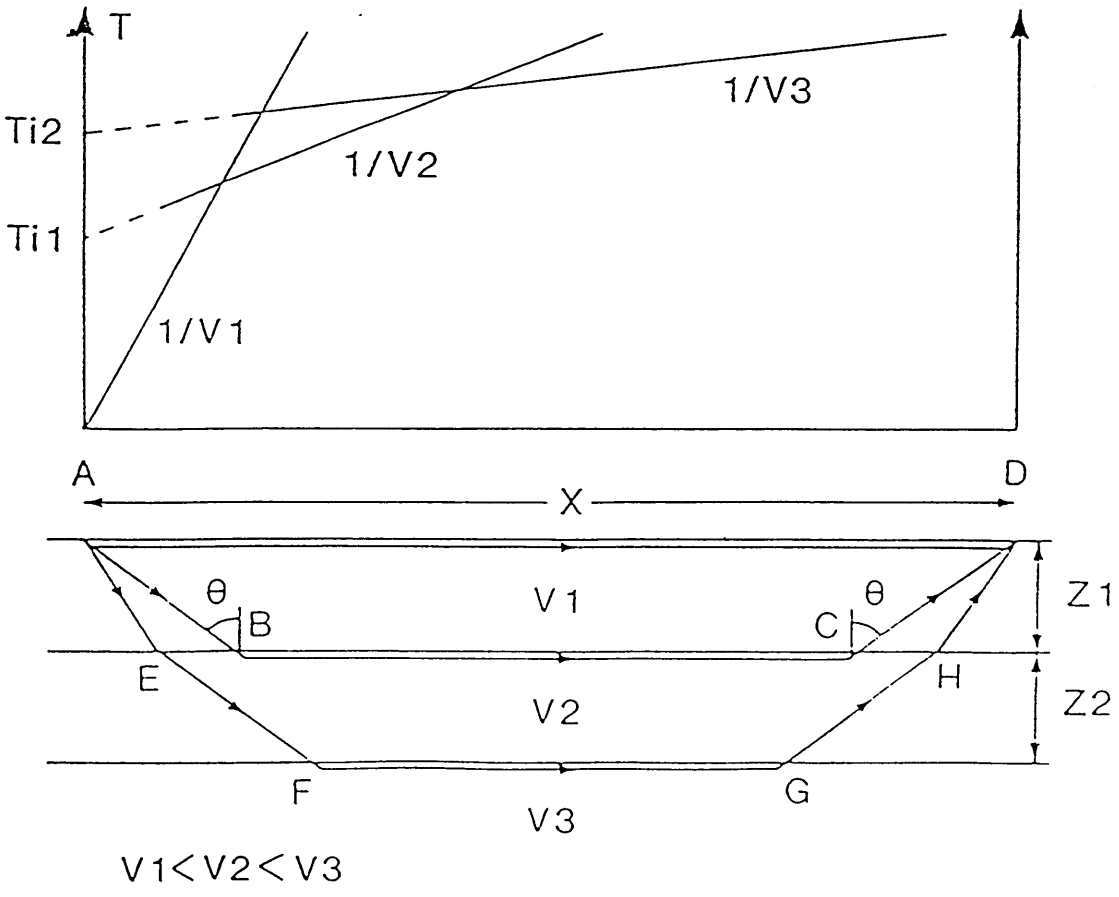

Fig. 4.20 Travel-time curves and ray-paths resulting from the critical refraction of rays at horizontal interfaces between constant velocity layers.

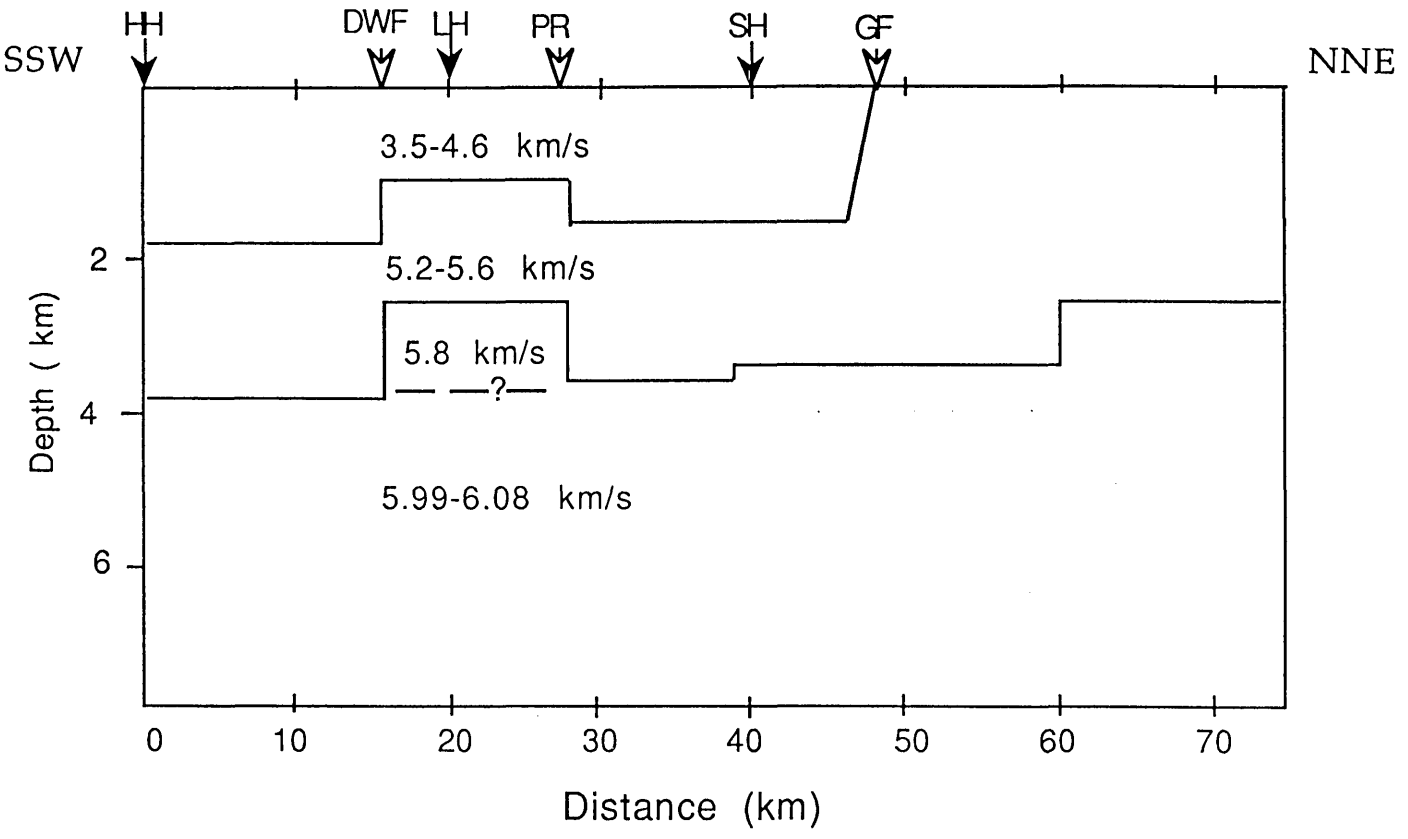

Fig. 4.21 Upper crustal model of the main line after applying horizontal layer interpretation. Solid arrows indicate quarry sources: HH - Hillhouse, LH - Loanhead, SH - Sheephill. Major faults are open arrows: DWF - Dusk Water Fault, PR - Paisley Ruck, GF - Gartness Fault.

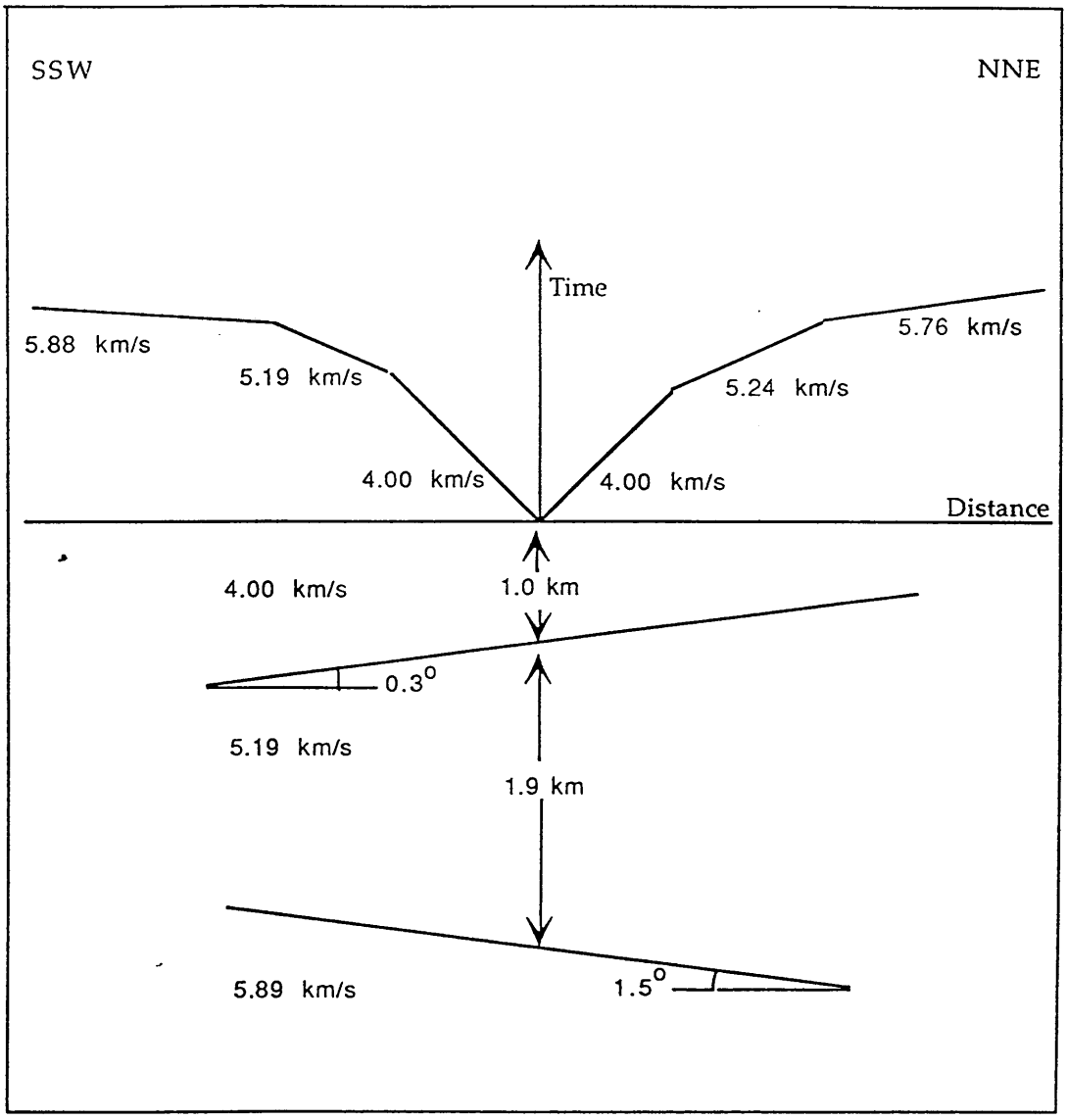

Fig. 4.23 Application of the split spread method to the Loanhead data.

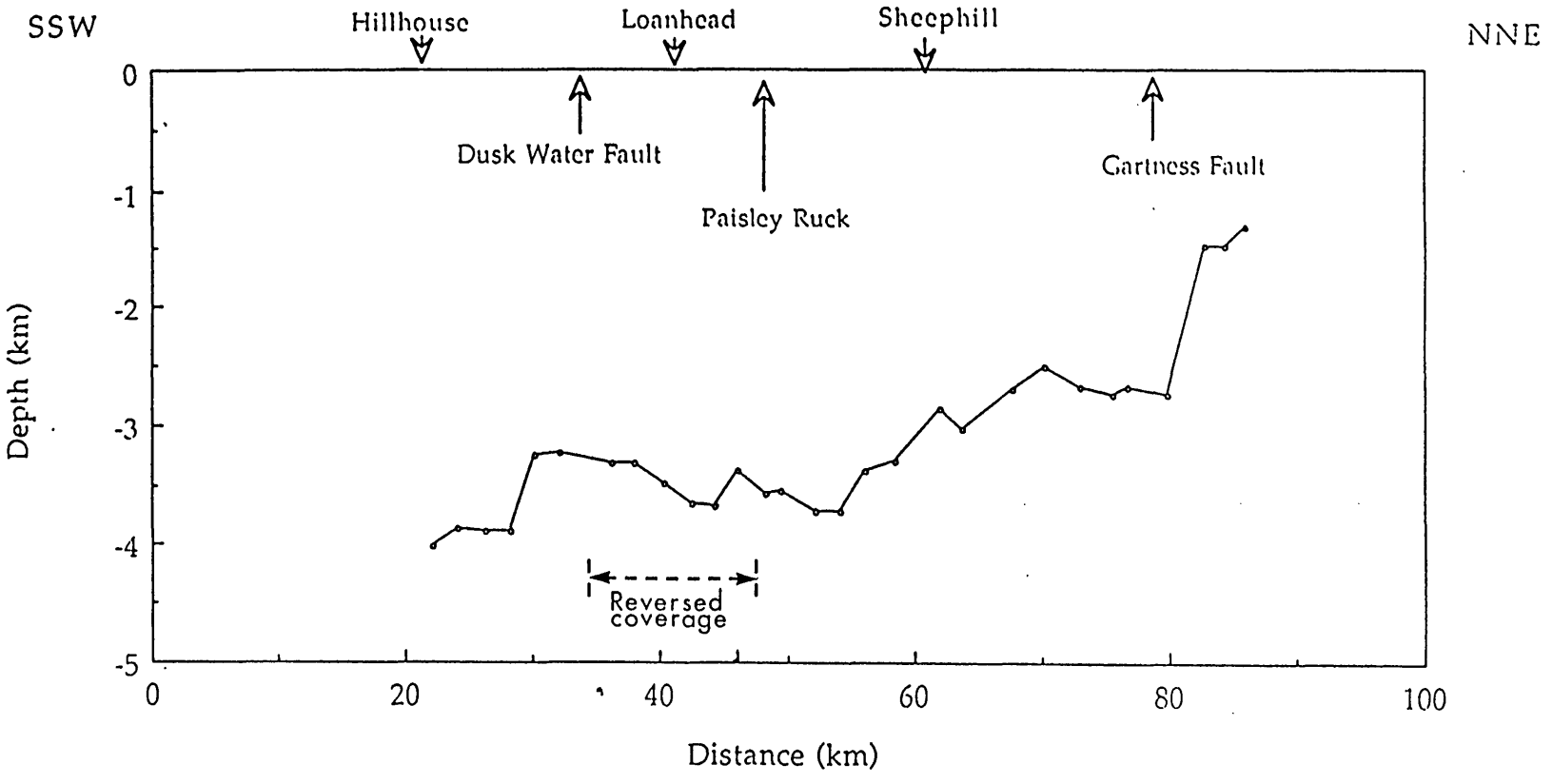

Fig. 4.24 Plus-minus interpretation of crystalline basement beneath the main line. Dashed line shows the reverse coverage from which the minus-time velocity (5.99 ± 0.03 km/s) was obtained.

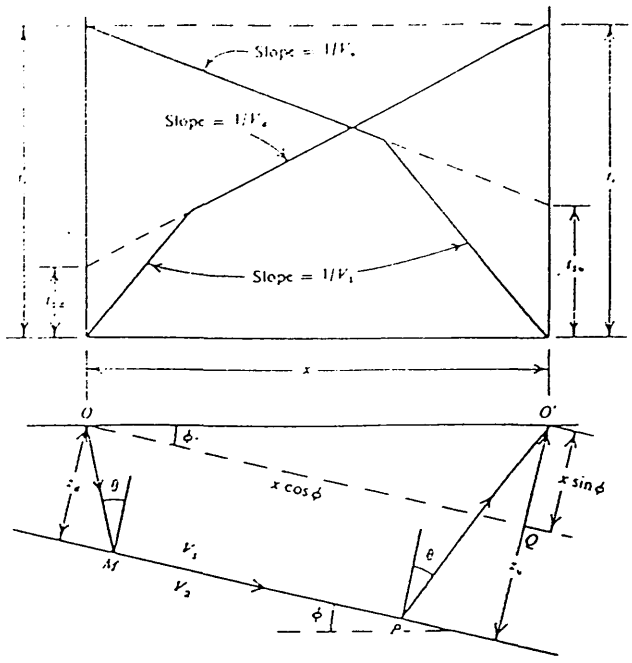

Fig. 4.22 Ray-paths and traveltime curves for a dipping refractor (after Telford *et al.* 1987).

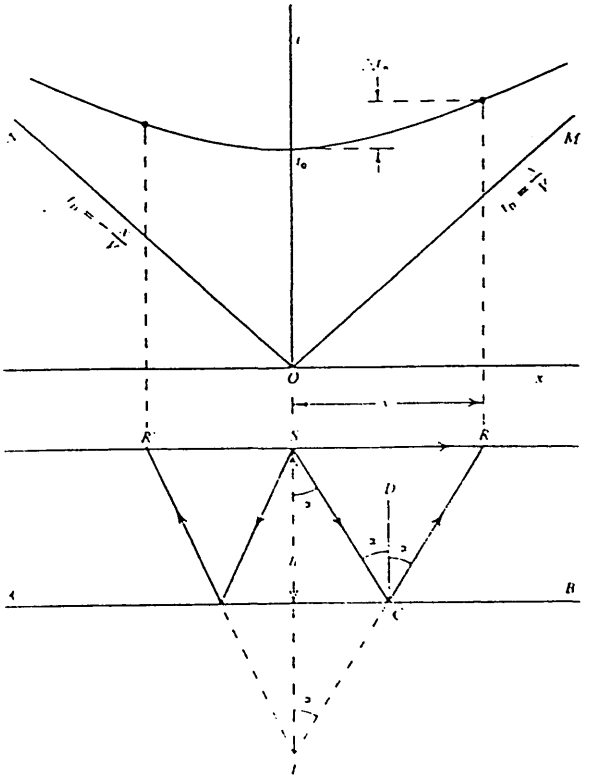

Fig. 4.25 Travel-time curve for a horizontal reflector (after Telford *et al.* 1987).

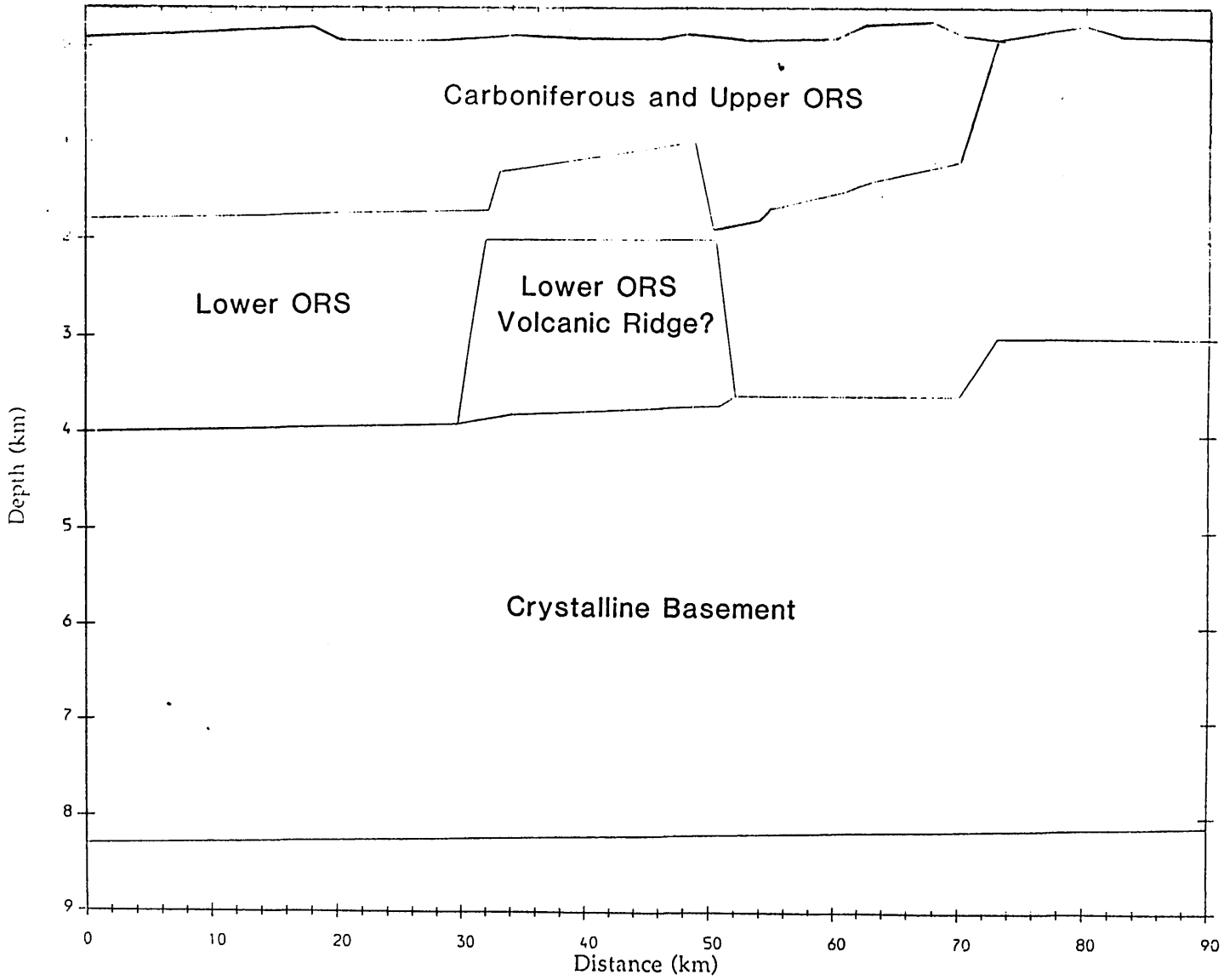

Fig. 4.26 Geological model of the main line upper crustal raytrace model.

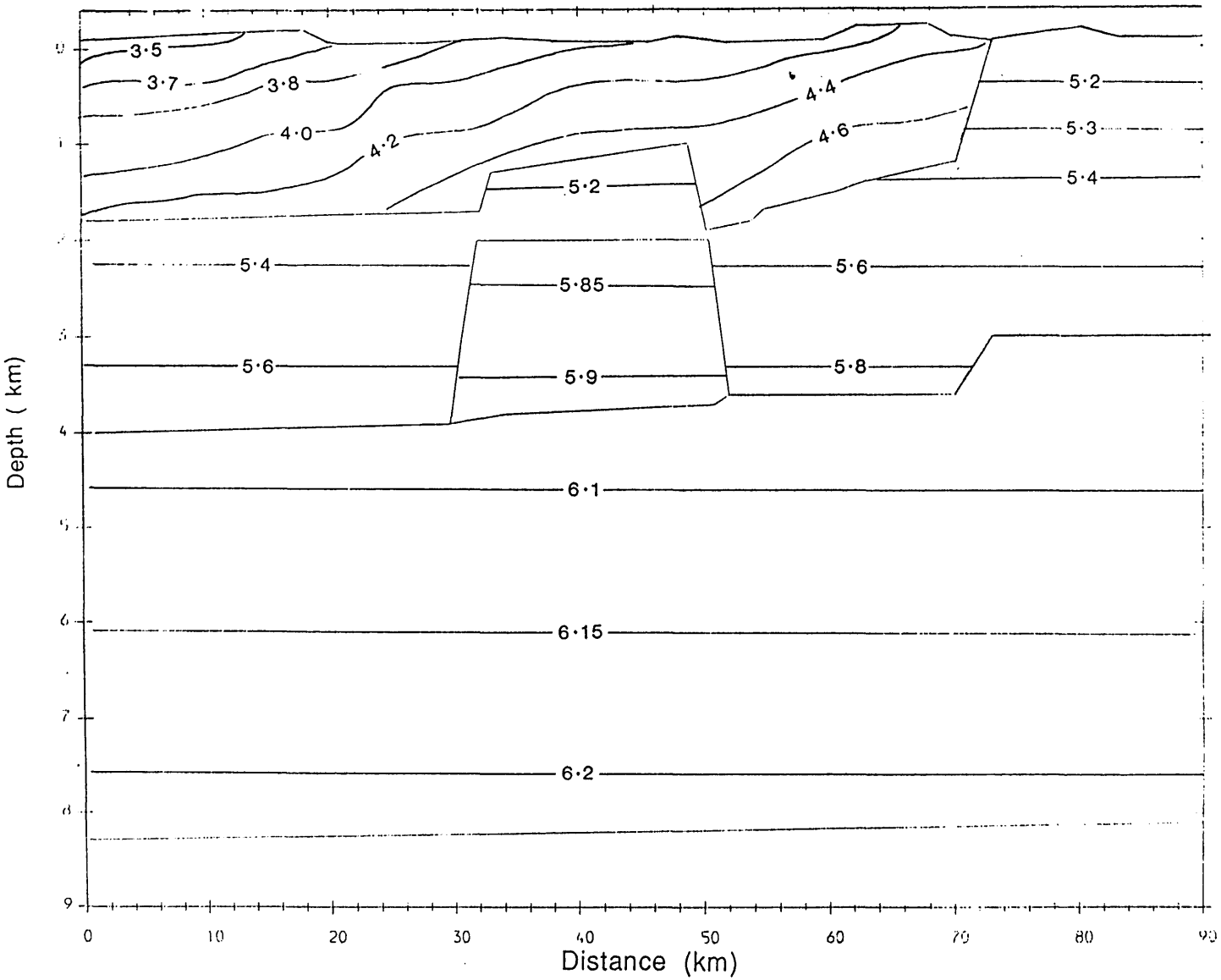

Fig. 4.27 P-wave velocity distribution of the upper crustal raytrace model of the main line.

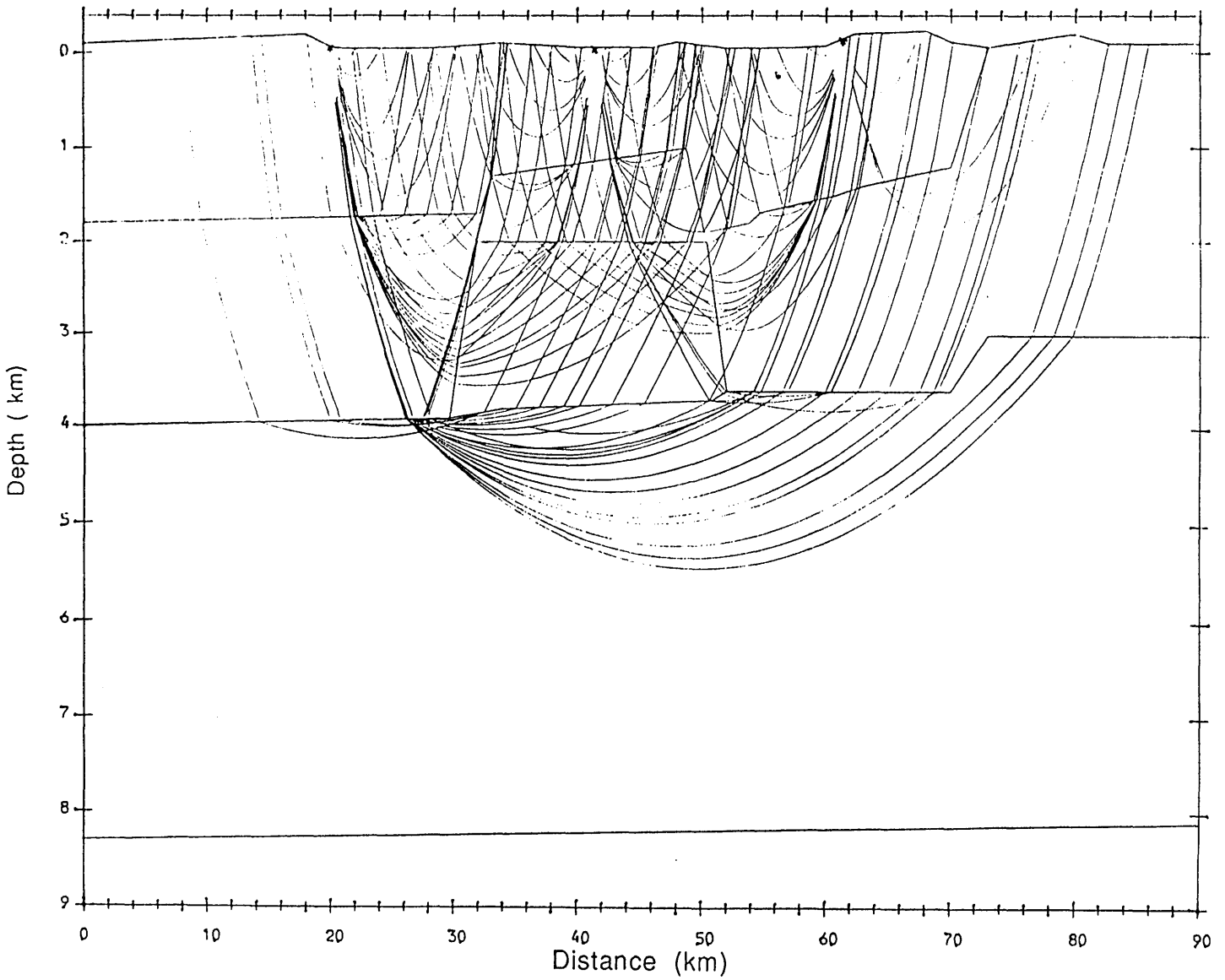

Fig. 4.28 Rays used to determine the upper crustal model of the main line.

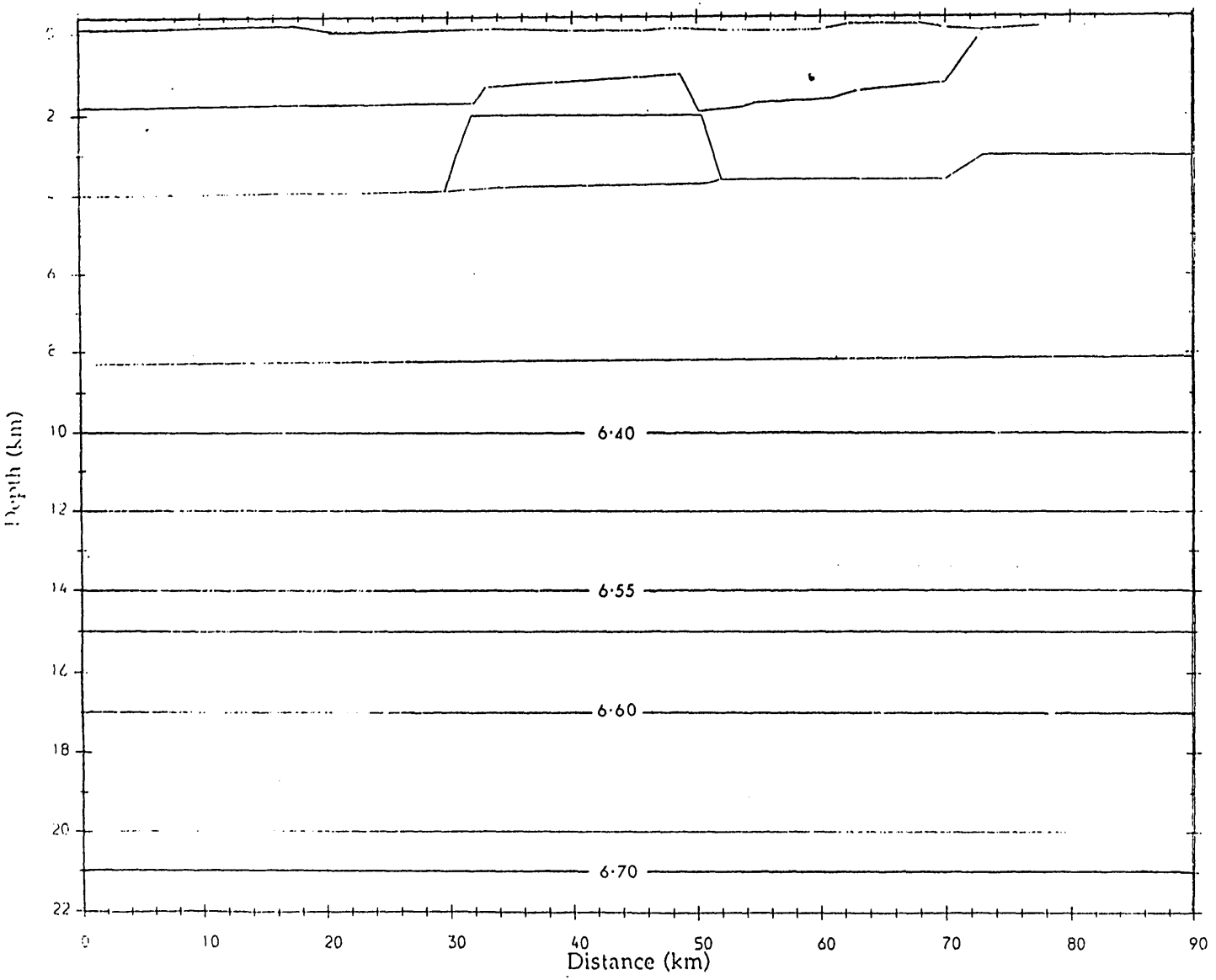

Fig. 4.29 Velocity distribution of the lower layers of the complete raytrace model of the main line. Velocities of upper layers are shown in Fig. 4.27.

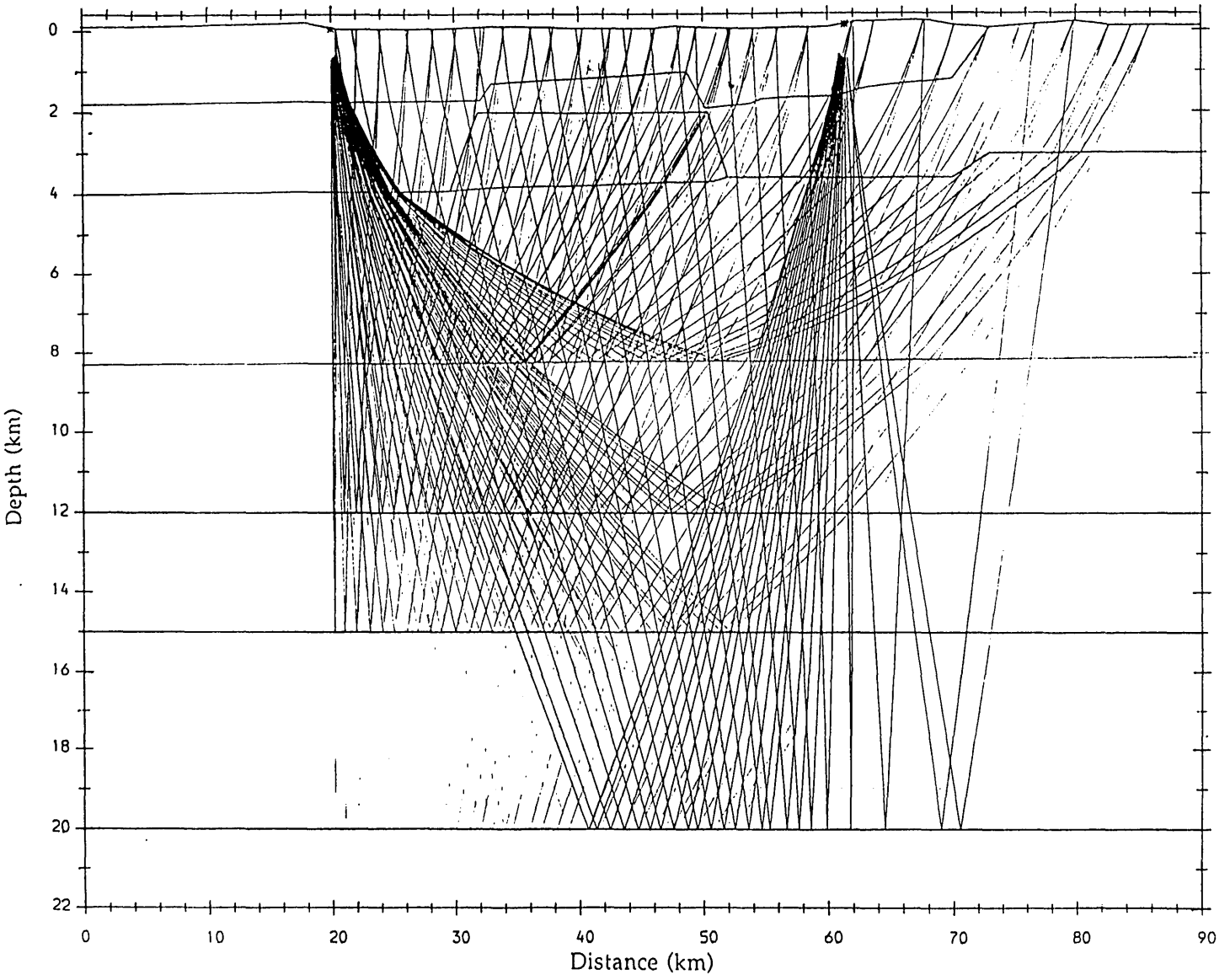

Fig. 4.30 Reflection raypaths of the deeper horizons of the main line.

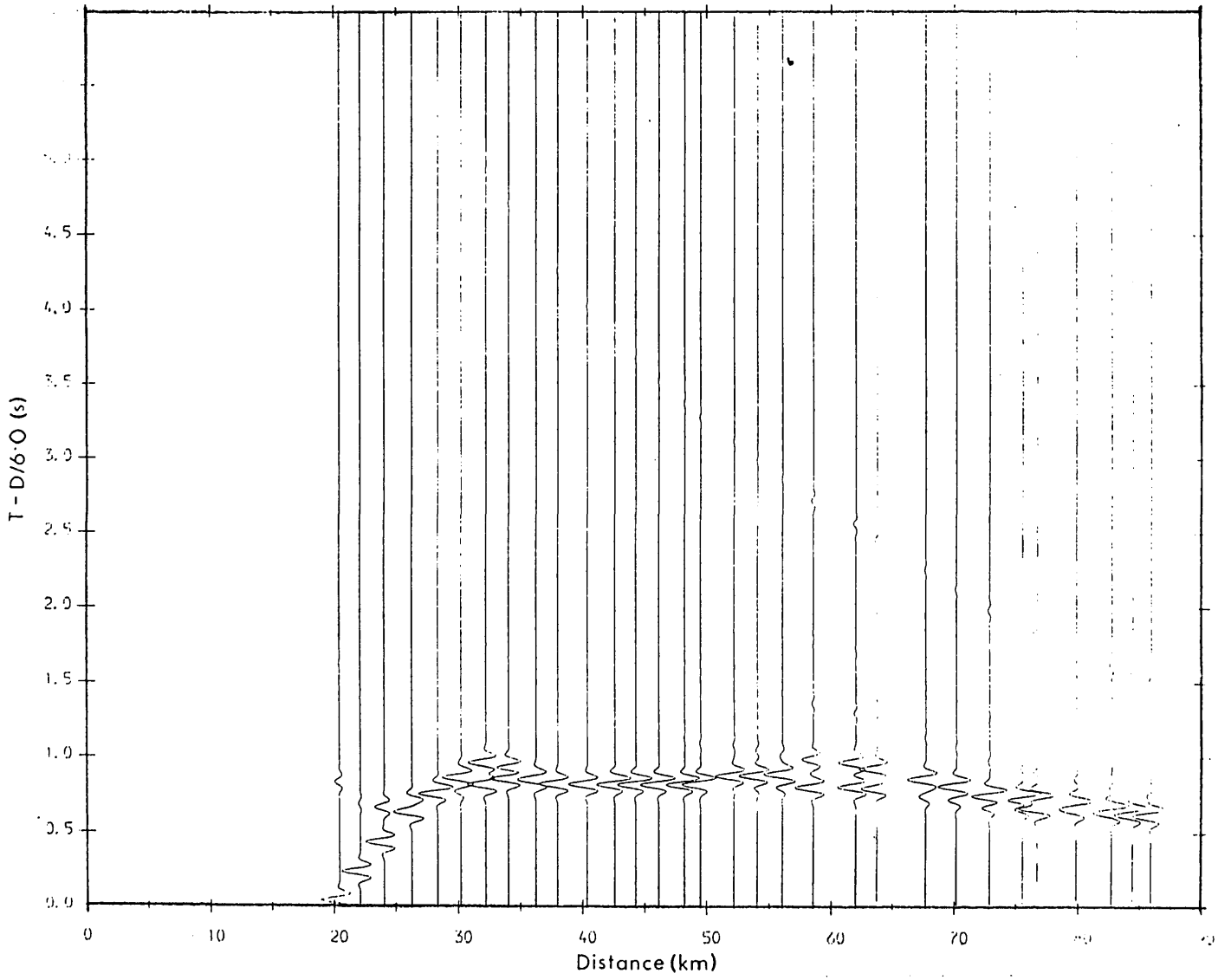

Fig. 4.31a Synthetic seismograms obtained from the raytracing model of the main line for the Hillhouse shotpoint.

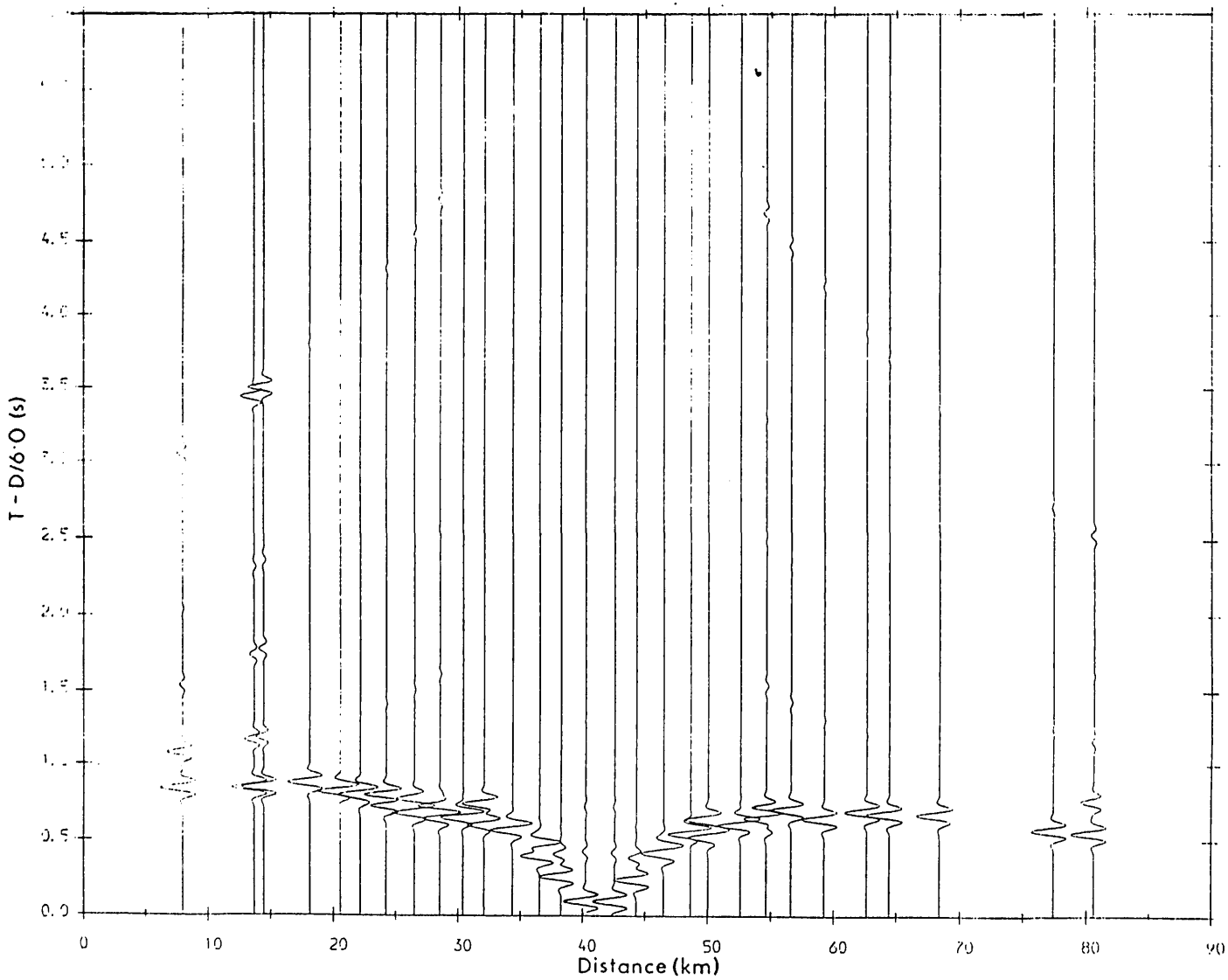

Fig. 4.31b Synthetic seismograms obtained from the raytracing model of the main line for the Loanhead shotpoint.

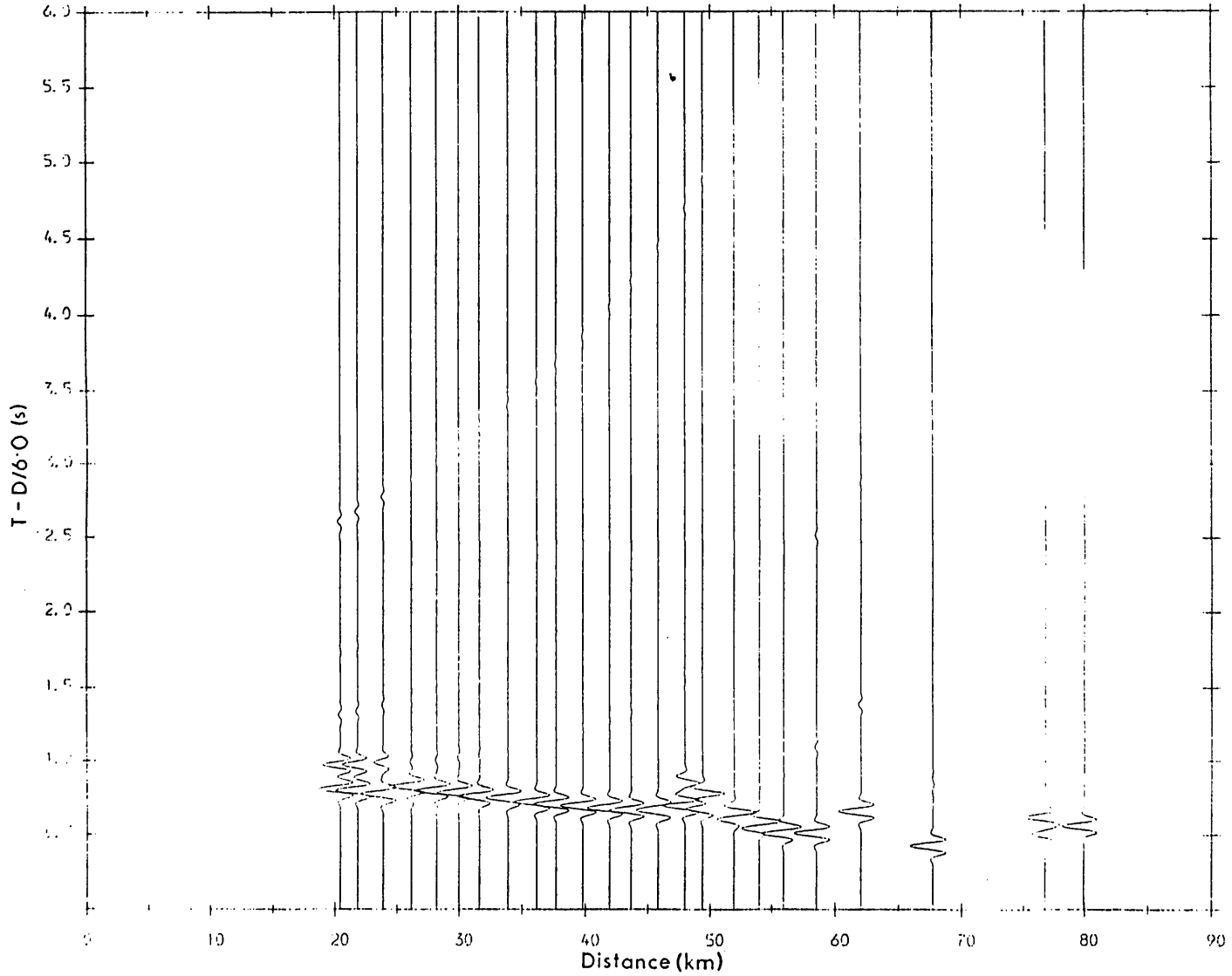

Fig. 4.31c Synthetic seismograms obtained from the raytracing model of the main line for the Sheephill shotpoint.

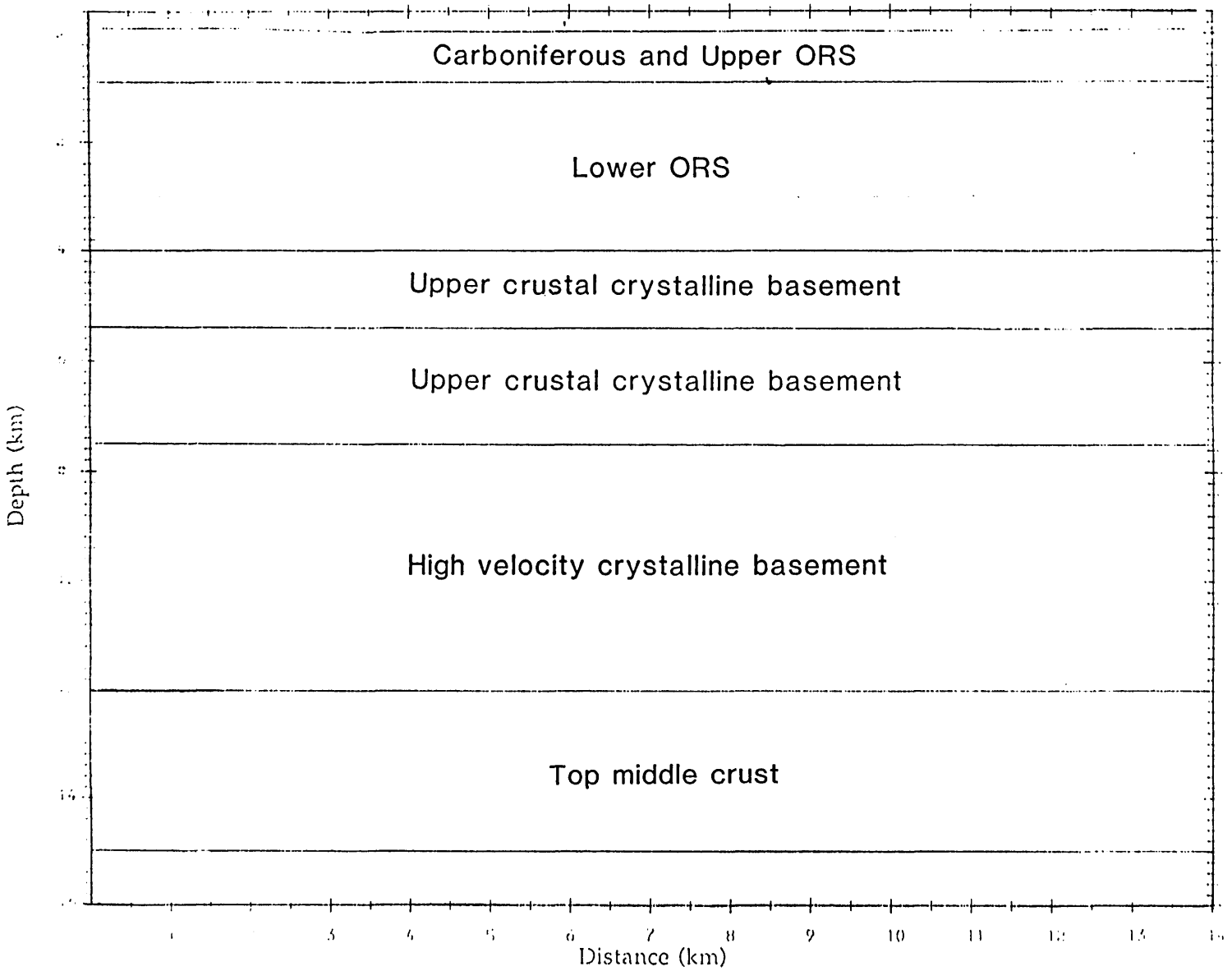

Fig. 4.32 Geological model of the Hillhouse-Kilmarnock line.

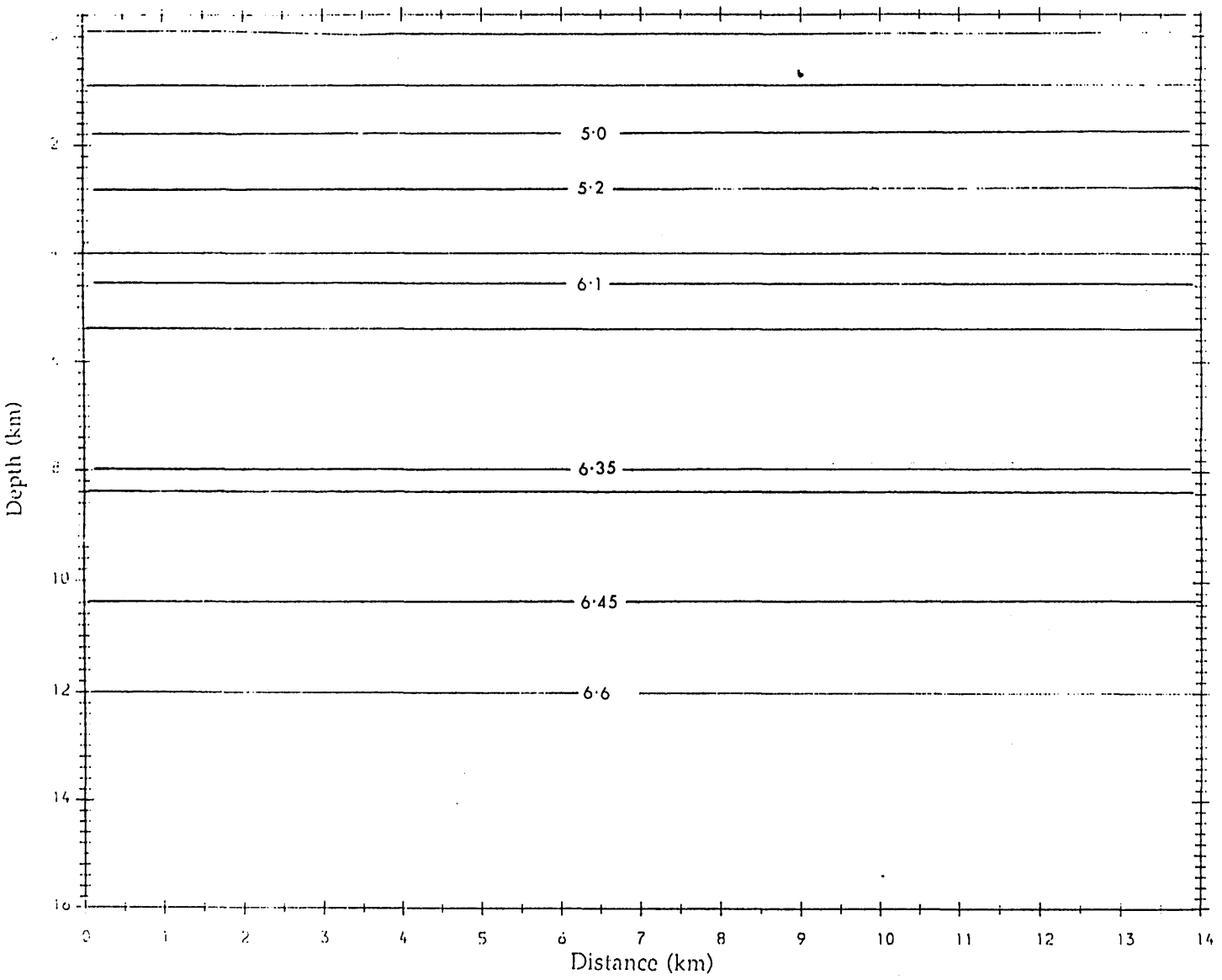

Fig. 4.33 P-wave velocity distribution of the Hillhouse-Kilmarnock line model.

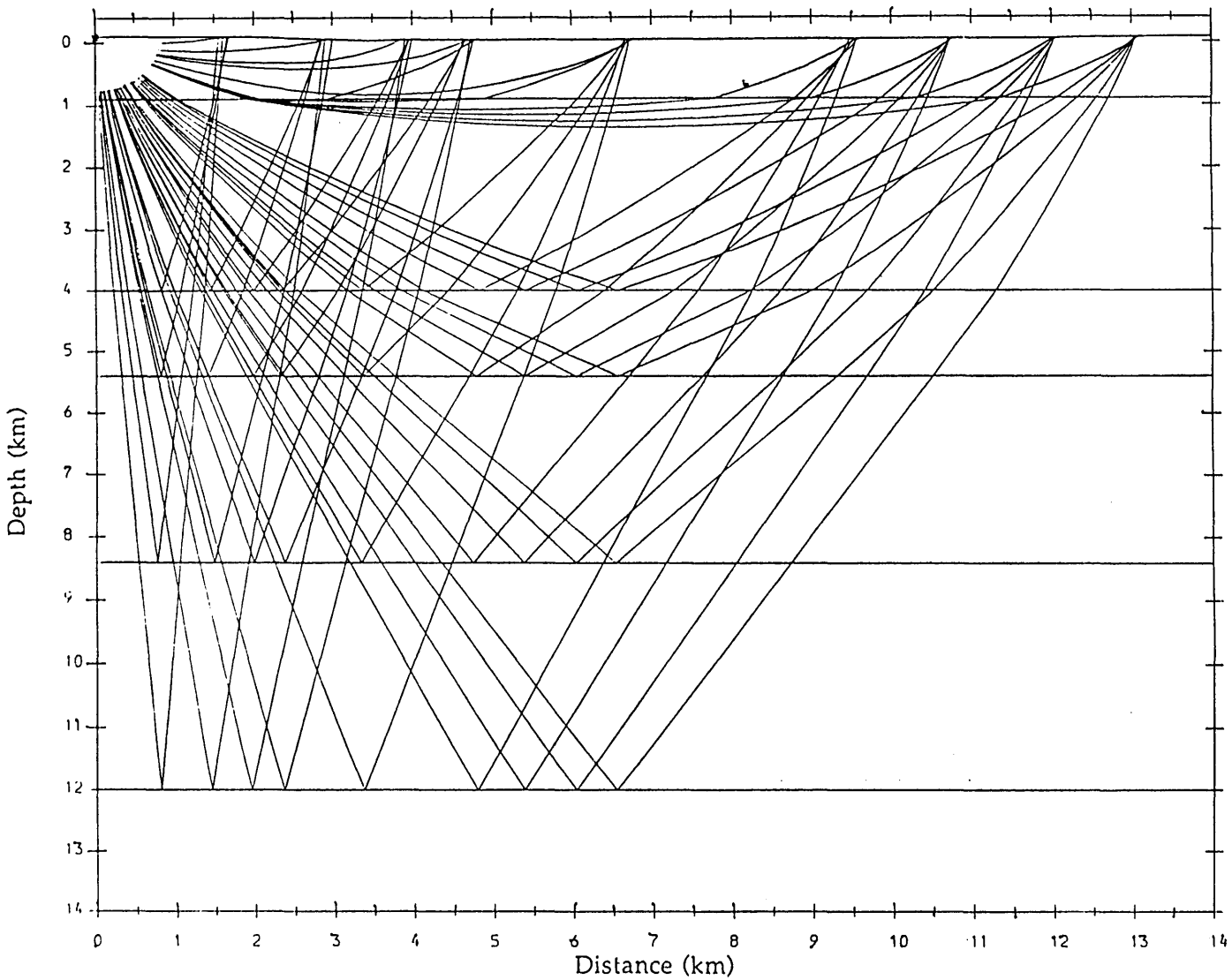

Fig. 4.34 Rays used to obtain the Hillhouse-Kilmarnock line model.

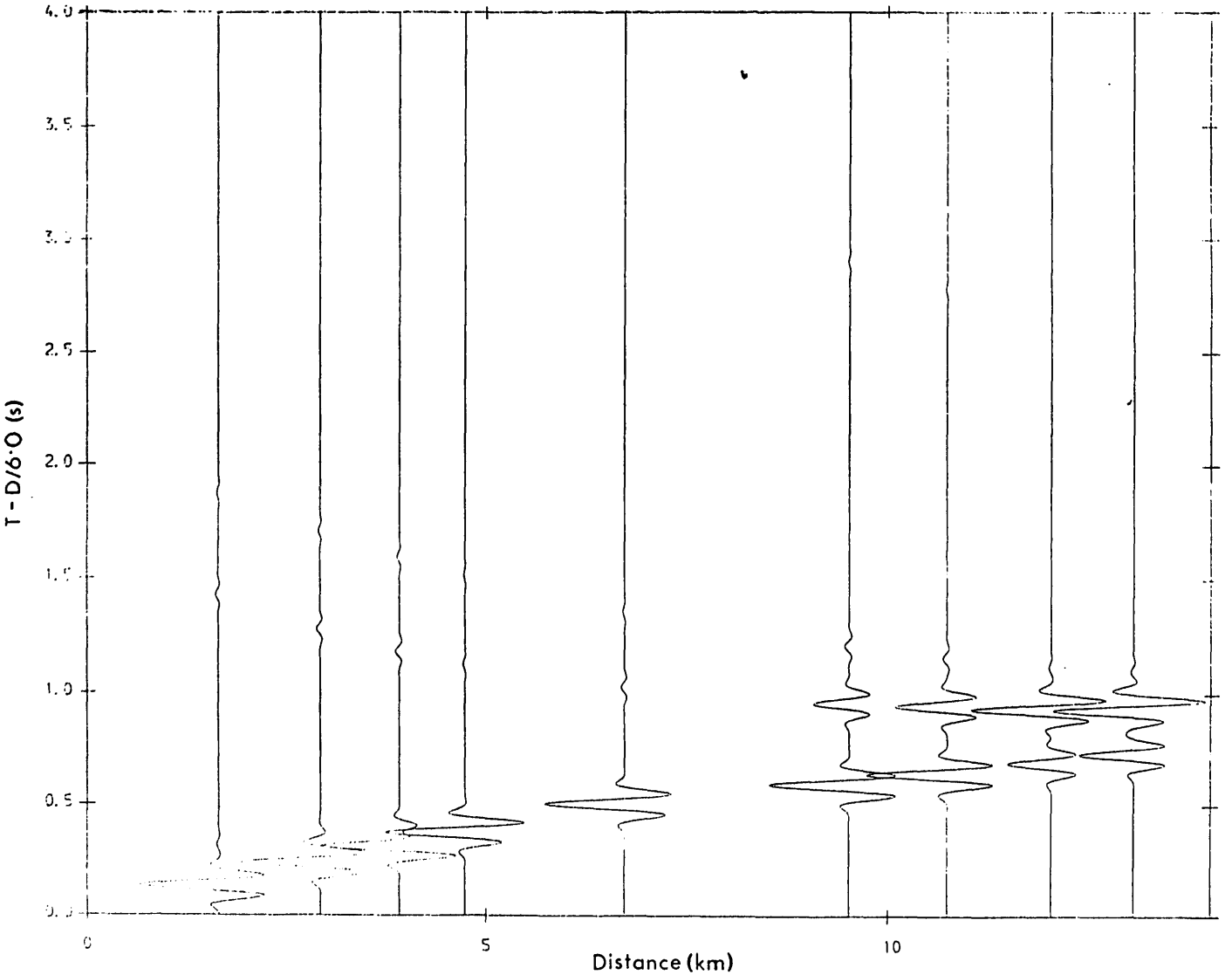

Fig. 4.35 Synthetic seismograms obtained from the Hillhouse-Kilmarnock line model.

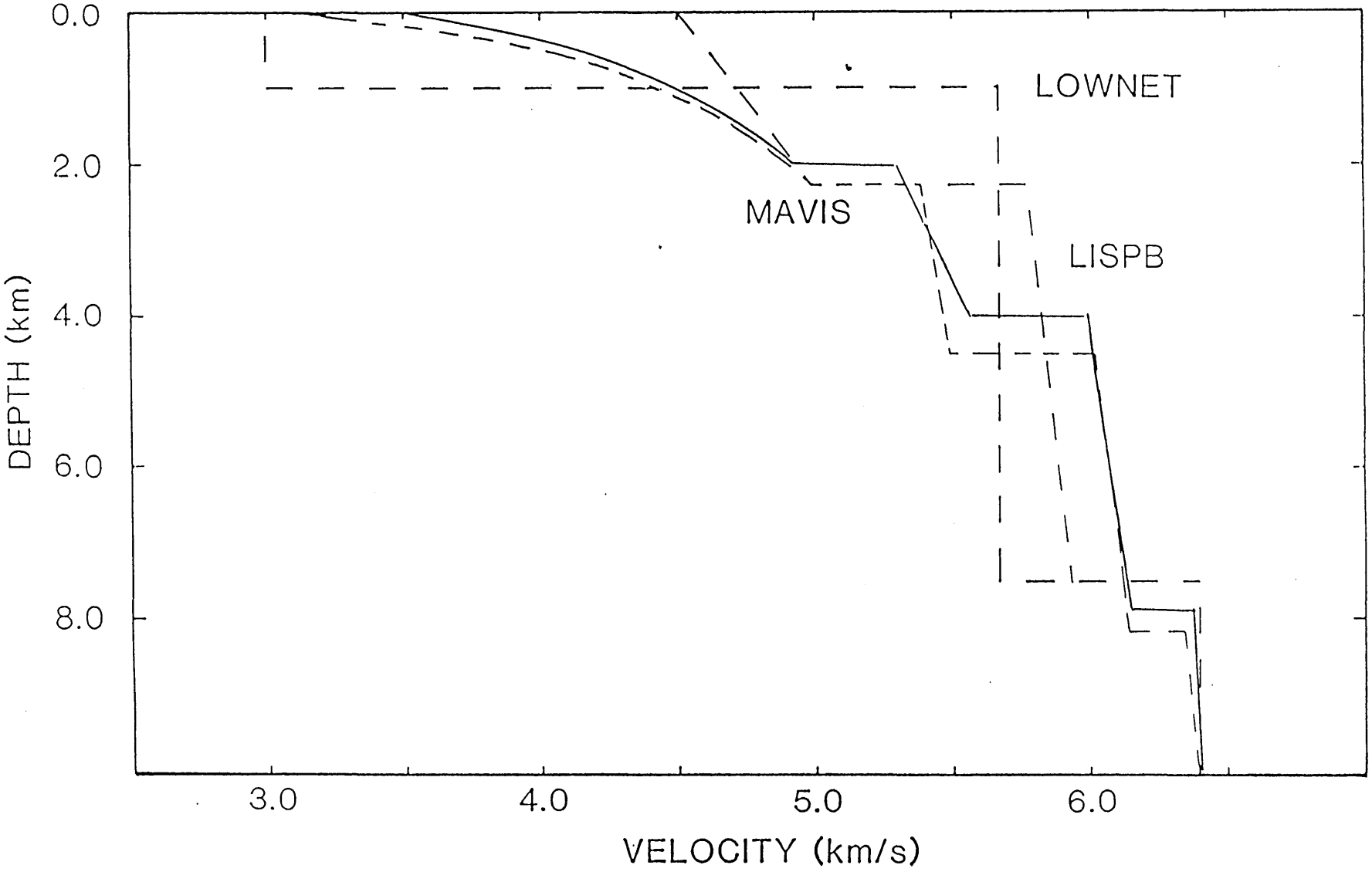

Fig. 5.1 Comparison of the average velocity-depth profiles of this and previous studies.

APPENDIX 7

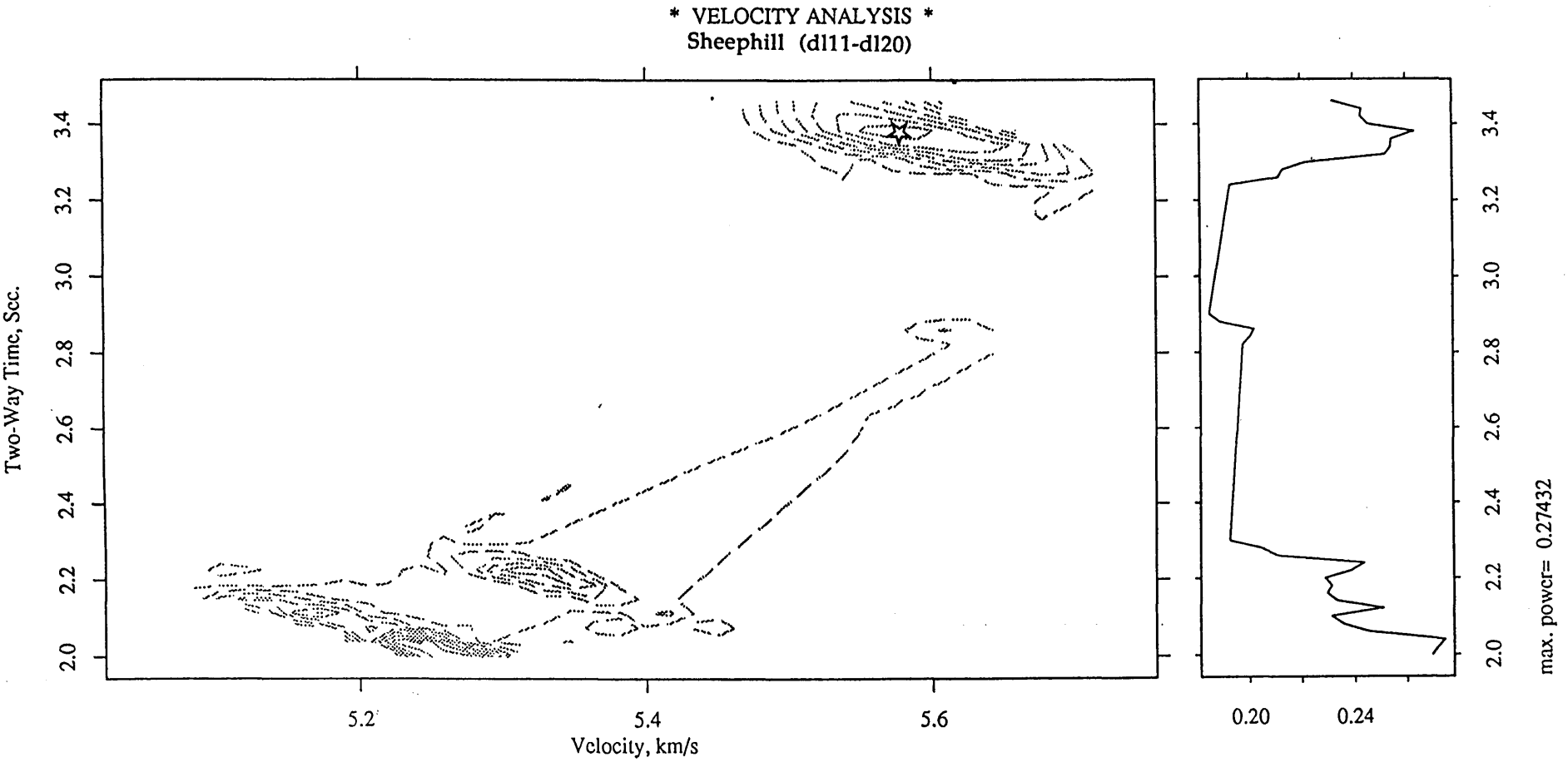

SEMB. METHOD FOR REFL. DATA
WINDOW (LENGTH, STEP)= 305, 20 MSEC.
VELOCITY STEP = 0.010 KM/S
CONTOUR (MIN,MAX,INT)= 0.19 0.27 0.01

WINDOW
PEAKS LOG

Semblance velocity analysis for stations dl11-20 from Sheephill to investigate reflection arrival (a7)

SHEEPHILL QUARRY

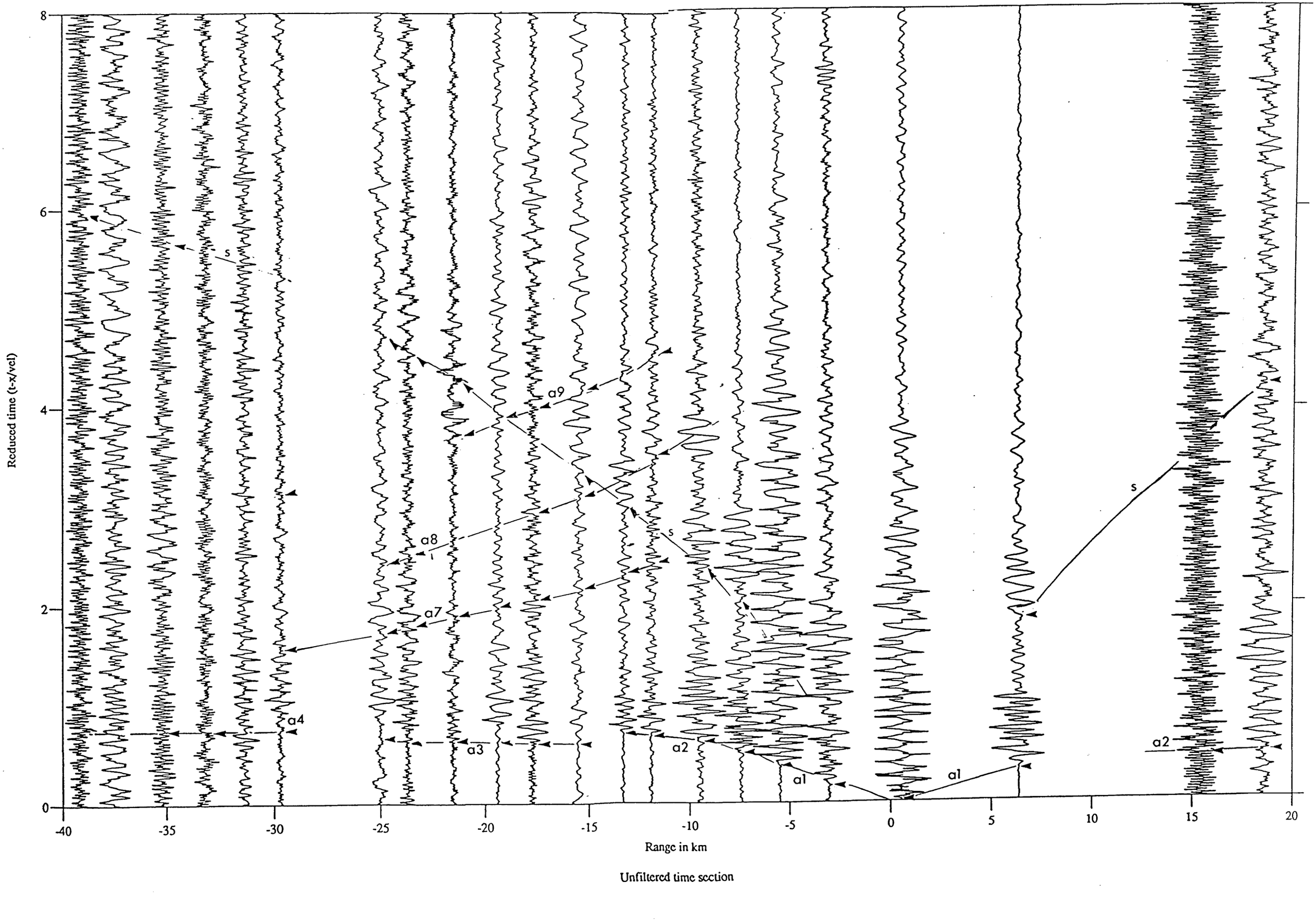

Unfiltered time section

SHEEPHILL QUARRY

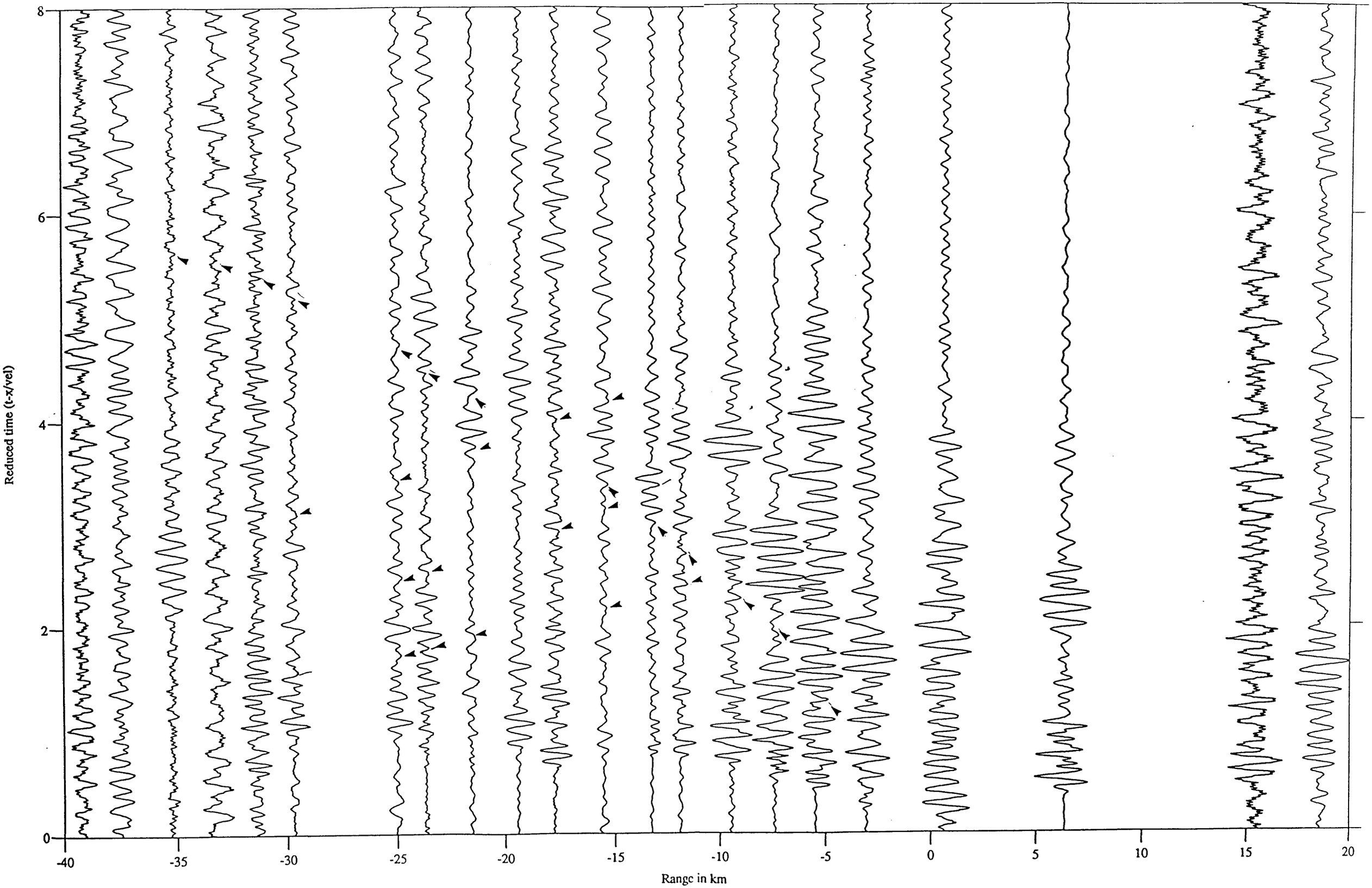

Sheephill (main line) vertical component data filtered with a minimum-phase, low-pass 8.0 Hz filter with a 0.25 s Hamming window. Reduction velocity 6.0 km/s.

SHEEPHILL QUARRY

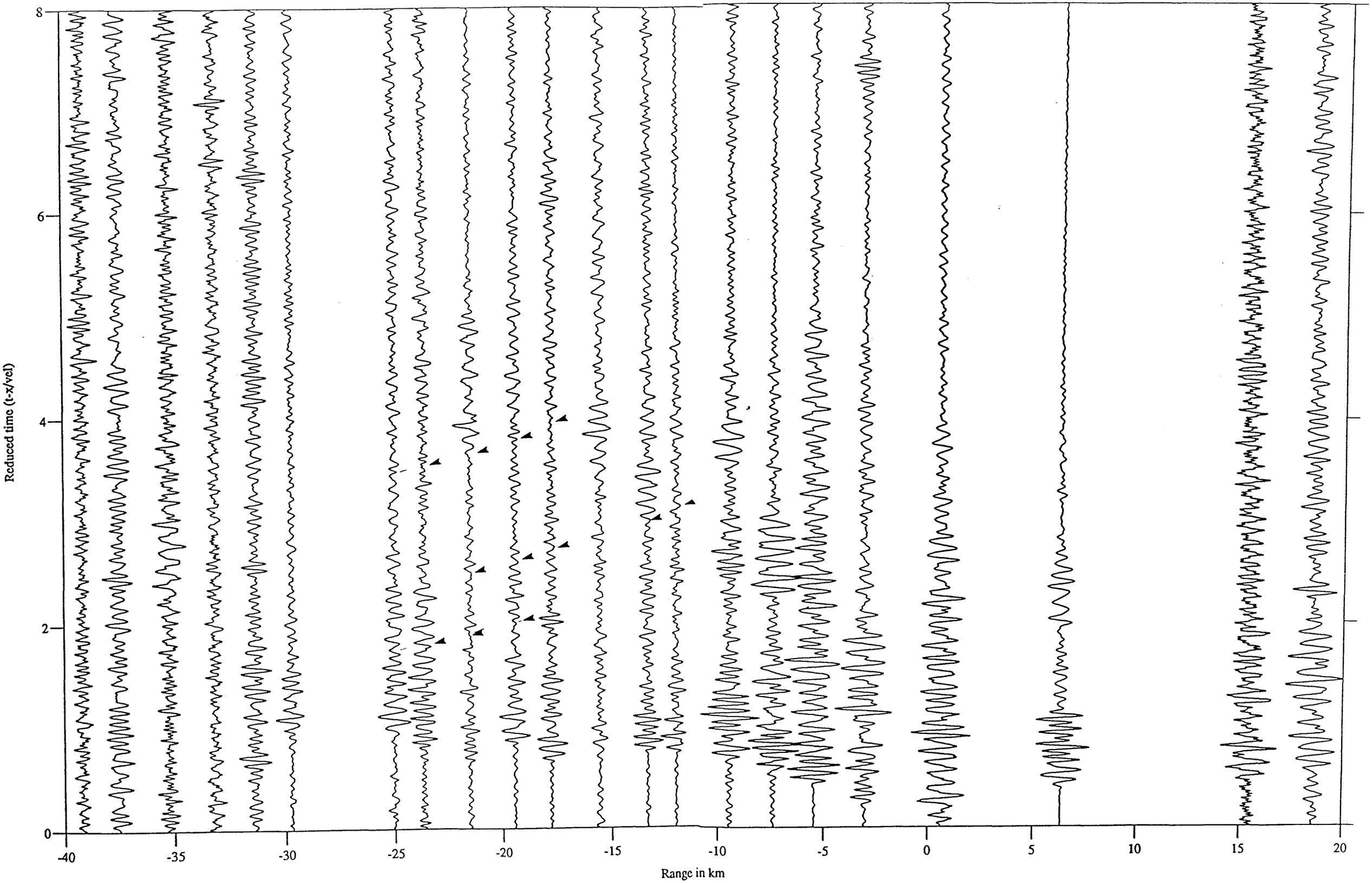

Sheephill vertical component data filtered with a minimum-phase, band-pass 8.0-16.0 Hz filter with a 0.25 s Hamming window. Reduction velocity 6.0 km/s.

SHEEPHILL QUARRY

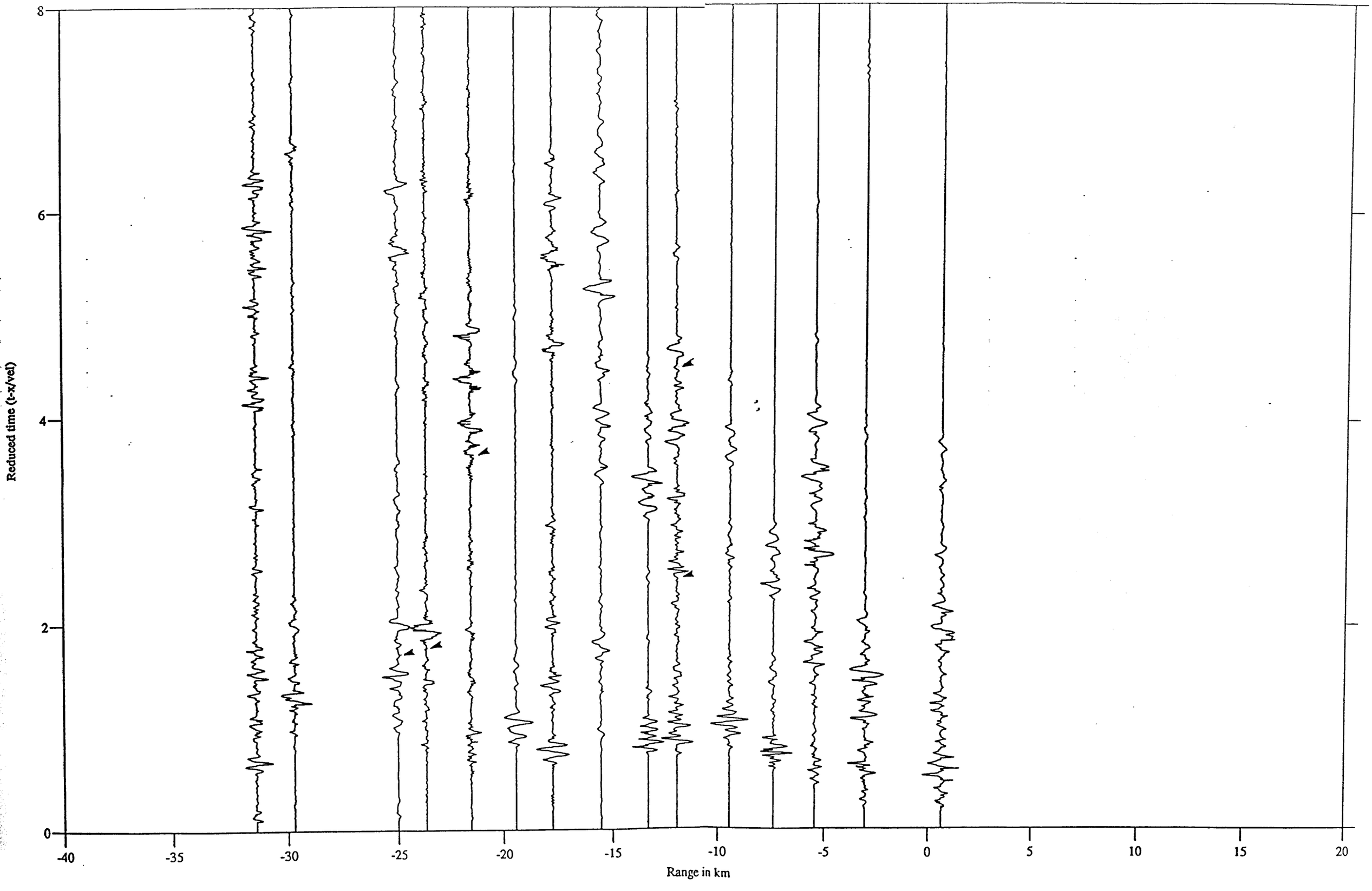

Sheephill vertical component data with polarization filtering, reduction velocity 6.0 km/s.

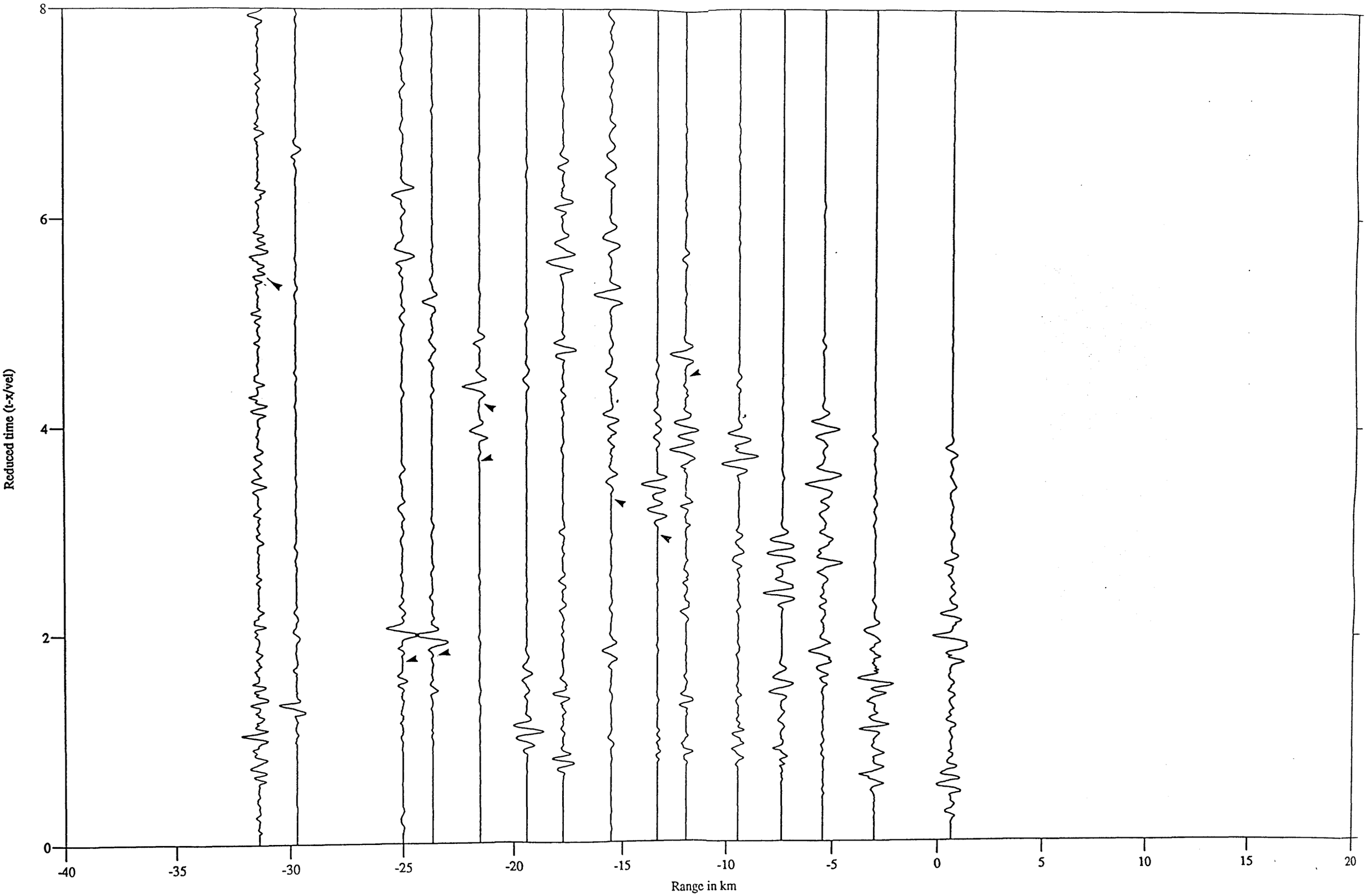

Sheephill vertical component data filtered with lowpass and polarization filter, reduction velocity 6.0 km/s. Filter parameters were: minimum-phase, lowpass 8.0 Hz frequency filter with a 0.25 s Hamming window; polarization filter window length 0.20 s.